

Fakultät für Chemie der Technischen Universität München

Name der promotionsführenden Einrichtung

Application and Development of Resorcin[4]arene-Based Supramolecular Catalysts

Titel der wissenschaftlichen Abhandlung

Lorenzo Catti

Vorname und Name

Vollständiger Abdruck der von der promotionsführenden Einrichtung

Fakultät für Chemie

der Technischen Universität München zur Erlangung des akademischen Grades

eines Doktors der Naturwissenschaften

genehmigten Dissertation.

Vorsitzende/-r: Prof. Dr. Kathrin Lang

Prüfende/-r der Dissertation:

1. Prof. Dr. Konrad Tiefenbacher

2. Prof. Dr. Tobias A. M. Gulder

3. Prof. Dr. Corinna Hess (mündliche Prüfung); Prof. Dr. Christof Sparr (schriftliches Gutachten)
(Universität Basel)

Die Dissertation wurde am 13.02.2017 bei der Technischen Universität München
eingereicht und durch die promotionsführende Einrichtung
Fakultät für Chemie am 13.03.2017 angenommen.

Der größte Teil der vorliegenden Arbeit wurde in der Zeit zwischen November 2013 und Mai 2016 unter Leitung von Prof. Konrad Tiefenbacher an der *Juniorprofessur für Organische Chemie* der *Technischen Universität München* angefertigt. Die Arbeit wurde unter Leitung von Prof. Konrad Tiefenbacher an der *Assistenzprofessur (mit Tenure Track) für Synthesis of Functional Modules* der *Universität Basel* im Februar 2017 fertiggestellt.

Teile dieser Arbeit wurden veröffentlicht:

Catti, L.; Pöthig, A.; Tiefenbacher, K.* *Adv. Synth. Catal.* **2017**, in press,
DOI:10.1002/adsc.201601363.

Zhang, Q.; Catti, L.; Kaila, V. R. I.; Tiefenbacher, K.* *Chem. Sci.* **2017**, *8*, 1653.

Catti, L.; Bräuer, T.; Zhang, Q.; Tiefenbacher, K.* *Chimia* **2016**, *70*, 810.

Catti, L.; Zhang, Q.; Tiefenbacher, K.* *Chem. Eur. J.* **2016**, *22*, 9060.

Catti, L.; Zhang, Q.; Tiefenbacher, K.* *Synthesis* **2016**, *48*, 313.

Catti, L.; Tiefenbacher, K.* *Chem. Commun.* **2015**, *51*, 892.

Acknowledgements

First of all, I would like to express my deepest gratitude to my supervisor Prof. Konrad Tiefenbacher for his excellent guidance over the course of my PhD studies. I am truly thankful to have been involved in such a fascinating research project and I appreciate the ambitious long-term goal of this endeavor. Without his support, his great ideas and his constant availability, this dissertation would not have been possible. I enjoyed a lot of freedom in my research, which allowed me to learn from my own mistakes and grow as a chemist. His ability to create a pleasant working atmosphere has to be emphasized. Overall, I truly consider myself fortunate to have had the opportunity to work under the guidance of such a talented professor.

I would also like to thank Prof. Thorsten Bach for his continuous support. His deep knowledge of organic chemistry is truly admirable. Likewise, I want to thank all the members of his group, who were always helpful and willing to discuss chemistry. I am also thankful to Prof. Stefan Huber and his group for their support and the pleasant time we spent together at the TU Munich. In addition, Ms. Kerstin Voigt is acknowledged for all the organizational efforts.

I am truly grateful to all the members of the Tiefenbacher group for the very pleasant working atmosphere and their constant support. I am also very thankful for the fun time we spent together outside the laboratory. Especially I would like to thank Qi Zhang and Johannes Richers. Qi taught me the basics of resorcin[4]arene chemistry and I deeply appreciate his friendly and calm personality. Johannes taught me a lot about the practical aspects of organic chemistry, since the time I was a research student in his laboratory. I appreciate his passion for chemistry and his eagerness to discuss it. I also admire his skills in the area of graphical design and agree with him on the profound connection between science and art. I furthermore was blessed to work with a number of very talented students over the course of my PhD studies and I am thankful for the wonderful time we had together: Andreas Herdlitschka (Bachelor`s Thesis), Nadine Truchan, Michael Neumeier, Daniel Di Carlo, Vivien Lechner, Jacob Sag, Michael Wiedemann, Ramona Baiertl, Philip Böhm (Bachelor`s Thesis), Severin Merget (Master`s Thesis) and Fabian Bissegger (Master`s Thesis).

In addition, I want to thank Prof. Christof Sparr and his group for their support. I especially appreciate the warm welcome they gave me during my first days in Basel. I would also like to thank the staff of the University of Basel, who helped me during my first days and who helped

me set up the new laboratories. I also want to mention the help of PD Dr. Daniel Häussinger regarding NMR measurements, in particular DOSY measurements. Furthermore, I want to thank Mihai Lomora and the members of the Palivan group for the interesting collaboration on the incorporation of hexameric assemblies into the membrane of polymersomes. Dr. Felix Rudolphi is acknowledged for his help with the software “Sciformation”. Additionally, Ms. Audrey Fischer is acknowledged for organizational efforts.

I also want to mention the great time I had during the supervision of the OCA (OC practical course) and the nice people I got to know during that time. Teaching young scientists the basics of organic chemistry helped me consolidate my own knowledge. The experience also taught me the great responsibility that comes with heading a laboratory.

Last but not least I owe gratitude to my friends, especially Klemens Thaler, who supported me during all those years. Likewise, I want to thank my parents, who made it possible for me to study chemistry. Especially my mother is acknowledged for her unconditional support.

English abstract

Self-assembled supramolecular structures based on the resorcin[4]arene motif **54b** represent readily available systems for the investigation of enzyme-like catalysis. The hydrogen bond-based hexameric assembly **XI**, formed by subunit **54b**, encloses a volume of about 1400 Å³, is capable of reversible guest-encapsulation and has been shown stabilize cationic molecules via extensive cation- π interactions with the aromatic cavity walls. The discovery of the Brønsted acid character of hexamer **XI** ($pK_a \approx 5.5-6.0$) in 2013 triggered intensive investigations regarding its application in supramolecular acid catalysis.

One of the first catalytic applications was achieved in the intramolecular hydroalkoxylation of unactivated hydroxy olefins under mild conditions. The capability of hexamer **XI** to stabilize cationic transition states could be harnessed to synthesize several tetrahydropyran and oxepane derivatives in generally good to excellent yields. The concept of using the resorcin[4]arene hexamer cavity as a reaction chamber was subsequently extended to a dehydrative cyclization-rearrangement cascade reaction, which had previously only been reported with an excess of strong Brønsted acid. The study furthermore led to the discovery of an unprecedented cyclobutanone formation via an intramolecular 1,5-hydride transfer within the cavity of hexamer **XI**. In addition, first preliminary experiments were conducted regarding the hexamer **XI**-catalyzed intermolecular Friedel-Crafts alkylation. Moreover, certain limitations of the current system could be overcome by utilizing camphorsulfonic acid as an encapsulated acid co-catalyst. In addition, the photoacidity of the system was studied as an alternative, unconventional approach to increase the acidity of the catalyst.

In order to design and construct novel hydrogen bond-based supramolecular catalysts, the molecular mechanisms responsible for the catalytic activity of host system **XI** were investigated by comparing its properties with those of the closely related pyrogallol[4]arene hexamer **XII**, which is catalytically inactive in cationic reactions. Research on this subject was further advanced by successfully synthesizing derivatives of the resorcin[4]arene monomer **54b** that were demonstrated to self-assemble in solution. In this context, the tetra-amide **140d** was developed which features an alternative mode of connectivity based on amide dimerization. In addition, introduction of fluorine atoms in 2-position was achieved for the first time. Finally, first steps into the direction of an inherently chiral resorcin[4]arene hexamer catalyst were taken by mono-propylation of subunit **54b**.

Deutsche Zusammenfassung

Selbstassemblierte supramolekulare Strukturen, die auf dem Resorcin[4]aren Motiv **54b** basieren, dienen als leicht zugängliche Systeme für die Untersuchung artifizierlicher, enzym-ähnlicher Katalyse. Die auf Wasserstoffbrückenbindungen basierende hexamere Kapselstruktur **XI**, die sich in Lösung spontan aus Monomer **54b** assembliert, umfasst ein Volumen von etwa 1400 Å³. Das System ist zur reversiblen Gastaufnahme befähigt und ist in der Lage kationische Moleküle über Kation- π Wechselwirkungen mit der aromatischen Kavität zu stabilisieren. Im Jahr 2013 zeigten interne Studien, dass die molekular Kapsel **XI** als milde Brønsted-Säure ($pK_a \approx 5.5-6.0$) fungiert. Dieser Beobachtung folgten intensive Studien zur Anwendung von Hexamer **XI** auf dem Gebiet der supramolekularen Säure-Katalyse.

Eine der ersten katalytischen Anwendungen erfolgte in der intramolekularen Hydroalkoxylierung nicht-aktivierter Hydroxyolefine unter milden Reaktionsbedingungen. Unter Ausnutzung der Stabilisierung kationischer Übergangszustände durch Hexamer **XI** konnten mehrere Tetrahydropyran- und Oxepan-Derivate in allgemein guter bis sehr guter Ausbeute synthetisiert werden. Das Konzept wurde nachfolgend auf eine kationische, durch Dehydratisierung tertiärer Alkohole initiierte, Kaskadenreaktion in der Kavität von Hexamer **XI** ausgeweitet. Dabei durchgeführte Studien resultierten in der Entdeckung einer bisher nicht bekannten Cyclobutanon-Synthese, basierend auf einem intramolekularen 1,5-Hydrid-Transfer. Des Weiteren wurden erste Studien zu Hexamer **XI**-katalysierten intermolekularer Friedel-Crafts-Alkylierungen durchgeführt. Zusätzlich gelang es die Eigenschaften des katalytischen Systems durch Einkapsulierung eines Säure-Cokatalysators (Campher-sulfonsäure) zu modulieren. Als weitere Alternative zur Modulierung des Systems wurde die Induzierung von Photoacidität durch Bestrahlung des Katalysators untersucht.

Um gezielt neuartige Wasserstoffbrücken-basierte Katalysatoren zu entwickeln, wurden die Grundlagen der katalytischen Aktivität von Hexamer **XI** durch Vergleich mit Wirtstruktur **XII** erforscht, die strukturell verwandt ist, jedoch keine katalytische Aktivität aufweist. Aus demselben Motiv heraus wurden Derivate des Resorcin[4]aren Monomers **54b** synthetisiert, deren Fähigkeit zur Selbstassemblierung in Lösung demonstriert werden konnte. Das in diesem Zusammenhang synthetisierte Tetraamid **140d** verfügt über ein alternatives Konnektivitätsmuster und assembliert über Amid-Dimerisierung. Zusätzlich gelang zum ersten Mal die Einführung von Fluorid-Substituenten in *ortho*-Position zu den Phenoleinheiten. Abschließend

wurde erste Schritte in Richtung eines inhärent chiralen Resorcin[4]aren-Hexamer Katalysators durch Monopropylierung von Untereinheit **54b** eingeleitet.



Table of contents

Acknowledgements	III
English abstract	VII
Deutsche Zusammenfassung	IX
1. Introduction	1
2. Enzyme catalysis	2
2.1 Basic principles of enzyme catalysis	2
2.2 Terpene cyclases.....	2
2.2.1 Biomimetic terpene/polyene cyclizations	5
3. Supramolecular hosts	9
3.1 Covalently-linked supramolecular hosts	9
3.2 Self-assembled supramolecular hosts	13
3.2.1 Hexameric capsules of resorcin[4]arene and pyrogallol[4]arene	22
4. Catalytic and stoichiometric chemistry in self-assembled supramolecular hosts	28
4.1 Advantages of chemistry within supramolecular hosts	28
4.2 Examples of catalysis and stoichiometric chemistry in self-assembled hosts.....	30
5. Objective of this thesis	48
6. Results and discussion.....	50
6.1 Publication summaries.....	50
6.1.1 Intramolecular hydroalkoxylation catalyzed inside a self-assembled cavity of an enzyme-like host structure	50
6.1.2 Host-catalyzed cyclodehydration-rearrangement cascade reaction of unsaturated tertiary alcohols.....	52
6.2 Application: Friedel-Crafts alkylation.....	54
6.3 Modulation: acid co-catalyst and photoacidity.....	57
6.4 Elucidation: reasons for the catalytic inactivity of the pyrogallol[4]arene hexamer XII	63
6.5 Derivatization: towards new hydrogen bond-based supramolecular catalysts.....	66
6.5.1 Inherently chiral mono-functionalized C-undecylcalix[4]resorcinarenes.....	66
6.5.2 Achiral tetra-functionalized C-undecylcalix[4]resorcinarenes	74
6.5.2.1 Tetra-benzyl alcohol 140a and tetra-aldehyde 140b	74
6.5.2.2 Tetra-carboxylic acid 140c and tetra-amide 140d	79
6.5.2.3 Tetra-fluoride 140e	94

7. Summary and outlook	104
8. Experimental section	109
8.1 General information.....	109
8.2 General procedures for hexamer studies	111
8.2.1 General procedure for catalytic tests with hexamer XI	111
8.2.2 General procedure for the control experiments with inhibitor Bu ₄ NBr.....	112
8.2.3 General procedure for the modulation experiments with camphorsulfonic acid...	113
8.2.4 General procedure for the modulation experiments using photoacidity	113
8.2.5 General procedure for the THT cyclizations with hexamer XIII and (189) ₆	113
8.2.6 Acetal hydrolysis with hexamer XIII	114
8.2.7 Encapsulation studies with hexamer XIII and (189) ₆	116
8.2.8 Self-recognition studies with compounds 140e and 54b	116
8.2.9 Determination of the p <i>K</i> _a value of hexamer XIII	117
8.3 Synthetic procedures.....	120
9. Index of abbreviations	138
10. References	140
11. Bibliographic data of complete publications.....	150
12. Reprint permissions and reprints	153
12.1 The Royal Society of Chemistry	153
12.2 John Wiley and Sons	153



1. Introduction

Supramolecular chemistry, often defined as chemistry beyond the molecule,¹ seeks to develop advanced chemical systems from building blocks interacting through noncovalent intermolecular interactions. Based on the concept of molecular information, this research area aims at controlling the structural and dynamic features of molecular entities and their complexification by self-organization.² Components capable of self-organization spontaneously self-assemble into defined, well-organized and functional supramolecular architectures. Self-assembly represents the driving force responsible for the creation of life from inanimate matter.³ The reversibility of noncovalent interactions allows these systems to respond to external stimuli and therefore enables evolution. Adaptation to the environment as well as self-assembly rely on molecular recognition via noncovalent interactions. Molecular recognition marks one of the key features of enzymes and enables their selective complexation of specific substrates in complex mixtures. The three-dimensional structure of enzymes, which results from the information encoded in their amino acid sequence, creates a unique microenvironment for catalysis that is separated from its surroundings. Compartmentalization of this kind is of fundamental importance in biology as it defines cell structure and allows different metabolic activities in close proximity. The reaction profile of a substance enclosed within an enzyme is highly controlled by the functionalities incorporated into the enzyme pocket and the influence of the confined environment on the guest conformation. The efficiency of enzyme catalysis regarding acceleration and selectivity remains unrivaled to this day by man-made catalysts. Supramolecular catalysis aims to overcome the limitations of conventional catalysts by mimicking the basic principle of operation displayed by enzymes. The required supramolecular systems are designed to only mimic the catalytically active portion of the enzyme, which reduces the complexity of the overall architectures. A common strategy for the construction and design of supramolecular catalysts relies on the synthesis of simple building blocks, which self-assemble in solution via noncovalent interactions. Hydrogen bonding, which is ubiquitous in nature and responsible for the secondary structure of enzymes, has become an established tool for the construction of such assemblies.

This thesis describes the application of a hydrogen bond-based hexameric assembly as a catalyst in reactions involving cationic transition states. Novel derivatives of this catalyst are reported and studied regarding their properties and reactivity in monoterpene cyclizations. Additionally, strategies to modulate the catalytic activity of the original hexameric structure are presented.

2. Enzyme catalysis

2.1 Basic principles of enzyme catalysis

The three-dimensional structure of an enzyme creates a hydrophobic pocket in an aqueous environment, which selectively isolates substrates of complementary size and shape from the solvent. This desolvation process strongly influences the binding affinity of the substrate, both entropically and enthalpically.⁴ It furthermore protects the catalyzed reaction from the intrinsic reactivity of the solvent. In the case of intermolecular reactions, the co-encapsulation of the reaction partners brings them in close proximity and facilitates their reaction via an increase in their local concentration. Enzymes use a large variety of molecular mechanisms to accelerate the rate of the catalyzed reaction. Lowering of the activation free energy plays the dominant role and can be achieved via different modes:⁵ 1) enzymes preferentially bind and therefore stabilize the transition state of the reaction rather than the substrate or the product (transition state stabilization). This often involves the stabilization of developing charge in the transition state. 2) Upon encapsulation, the substrate experiences a certain strain and is forced to adopt a reactive orientation and/or conformation (ground state destabilization). Additionally, noncovalent interactions with the amino acids in the active center can result in activation of the substrate by increasing its reactivity. 3) Substrate activation can also result from transient covalent bond formation with residues in the enzyme pocket (covalent catalysis).⁶ Alternatively, quantum mechanical tunneling through the activation barrier can also result in a sizeable contribution to the rate acceleration.⁵ Two more recently identified contributions to the catalytic efficiency of enzymes include matching of the pK_a values in the transition state and protein dynamics.⁷ Multiple activation modes can work in parallel and create rate accelerations as large as a factor of 10^{19} .⁸ After successful transformation, the product is released into the bulk solvent to complete the catalytic cycle.

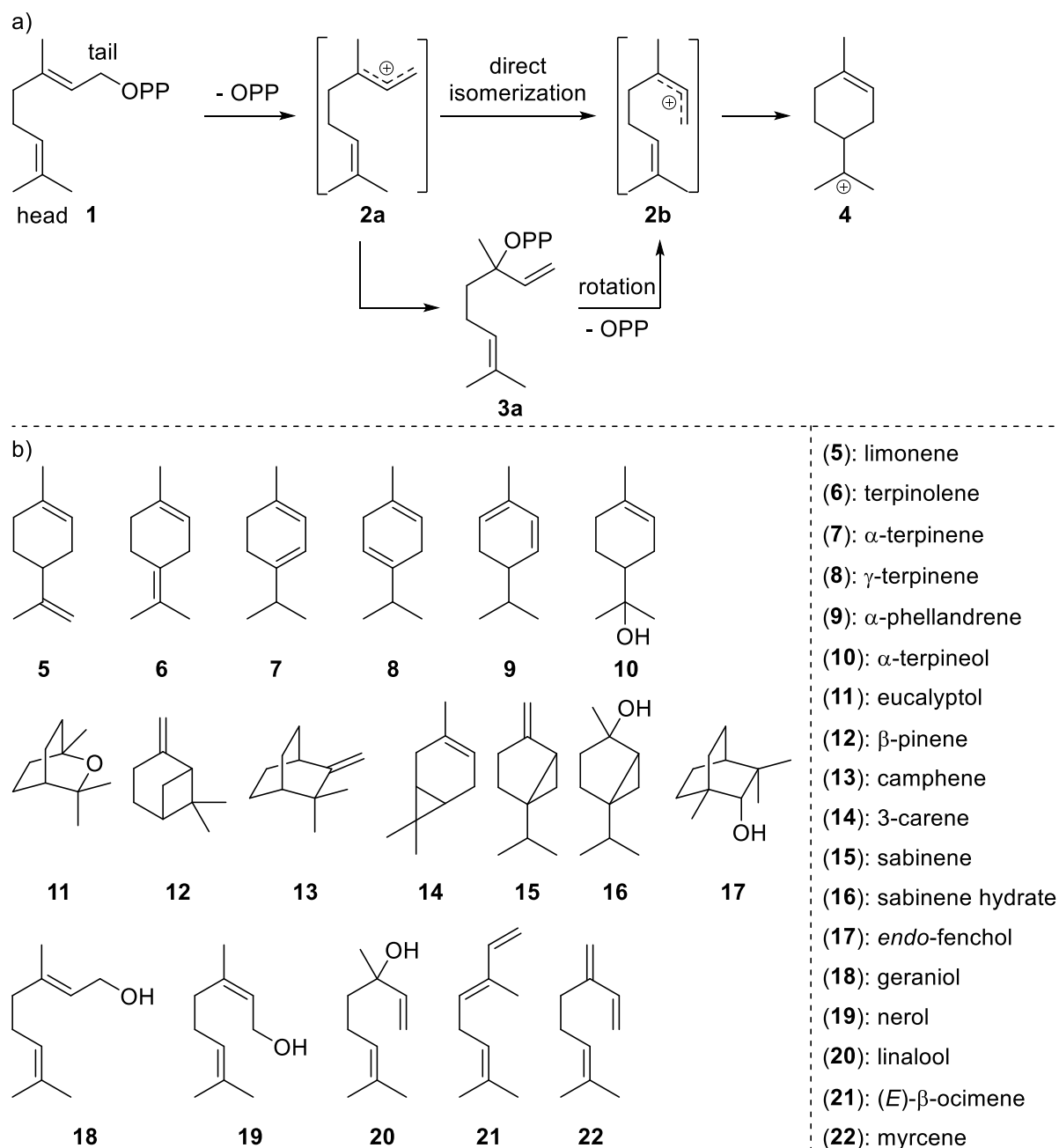
2.2 Terpene cyclases

Terpenes represent the largest and most diverse group of natural products, comprising more than 30 000 known members to date.⁹ Many terpenes feature biological activity and are used to treat diseases like cancer (paclitaxel)¹⁰ or malaria (artemisinin).¹¹ Yet, the whole spectrum of terpene structures derives from the cyclization of only a handful of acyclic precursors. Based on their number of carbon atoms (isoprene units), terpenes are classified into hemi- (C_5), mono- (C_{10}), sesqui- (C_{15}), di- (C_{20}), sester- (C_{25}) and triterpenes (C_{30}). Even larger members like tetraterpenes (C_{40}) exist. The different terpene precursors are the product of a chain elongation

reaction catalyzed by prenyltransferases.¹² Isopentenyl diphosphate and dimethylallyl diphosphate are utilized as C₅-building blocks for the chain elongation and themselves are biosynthetically produced by the mevalonate and deoxyxylulose phosphate pathway.⁹

Cyclization of the acyclic terpene precursors, by enzymes called terpene cyclases, into highly elaborate carbon skeletons is considered as one of the most complex reactions encountered in nature. The reaction is initiated by generation of a highly reactive carbocation within the enzyme pocket. Two different classes of terpene cyclases are distinguished, which differ in their mode of carbocation formation. Type I cyclases trigger cation formation via the cleavage of the allylic diphosphate leaving group utilizing a trinuclear metal (mostly Mg²⁺) cluster, which is complexed by conserved amino acid residues in the active site. In contrast, type II cyclases initiate the cyclization by protonation of a C–C double bond or an epoxide moiety. A related activation mode relies on the formation of an intermediary halonium ion and is responsible for the multitude of halogenated cyclic terpene products. Both activation modes furthermore differ by the direction of charge propagation during the cyclization cascade. The activation of the terminal double bond (head) results in a so-called head-to-tail terpene (HTT) cyclization, while cleavage of the allylic diphosphate group (tail) leads to a tail-to-head terpene (THT) cyclization.¹³ In both cases, the formed cation undergoes cyclization by the intramolecular attack of a double bond. The resulting cation can undergo further cyclizations, Wagner-Meerwein rearrangements and hydride migrations, until the cascade is terminated by elimination or attack of a nucleophile like water. Complexation of the cleaved diphosphate unit by the trinuclear metal cluster prevents premature quenching during the THT cyclization and allows for a non-stop reaction mode. The formed carbocations are stabilized by cation-dipole and cation- π interactions within the enzyme pocket during the reaction. Stabilization of cationic intermediates via cation- π interactions with aromatic residues avoids the danger of alkylation and therefore suicide inhibition of the enzyme. Despite the wide range of alternative reaction pathways, more than half of the known mono- and sesquiterpene cyclases catalyze the formation of a single product. Equally impressive is the transfer of stereoinformation from the chiral environment of the enzyme to the prochiral sp²-hybridized carbons of the terpene precursor. Due to the high reaction rate of cationic cyclizations, extensive conformational changes of the intermediates are considered unlikely. This makes the initial substrate conformation, induced by the enzyme pocket, decisive for the observed reaction outcome. It is noteworthy that terpene cyclases and prenyltransferases are structurally and mechanistically related and likely diverged from a common primordial ancestor.¹²

Monoterpene cyclases produce acyclic, mono- and bicyclic terpenes using geranyl diphosphate (**1**) as a substrate (Scheme 1). The activation occurs via ion-dependent phosphate cleavage to give allylic cation **2a**, which is unable to cyclize directly due to its (*E*)-configuration. It is postulated that cation **2a** is first converted to linalyl diphosphate (**3**), which allows rotation around the former double bond. A second ionization-step creates the *cisoid*-isomer **2b**, which can be attacked by the internal double bond to yield α -terpinyl cation (**4**), the common intermediate of all cyclic monoterpenes. However, new results indicate that a direct isomerization from the *transoid*-cation **2a** to the *cisoid* isomer **2b** might be feasible.¹⁴ Cation **4** can subsequently be deprotonated to give either limonene (**5**) or terpinolene (**6**). If the deprotonation is preceded by a 1,2- or 1,3-hydride migration step, formation of α -terpinene (**7**), γ -terpinene (**8**) or α -phellandrene (**9**) is observed. However, if a residual water molecule is present in the enzyme pocket, α -terpinyl cation (**4**) can be converted to α -terpineol (**10**). Intramolecular hydroalkoxylation of alcohol **10** can lead to formation of the bicyclic ether eucalyptol (**11**). Alternative bicyclic reaction products comprise β -pinene (**12**), camphene (**13**), 3-carene (**14**) and sabinene (**15**). Furthermore, trapping of intermediary bicyclic cations by water can lead to compounds like sabinene hydrate (**16**) and *endo*-fenchol (**17**). If the initial ionization step is followed by proton loss or attack of water, acyclic products are formed. Geraniol (**18**), nerol (**19**), linalool (**20**), (*E*)- β -ocimene (**21**) and myrcene (**22**) belong to this class of compounds. Additionally, also products that arise from attack of the initially cleaved diphosphate group can be found. The absolute configuration of the product can be traced back to the helical conformation fold of geranyl diphosphate (**1**), which gives rise to the corresponding enantiomer of the α -terpinyl cation (**4**). If more than a single product is formed by the cyclase, the different monoterpene products usually all share the same absolute configuration.

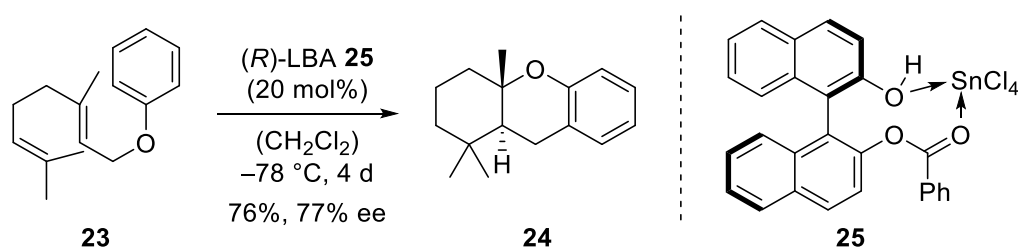


Scheme 1: (a) Biosynthetic formation of α -terpinyl cation (4) (PP = diphosphate); (b) common cyclic and acyclic monoterpenes.

2.2.1 Biomimetic terpene/polyene cyclizations

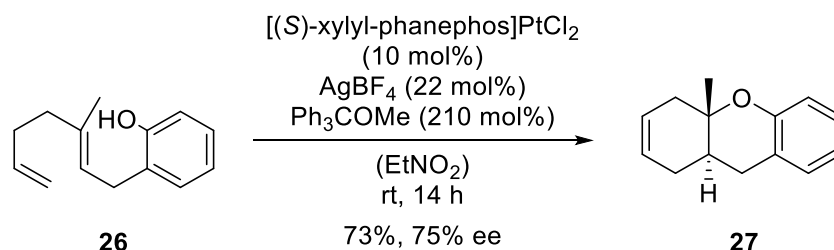
The complexity of polycyclic terpene natural products has intrigued chemists over the last decades and has led to the development of efficient biomimetic polyene cyclizations. Those methodologies contrast the prevalent approach of sequential ring construction by establishing the polycyclic carbon framework in a single concerted step. Early approaches accomplished cyclization by protonation of olefins or the activation of leaving groups under harsh conditions. The stereochemistry of those cyclizations was independently rationalized by *Stork* and

Eschenmoser on the basis of concerted *anti*-additions via a poly-chair-like transition state.¹⁵ However, it took until 1999 before the first enantioselective polyene cyclization was reported by *Yamamoto et al.*¹⁶ The enantioselectivity was achieved by combining a Lewis acid with a chiral Brønsted acid to yield a highly acidic proton in a chiral environment. Catalytic amounts of this Lewis acid-assisted chiral Brønsted acid (LBA) **25** could be employed to convert polyene **23** via a formal 1,3-rearrangement into tricycle **24** in 76% yield and 77% ee (Scheme 2). However, low temperatures and a long reaction were necessary to achieve a high ee.



Scheme 2: First enantioselective polyene cyclization, utilizing chiral LBA **25**.

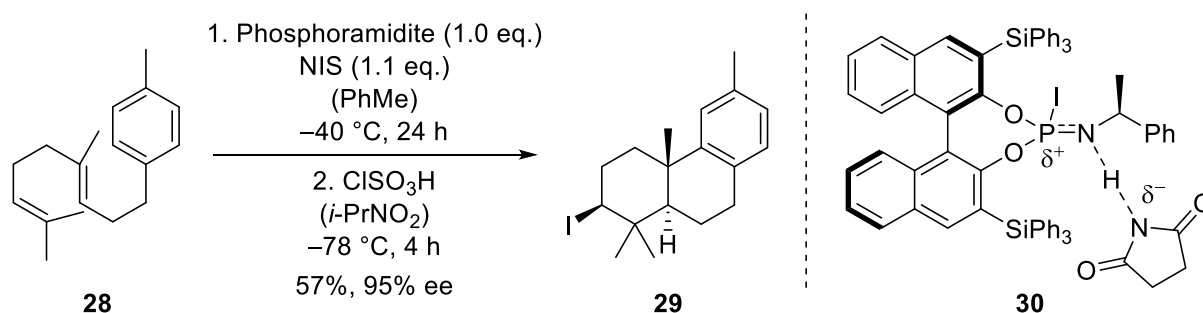
An alternative approach was developed by *Gagné et al.* utilizing a chiral transition metal catalyst.¹⁷ The group exploited the ability of the cationic platinum(II) complex to chemoselectively activate terminal double bonds. In a subsequent ligand screening, a non-BINAP derived bisphosphine ligand was shown to give the highest enantioselectivity. Utilizing the optimized conditions, phenol **26** could be cyclized into product **27** in 73% yield and 75% ee (Scheme 3). Since the final reaction step involves a β -hydride elimination, methyl trityl ether had to be employed as a hydride abstractor to achieve catalytic turnover. The method was later adapted to achieve a tandem cyclization-fluorination cascade, by using XeF_2 as a fluorine source, which effectively competes with the β -hydride elimination step.¹⁸ Analog methodologies utilizing gold and iridium catalysts have also been reported.¹⁹



Scheme 3: Enantioselective transition metal-catalyzed polyene cyclization.

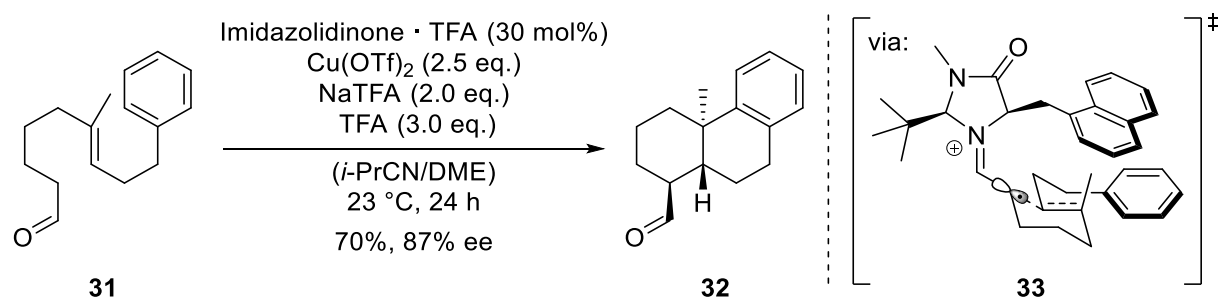
The first enantioselective halonium-triggered polyene cyclization was reported by *Sakakura et al.*²⁰ The chiral information was transferred by employing a chiral phosphoramidite that acts

as a Lewis base to activate *N*-iodosuccinimide (NIS). Stoichiometric amounts of the formed adduct **30** promoted the conversion of substrate **28** into tricycle **29** in 57% yield and 95% ee (Scheme 4). Bicyclic side products that resulted from premature quenching could be converted into the final product under acidic conditions. The use of toluene as a solvent enables species **30** to form a tight ion pair in solution, which proved essential for the enantioselectivity. The methodology turned out to be limited to the use of NIS, since the use of *N*-bromo- or *N*-chlorosuccinimide significantly reduced either enantioselectivity or reactivity, respectively. Bromodiethylsulfonium bromopentachloroantimonate (BDSB), developed by the *Snyder* group, represents a highly selective and mild, but achiral agent for polyene cyclizations. Initial investigations using chiral derivatives of BDSB afforded no asymmetry in cation- π cyclizations so far.²¹



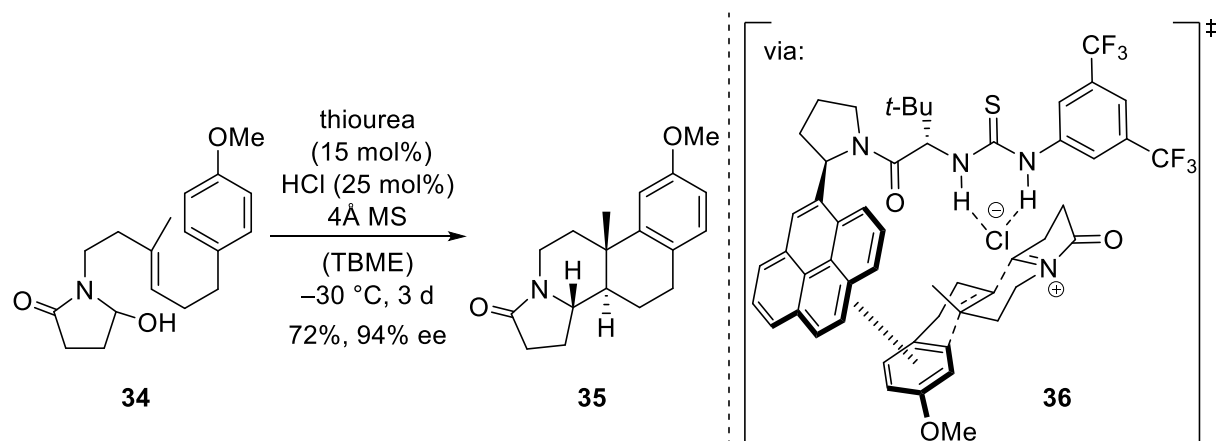
Scheme 4: First enantioselective halonium-induced polyene cyclization.

The first example of a catalytic enantioselective radical-based polyene cyclization was presented by *MacMillan et al.* in 2010.²² The method was developed based on one of their previous studies regarding enamine oxidation in enantioselective organocatalysis.²³ Using a chiral imidazolidinone and a polyene aldehyde, the group was able to achieve high enantioselectivities in radical-triggered cyclizations. Treating aldehyde **31** with the chiral catalyst and Cu(OTf)₂ as the oxidant gave product **32** in 70% yield and 87% ee via the radical transition state **33** (Scheme 5). The methodology could even be extended to the synthesis of pentacyclic compounds. However, this required the installation of nitrile moieties in the substrate to render the propagating radical sufficiently electrophilic.



Scheme 5: Enantioselective radical polycyclization.

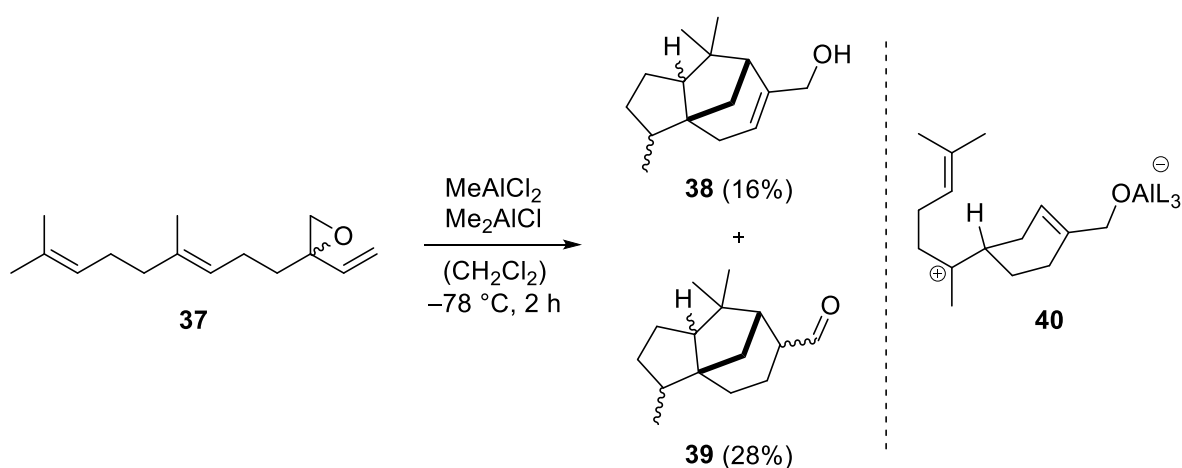
In order to simulate the aromatic environment of a cyclase active site, *Jacobsen et al.* developed a series of thiourea derivatives with attached aromatic residues.²⁴ A screening unambiguously demonstrated that an increase in size of the aromatic residue resulted in a significant increase in reactivity and enantioselectivity. Using a pyrene containing thiourea catalyst, they were able to cyclize hydroxylactam **34** to tetracycle **35** in 72% yield and 94% ee (Scheme 6). The reaction proceeds via transition state **36**, in which the substrate is tightly coordinated to the thiourea unit by anion binding and the pyrene moiety interacts with the developing positive charge through cation- π interactions. This study demonstrated the possibility of utilizing cation- π interactions with a small-molecule catalyst to induce high levels of stereocontrol.



Scheme 6: Thiourea-catalyzed polyene cyclization.

Despite the intensive study of HTT polycyclizations, it was not before 2012 that *Shenvi et al.* reported the first non-stop THT polycyclization in solution.¹³ In contrast to HTT cyclizations, the THT cascade contains multiple cationic branching points, which are prone to undergo elimination (E1) or nucleophilic attack (S_N1) in solution.²⁵ This results from Coulombic interactions that hold the counteranion of the activating agent in close proximity to the intermediate carbocation. In cyclase enzymes, the diphosphate counteranion is sequestered by complexation to a trinuclear metal cluster in an aspartate rich binding motif. The group

simulated this strategy by employing an epoxide as an initiator unit in combination with a mixture of aluminum Lewis acids that feature non-dissociating ligands. This kept the aluminate anion bound to the oxygen (intermediate **40**) and allowed for full propagation of the cationic charge. This approach allowed for the synthesis of a mixture of polycycles **38** and **39** from vinyl epoxide **37** (Scheme 7). Polycycle **39** was further converted in two steps to a mixture of β -cedrenes and β -funebrenes, which marked the first synthesis of a member of the funebrene class. In contrast to the well-defined chair-like transition states in HTT cyclizations with the preference for *trans*-anti-*trans* decalin frameworks, the lack of stereocontrol in this cyclization cascade can be considered a shortcoming of the methodology.



Scheme 7: First example of a THT polycyclization in solution.

3. Supramolecular hosts

3.1 Covalently-linked supramolecular hosts

Molecular recognition marks the first step in enzyme catalysis. The enzyme selectively isolates the substrate from the solvent and provides a functionalized template for the chemical transformation. A biomimetic strategy to simulate this mode of operation relies on substrate encapsulation within a supramolecular host. Encapsulation into the hydrophobic host cavity grants control over the local chemical environment of the guest, which can lead to altered or even unprecedented reactivity, not observed in nature. The guest binding is based on noncovalent interactions and depends on the investigated host as well as the employed solvent.^{4,26} Like any spontaneous process, the binding has to be associated with a negative binding free energy ΔG . Therefore, the binding event can either be entropically- or enthalpically-driven. Although many methods like NMR spectroscopy or mass spectrometry exist to study the thermodynamics of guest binding, isothermal titration calorimetry (ITC) is

still considered the most reliable way to determine ΔH and ΔS values, at least for simple 1:1 complexes.^{26a}

The noncovalent forces that are responsible for guest binding in enzymes also apply to artificial host-guest complexes. Most of the early examples in host-guest chemistry, including crown ethers, cryptands and spherands, are based on ion-dipole interactions.²⁷ The important role of cation- π interactions in the complexation of quaternary ammonium ions by water-soluble cyclophanes was elucidated by *Dougherty et al.*²⁸ Based on the electrostatic model for cation- π interactions, they showed that the electrostatic potential (ESP) surface of the aromatic host provides a qualitative measure for the potential strength of the cation- π interaction.²⁹ Other common interactions with aromatic surfaces include π -stacking, either parallel-displaced, edge-to-face or eclipsed,³⁰ and CH- π interactions. Anion- π interactions represent a less common mode of interaction and only recently have shifted into the focus of investigation and catalysis.³¹ In aqueous media, the binding is mainly dictated by the hydrophobic effect. According to the classical hydrophobic effect, the binding is entropy-driven and results from release of ordered water around a hydrophobic solute upon its aggregation. The non-classical hydrophobic effect describes binding that is enthalpy-driven and that benefits from a gain in dispersive interactions, based on the attraction of fluctuating dipoles, and a gain in solvent cohesive interactions. In an empirical study, *Rebek et al.* showed that optimal binding is observed when the guest occupies about 55% of the host volume. A larger occupancy, however, can be favored by strong intermolecular forces.³² Arguably the most important specific interactions in recognition are hydrogen bonds. Hydrogen bonds (HB) require a non-competitive solvent, are highly directed and generally form along the direction of the unpaired electrons of the acceptor atom. In general, the strength of the hydrogen bond increases with increasing acidity of the HB donor and increasing basicity of the HB acceptor.³³ A single hydrogen atom can participate in two weaker and therefore longer hydrogen bonds, which is called a bifurcated HB.³⁴ Cooperative hydrogen bonding, like in carbohydrate recognition, occurs, when a OH-group participates both as a donor and acceptor. This increases the bond polarization and therefore the strength of the individual HBs.³⁵ Furthermore secondary electrostatic interactions have to be considered in HB arrays, which can be either attractive or repulsive.³⁶ Aromatic rings can also participate as acceptors in so-called weak hydrogen bonds. Halogen bonding represents a related interaction and is based on the interaction of Lewis bases with the positive area (σ -hole) of electrostatic potential opposite to C-X bonds. The strength of the halogen bond (XB) increases with decreasing hybridization state of the carbon atom of the XB donor and with increasing size of

the halogen atom. In general, the XB shows a strong preference for linear arrangements.³⁷ Several other attractive forces like S- π and orthogonal dipolar interactions exist,³⁸ but possess no major significance in host-guest chemistry.

Early efforts to mimic biological catalysts relied on covalently linked host structures. Among them, cyclodextrins were the first to be applied as simple enzyme models. Cyclodextrins are naturally occurring sugars that are soluble in water and possess a hydrophobic pocket for guest binding. This property was exploited by *Breslow et al.*, who could show that α -cyclodextrin (**41**) accelerates the chlorination of anisole and suppresses formation of the *ortho*-regioisomer (Figure 1).³⁹ Other examples include an intermolecular acyl transfer reaction catalyzed within the cyclic porphyrin **42**,⁴⁰ an accelerated auto-acylation by guest binding using spherand **43**,⁴¹ and the catalytic oxidation of aromatic aldehydes to their corresponding methyl esters in a cyclophane structure.⁴²

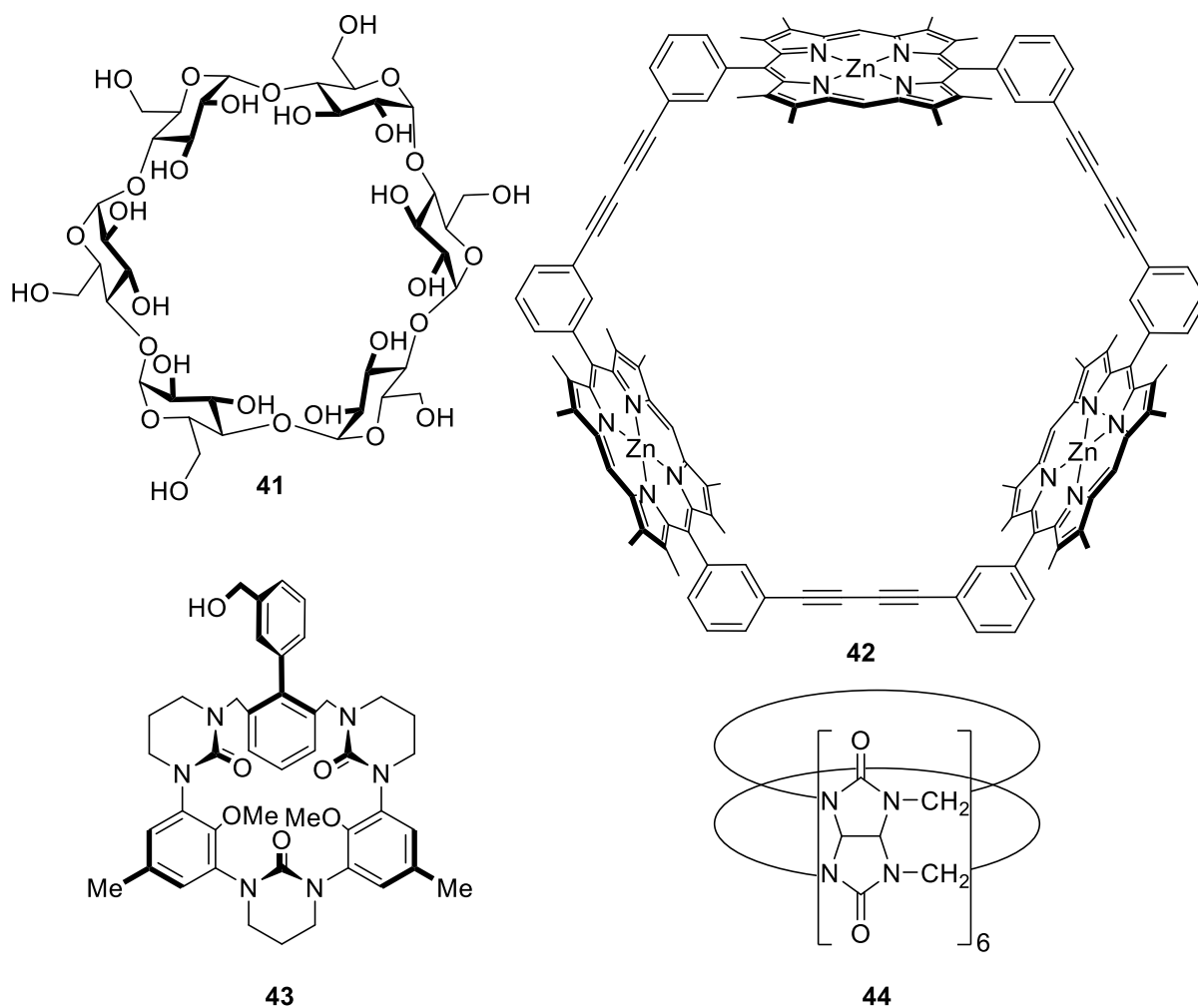
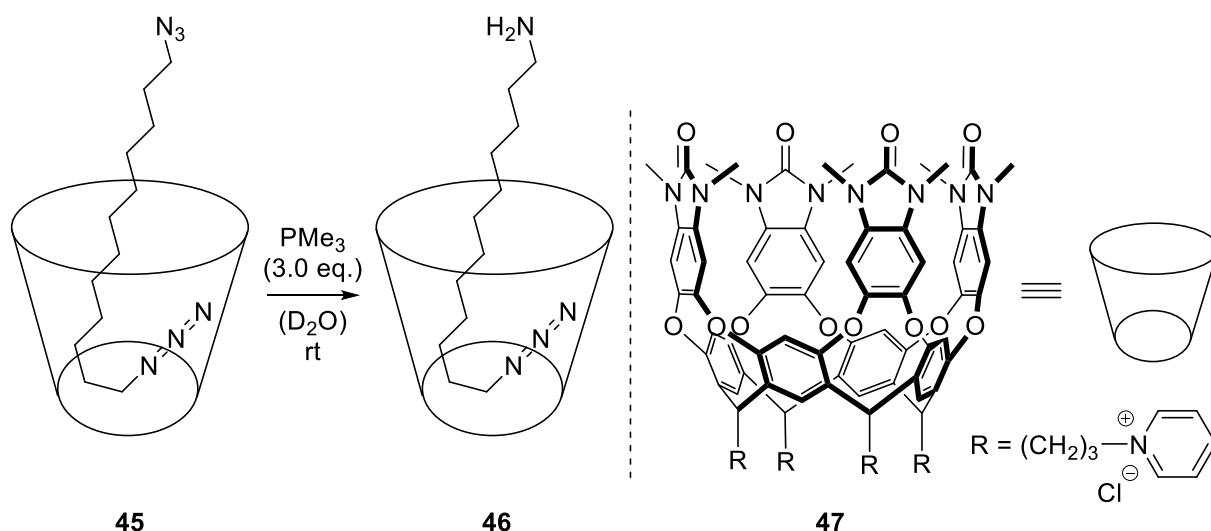


Figure 1: Examples of covalently linked hosts, investigated as enzyme-like catalysts.

Another potent class of covalently-linked host structures comes in the form of cucurbiturils. They belong to a family of macrocyclic oligomers that are easily accessible via the copolymerization of glyoxal, formaldehyde and urea. Due to favorable strain and hydrogen bonding, cucurbit[6]uril (**44**) is the only reaction product under the standard reaction conditions. Cucurbiturils strongly bind cationic guests due to ion-dipole interactions with the oxygen atoms that line each end of the cavity. This property was exploited in the catalytic 1,3-dipolar cycloaddition between an azide and an alkyne, both bearing a pendant ammonium group.⁴³ Due to the cationic charge in the product species, considerable product inhibition was observed. Despite their favorable properties, cucurbiturils as well as cyclodextrins lack an easy access to larger derivatives, needed for more complex and sophisticated reactions.

Deep, water-soluble cavitands like **47**, developed by *Rebek et al.*, represent another family of covalent bond-based enzyme mimics. They can be accessed by bridging the hydroxy moieties of a resorcin[4]arene, creating a hydrophobic cavity that can either exist in the depicted “vase” or a more open, fold-back “kite” conformation. Their solubility can be controlled via variation of the pendant R groups. Recent efforts by the *Rebek* group have been directed towards applying cavitands **47** as a vessel for organic reactions in water. In one example, the group used cavitand **47** as a stoichiometric, supramolecular protecting group in the selective reduction of diazide **45** to monoazide **46** (Scheme 8). After the first reduction, the substrate is fixed in a conformation, in which the amine is exposed to the solution and the azide is buried deep within the hydrophobic pocket, inaccessible for reduction.⁴⁴ The enforced folding of long chain substrates within water-soluble cavitands was furthermore explored in the macrocyclization of diamines⁴⁵ and the monohydrolysis of diesters.⁴⁶ However, all of these reactions utilize stoichiometric amounts of the cavitand.



Scheme 8: Application of water-soluble cavitand **47** in the selective mono-reduction of diazide **45**.

3.2 Self-assembled supramolecular hosts

The main disadvantage of more sophisticated, covalently-linked supramolecular hosts stems from their time-consuming and non-trivial preparation. For example, *Diederich et al.* had to invest 18 steps into the synthesis of a catalytically active cyclophane host structure.⁴² Additionally, the host is often obtained in low yields and contaminated with by-products, which results from the entropic penalty that arises from the construction of a preorganized, entropically disfavored structure. Different strategies have been developed to overcome those problems, like templated cyclization, but most of the required reactions are still performed under high dilution conditions. Furthermore, the covalent structure is often tailored for a certain guest and in many cases *de novo* syntheses have to be performed to accommodate different guests. Other disadvantages are their lack in responsiveness towards external stimuli and their often observed reluctance regarding guest release.

Those deficits resulted in an increased interest in noncovalently self-assembled hosts structures. Self-assembly represents a thermodynamic process by which two or more components form a more organized system as a consequence of local, noncovalent interactions. Although the individual connections are reversible and weak, the accumulation of a multitude of such interactions results in a thermodynamically stable assembly, which can be applied as a host for chemical reactions. The components used for self-assembly are usually decorated with designed functionalities to dictate the formation of a desired architecture. Overall less synthetic effort is required for the construction of the small components than for covalently-linked assemblies. Furthermore, the reversibility of the connectivities results in a more dynamic system with a

higher resemblance to enzymes.⁴⁷ Dynamic covalent chemistry has developed as a strategy to combine the strength of the covalent bond with the reversibility of noncovalent bonds. It applies reversible covalent bond formation under thermodynamic control for the self-assembly process. Bond types of this class include imines,⁴⁸ disulfides,⁴⁹ orthoesters⁵⁰ and boronic esters.⁵¹ However, most self-assembly strategies take advantage of metal-ligand interactions,⁵² hydrogen bonds⁵³ or the hydrophobic effect.⁵⁴ Less utilized design strategies make use of ion pair interactions⁵⁵ and halogen bonding⁵⁶ for capsule formation. In the following, selected examples of self-assembled host structures are presented with application in stoichiometric or catalytic chemistry or potential application in the future.

Metal-ligand assemblies represent the largest and best-studied class of supramolecular reaction vessels. Careful selection of component geometry allows for a controlled and highly modular construction of multimeric assemblies. The field was pioneered by the *Fujita* laboratory, which perfected the methodology to prepare a wide range of assemblies displaying different shapes, metal-ligand stoichiometries and cavity sizes. Very recently, the group succeeded in forming the largest self-assembled capsule to date, composed of 144 small components.⁵⁷ Studies regarding supramolecular catalysis have mainly focused on the octahedral cage **I**, which quantitatively self-assembles from dimethylethylenediamine end-capped Pd^{II} ions and 1,3,5-tris(4-pyridyl)triazine in a 6:4 ratio (Figure 2).⁵⁸ The diamine capping is used to enforce the *cis* geometry around the square planar Pd^{II} ions. The cage is highly water-soluble and reversibly encapsulates organic molecules within the hydrophobic cavity. Furthermore, the cage can be rendered chiral by simply replacing the ethylenediamine with a chiral diamine. Despite carrying the chiral centers on the periphery, modest chiral induction was observed in a [2+2] photocycloaddition, since the walls of the cage slightly rearrange upon diamine substitution.⁵⁹ The group also synthesized the more “open” square-pyramidal host **II** by changing the original ligand to a tris(3-pyridyl)triazine ligand. Due to the bowl-shaped hydrophobic cavity, this structure is also capable of reversibly encapsulating organic molecules in aqueous media. Related cages of M₂L₄ stoichiometry, commonly constructed via pyridine-palladium interactions, represent a relatively new class of cages with potential application in catalysis.⁶⁰ Key contributions to this research field have been provided by the laboratories of *Clever*⁶¹ and *Yoshizawa*.⁶²

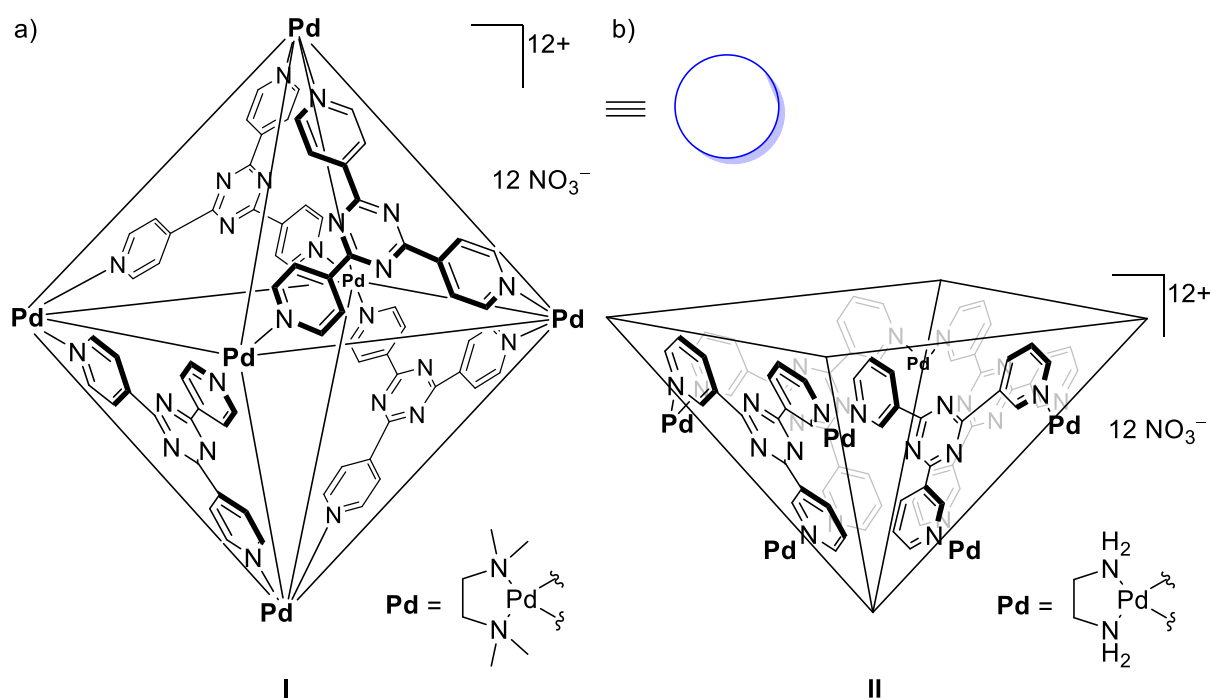


Figure 2: (a) Metal-ligand cages designed by the *Fujita* group; (b) symbolic representation of cage **I** (blue circle).

The most established supramolecular catalyst based on metal-ligand interactions was developed by *Raymond et al.* in 1998.⁶³ The water-soluble tetrahedral cage **IIIa** forms upon mixing of gallium(III) salt and naphthalene-based catecholate ligands in a ratio of 4:6 (Figure 3a). In contrast to host **I** and **II**, the cage has an overall negative charge and therefore has a high affinity for cationic guest molecules. Cationic guests additionally experience strong cation- π interactions within the cavity, but neutral molecules are encapsulated as well. The hydrophobic cavity has a volume of about 450 Å³ and allows guest exchange through a nondissociative mechanism that involves partial deformation of the host.⁶⁴ Based on the octahedral coordination of the gallium ion by three bidentate ligands, the individual complexes have helical chirality (Figure 3c). Interestingly, the mechanical coupling between the four gallium centers results in the exclusive formation of the homochiral $\Delta\Delta\Delta\Delta$ - and $\Lambda\Lambda\Lambda\Lambda$ -assemblies. Although resolution of the enantiomers is possible, the group discovered that enantiopure ligands bias the helical chirality of the metals and lead to the formation of enantio- and diastereopure hosts.⁶⁵ Besides dictating the chirality, the new ligands also resulted in a higher stability against temperature and oxidation. Detailed mechanistic studies furthermore showed that guest ingress is entropy-based due to displacement of solvent molecules from the cavity.⁶⁶

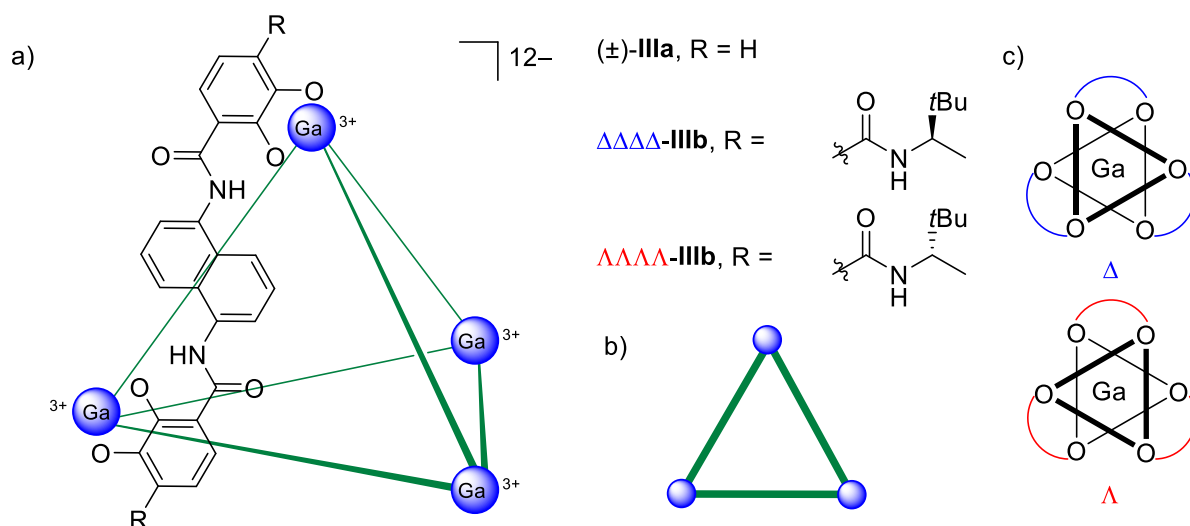


Figure 3: (a) M_4L_6 cages developed by the *Raymond* group; (b) schematic representation of the cage; (c) helical chirality.

Two structurally related tetrahedral M_4L_6 cages were reported by the *Nitschke* group (Figure 4). Cage **IVa** spontaneously assembles from four iron(II) ions and six imine ligands, which are produced *in situ* from six molecules of 4,4'-diaminobiphenyl-2,2'-disulfonic acid and twelve molecules of 2-formylpyridine. The cavity of the anionic $[Fe_4L_6]^{4-}$ cage **IVa** has a volume of 141 \AA^3 and through extensive deformation is capable of tightly binding a variety of hydrophobic guests like cyclohexane in a 1:1 complex.⁶⁷ The small cavity size, however, limits the range of suitable guests to molecules with six or less carbon atoms.⁶⁸ The rate of encapsulation is strongly influenced by the guest size with small and more planar molecules showing an increased uptake rate. Furthermore, no affinity was observed for similarly sized alcohols or organic cations. This substantial selectivity for neutral, hydrophobic molecules was attributed to the hydrophobic effect. The lack of affinity for cationic molecules, which stands in contrast to anionic cage **III**, is believed to result from a lesser overall charge and the guest's greater shielding from the externally oriented sulfonate groups, which mainly induce the high water solubility of the host. An interesting aspect of the cage's behavior is that it can be reversibly opened via alteration of the pH of the aqueous solution. Below a pH of 3.5 the imine functionality of the ligand is hydrolyzed causing encapsulated guests to be released into solution.⁶⁷ Using a longer diamino terphenylene subcomponent with chiral glyceryl residues, the *Nitschke* group was able to form a larger water-soluble $[Fe_4L_6]^{8+}$ analog of their original cage bearing a chirotopic internal void.⁶⁹ By choosing the stereochemistry of the glyceryl groups, the corresponding $\Delta\Delta\Delta\Delta$ - and $\Lambda\Lambda\Lambda\Lambda$ -host structures **IVb** can be obtained in an enantiopure fashion. The outwardly directed glyceryl groups close the faces of the cage, thereby creating a hydrophobic cavity with a calculated volume of 418 \AA^3 . This allows for the encapsulation of a wider range of primarily hydrophobic guests.

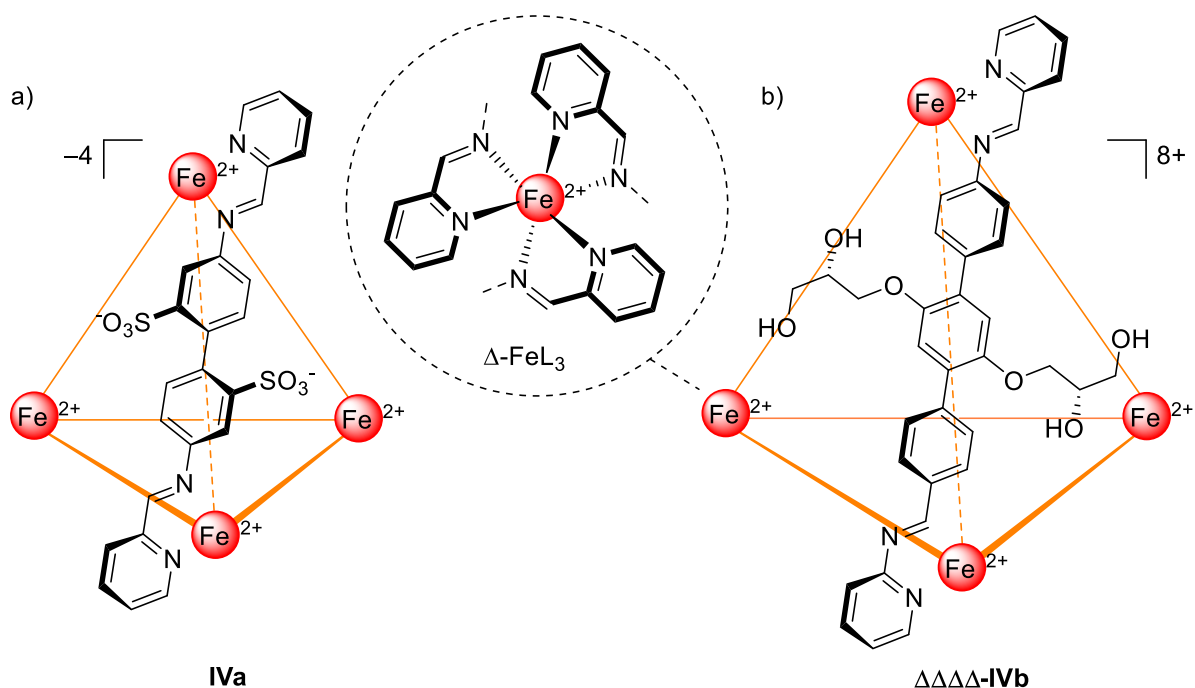


Figure 4: (a) Schematic representation of the $[\text{Fe}_4\text{L}_6]^{4-}$ cage **IVa**; (b) enantiopure $[\text{Fe}_4\text{L}_6]^{8+}$ analog **IVb**.

A host that has only recently been applied to catalysis is the $[\text{Co}_8\text{L}_{12}]^{16+}$ cubic coordination cage **V**, developed by the *Ward* group (Figure 5).⁷⁰ The cage contains a high-spin Co(II) ion at each vertex and twelve bidentate pyrazolyl-pyridine ligands are spanning each edge of the cube. The 24 external hydroxy groups installed at the ligands make the cage water-soluble. Due to the strongly hydrophobic cavity of about 400 \AA^3 , the cage binds hydrophobic molecules with binding constants of up to $1 \times 10^8 \text{ M}^{-1}$.⁷¹ Guest ingress and egress occurs through small apertures in the center of each face. The cage selectively encapsulates neutral molecules in the presence of anionic and cationic guests, which show little affinity for the cavity due to their hydrophilic nature. Combined with the high stability of the cage over a wide pH range, this can be utilized for pH-dependent binding of ionizable guests.⁷² Additionally, the paramagnetic nature of the Co(II) ions acts as a shift reagent, which improves NMR-based analysis of guest encapsulation.

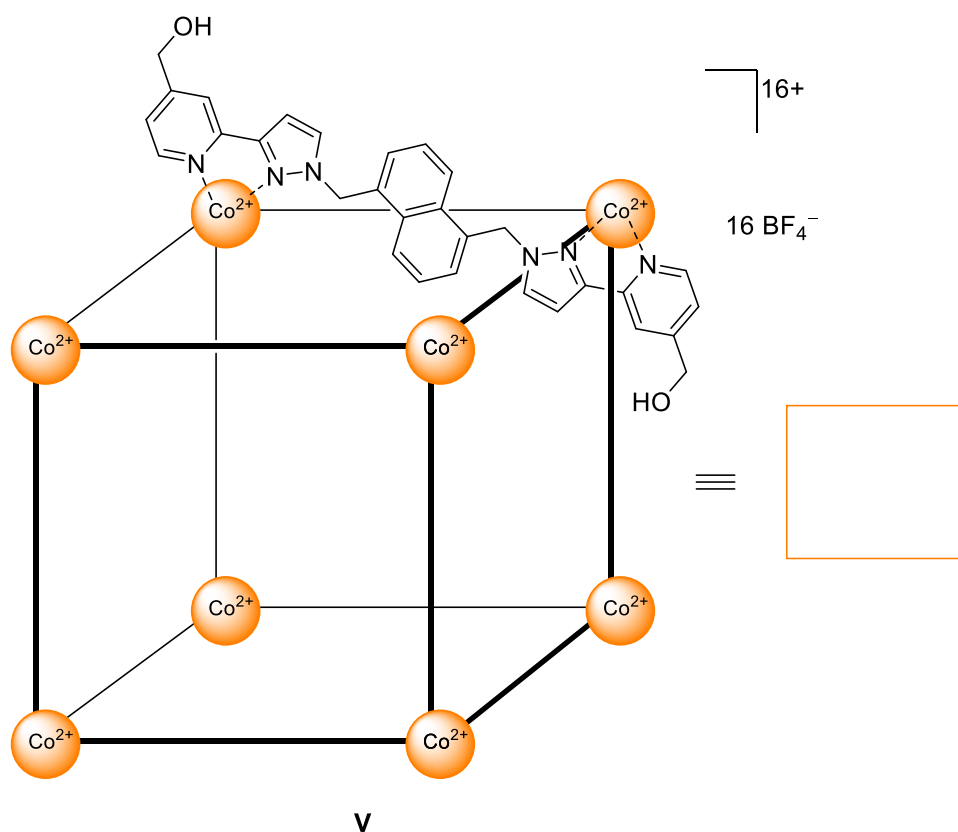
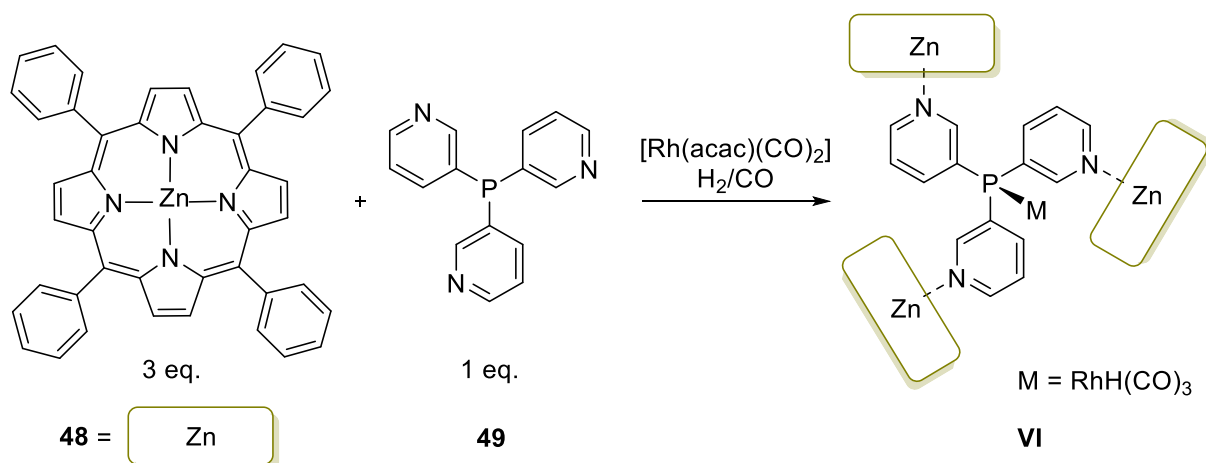


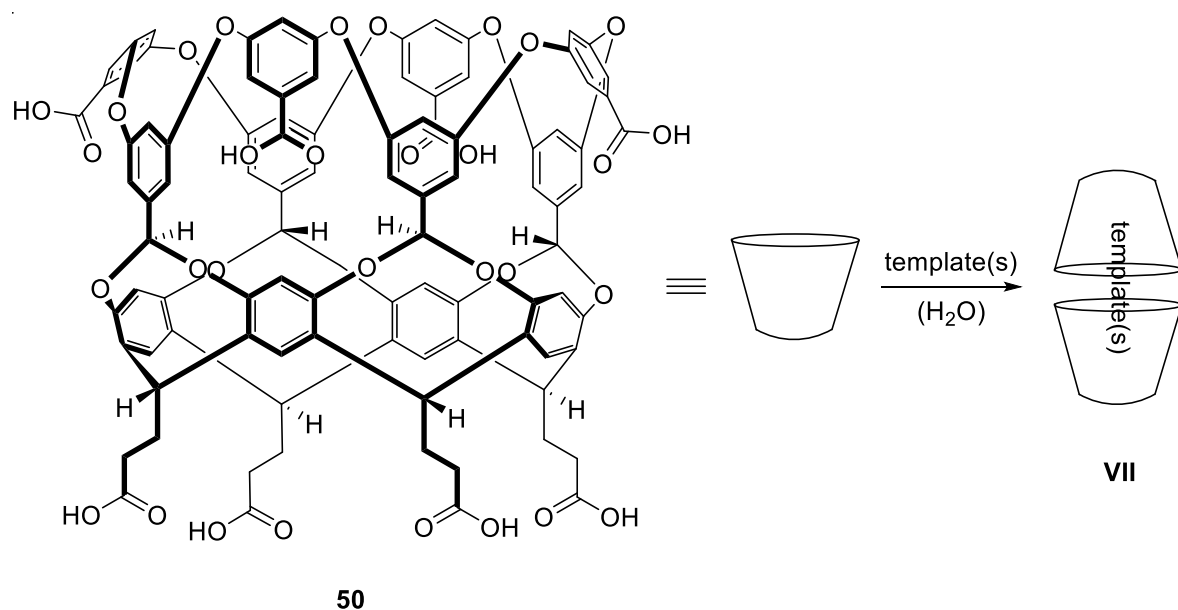
Figure 5: Schematic and symbolic representation of the cubic $[\text{Co}_8\text{L}_{12}]^{16+}$ cage **V**, developed by the *Ward* group.

By applying the ligand-template strategy,⁷³ the *Reek* laboratory has blurred the line between conventional transition metal catalysis and supramolecular catalysis. The strategy relies on a ligand that features additional multiple binding sites for metal complexes like porphyrins, and thereby creates a second coordination sphere around the catalytically active metal-ligand complex. Host **VI**, which is based on this design, is depicted in Scheme 9 and forms via self-assembly from three zinc(II) tetraphenylporphyrins (**48**) and one *meta*-tris-pyridylphosphine ligand (**49**). To create a supramolecular hydroformylation catalyst, the phosphine ligand, embedded within the cavity created by the porphyrins, binds to a catalytically active $[\text{RhH}(\text{CO})_3]$ complex.⁷⁴ Steric reasons prevent the formation of a bis-phosphine complex. The approach is highly modular and variation of the porphyrin unit gives access to a wide range of host structures. Additionally, the *Reek* group recently established a large cage with endohedral binding sites that preorganize a catalytically active complex and a substrate in close proximity.⁷⁵



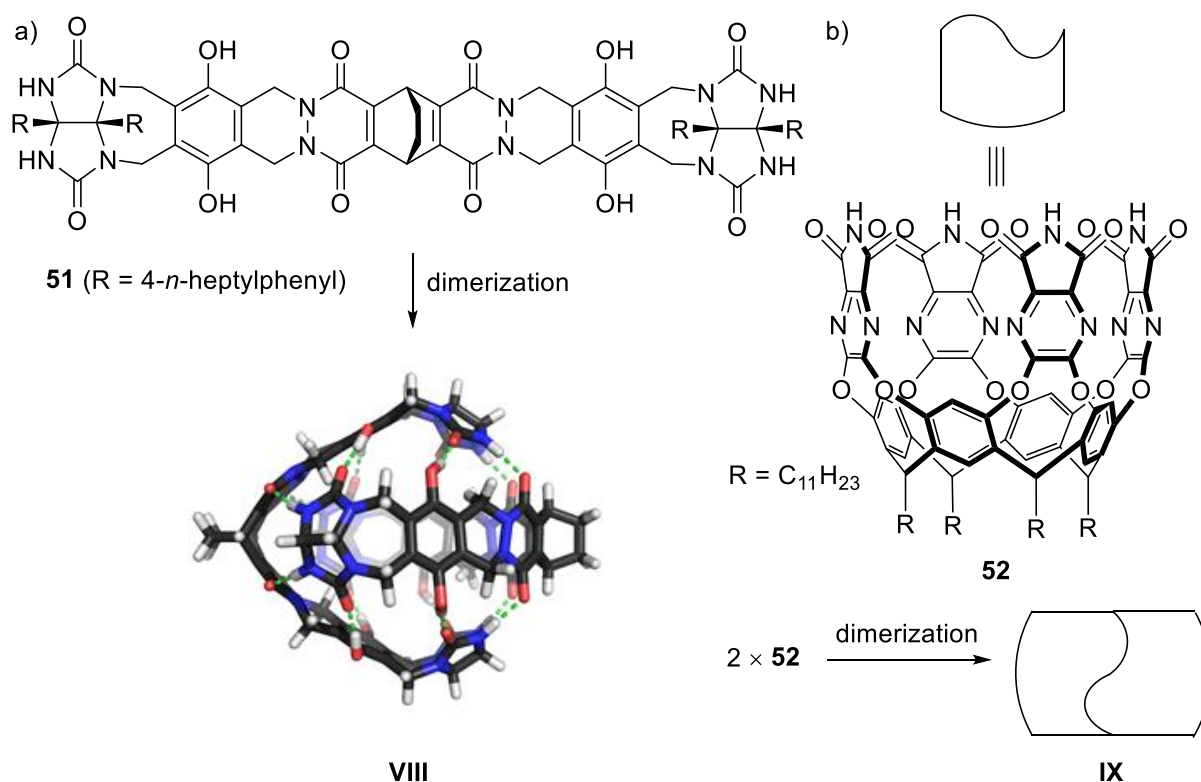
Scheme 9: Supramolecular hydroformylation catalyst **VI**, based on the ligand-template approach.

Self-assembly via the hydrophobic effect represents a less developed field in supramolecular chemistry and is mainly based on octa-acid **50** and derivatives thereof (Scheme 10).⁵⁴ Octa-acid **50** belongs to the class of deep cavitands and is easily accessible in gram scale from the corresponding resorcin[4]arene scaffold. The good water-solubility arises from the eight carboxylic acids that line the outer surface of the cavitand. At a pH of around 10 and a concentration of 1 mM, octa-acid **50** exists essentially as a monomer, as confirmed by DOSY spectroscopy.⁷⁶ However, as soon as a suitable guest like butane is added, the cavitand dimerizes via the hydrophobic effect to give host structure **VII**. Dimer **VII** has almost exclusively been applied in photochemical reactions. The reactions show an interesting change in product selectivity, compared to bulk solution, but no catalytic application has yet been reported.⁷⁷



Scheme 10: Formation of host **VII** via dimerization of octa-acid **50** in the presence of a suitable template.

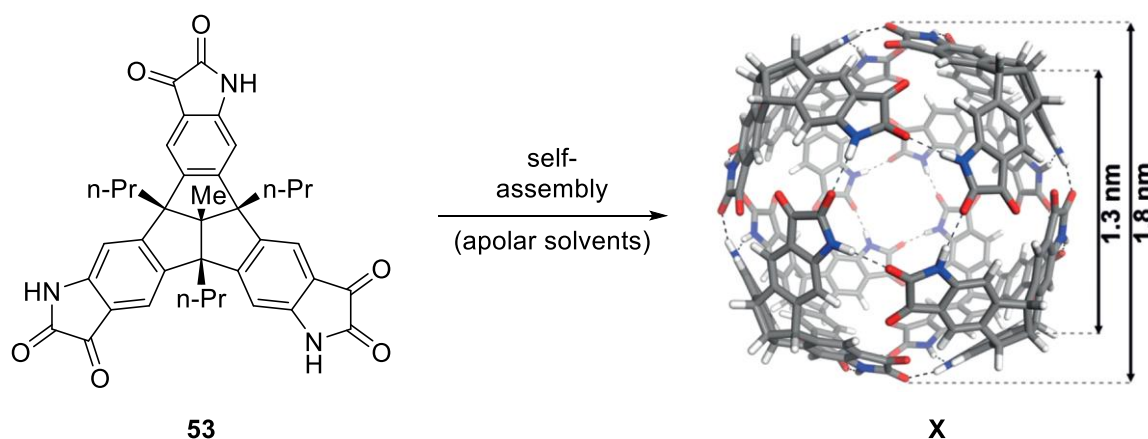
Three-dimensional assemblies based on hydrogen bonding differ from metal-ligand assemblies in several aspects. First, the self-assembly requires a solvent, which does not compete for hydrogen bonds, which excludes hydrogen bond acceptors and donors like water. Second, the lack of an intrinsic geometry preference requires the building blocks to incorporate some degree of curvature. Third, due to the weaker mode of interaction, guest exchange usually proceeds via partial or complete disruption of the hydrogen bond network and the systems show an overall increased degree of dynamic flexibility. The application of hydrogen bonds for self-assembly was initiated by *Rebek et al.* using two glycoluril units connected by a tether. In apolar solvents, two copies of the naturally curved unit **51** self-assemble via the formation of up to 16 intermolecular hydrogen bonds to give a “softball”-like structure (Scheme 11). Host **VIII** features a cavity of about 320 \AA^3 and is capable of reversible guest encapsulation. Hydrophobic guests like adamantane are bound well within the cavity via van der Waals interactions, while guests capable of hydrogen bonding form intermolecular hydrogen bonds to the interior surface of the cavity.⁷⁸ Furthermore, guest binding is entropically driven, at least in the cases where one large guest displaces two encapsulated solvent molecules.⁷⁹ Another hydrogen bond-based host that has been applied as a reaction vessel is the cylindrical dimer **IX** (Scheme 11). It forms from two copies of cavitand **52** and is stabilized by a seam of eight bifurcated hydrogen bonds.⁸⁰ The cavity of about 400 \AA^3 is large enough to encapsulate between one and three guests, depending on their size. The guest ingress and egress occurs via opening of a single flap and ITC as well as NMR show that the binding is entropically driven.⁸¹



Scheme 11: (a) Self-complementary hydrogen bonding motif of “softball” **VIII** (color code for models used throughout the text: C = black/grey; O = red; N = blue; H = white); (b) dimerization of cavitand **52** to capsule **IX**. The scheme is partly reproduced from reference⁸² with permission of “John Wiley and Sons”.

A very recent contribution to the class of hydrogen bond-based assemblies was made by the *Mastalerz* laboratory. The group developed a novel, octameric cube-shaped assembly based on enantiopure tris(isatin) **53** (Scheme 12).⁸³ The use of an enantiopure monomer proved highly beneficial for the self-assembly process, since racemic monomer mostly gave ill-defined aggregates upon dissolution. This chirality-assisted synthesis approach, developed by *Schneebeli et al.*, shows great potential in overcoming synthetic limitations in generating sophisticated assemblies.⁸⁴ The very large cavity of about 2300 Å³ allows the reversible encapsulation of multiple guest molecules. Cationic guests like tetraalkylammonium ions show a high affinity towards the cavity due to cation- π interactions, but also neutral molecules like pyrene can be encapsulated by the host. Like it is often the case for hydrogen bond-based assemblies, the guest exchange is slow on the NMR timescale, which results in separate signals for free and bound species that can be integrated to determine the association constants. Assembly **X** is held together by 24 NH–O and 48 CH–O hydrogen bonds, which leads to a very high thermal stability of the assembly. The self-assembly in solution was confirmed by DOSY and ¹H NMR spectroscopy. Additionally, MALDI-TOF mass spectra showed ions corresponding to the octamer and complexes with ammonium guests. The counteranion of the ammonium salts appears to be not co-encapsulated, as indicated by reduced diffusion

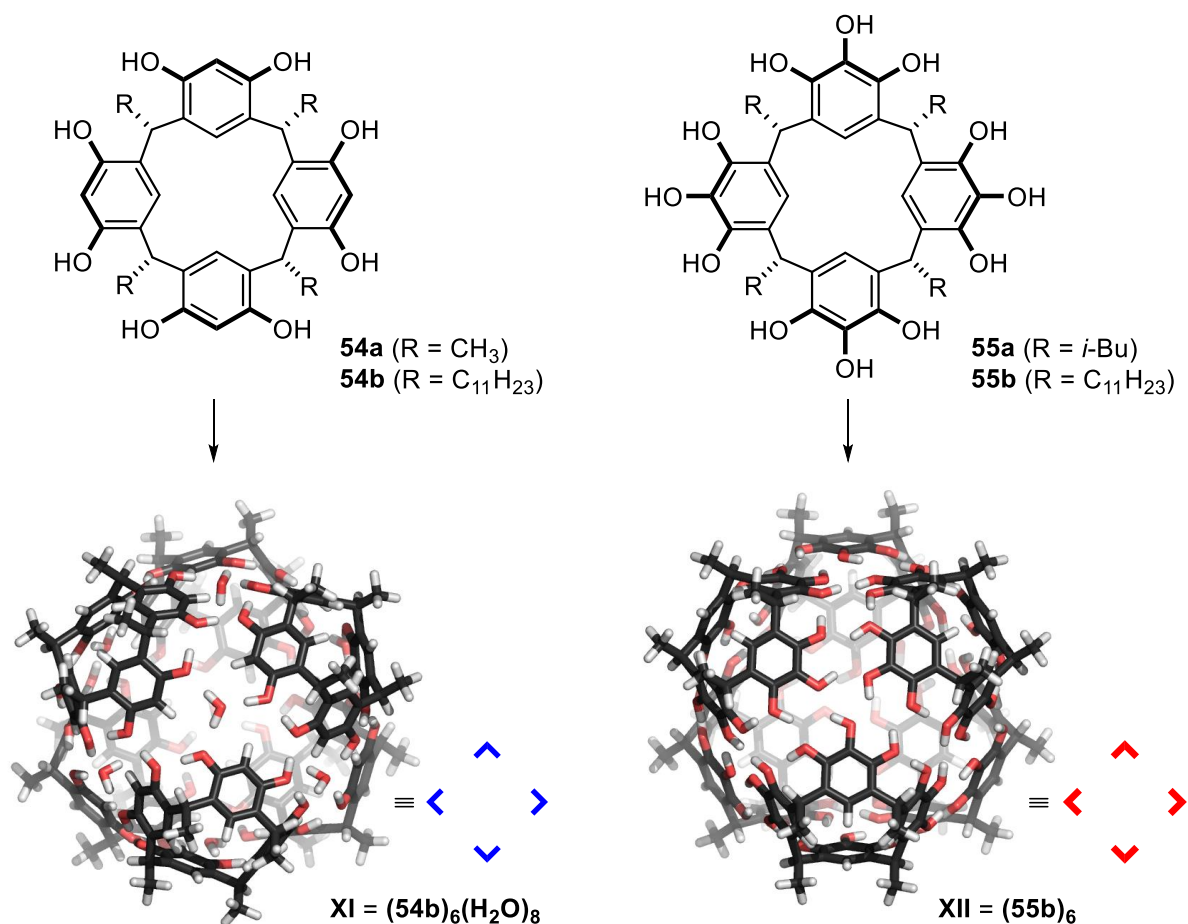
coefficients of the complexes. Exohedral bound, solvated anion clusters are believed to slow down the diffusion of the octamer. Furthermore, ion-pairs within the cavity should be in principle detectable via MALDI-TOF mass spectrometry. Application of host **X** as a supramolecular catalyst is currently under investigation.



Scheme 12: Self-assembly of enantiopure building block **53**, yielding octameric hydrogen-bonded capsule **X**. The scheme is partly reproduced from reference⁸³ with permission of “John Wiley and Sons”.

3.2.1 Hexameric capsules of resorcin[4]arene and pyrogallol[4]arene

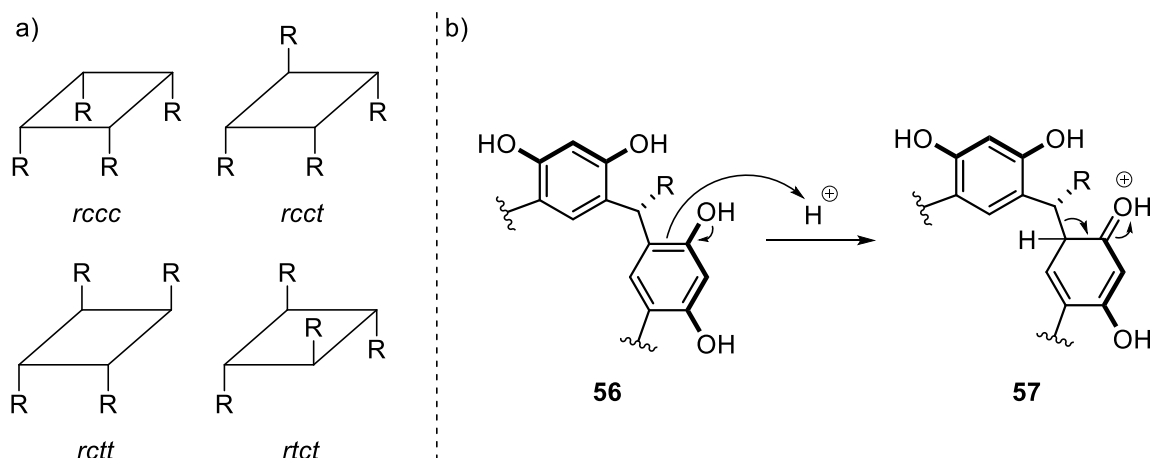
The hexameric capsules of resorcin[4]arene and pyrogallol[4]arene **XI** and **XII** represent the most investigated class of hydrogen bond-based assemblies. Research in this field was triggered in 1997 by the seminal publication by *Atwood* and *MacGillivray* that reported on the hexameric crystal structure of *C*-methyl resorcin[4]arene (**54a**) (Scheme 13).⁸⁵ This discovery was soon followed by a report from *Mattay et al.* on the hexameric assembly of *C*-*iso*-butyl pyrogallol[4]arene (**55a**) in the solid state.⁸⁶ The hexameric structure of resorcin[4]arene **54a** is held together by 60 hydrogen bonds and contains one water molecule at each corner of the cube-like structure. The cavity formed by the assembly has a volume of about 1400 Å³. In contrast, the pyrogallol[4]arene hexamer is assembled via 72 hydrogen bonds and due to the additional hydroxy groups lacks incorporated water molecules. The reported volumes of the cavity range between 1200 and 1520 Å³.⁸⁷ Subsequent investigations by the *Rebek* and *Cohen* groups showed that lipophilic derivatives of resorcin[4]arene and pyrogallol[4]arene like **54b** and **55b** form hexameric assemblies, identical to their crystal structure, upon dissolution in apolar solvents. This led to an intensive investigation of their supramolecular solution phase properties that is still ongoing.



Scheme 13: Hexameric assemblies of resorcin[4]arene and pyrogallol[4]arene (alkyl groups have been omitted for clarity throughout the text in the case of SPARTAN models) and their symbolic representation (adapted from reference⁸⁸).

The attractiveness of the resorcin[4]arene system is partly based on its easy accessibility. The macrocycle can be synthesized in multi-gram scale in a single step from resorcinol and the corresponding aldehyde under acidic conditions. Under standard reaction conditions, the synthesis yields the all-*cis* (*rccc*) stereoisomer, which represents the thermodynamic reaction product (likely due to optimal lipophilic interactions of the aliphatic chains).⁸⁹ The stereoisomer-nomenclature refers to the orientation of the alkyl chain with regard to the reference chain. All four possible isomers are schematically depicted in Scheme 14.⁹⁰ The reversibility of the macrocyclization can be explained by protonation of intermediate **56**, which yields the stabilized oxonium ion **57**. Subsequent C–C bond cleavage gives monofunctionalized resorcinol and a benzylic cation, which can undergo another Friedel-Crafts alkylation. Although trimers and other oligomers are formed during the reaction, the cyclotetramer is obtained selectively due to its fast cyclization because of intramolecular hydrogen bonding in the slightly folded conformation.⁹¹ A wide variety of aldehydes can be utilized for the cyclization reaction, but starting from resorcinol derivatives with substituents at the 2-position (*ortho* to both hydroxy groups) usually gives inseparable mixtures of acyclic and cyclic oligomers as well as

mixtures of stereoisomers.⁸⁹ Long chain aldehydes are utilized to ensure solubility in apolar solvents, which are required for hydrogen bond-based hexamer formation.



Scheme 14: (a) Four possible stereoisomers of resorcin[4]arene (r = reference; c = *cis*; t = *trans*); (b) mechanism explaining the reversibility of the resorcin[4]arene formation.

Additionally, the macrocyclic ring can adopt five symmetrical conformations: crown (or bowl/cone), saddle, diamond, boat and chair (Figure 6). The crown conformation is preferred, since it allows the maximum amount of intramolecular hydrogen bonds. Functionalization of the hydroxy groups as well as of the 2-position, however, allows observation of different conformations like the boat isomer. The crown isomer is preferred in host-guest chemistry due to its defined binding pocket. The crown conformation can be artificially fixed by linking the hydroxy groups together, for example with methylene bridges. This represents the starting point of cavitand and carcerand chemistry and further allows for an easier post-cyclization functionalization of the 2-position.⁹²

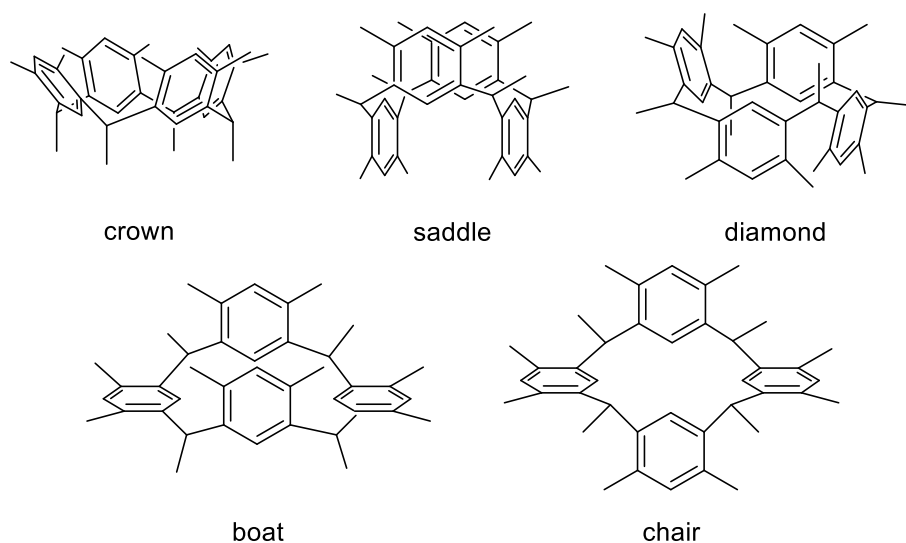


Figure 6: Conformations of resorcin[4]arene (residues have been omitted for clarity).

Pyrogallol[4]arene synthesis, on the other hand, starts from 1,2,3-trihydroxybenzene (pyrogallol) and likewise forms the *rccc* cyclotetramer as the primary product. The crown conformation is again favored by intramolecular hydrogen bonds.

Initial solution phase studies focused on the guest encapsulation behavior of hexamers **XI** and **XII** in CDCl_3 . For both hexamers, guest encapsulation and release is believed to occur via a pentameric intermediate, which requires several hydrogen bonds to break.⁹³ This process is slow on the NMR timescale, which results in different signals for free and encapsulated guests. The observed upfield shift for encapsulated guests arises from anisotropy effects caused by the aromatic cavity. In general, the guest affinity is affected by steric and electronic parameters. In case of identical functionality, larger guests usually show slower encapsulation than smaller guests. On the other hand, larger guests often experience a stronger interaction with the cavity, which reduces the observed rate of release.⁹⁴ Additionally, the limited space of the cavity can induce folding of larger guest molecules.^{87,95} However, this effect is generally less pronounced for hexamers **XI** and **XII** due to their large internal volume. If the guest is too large, uptake into the cavity is no longer possible. The resorcin[4]arene hexamer **XI** encapsulates both neutral, tertiary amines and charged quaternary ammonium ions. The stabilization of cationic charges within hexamer **XI** results from cation- π interactions with the aromatic cavity. In contrast, pyrogallol[4]arene hexamer **XII** shows no encapsulation of ammonium ions like tetrahexylammonium bromide in CDCl_3 . Neutral amines are encapsulated by **XII**, but *in situ* protonation of the amine via addition of DCl leads to rejection of the formed cation.⁹⁶ This contrasting encapsulation behavior remained puzzling for over a decade, but now seems to be solved by a recent publication on this subject (see chapter 6.4).⁸⁸ Additionally, a recent study has shown that tetraalkylammonium ions can in fact be encapsulated by host **XII** by changing the solvent to benzene.⁹⁷ This emphasizes the necessity in host-guest chemistry to consider the affinity of the solvent for the cavity, since solvent molecules are usually co-encapsulated to achieve an optimum packing coefficient. As suggested by *Cohen. et al.*, the smaller number of guests that were found to be encapsulated by host **XII** might arise from the higher affinity of solvent molecules for the cavity of the pyrogallol[4]arene hexamer. The very structured ^1H NMR spectra obtained for encapsulated solvents within **XII** seem to support this theory.⁹⁸ This was further corroborated by analysis of hexamer **XII** powders with magic angle spinning solid-state NMR.⁹⁹ To exclude competition of solvent molecules, the *Purse* group developed an efficient method for kinetic trapping of neutral guest molecules within **XII** by melting host **XII** in the presence of the guest. Using this method, the group could successfully encapsulate a

number of hydrocarbon guests, which are slowly replaced by solvent molecules upon dissolution.¹⁰⁰ The encapsulation behavior of hexamer **XII** was furthermore studied by employing pyrene butyric acid (PBA) as a fluorescent guest molecule. It was shown that two molecules of PBA within the cavity prefer to interact with the cavity rather than with each other. Encapsulation of PBA additionally increased its emission intensity in solution, since the shielded environment reduces radiationless excited-state decay pathways through collision with solvent molecules.¹⁰¹ The thermodynamic aspects of the guest encapsulation process were studied by the *Rebek et al.*. They could show that encapsulation of ammonium salts by the resorcin[4]arene hexamer **XI** is entropically favored by the replacement of solvent molecules. However, the entropy gain decreases with the size of the ammonium salt, probably due to bending and reduced mobility of the cation within the cavity.⁹⁵ The encapsulation was furthermore shown to be endothermic. Unfortunately, all attempts to study the system via ITC have failed so far. The study also revealed that an excess of salt leads to decomposition of the hexamer. This can be explained by competition of the counteranion for the hydrogen bonds of the assembly. Besides amines and ammonium ions, hexamer **XI** has been shown to encapsulate a wide range of molecules including alcohols,¹⁰² carboxylic acids,¹⁰³ metal complexes¹⁰⁴ and radical species.¹⁰⁵ Pyrogallol[4]arene hexamer **XII** on the other hand is additionally capable of encapsulating hydrocarbons,⁸⁷ certain alcohols⁸⁸ and under controlled conditions hydrogen gas.¹⁰⁶

DOSY NMR spectroscopy proved essential in the understanding of both hexamers in solution phase. This tool allows the determination of diffusion coefficients in a multicomponent system. The diffusion coefficient depends on the molecular weight, the effective size and the shape of the component.¹⁰⁷ Using DOSY spectroscopy, *Cohen et al.* could prove that the hexameric capsules are indeed the resting state of lipophilic pyrogallol[4]arene and resorcin[4]arene in chloroform. They could also show that no additional guest molecule is needed as a template for hexamer formation and that the cavity is filled with six chloroform molecules in the absence of a guest. Encapsulation of ammonium salts was also verified via DOSY experiments that showed the same diffusion coefficient for signals of encapsulated guest and hexamer.¹⁰⁸ DOSY spectroscopy was also used to probe the stability of both hexamers via titration with competing solvents like DMSO and methanol. Those experiments showed that more DMSO is needed in the case of the pyrogallol[4]arene hexamer **XII** to achieve complete disassembly. The higher stability of hexamer **XII** results from its additional hydrogen bonds and its reduced number of components. Furthermore, the integration of eight water molecules into the assembly of the

resorcin[4]arene hexamer **XI** was revealed to hold true for the solution phase, which explains the common use of water-saturated chloroform (w-CDCl₃) in resorcin[4]arene chemistry. Those water molecules are in fast exchange with surrounding bulk water, which explains the observation of a single water signal in the ¹H NMR. Interestingly, *Cohen et al.* could also demonstrate that certain alcohol molecules are able to replace integrated water molecules,¹⁰² confirming an observation that was already made in the solid state.¹⁰⁹ This is based on the fact that four of the integrated water molecules only act as a single hydrogen bond donor. DOSY experiments also suggest that the counteranion of the ammonium salt influences the nature of the assembly and that certain ammonium salts can lead to the formation of hexamers without integrated water molecules, owing to the templating effect of the salt.¹¹⁰ Indications that ammonium salts also strongly interact with the external surface of the hexamer were likewise provided by DOSY experiments.¹¹¹ In parallel, the absence of water molecules in the structure of pyrogallol[4]arene hexamer **XII** in solution was proven. This enabled *Rebek et al.* to study the self-assembly of hexamer **XII** in dry aliphatic hydrocarbons like *n*-octane.⁸⁷ DOSY spectroscopy proved again essential when studying the self-sorting properties of the two hexamers. It could be shown that resorcin[4]arenes and pyrogallol[4]arenes show narcissistic self-sorting behavior and only form homo-hexamers when mixed together. However, combining two resorcin[4]arenes or two pyrogallol[4]arenes that differ in their alkyl chains gave a single diffusion coefficient after slow equilibration, indicative of hetero-hexamer formation. Those observations could be confirmed by utilizing monomer building blocks labeled with donor and acceptor fluorophores in fluorescence resonance energy transfer (FRET) studies.¹¹² However, resorcin[4]arene **54b** can in fact form hetero-dimers with cavitand **52** in the presence of a templating guest, as reported by *Rebek et al.*¹¹³

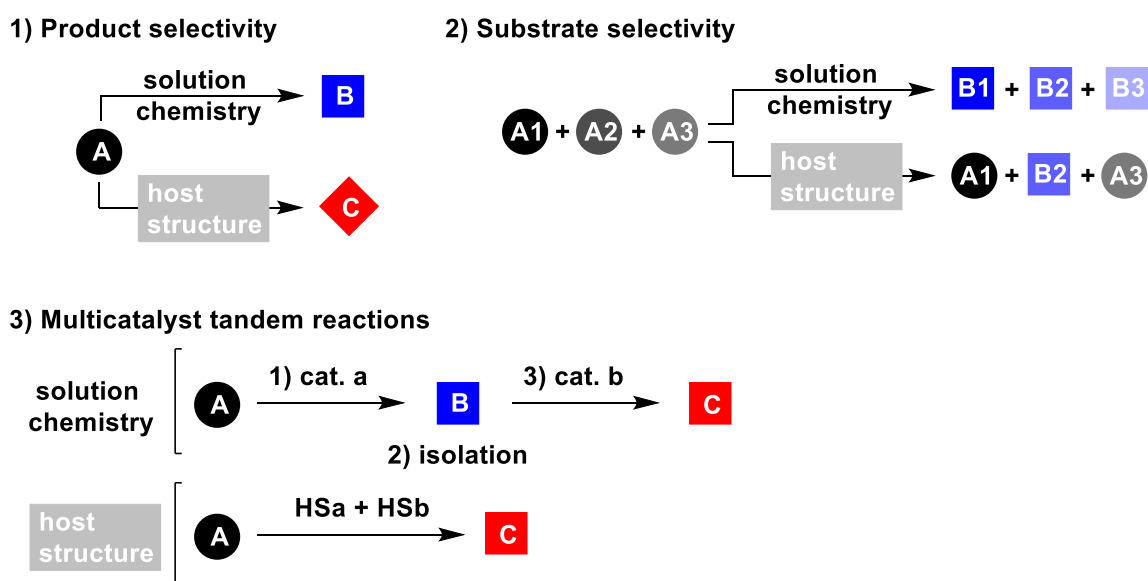
The tendency of resorcin[4]arene hexamer **XI** to encapsulate ammonium ions and alcohol species is based on cation- π and hydrogen bonding interactions, respectively. However, the good encapsulation of neutral, tertiary amines indicated another form of interaction, especially since the corresponding hydrocarbon analogs showed no encapsulation. Intrigued by this contradiction, *Zhang and Tiefenbacher* could show that tertiary amines are in fact protonated by hexamer **XI** and encapsulated as a charged species that experiences cation- π interactions inside the cavity.¹¹⁴ Using detailed NMR studies, they could ascribe the assembly a p*K*_a of about 5.5-6.0. The unexpectedly high Brønsted acidity of the phenol moieties was explained by the formation of a thermodynamically more stable complex due to attractive cation- π and Coulomb interactions with the negatively charged assembly. Additionally, the stabilization of the anionic

charge by delocalization via proton migration contributes to the lowering of the pK_a . The intactness of the hexameric assembly after deprotonation was confirmed by DOSY spectroscopy. Amines that are sterically too demanding for encapsulation were shown to be protonated on the outside of the cavity. Interestingly, an increase of the acidity of hexamer **XI** was observed upon encapsulation of an ammonium ion. This could in principle result from the gain in Coulomb interactions between the negatively charged host and the cationic ammonium guest.

4. Catalytic and stoichiometric chemistry in self-assembled supramolecular hosts

4.1 Advantages of chemistry within supramolecular hosts⁸²

Limiting the place of a reaction to a certain compartment that is shielded from its surroundings and controlling the local chemical environment of the reactive species by encapsulation within a host can provide distinctive advantages over classical chemistry in bulk solution. Especially hosts that allow catalysis within their hydrophobic cavities are increasingly investigated as artificial enzyme mimics. Catalytic activity of supramolecular hosts can arise from the intrinsic properties of the cavity or by encapsulation of a catalytically active guest, for example a transition metal catalyst. The three main advantages of host-controlled chemistry can be divided into the following three aspects (Scheme 15):



Scheme 15: Three main advantages of performing chemistry within active host structures (HS).

- 1) **Product selectivity:** Reactions within a host structure can lead to different products than in bulk solution. This can arise from interactions between the substrate and the host, which favor an alternative reaction pathway. Additionally, a different product can result from protection of an intermediate from nucleophilic attack by solvent molecules or counteranions via encapsulation. Differences in both stereochemistry and regiochemistry can be achieved by performing a reaction within a host. Furthermore, products that differ in their chemical formula from the counterparts in a solution experiment might be formed. The possibility of opening up new reaction pathways not accessible in solution is one of the most intriguing aspects of supramolecular chemistry. However, those changes in product selectivity are usually difficult to predict. A real control over the alternative pathways is currently still lacking and requires a better understanding of host-guest interactions. Additionally, hosts that are either tailored towards a certain transformation or highly modifiable need to be developed.

- 2) **Substrate selectivity:** Due to the limited size of the cavity and of the portals that allow guest exchange, only substrates of suitable size and shape can be converted. This allows the selective conversion of one substrate in the presence of other substrates that show similar reactivity but do not fit the cavity. This key feature of supramolecular chemistry cannot be reproduced using conventional chemistry in solution. Substrate-selective conversion furthermore can be used as a control experiment to exclude that the observed reaction proceeds on the outer surface of the host or in bulk solution. Additionally, a future industrial application of this property might include the use of impure starting materials, for example mixtures of differently sized olefins. This could reduce costs associated with substrate purification.

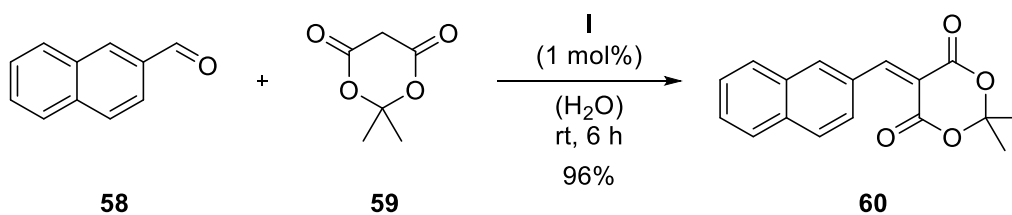
- 3) **Multicatalyst tandem reactions:** Multicatalyst tandem reactions avoid cost-intensive and time-consuming workup steps after each reaction. Although such reactions can also be achieved in solution,¹¹⁵ usually thorough optimization of the reaction conditions is required. This could be circumvented by supramolecular hosts, which spatially segregate the different catalysts from each other within their cavities. This allows the application of catalysts in one-pot, which are usually not compatible with each other. Tandem reactions furthermore require a defined sequence of substrate conversion. This requirement can be addressed by supramolecular hosts utilizing their size- and shape-selectivity.

Despite offering several advantages, supramolecular catalysis is often hindered by strong binding of the product species, which reduces the turnover rate or completely stops further conversion. Bimolecular reactions are especially prone to product inhibition, since the binding of the product is entropically favored. However, some strategies have been developed to circumvent this disadvantage, for example the *in situ* conversion of the product to a species with a lower binding affinity or modification of the substrate. The problem of product inhibition is less observed in reactions that feature a charged transition state but a neutral product. Reactions with a neutral transition state like the Diels-Alder reaction still pose a major problem with regard to product inhibition, due to the structural similarity between transition state and product species.

4.2 Examples of catalysis and stoichiometric chemistry in self-assembled hosts¹¹⁶

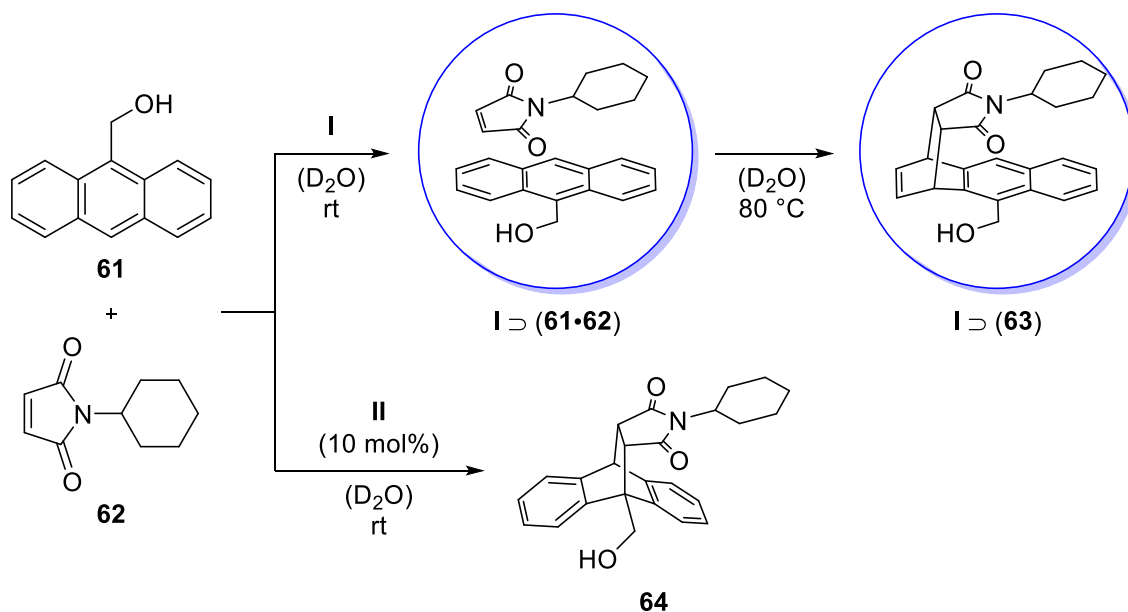
Supramolecular hosts often accelerate reactions by bringing two reacting species into close proximity within their cavity, thereby increasing their local concentration. Additionally, hosts can operate via stabilization of the transition state via noncovalent interactions or via induction of unusual guest conformations (preorganization).¹¹⁷ In recent years, efforts to mimic natural enzymes using supramolecular structures have increased significantly and have resulted in a wide variety of catalyzed reactions, with some even showing accelerations comparable to enzyme catalysis.¹¹⁸ Due to the size of this field, the following chapter only highlights selected examples without providing detailed mechanisms. Focus has been placed on reactions within the resorcin[4]arene hexamer **XI**.

The first true catalytic application of *Fujita*'s octahedral coordination cage **I** was achieved in the Knoevenagel condensation between 2-naphthaldehyde (**58**) and Meldrum's acid (**59**) (Scheme 16).¹¹⁹ Blocking cage **I** with strongly binding 1-adamantol completely inhibited the reaction, indicating the essential character of the cavity for the reaction. Furthermore, in the absence of cage **I**, only 4% of adduct **60** were observed after 6 h. Catalytic turnover is believed to result from the poor fit of product **60** to the cavity. Additionally, the group provided indication that the acceleration is based on the stabilization of the anionic transition state leading to the oxyanion intermediate by Coulomb interactions with the cationic palladium centers. Indeed, when replacing cage **I** with square-pyramidal host **II**, which features more remote palladium centers, the yield of product **60** was significantly reduced, even with stoichiometric amounts.



Scheme 16: Cage **I**-catalyzed Knoevenagel reaction.

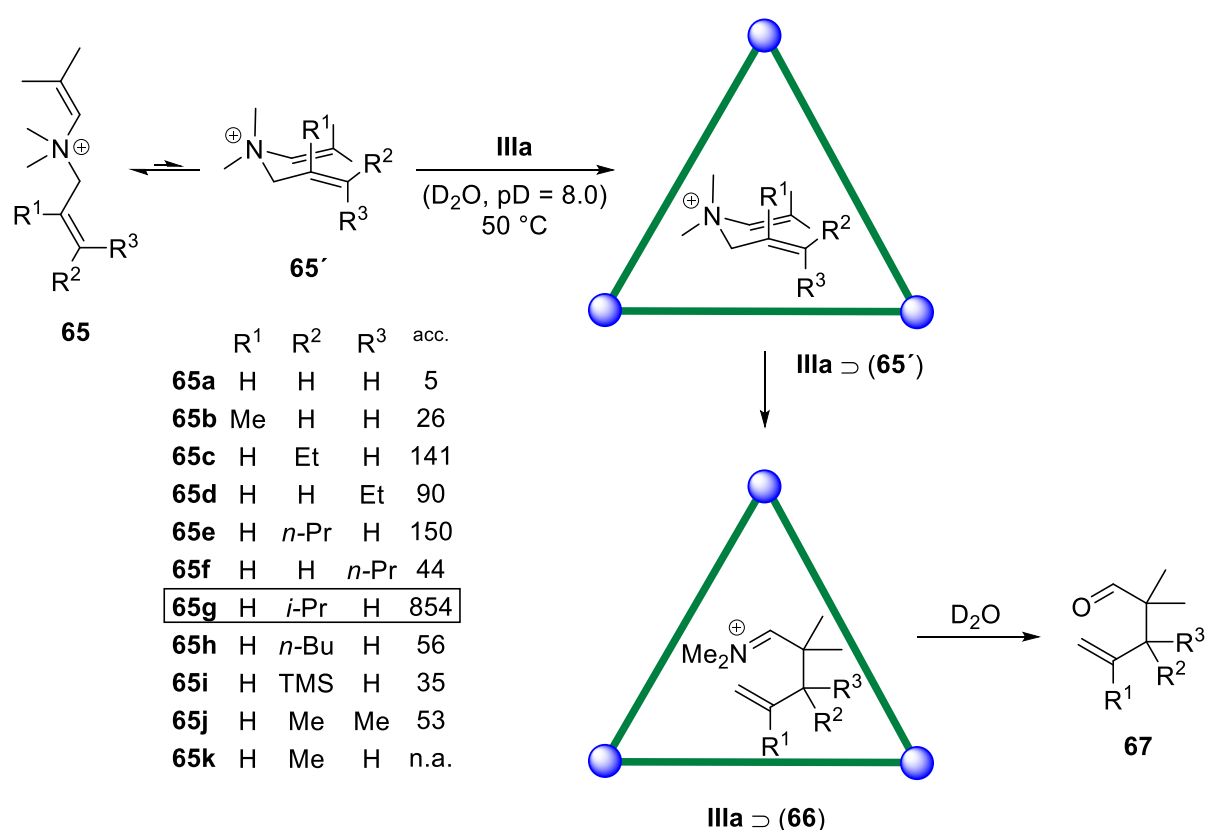
An interesting example of unusual product selectivity was observed in the Diels-Alder reaction between diene **61** and dienophile **62** inside the cavity of cage **I**. Cage **I** selectively encapsulates a pair of substrate **61** and **62** to give inclusion complex **I** \supset (**61**·**62**) (**I** \supset denotes encapsulation within **I**) (Scheme 17).¹²⁰ Upon heating, the Diels-Alder reaction takes place to give product **63**, showing an unusual regioselectivity due to the constrictive binding within the hydrophobic reaction pocket. However, strong binding of the reaction product prevents catalytic turnover. Interestingly, application of the more “open” host **II** allows catalytic turnover due to the weak binding of the Diels-Alder reaction product, but yields the conventional regioisomer **64**, which is also observed in solution.



Scheme 17: Unusual regioselectivity observed in a Diels-Alder reaction within cage **I**.

By far the most examples of catalysis have been reported with the tetrahedral metal-ligand cage **IIIa**, developed by the *Raymond* group. The first reported example describes the acceleration of the aza-Cope rearrangement of allylenammonium salts within the cavity of host **IIIa** (Scheme 18).¹²¹ The cationic ammonium salt **65** shows a high affinity towards the cavity, based on cation- π interactions. Encapsulation of the substrate into the small cavity requires the compact, chair-like conformation **65'**, similar to the transition state of the reaction. This

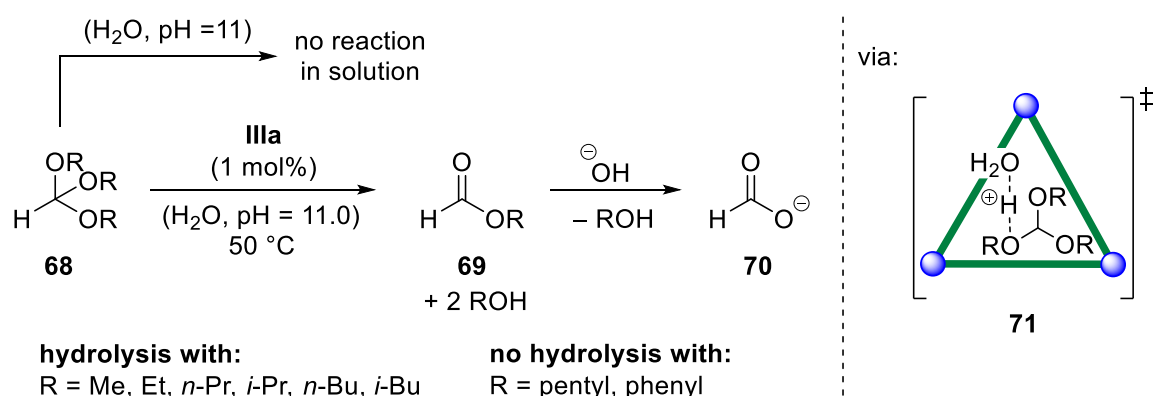
preorganization of the substrate lowers the entropic barrier for the rearrangement and is the main reason for the observed accelerations of up to a factor of 854 (**65g**). Hydrolysis of the rearranged intermediate **66** outside of the cavity finally gives aldehyde **67**. The reaction could be realized with only 13 mol% of cage **IIIa**. Furthermore, application of the enantiopure analog $\Delta\Delta\Delta$ -**IIIa** gave enantioselectivities of up to 64% ee under the standard reaction conditions. In a subsequent study, the successful acceleration of the aza-Cope rearrangement of less reactive propargylenammonium ions within **IIIa** was described.¹²²



Scheme 18: Acceleration of the aza-Cope rearrangement within cage **IIIa**.

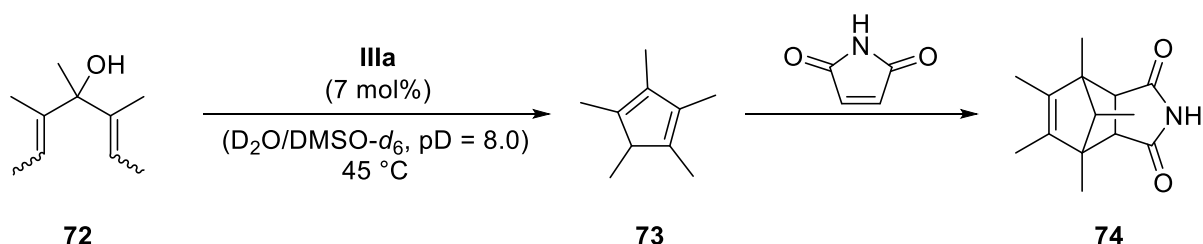
An impressive example of the unique microenvironment provided by host cavities was reported in form of the orthoformate hydrolysis in basic solution (Scheme 19).¹²³ Orthoformates **68** are stable under basic conditions, but the presence of 1 mol% of cage **IIIa** is sufficient to efficiently catalyze conversion to the corresponding formates **70**. The hydrophobic effect drives uptake of the neutral substrate, which is converted within the cavity to the protonated form of ester **69**. Subsequent release and hydrolysis yields the final product. Protonation of the orthoester via transition state **71** is enabled by the cation-stabilizing environment of cage **IIIa**. As a result of the limited space within **IIIa**, only small substrates showed hydrolysis to their formates. This clear size-selectivity provides strong evidence that the reaction indeed proceeds within the

cavity. Additionally, the group was able to extend this methodology to the hydrolysis of dimethyl acetals under basic conditions.¹²⁴



Scheme 19: Size-selective hydrolysis of orthoformates under basic conditions within cage **IIIa**.

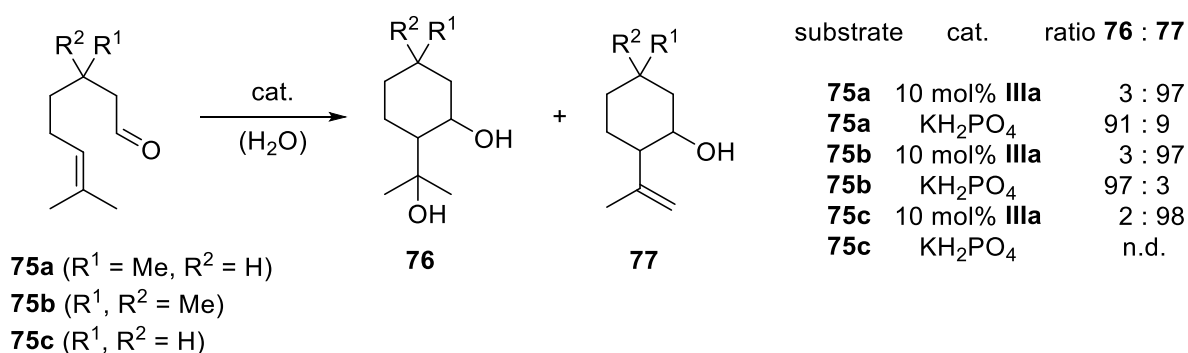
In cooperation with the *Bergman* group, *Raymond et al.* reported one of the largest rate accelerations to date in supramolecular catalysis. The Nazarov cyclization of tertiary alcohol **72** to cyclopentadiene **73** shows a rate acceleration on the order of 10⁶ in the presence of 7 mol% of cage **IIIa** (Scheme 20).¹¹⁸ Detailed mechanistic studies revealed three different aspects to be responsible for the high rate acceleration. First, the substrate is bound in its reactive U-shape conformation. Second, the basicity of the alcohol is dramatically increased within the cavity, due to its cation-stabilizing effect, based on Coulomb and cation- π interactions. Third, mechanistic data indicates a strong stabilization of the cationic transition state.¹²⁵ The strong binding product was converted *in situ* to the low-affinity adduct **74** via a Diels-Alder reaction with maleimide. Like in their other studies, addition of a strong binding ammonium ion blocked the cavity and stopped conversion of substrate **72**.



Scheme 20: Nazarov cyclization catalyzed by cage **IIIa**.

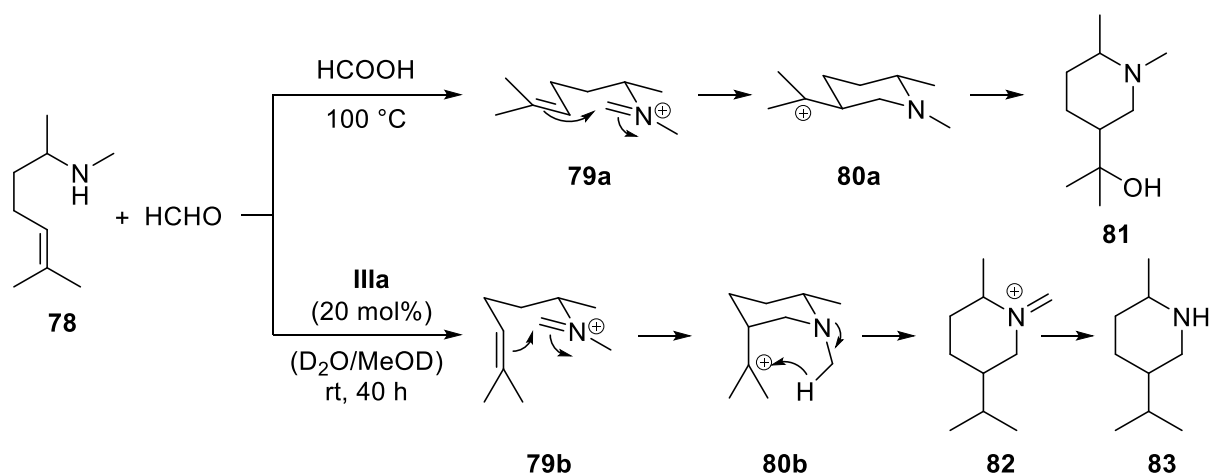
Inclusion within a cavity can protect reactive intermediates from nucleophilic attack by solvent molecules. This was demonstrated in the cage **IIIa**-catalyzed Prins cyclization of substrate **75** (Scheme 21).¹²⁶ The intermediary cyclohexyl cation can in principle either react in a S_N1-mechanism with water to diol **76** or undergo elimination to yield compound **77**. Due to the

hydrophobic environment within the cavity of **IIIa**, a high selectivity for the corresponding alkene products was observed. In acidic (pH = 3.2), aqueous solution however, the diols were formed preferentially. Interestingly, substrate **75c** only gave a complex mixture in solution. Using cage **IIIa**, the lack of intrinsic conformational constraint was compensated by the constrictive environment within the cavity. Enantioselective catalysis was achieved by utilizing related host **IIIb**, which, under optimized conditions, gave an enantiomeric excess of 69% ee with substrate **75b**.⁶⁵



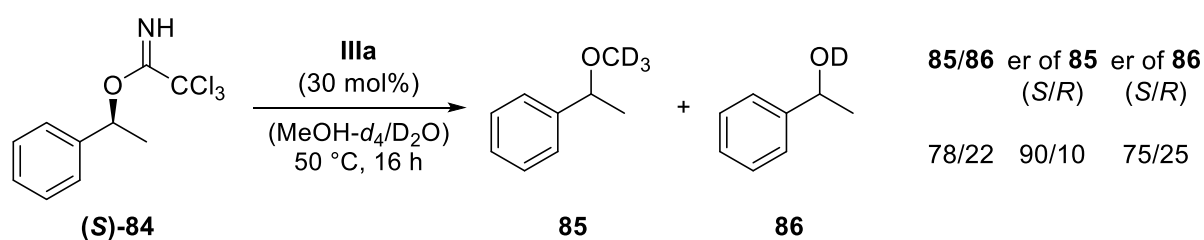
Scheme 21: Chemoselectivity in the cage **III**-catalyzed Prins cyclization.

An unexpected discovery was made, when the groups of *Raymond*, *Bergman* and *Toste* studied the aza-Prins cyclization of iminium ions.¹²⁷ While in solution the expected tertiary amine product **81** was formed, the presence of 20 mol% of **IIIa** changed the product species to secondary amine **83** (Scheme 22). The authors could show, that after the cyclization of **79b**, formed from amine **78**, an intramolecular 1,5-hydride transfer was occurring inside the supramolecular host. The steric confinement inside **IIIa** enforces the formation of the more compact configurational isomer **80b**, as compared to the less strained isomer **80a** in the solution experiment. In the strained intermediate **80b**, the orbitals are well aligned for the observed hydride shift, which gives intermediate **82**. In the relaxed solution isomer **80a**, such a hydride migration is not feasible and the carbocation **80a** is intercepted by water as a nucleophile, generating product **81**.



Scheme 22: Pronounced deviation in product selectivity, observed in the aza-Prins cyclization using cage **IIIa**.

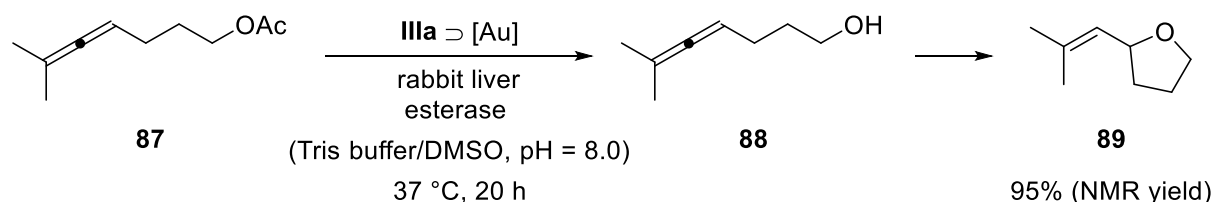
Influence on the stereochemical outcome of a reaction is highly desired and can indeed be achieved by exploiting the confined environment of a supramolecular host. In methanol- d_4 solution, treatment of enantiopure trichloroacetimidate (*S*)-**84** with 5 mol% of an achiral phosphoric acid gives benzyl ether **85** with 84% inversion of stereochemistry, which confirms an S_N2 -reaction mechanism. However, utilizing 30 mol% of **IIIa** in a mixture of methanol and water gives ether **85** and alcohol **86** with high degree of stereoretention (Scheme 23). The authors could prove that the reaction proceeds within the cavity and also could exclude a stereoretentive double inversion mechanism. The stereoretention is believed to result from shielding of one side of the transiently formed benzylic cation by the cavity wall via cation- π interactions.¹²⁸



Scheme 23: Control over the stereochemical outcome of a reaction via encapsulation within **IIIa**.

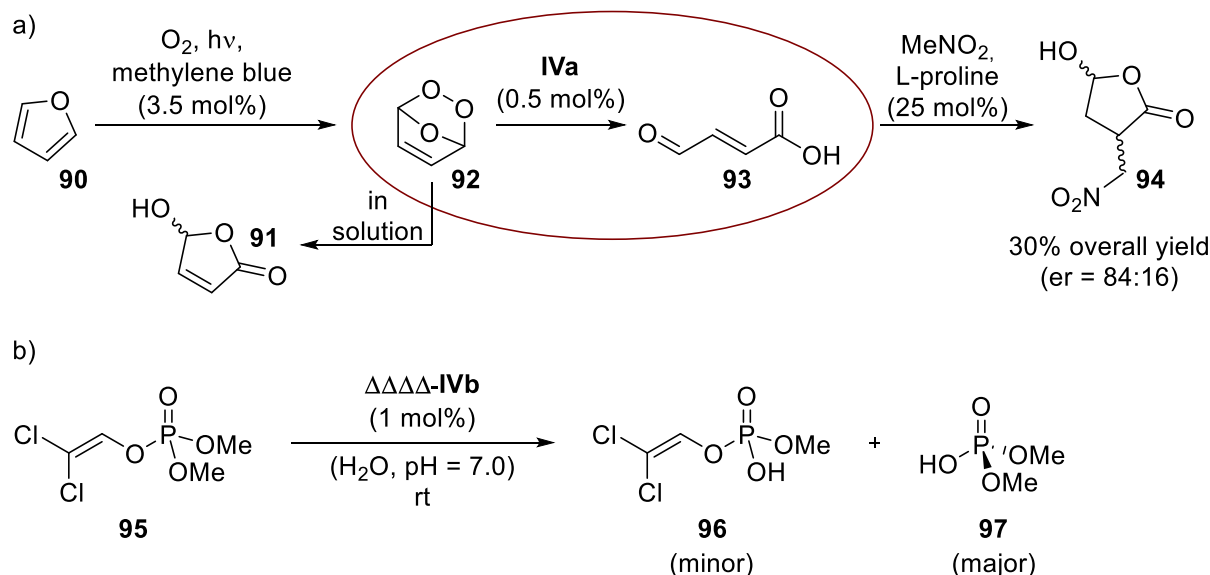
A remarkable example of a multicatalyst tandem reaction is the hydrolysis-cyclization tandem reaction in the presence of rabbit liver esterase and **IIIa** \supset (Me_3PAu^+) (Scheme 24).¹²⁹ In a previous study, the encapsulation of Me_3PAu^+ within **IIIa** was shown to accelerate the hydroalkoxylation of alcohol **88** to tetrahydrofuran **89** by a factor of eight.¹³⁰ Based on these results, a tandem reaction with an enzyme was envisioned starting from acetate **87**. Indeed, complete compatibility was observed between the two catalysts and tetrahydrofuran **89** was formed in high yield and selectivity. Interestingly, the free gold catalyst did significantly reduce

the rate of the enzyme-catalyzed hydrolysis step. This highlights the advantage of spatially segregating catalysts using supramolecular hosts. Recently, encapsulation of a gold catalyst within **IIIa** was also shown to dramatically accelerate an alkyl-alkyl reductive elimination step.¹³¹



Scheme 24: Hydrolysis-cyclization tandem reaction favored by encapsulation of the gold catalyst.

A second example of a multicycatalytic tandem reaction was provided by the Nitschke group utilizing host **IVa** (Scheme 25a).¹³² Remarkably, host **IVa** self-assembles in the presence of the other two catalysts and the reagents despite incomplete orthogonality due to the reversibility of the side reactions and the thermodynamic stability of the host structure. The reaction sequence starts with a Diels-Alder reaction between singlet oxygen and furan (**90**). Endoperoxide **92** is subsequently hydrolyzed by host **IVa** to the α,β -unsaturated aldehyde **93**, which undergoes a L-proline catalyzed 1,4-addition of nitromethane to yield the final product **94**. Strikingly, the absence of host **IVa** leads to a different product (hydroxyfuranone **91**).

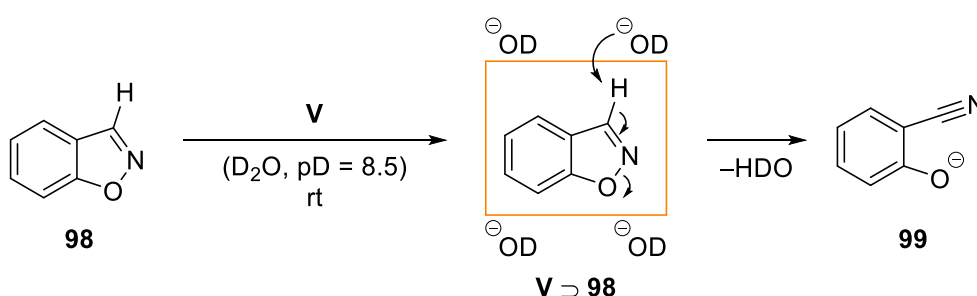


Scheme 25: (a) Multicycatalytic system that utilizes host **IVa**; (b) accelerated hydrolysis of dichlorvos (**95**) in the presence of host $\Delta\Delta\Delta\Delta\text{-IVb}$.

The related host $\Delta\Delta\Delta\Delta\text{-IVb}$ was shown to accelerate the hydrolysis of dichlorvos (**95**) to a mixture of phosphoric acid **96** and dimethyl phosphoric acid (**97**) (Scheme 25b).⁶⁹ Control

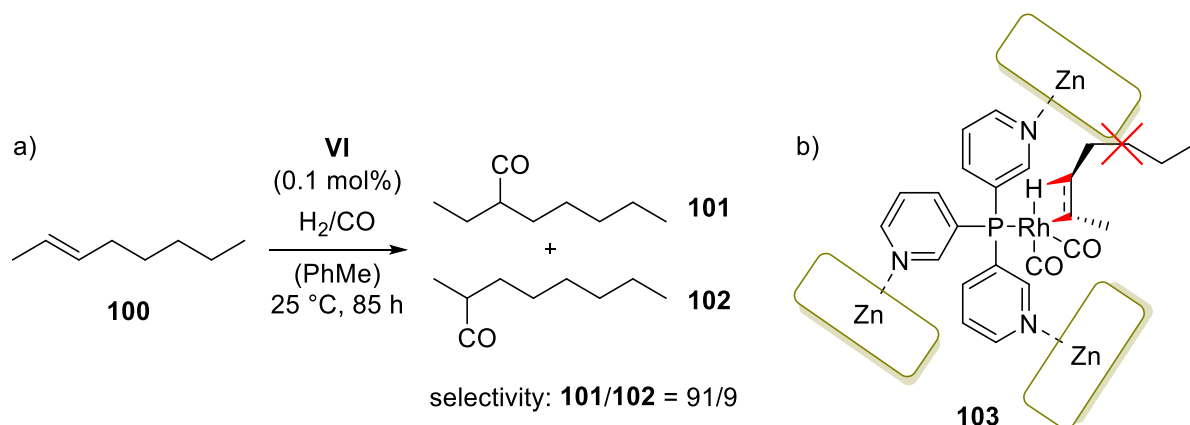
experiments indicated that indeed the complete capsule structure is necessary, since its subcomponents alone did not change the rate significantly. Additionally, tightly binding guests (e.g. cyclooctane) efficiently slow down the reaction by blocking the cavity. A possible explanation for the observed acceleration might be the polarization of the encapsulated substrate by the positively charged host structure.

An example for acceleration via increase in the local concentration of reactants was provided by the *Ward* group using metal-ligand cage **V** (Scheme 26).¹³³ In basic medium, an acceleration of up to 10^5 was observed in the Kemp elimination of benisoxazole (**98**) to 2-cyano-phenolate (**99**). The high catalytic efficiency of the reaction was shown to result from 1) a high local concentration of partially desolvated deuteroxide ions around the positively charged vertices of the cage and 2) binding of the hydrophobic substrate in the cavity. The importance of both orthogonal binding sites was verified by competition experiments. Catalytic turnover is possible due to the weak binding of the anionic product species.



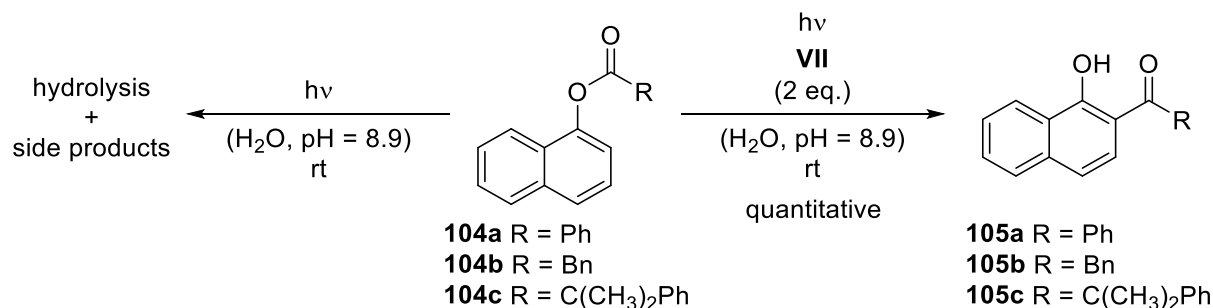
Scheme 26: Acceleration of the Kemp elimination using metal-ligand cage **V**.

Unprecedented regioselectivity was achieved in the hydroformylation of *trans*-2-octene (**100**) using host structure **VI** (Scheme 27a).¹³⁴ In solution, the incorporated rhodium catalyst yields a 50:50 mixture of the aldehydes **101** and **102**. Upon encapsulation, the selectivity changes remarkably to 91:9 in favor of the C3-branched aldehyde. Detailed studies indicate that the selectivity is established during the hydrometalation step. In the transition state **103**, which leads to the minor aldehyde product, CH- π interactions that are present between the porphyrin units have to be disrupted for hydrometalation (Scheme 27b). Further studies showed that simple variation of the porphyrin units allows a controlled reversal in selectivity.⁷⁴ Additionally, high enantioselectivity could be achieved by employing a chiral second coordination sphere.¹³⁵



Scheme 27: High regioselectivity in a hydroformylation reaction achieved with supramolecular catalyst **VI**.

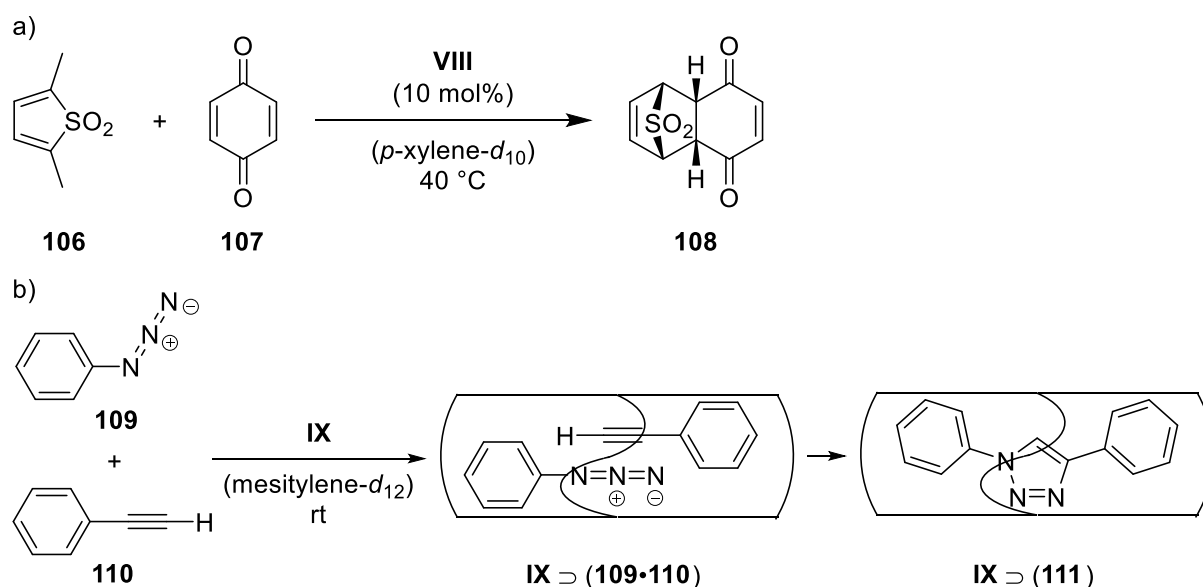
The restricted mobility of highly reactive species within dimer **VII** was exploited in the photo-Fries reaction of naphthyl esters **104** (Scheme 28).¹³⁶ In basic aqueous solution, the reaction gives multiple side products and suffers from hydrolysis of the starting material. Encapsulation of the ester by dimer **VII**, however, prevents hydrolysis and leads to quantitative formation of the rearranged products **105**. The selectivity is believed to arise from the restricted mobility of the intermediary singlet radical pair within the cavity and from an increased rate of radical recombination. An excess of dimer **VII** was employed to ensure complete encapsulation of the substrate.



Scheme 28: Selective photo-Fries reaction in basic aqueous solution using dimer **VII**.

The first example of true catalysis within a self-assembled hydrogen bond-based host structure was reported by *Rebek et al.* in 1998.¹³⁷ The study showed that the presence of 10 mol% of dimeric host **VIII** accelerates the Diels-Alder reaction between thiophene **106** and *p*-benzoquinone (**107**) by a factor of 10 as compared to the background reaction (Scheme 29a). Weak binding of product **108** enabled entropically disfavored replacement with two substrate molecules and therefore catalytic turnover. Significantly higher rate accelerations were achieved with alternative diene/dienophile combinations, but in those cases strong product inhibition was observed.

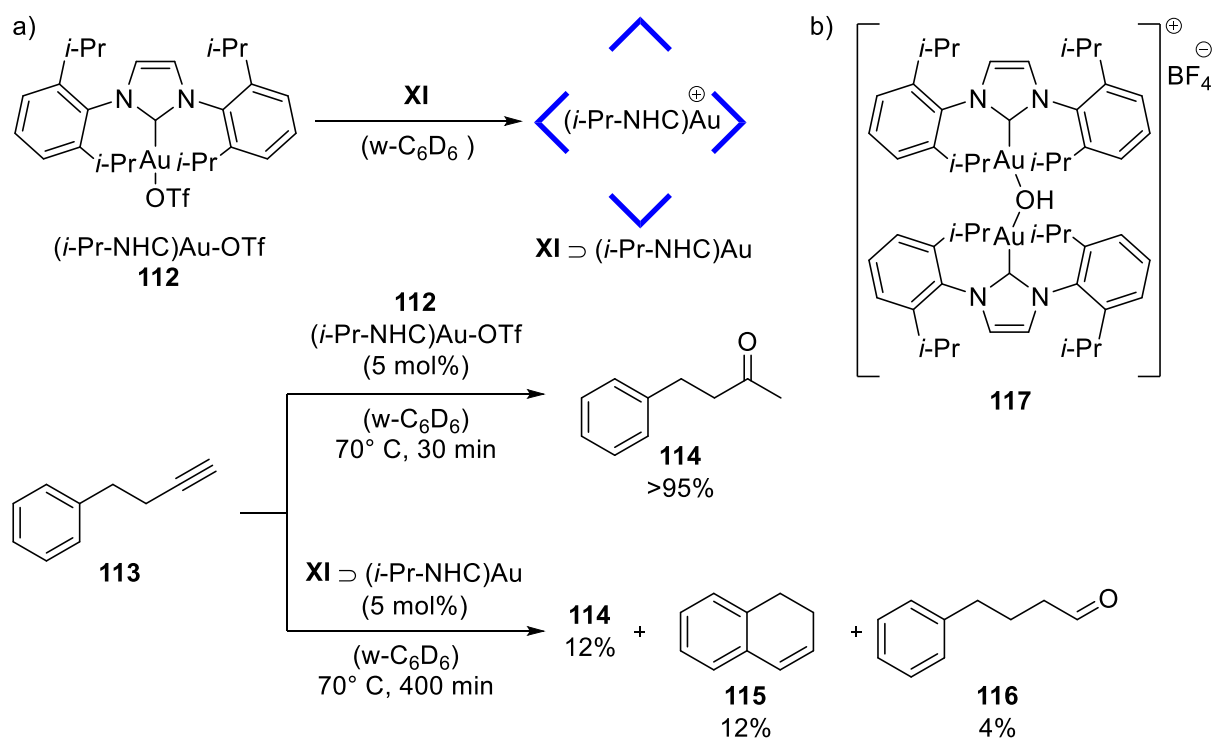
Another early report by the *Rebek* group deals with the high regioselectivity obtained in the 1,3-dipolar cycloaddition between phenyl azide (**109**) and phenylacetylene (**110**) within hydrogen-bonded dimer **IX** (Scheme 29b).¹³⁸ In solution, the cycloaddition between the two substrates yields a nearly equimolar mixture of the 1,2- and 1,4-adduct. Encapsulation of the substrates within dimer **IX** only allows for an antiparallel alignment, orienting the two polar functionalities near the seam of hydrogen bonds. This results in a complete selectivity in favor of the 1,4-regioisomer (**111**). Despite the high rate acceleration, application of the methodology is restricted by severe product inhibition.



Scheme 29: Early examples of chemistry within self-assembled hydrogen bond-based host structures.

The first example of catalysis within the self-assembled resorcin[4]arene hexamer **XI** was achieved by *Reek et al.* in 2011 by encapsulation of a gold(I)-catalyst.¹³⁹ Addition of complex **112** to a solution of hexamer **XI** in water saturated benzene-*d*₆ (w-C₆D₆) led to complete uptake of the catalytically active cationic species (Scheme 30a). The triflate anion was shown by ¹⁹F NMR to reside outside of the cavity. To probe the influence of encapsulation on the catalytic activity, alkyne **113** was added to 5 mol% of **XI** \supset (*i*-Pr-NHC)Au and the reaction was monitored at 70 °C. Interestingly, compared to the free catalyst, a change in product selectivity was observed. In addition to ketone **114**, which is the sole product in solution, dihydronaphthalene (**115**) and the anti-Markovnikov product **116** were formed. The formation of dihydronaphthalene (**115**), which is usually only formed in the absence of water, can be explained by the hydrophobic character of the cavity space. Anti-Markovnikov product **116** is believed to be a direct result of the confined space within the cavity and has not been observed before in significant amounts with gold catalysis. Encapsulation of the catalyst results in a

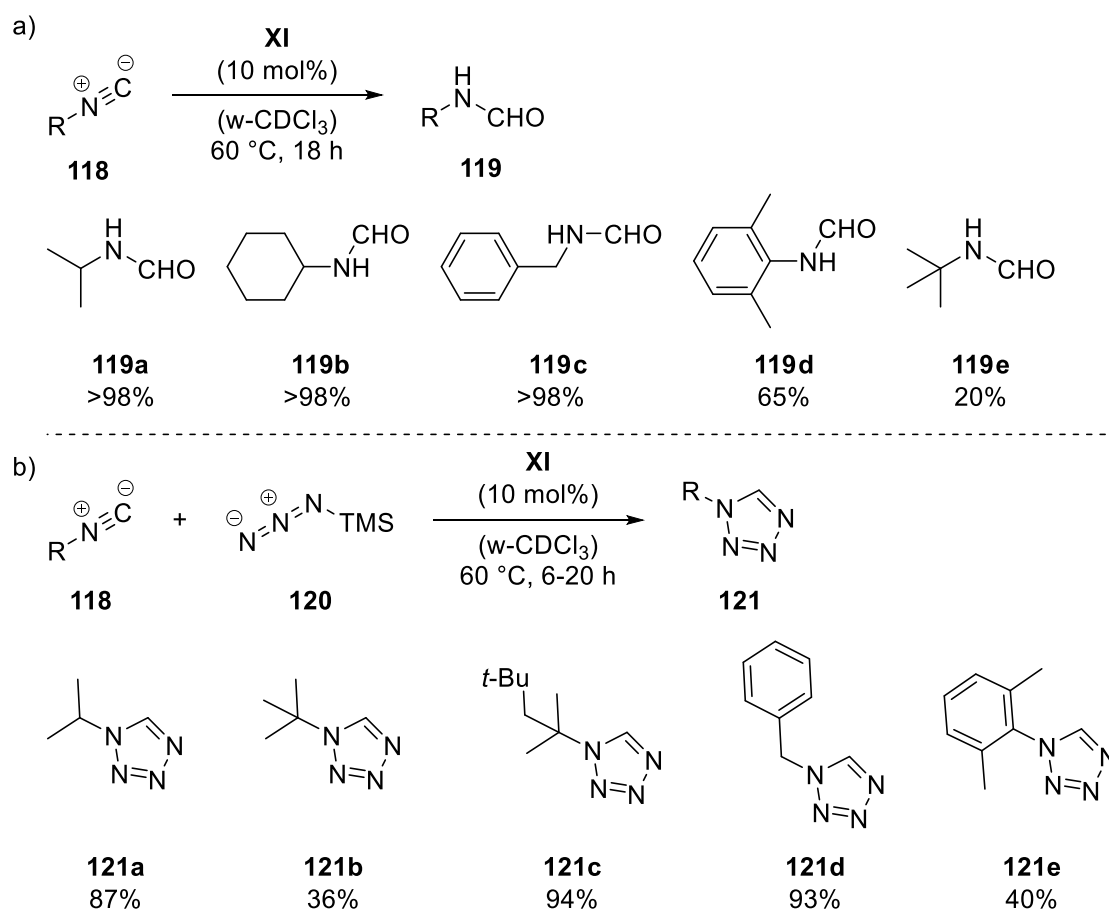
significant reduction of the reaction rate. Furthermore, blocking of the cavity with a strong binding ammonium ion restores the original selectivity of the catalyst. A subsequent study explored the effect of encapsulation on the substrate selectivity of the gold(I)-catalyst. Indeed, contrary to solution, size and shape effects now dominated the substrate reactivity.¹⁴⁰ Very recently, the group extended the methodology to switch between the dinuclear gold complex **117** and its mononuclear analog (Scheme 30b).¹⁴¹ Dinuclear gold complex **117** converts substrate **113** via a dual activation mode into a mixture of dimers. In the presence of hexamer **XI**, the dinuclear complex is broken into encapsulated mononuclear species. This restores the original reactivity described in their previous study (Scheme 30a). By adding a strongly binding ammonium ion, the gold catalyst is expelled from the cavity and resumes its dual activation mode.



Scheme 30: (a) Encapsulation of a gold catalyst within hexamer **XI**; (b) switchable dinuclear gold complex.

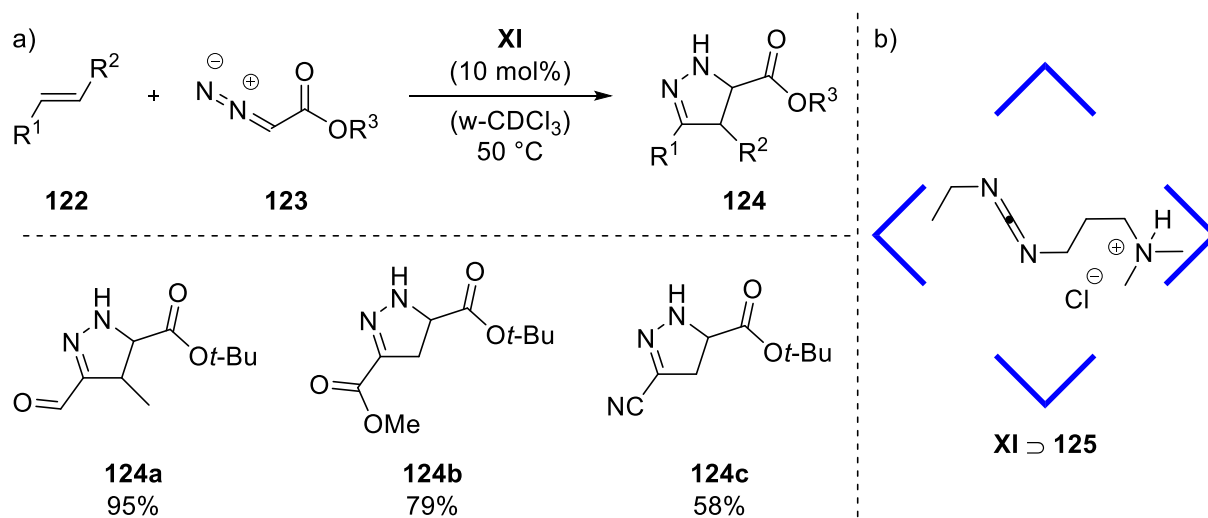
The groups of *Scarso* and *Strukul* utilized the same concept to switch between an active and inactive photoredox catalyst. Encapsulation of $[\text{Ru}(\text{bpy})_3]^{2+}$ by hexamer **XI** turns off its catalytic activity in the aerobic oxidation of aliphatic sulfides. Subsequent addition of a competitive cationic guest releases the photocatalyst and restores the catalytic activity.¹⁴² The collaboration continued with a report on the efficient isonitrile hydrolysis within hexamer **XI**, utilizing the intrinsic catalytic activity of the assembly.¹⁴³ They could show that 10 mol% of hexamer **XI** are sufficient to produce the corresponding formylamides **119a-e** in water-

saturated chloroform- d_1 at 60 °C (Scheme 31a). The reaction likely proceeds via protonation of the isonitrile carbon atom, followed by attack of a water molecule that is incorporated into the assembly. Inhibition of the reaction by addition of a strongly binding ammonium ion provided evidence that the reaction proceeds within the cavity. Furthermore, no conversion was observed in the absence of the catalyst. A follow-up study utilized the good binding of isonitriles for the catalytic [3+2] cycloaddition with trimethylsilyl azide (TMSN₃, **120**) to construct a series of 1-substituted 1*H*-tetrazoles (Scheme 31b).¹⁴⁴ The authors could show that the 1*H*-tetrazoles **121a-e** are formed directly without intermediary formation of the corresponding formylamides, despite using nearly identical reaction conditions as in their previous study. Control experiments with acetic acid ($pK_a = 4.8$),¹⁴⁵ which is an even stronger acid than hexamer **XI**, showed no conversion, excluding an acid-based mechanism. Interestingly, a large excess of a tetraalkylammonium ion did not completely inhibit the reaction, which indicates that the residual space within the cavity is still sufficient to catalyze the reaction to some degree. Again, no conversion was observed in the absence of the catalyst.



Scheme 31: (a) Hexamer **XI**-catalyzed hydrolysis of isonitrile **118**; (b) [3+2] cycloaddition catalyzed by hexamer **XI** (selected examples).

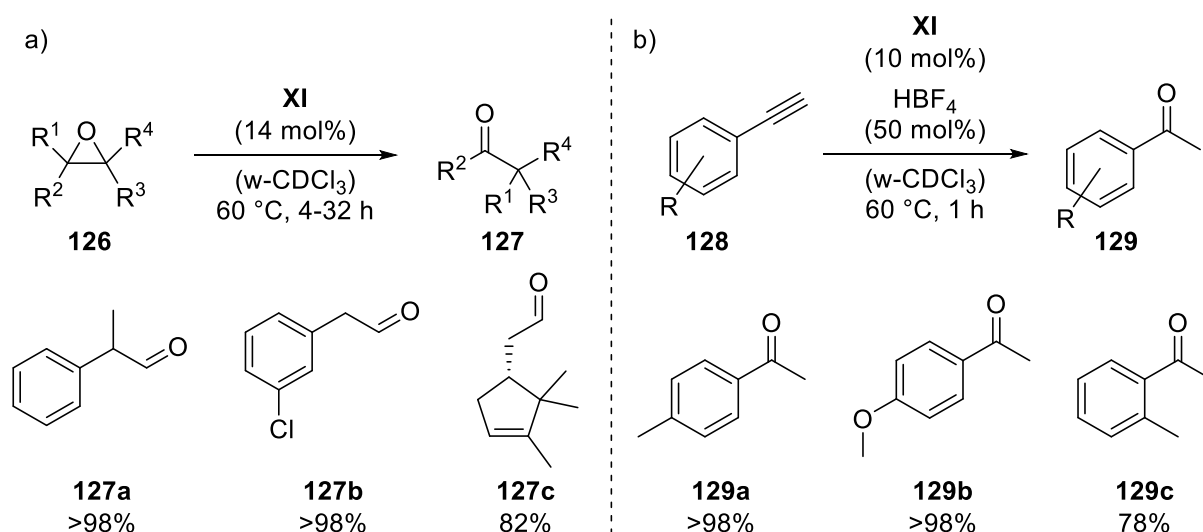
The groups of *Scarso* and *Strukul* also demonstrated that hexamer **XI** is capable of catalyzing the 1,3-dipolar cycloaddition between electron-poor alkene **122** and diazoacetate ester **123** (Scheme 32a).¹⁴⁶ Efficient encapsulation of the neutral diazoacetate ester **123** was proven by ¹H NMR and DOSY experiments. The presence of the hexamer not only accelerated the reactions but also enabled some that were not possible in bulk solution. This positive effect is believed to arise from weak interactions with the electron-rich surface of the cavity and additionally from an increased effective concentration inside the host. Formation of the 4,5-dihydro-1*H*-pyrazoles **124** was substantially inhibited by addition of a competitive high-affinity guest. Catalyst **XI** even showed a modest substrate selectivity, favoring the conversion of smaller substrates, likely due to a better packing of smaller reagent combinations within the cavity. The substrate selectivity, imparted by hexamer **XI**, was utilized in a subsequent study to control amide formation by encapsulation of the coupling reagent **125** (Scheme 32b).¹⁴⁷ While in solution pairs of differently-sized carboxylic acids react similarly with a given primary amine, in the presence of **XI** \supset **125** the formation of the shorter amide is significantly favored.



Scheme 32: (a) 1,3-Dipolar cycloaddition catalyzed by hexamer **XI** (selected examples); (b) encapsulation of a coupling reagent within the cavity of **XI**.

The ability of hexamer **XI** to act as a weak Brønsted acid and to stabilize cationic intermediates and transition states allows its application in reactions that are not possible with conventional Brønsted acids with comparable acidity. This was illustrated by the isomerization of epoxides **126** to their corresponding carbonyl compounds **127** (Meinwald isomerization) (Scheme 33a).¹⁴⁸ While no conversion was observed with acetic acid, the epoxides readily isomerized in the presence of 14 mol% of hexamer **XI**. This highlights the favorable effect of the unique microenvironment for the observed isomerization. As in previous studies, addition of a

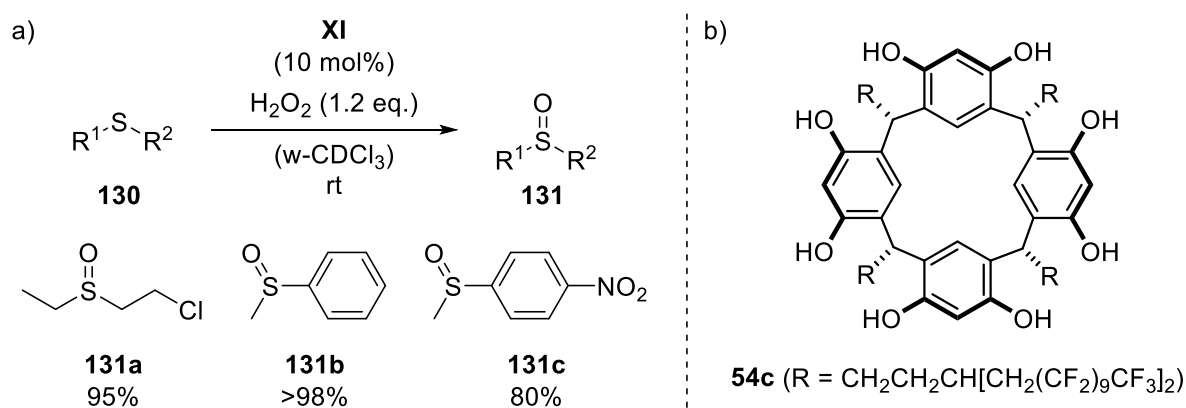
competitive cationic guest led to inhibition of the reaction. Several aromatic epoxides were isomerized in excellent yield, with less electron-rich substrates requiring a longer reaction time. Even some strained aliphatic epoxides like α -pinene oxide could be converted within the cavity. However, very electron-poor derivatives turned out to be completely inactive. The limitations resulting from the weak acidity of hexamer **XI** can be overcome by utilizing an acid co-catalyst, as demonstrated in a separate study by *Scarso* and *Strukul*. Neither catalytic amounts of hexamer **XI** nor catalytic amounts of HBF_4 are able to induce the hydration of phenylacetylene **128** alone. However, formation of methyl ketone **129** occurs rapidly as soon as both reagents are combined (Scheme 33b).¹⁴⁹ It is believed that the reaction requires an initial rate-determining protonation by the strong acid HBF_4 . It is argued that this step has to occur within the host to experience the stabilizing effect of the aromatic cavity.



Scheme 33: (a) Meinwald isomerization catalyzed by host **XI** (selected examples); (b) catalytic hydration of aromatic alkynes (selected examples).

The hexamer **XI**-catalyzed activation of hydrogen peroxide in the sulfoxidation of thioethers represents another example that does not rely on the acidity of the hexamer. The groups of *Scarso* and *Strukul* could show that the presence of 10 mol% of hexamer **XI** accelerate the oxidation of thioether **130** to sulfoxide **131** (Scheme 34a).¹⁵⁰ The acceleration effect was not observed when the hexamer was replaced by acetic acid. Additionally, the formation of sulfones was not detected, even when using a sulfoxide as the substrate. The authors suggest that the acceleration results from a dual synergic effect: 1) hydrogen peroxide replaces water molecules that are incorporated into the hexameric structure and thereby becomes more electrophilic and 2) the polar transition state of the reaction is stabilized by interactions with the electron-rich surface of the cavity. Interestingly, the addition of tetraethylammonium tetrafluoroborate only

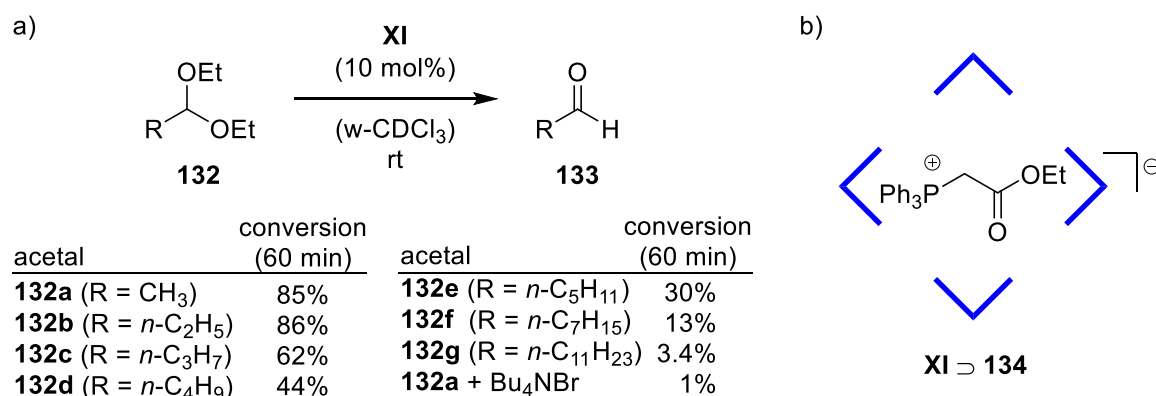
led to a modest reduction of the acceleration. It is likely that the residual space of the cavity allows co-encapsulation and oxidation of small substrates. Another application that does not require the acidity of the hexamer was reported by *Shimizu et al.*¹⁵¹ The group utilized their previous discovery that resorcinarene **54c**, which bears fluororous alkyl chains, forms hexameric assemblies in wet fluororous solvents (Scheme 34b). This hexamer was shown to modestly accelerate (2.3- to 21-fold increase in yield after 6 h) the Diels-Alder reaction between a series of dienes and dienophiles in a fluororous biphasic system. In this case, the acceleration likely results from the fluorophobic effect that forces the organic substrates into the cavity and increases their local concentration. Indeed, when reducing the fluororous content of fluororous solvent mixtures, a decrease in acceleration was observed. Additionally, the cavity space influenced the *endo/exo* ratio of the obtained products, favoring the more compact *endo* form. Furthermore, the biphasic system allowed efficient catalyst recovery by simple decantation.



Scheme 34: (a) Hexamer **XI**-catalyzed sulfoxidation of thioethers (selected examples); (b) resorcin[4]arene derivative that allows hexamer formation in wet fluororous solvents.

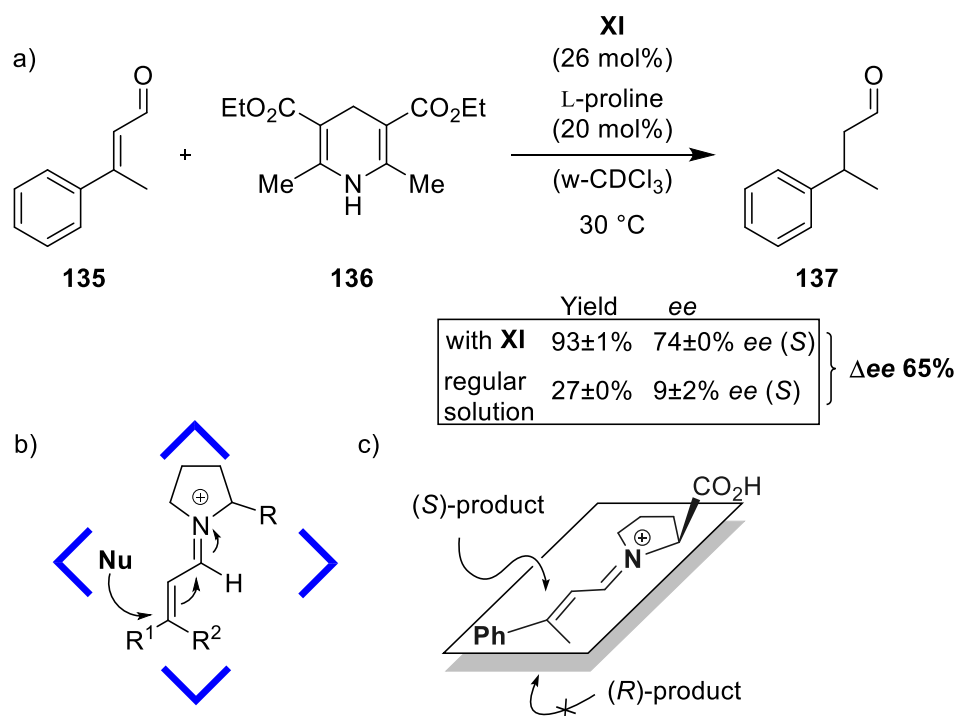
The disclosure of the Brønsted acidity of hexamer **XI** by the *Tiefenbacher* group was accompanied by a report on its first intentional application in acid catalysis.¹¹⁴ The authors could show that hexamer **XI** is able to catalyze the hydrolysis of acetal **132** to its corresponding aldehyde **133** in water-saturated chloroform (Scheme 35a). Despite the hydrophobic character of the cavity, water is apparently able to enter the cavity and react with the substrate. Due to less efficient uptake, the longer substrates showed significantly reduced reaction rates. This observation could be utilized for the size-selective conversion of a small substrate in the presence of larger one. Additionally, blocking of the cavity with tetrabutylammonium bromide (TBAB) inhibited the reaction. The group furthermore utilized hexamer **XI** as a control element in a size-selective Wittig reaction. A small Wittig ylide was irreversibly encapsulated in its protonated form **134**, while a large analog, too bulky to fit the cavity, only underwent reversible protonation on the outside of the cavity (Scheme 35b). Addition of propanal to a mixture of

both ylides and stoichiometric amounts of hexamer **XI** therefore led to a selective conversion of the larger ylide.



Scheme 35: (a) Size-selective acetal hydrolysis catalyzed by hexamer **XI**; (b) Selective encapsulation of a small Wittig ylide.

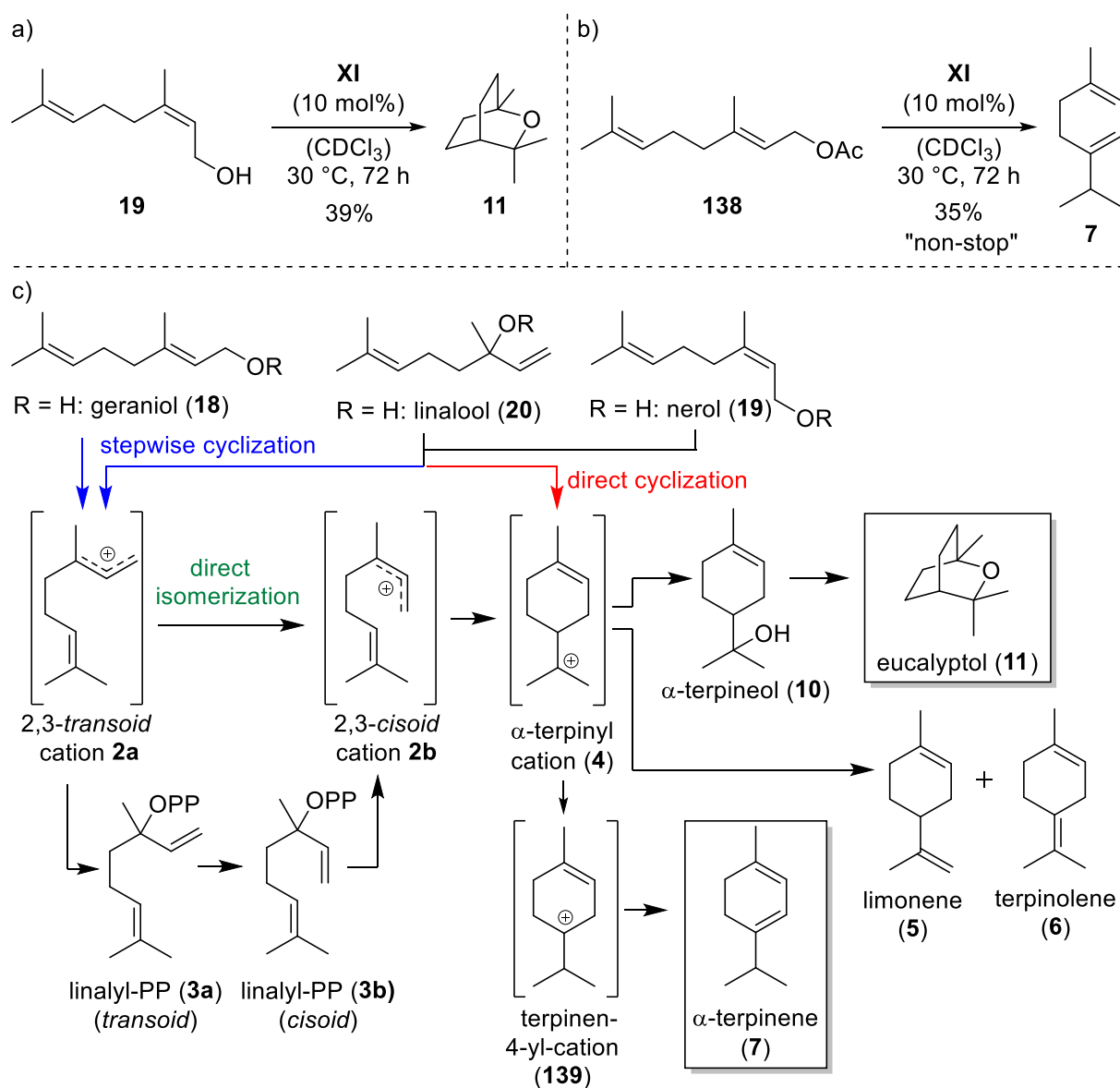
The *Tiefenbacher* group also reported the first example of iminium catalysis within a supramolecular structure, utilizing hexamer **XI**.¹⁵² *In situ* condensation between the α,β -unsaturated aldehyde **135** and L-proline yields an iminium ion with high affinity for the cavity. After rapid encapsulation, the iminium ion is attacked by Hantzsch ester (**136**) to yield the saturated aldehyde **137** (Scheme 36). Strikingly, the enantiomeric excess differs significantly from the value obtained in the corresponding solution experiment. It is argued that the iminium ion binds via cation- π interactions to the inner surface of the cavity from its sterically less hindered face. This binding mode favors attack of the Hantzsch ester from the top side, which results in more (*S*)-product than in the regular solution experiment. Control experiments provided further evidence that the reaction indeed proceeds within the cavity. A screening of the substrate scope indicated the importance of the phenyl moiety and the positive effect of *ortho*-substituents on the enantiomeric excess.



Scheme 36: (a) Iminium catalysis within hexamer **XI**; (b) nucleophilic attack on the encapsulated iminium ion; (c) hypothesis for the observed effect on the enantiomeric excess.

By far the most impressive example of catalysis within the resorcin[4]arene hexamer **XI** is the tail-to-head terpene (THT) cyclization of acyclic monoterpenes. Due to possible side reactions of the cationic intermediates, THT cyclizations are extremely hard to control in solution and usually give complex mixtures containing only traces of cyclic monoterpenes. However, *Zhang* and *Tiefenbacher* could show that hexamer **XI** is capable of activating commercially available monoterpenes like geraniol (**18**), nerol (**19**) and linalool (**20**) via protonation and induce their cyclization within the aromatic cavity.¹⁴ The mild cyclization of nerol using 10 mol% of hexamer **XI** yielded eucalyptol (**11**) in remarkable 39% yield (Scheme 37a). A comparable direct cyclization to eucalyptol had not been described before with an artificial catalyst. Formation of eucalyptol results from an intramolecular hydroalkoxylation of α -terpineol (**10**), which is generated by interception of the α -terpinyl cation (**4**) by the cleaved leaving group. In order to suppress interception by the cleaved water molecule, acetate was utilized as a less nucleophilic leaving group. Indeed, treating geranyl acetate (**138**) with hexamer **XI** gave α -terpinene (**7**) in good selectivity without the formation of any intermediates (Scheme 37b). This non-stop reaction likely involves formation of cation **139** via a 1,2-H shift of intermediate **4**. The non-stop reaction mechanism is enabled by the cavity, which stabilizes the intermediary cations via cation- π interactions with the electron-rich surface and excludes nucleophilic water molecules. Additionally, the hexamer acts a non-nucleophilic counteranion, although some degree of phenol alkylation, especially in the case of geranyl derivatives, could be observed.

Evidence for the importance of the cavity was provided by inhibition of the reaction in the presence of a high affinity ammonium guest. A striking conclusion that can be drawn from the non-stop cyclization of geranyl acetate (**138**) is the feasibility of a direct isomerization from the *transoid* cation **2a** to the *cisoid* cation **2b**, which had long been considered unlikely in the biosynthesis of terpenes (Scheme 37c). Furthermore, the ionization and isomerization of geranyl acetate (**138**) are considered to be slow, which gives the leaving group enough time to diffuse away from the reaction center. This prevents the leaving group from acting as a general base. In contrast, neryl and linalyl derivatives can react in a concerted S_N2/S_N2' like fashion, which increases the possibility of a leaving group-assisted deprotonation of cation **4**.



Scheme 37: (a) Hexamer **XI**-catalyzed cyclization of nerol (**19**) to eucalyptol (**11**); (b) non-stop cyclization of geranyl acetate (**138**); (c) reaction pathways of the monoterpene cyclization within hexamer **XI** with comparison to biosynthesis (**3a/3b**).

5. Objective of this thesis

The results documented in this thesis represent efforts towards the long-term goal of controlling THT cyclizations within supramolecular assemblies. In nature, THT cyclizations are catalyzed by enzymes with high selectivity inside a defined hydrophobic reaction pocket that constrains the flexible terpene chain to a defined conformation. The cationic intermediates are stabilized by cation- π interactions within the active site and protected from attack of nucleophiles. THT cyclizations create a vast variety of complex cyclic and often biologically active structures and, in contrast to HTT cyclizations, cannot be controlled in bulk solution. Supramolecular structures not only provide suitable mimics for enzyme catalysis but also enable the use of unnatural terpene precursors to generate derivatives of terpene natural products that are not accessible via other methods. The possibility to use commercially available alcohol substrates like nerol (**19**) instead of diphosphates for the THT cyclization further enhances the value of this methodology.

Despite the successful prove of concept study about monoterpene cyclization within hexamer **XI**, fundamental understanding of the prerequisites for catalytic activity of self-assembled hydrogen bond-based structures is lacking. The large symmetric cavity of hexamer **XI** is furthermore unable to induce a defined substrate conformation, which results in the formation of product mixtures. Additionally, the products are obtained as racemic mixtures due to the rapid racemization of assembly **XI** in solution. To overcome the current shortcomings and to develop novel hydrogen bond-based hexameric systems, two major goals have been devised for this thesis: 1) Improve the current understanding of the catalytically active system **XI** and 2) synthesize derivatives of hexamer **XI** and evaluate their properties.

The application of hexamer **XI** in reactions involving cationic transition states represents a valuable approach to learn more about the scope and limitations of the current system. Therefore, different cationic reactions will be studied within the supramolecular structure **XI**. Additionally, those applications represent valid contributions to the field of synthetic organic chemistry and catalysis in general. Furthermore, strategies to modulate the catalytic activity of hexamer **XI** will be investigated, since they are expected to be adaptable to related systems. In addition, the properties of the closely related, catalytically inactive system **XII** will be probed to gain insight on the molecular mechanisms responsible for the catalytic activity of hexamer **XI**.

The development of novel resorcin[4]arene-based supramolecular catalysts requires the derivatization of building block **54b**. Based on molecular modelling, all derivatives presented in Figure 7a are capable of forming hexameric assemblies. Furthermore, the residues introduced in **140a-d** are expected to replace the water molecules present in the original structure of the resorcin[4]arene hexamer **XI**. Additionally, modelling indicates that the assembly of subunit **140d** features unsaturated recognition sites on the surface, which could be used to modify the cavity via docking of internally directed guest molecules. Therefore, the synthesis of the derivatives **140a-e** will be attempted and the self-assembly of the structures will be investigated. In addition, the catalytic activity of successfully assembled structures will be evaluated using the monoterpene cyclization as a model reaction. If possible, the pK_a value and the ESP surface of the assembly will be determined.

In order to achieve enantioselective transformations, chiral enantiopure catalysts have to be developed. Therefore, the synthesis of chiral subunits of the general structure **141** will be attempted via mono-functionalization of **54b**, since their assembly is expected to provide a chirotopic internal environment (Figure 7b). Molecular modelling indicates the toleration of the Z-group by the hydrogen bond network of hexamer **XI**. Separation of the enantiomers formed by functionalization with achiral Z-groups will be attempted using chiral HPLC.

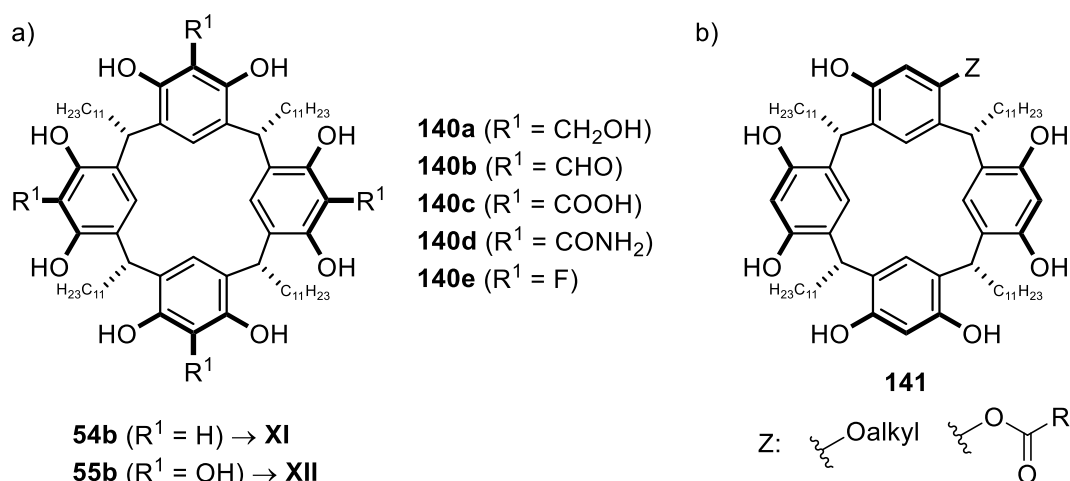


Figure 7: (a) Planned derivatives of the resorcin[4]arene monomer **54b**; (b) Chiral monomer **141**, prepared via mono-functionalization of **54b**.

6. Results and discussion

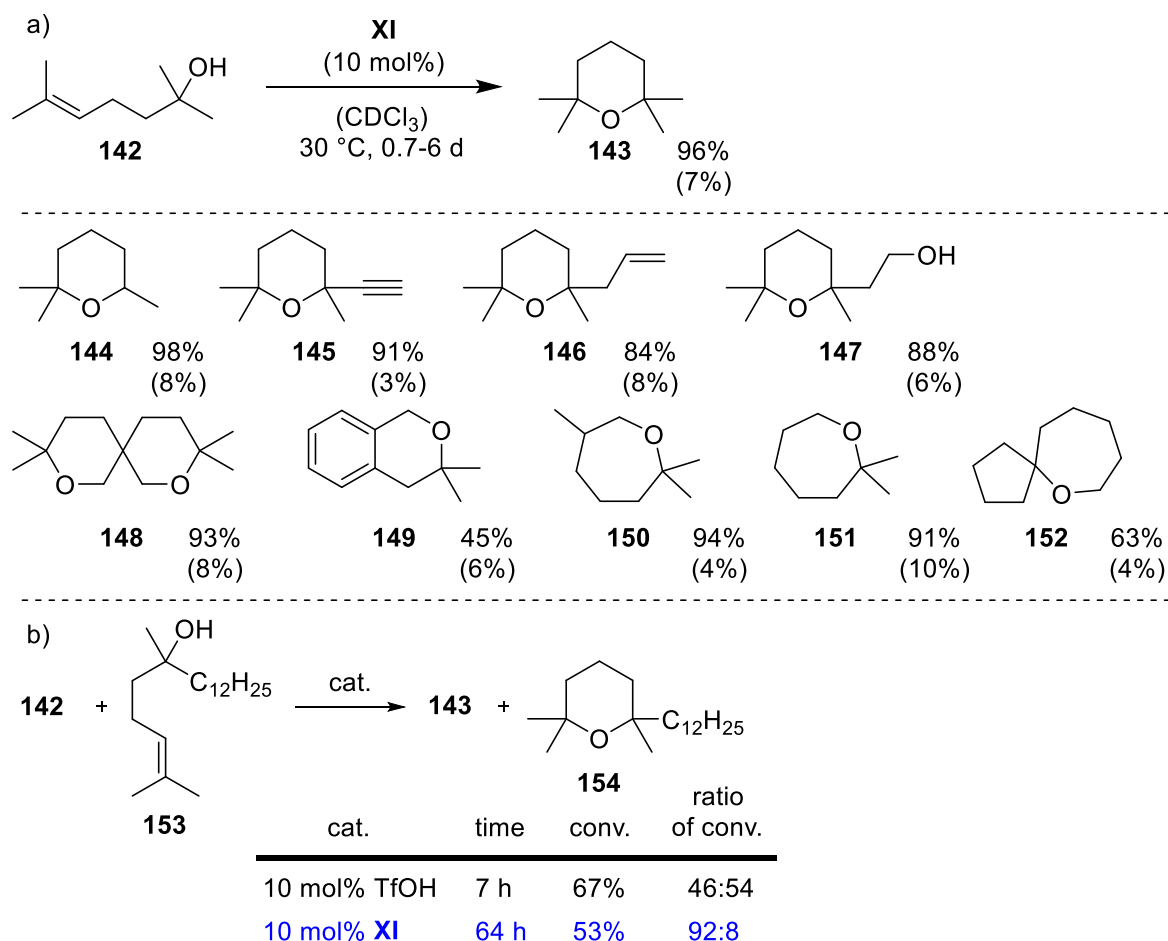
6.1 Publication summaries

This chapter functions as a short summary of the publications that were prepared during the course of this dissertation (excluding reviews, concept articles and co-authored publications (chapter 6.4)). At the beginning of this dissertation, only four examples of catalysis within self-assembled hydrogen bond-based structures were reported in the literature. The field has grown rapidly since then (see chapter 4.2).

6.1.1 Intramolecular hydroalkoxylation catalyzed inside a self-assembled cavity of an enzyme-like host structure¹⁵³

After successful catalytic application of the resorcin[4]arene hexamer **XI** in the cleavage of diethyl acetals, we set out to investigate its performance in the intramolecular hydroalkoxylation of unactivated alcohols, which show good uptake due to hydrogen bond interactions with the host. The resulting cyclic ethers were expected to show a low affinity to the cavity and thereby enable catalytic turnover. In a proof of concept experiment, 10 equiv. of alcohol **142** were added to a solution of hexamer **XI** in water-saturated chloroform (Scheme 38a). Encapsulation of the substrate was subsequently confirmed by ¹H NMR spectroscopy. The reaction was kept at 30 °C and monitored via NMR spectroscopy and GC analysis. After several days, formation of the desired cyclic ether **143** could be confirmed by isolation. Subsequent optimization showed that the rate of the reaction could be significantly increased by using regular chloroform instead of water-saturated one. It is believed that water molecules compete with the hydroxy group of the substrate for the protons of the catalyst. The low background reaction in the presence of tetrabutylammonium bromide (1.5 equiv.) provided good evidence that the reaction indeed proceeds within the capsule interior. Furthermore, no conversion was observed in the absence of the catalyst, which excluded a background reaction by DCI/HCl, which is present in chloroform due to photodegradation. We subsequently screened the scope of the reaction by employing different tetrahydropyran and oxepane precursors. The corresponding cyclic ethers **144-152** were usually obtained in good to excellent yields. Substrates bearing two hydroxy groups showed the highest reaction rates due to their strong affinity for the cavity. The reduced yield for cyclic ether **149** was ascribed to an oligomerization side reaction. Additionally, cyclic ether **152** was shown to exist in an equilibrium with its precursor under the reaction conditions. Substrates that would require the formation of an

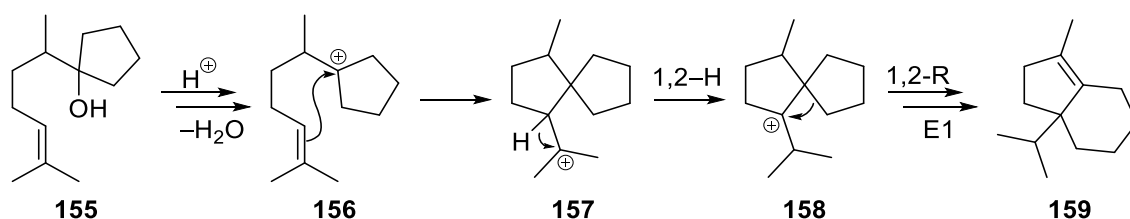
intermediary secondary cation showed no conversion under the applied reaction conditions. An attempt to favor the formation of a 13-membered cyclic ether via encapsulation failed, since the cavity is too large to induce significant folding of the substrate. The mild conditions employed in this study contrast the often harsh conditions required in solution. Although being a stronger Brønsted acid, acetic acid did not promote the reaction when utilized in catalytic amounts (10 mol%). The observed catalytic effect of hexamer **XI** is believed to result from the stabilization of reaction intermediates and transition states via cation- π interactions. The encapsulation-based conversion of the substrates was subsequently applied in the size-selective conversion of the small substrate **142** in the presence of its larger analog **153** (Scheme 38b). While the reaction proceeded highly selective in favor of the smaller substrate with hexamer **XI**, no selectivity was observed in solution with triflic acid as the catalyst.



Scheme 38: (a) Scope of the intramolecular hydroalkoxylation catalyzed by hexamer **XI** (conversions in the presence of 1.5 equiv. of TBAB in brackets); (b) size-selectivity achieved with hexamer **XI** that results in almost no formation of ether **154**.

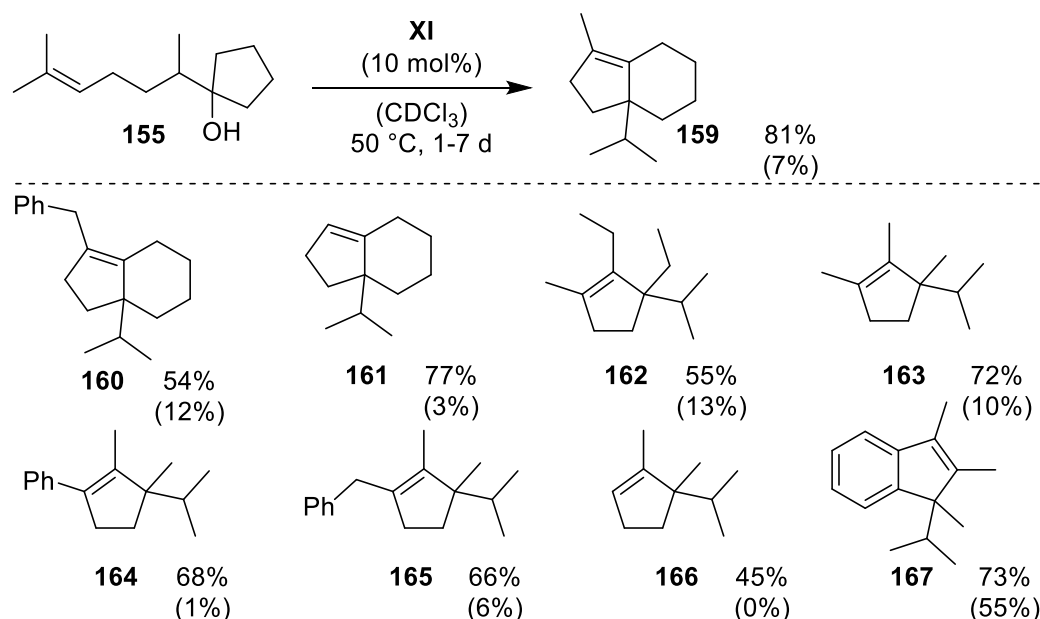
6.1.2 Host-catalyzed cyclodehydration-rearrangement cascade reaction of unsaturated tertiary alcohols¹⁵⁴

The concept of using hexameric assembly **XI** as a reaction chamber for unsaturated alcohols was further extended to a dehydrative cyclization-rearrangement cascade reaction. The strong delocalization of the negative charge via proton migration renders the deprotonated assembly a non-nucleophilic counteranion, which enables the investigation of cationic cascade reactions. Cyclization-rearrangement cascade reactions, similar to the depicted transformation of substrate **155**, have been shown to require an excess of Brønsted acid or to rely on expensive transition metal catalysts (Scheme 39). The reaction of substrate **155** proceeds via an initial protonation, followed by cleavage of water to yield cation **156**. An intramolecular attack of the double bond gives exocyclic cation **157**, which undergoes a 1,2-hydride shift. The formed cation **158** subsequently rearranges and the intermediary cation then eliminates to give compound **159** as the final product of the reaction cascade. We wondered if this reaction can be rendered catalytic by employing hexamer **XI** as a supramolecular catalyst.



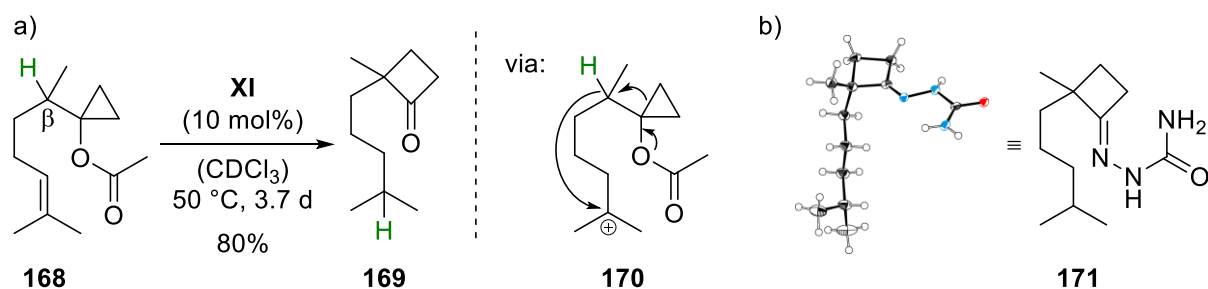
Scheme 39: Mechanism of the dehydrative cyclization-rearrangement cascade reaction of compound **155**.

To our delight, 10 mol% of hexamer **XI** were found to be sufficient to yield annulated cyclopentene **159** in 81% yield after 4 d at 50 °C. When hexamer **XI** was substituted by 10 mol% of trifluoroacetic acid (TFA), only 5% of product **159** were formed after 4 d at 50 °C, although the $\text{p}K_{\text{a}}$ of TFA is about five order of magnitude lower than that of hexamer **XI**. As in the previous study, addition of TBAB led to a significantly reduced product formation. Due to a lack of substrate scope in the literature, the formation of related cyclopentenes was investigated. In this course, several highly substituted cyclopentenes (**160-167**) could be formed in moderate to good yield (Scheme 40). However, the cyclobutyl and cyclopropyl analogs of substrate **155** failed to undergo the desired transformation. Evidence for a cavity-based conversion of the substrates was again provided by size-selective conversion.



Scheme 40: Scope of the hexamer **XI**-catalyzed cascade reaction (yields in the presence of 1.5 equiv. of TBAB in brackets).

Additionally, the influence of the leaving group was studied for substrates showing no or decreased product formation. The acetate group was chosen based on its positive effect on the THT cyclization within hexamer **XI**. Unfortunately, no substantial influence of the acetate group on the yield and the selectivity of the reaction was observed. However, in the case of substrate **168**, a completely different reaction path was induced (Scheme 41). The formed product was identified as cyclobutanone **169** via X-ray analysis of its derivative **171**. Product formation is believed to occur via cation **170**, which undergoes a concerted 1,5-hydride transfer and a ring expansion. Subsequent efforts were directed towards establishing this reaction as a general method for cyclobutanone formation starting from α -branched esters, which can be readily transformed to the corresponding cyclopropyl acetates in one step via *in situ* trapping of the Kulinkovich alcoholates with acetyl chloride. Unfortunately, variation of the β -residue led to unreactive substrates. Only a phenyl substituent in β -position gave rise to moderate cyclobutanone formation. Furthermore, substrates bearing the hydride acceptor at the leaving group failed to undergo the reaction, presumably due to insufficient orbital overlap in the transition state.¹⁵⁵

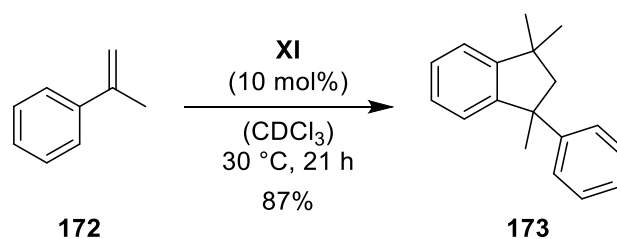


Scheme 41: (a) Hexamer **XI**-catalyzed cyclobutanone formation; (b) crystal structure of derivative **171**.

6.2 Application: Friedel-Crafts alkylation

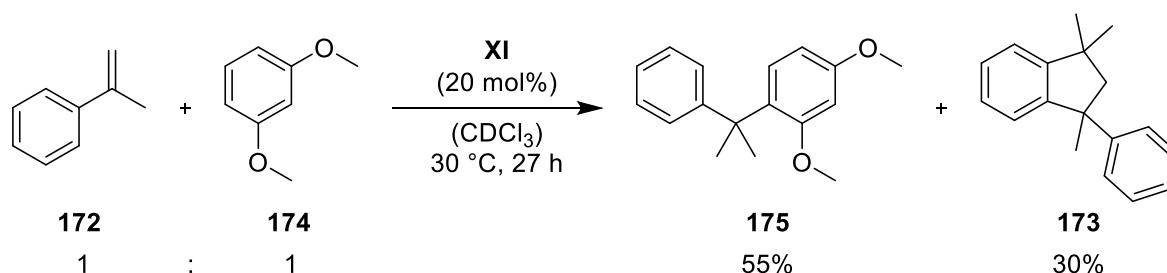
The Friedel-Crafts alkylation represents one of the oldest and most efficient methods for the functionalization of aromatic rings.¹⁵⁶ The original conditions relied on toxic and labile alkyl halides and stoichiometric or super stoichiometric amounts of Lewis acid. Ongoing research has replaced these conditions with catalytic processes under environmentally benign conditions.¹⁵⁷ Especially the use of alcohols or alkenes as electrophiles is desired, since only water or no byproduct is formed during the transformation.¹⁵⁸ Interestingly, despite the active research on catalytic methods, no valuable example of Friedel-Crafts chemistry within a supramolecular catalyst has been reported. Although gold-catalysis within hexamer **XI** has led to an unexpected intramolecular Friedel-Crafts cyclization (Scheme 30), the product is formed in low yield and together with side products. One of the potential advantages of performing Friedel-Crafts chemistry within a supramolecular host is the increased control over the regioselectivity. In addition, aromatic substrates usually show high affinity for hydrophobic cavities and often interact with the cavity surface via π - π interactions. Furthermore, the limited size of the cavity could be utilized to induce selective Friedel-Crafts oligomerizations. Intrigued by these conceptual advantages, some preliminary experiments have been conducted regarding hexamer **XI**-catalyzed Friedel-Crafts alkylations and are presented in the following.

An intermolecular Friedel-Crafts homodimerization was achieved within hexamer **XI** utilizing α -methylstyrene (**172**) as the substrate (Scheme 42). The reaction is highly selective at 30 °C and gives the dimeric species **173** in 87% according to ¹H NMR analysis. Furthermore, no conversion was observed in the presence of tetrabutylammonium bromide (2.4 equiv.). Dimerization was confirmed by comparing the ¹H NMR spectrum of the reaction mixture with literature data and by GC analysis (retention time shift). Interestingly, the reaction showed no conversion in benzene-*d*₆.



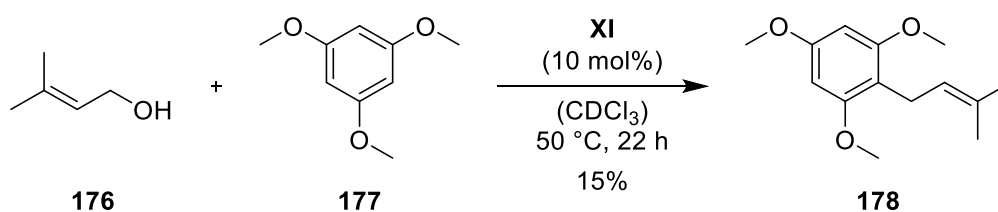
Scheme 42: Hexamer **XI**-catalyzed Friedel-Crafts homodimerization.

The homodimerization could be partially suppressed by addition of the electron-rich arene **174** (Scheme 43). Using 5 equiv. of each starting material, the hetero- and homoadduct were obtained in a ratio of 1.8:1. The structure of the heteroadduct **175** was verified by comparison of the ^1H NMR spectrum of the reaction mixture with literature data. The reaction was again completely inhibited by the addition of 2.4 equiv. of TBAB. The high selectivity for substitution in *o,p*-position is in accordance with the literature and results from directing and steric effects of the methoxy substituents. Complete suppression of the homodimerization might be achieved by using an excess of 1,3-dimethoxybenzene (**174**).



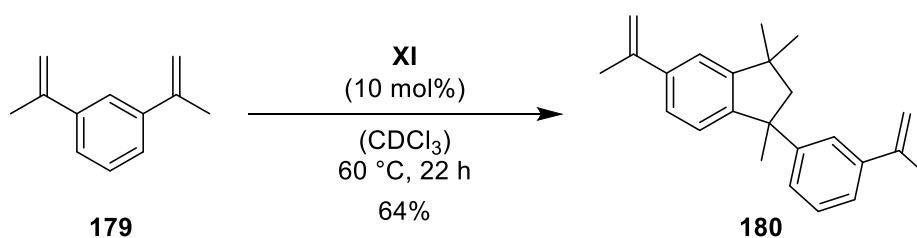
Scheme 43: Partial suppression of the homodimerization in the presence of 1,3-dimethoxybenzene (**174**).

Furthermore, the application of allylic alcohol **176** as the electrophile was investigated (Scheme 44). The starting materials were employed in a 1:1 ratio. Monitoring of the reaction via GC analysis showed complete conversion of the 10 equiv. of electrophile after only 1 h and about 12% yield of a substitution product. Addition of another 10 equiv. of alcohol **176** only led to a slight increase of the yield. Notably, a significant decrease in the conversion rate of the electrophile was observed. Both observations indicate a deactivation of the catalyst via alkylation of the phenol groups. Changing the ratio between electrophile and nucleophile to 1:3 resulted in an almost identical yield after a second addition of electrophile. The postulated product structure **178** is derived from comparison with similar reactions reported in the literature.¹⁵⁸ NMR analysis is required to confirm the product structure and to provide evidence for the alkylation of the catalyst. The reaction was additionally performed with *tert*-butanol as the electrophile. However, in this case no conversion of arene **177** was observed.



Scheme 44: Electrophilic aromatic substitution with an alcohol-based electrophile (yield not response factor-corrected).

Finally, a selective oligomerization of 1,3-diisopropenylbenzene (**179**) within the cavity of hexamer **XI** was attempted (Scheme 45). Due to very slow consumption of diene **179** at 30 °C, the reaction temperature was raised to 60 °C. Reaction monitoring via GC analysis indicated formation of a main product in 64% yield after 22 h, which is assumed to be compound **180** (see below). The yield derived from GC analysis only serves as an approximation because the response factor of the product is not known. Since the response factor mainly depends on the chemical formula, a significant difference between the response factors of compound **179** and **180** is expected. A NMR-based yield determination is prevented by the extensive overlap of signals. A conclusive structure verification via the ^1H NMR spectrum of the reaction mixture was not possible. However, comparison with data obtained from the dimerization of **173** strongly indicates formation of product **180**. It is noteworthy that a clear decrease in yield of product **180** was detected via GC after 6 d. This might indicate formation of a trimeric species, which can no longer be detected via GC analysis due to its high boiling point. Control reactions in solution with 60 mol% of TFA or 100 mol% of HCl in dioxane at 60 °C showed either no or only traces of product. The solution conditions have to be optimized in order to evaluate an encapsulation-derived product selectivity.



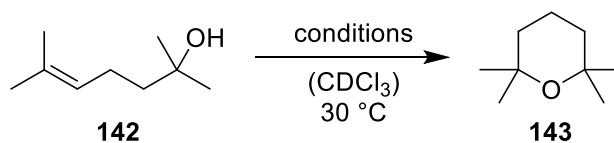
Scheme 45: Attempted oligomerization of diene **179** within the cavity of host **XI**.

6.3 Modulation: acid co-catalyst and photoacidity

Current drawbacks of the catalytic system **XI** comprise moderate reaction rates and a limited substrate scope due to the modest acidity of the assembly. The performed reactions within hexamer **XI** usually rely on the formation of intermediary tertiary or even better stabilized allylic/benzylic cations. This became especially evident during the studies on intramolecular hydroalkoxylation, when substrates requiring the formation of an intermediary secondary cation failed to react. In nature, enzymes often depend on noncovalently bound cofactors that enable, enhance or alter the catalytic process.¹⁵⁹ This analogy inspired the idea to utilize a noncovalently bound acid cofactor to increase the acidity of the hexameric catalyst system and additionally modify the available cavity space.

A short screening of Brønsted acids utilizing the cyclization of alcohol **142** as a model reaction revealed camphorsulfonic acid (CSA) ($pK_a = 1.2$)¹⁶⁰ as a suitable cofactor. Addition of 10 mol% of CSA to 10 mol% of hexamer **XI** resulted in full conversion of alcohol **142** after 24 h at 30 °C (Table 1). In comparison, 3.5 d were required in the absence of CSA to achieve full conversion. Remarkably, no conversion of alcohol **142** was observed with 10 mol% of CSA after 1 d if hexamer **XI** was omitted. Efficient binding of CSA to the cavity was expected due to its strong hydrogen donor and acceptor functionalities. This could be verified by ¹H NMR spectroscopy and a DOSY experiment (Figure 8). Titration of host **XI** with CSA furthermore indicated that at least two equiv. of CSA can be encapsulated by one hexamer unit. In addition, NMR data suggests strong competition between TBAB and CSA. This is also corroborated by 68% conversion of alcohol **142** in the presence of 1.5 equiv. of TBAB and 1.0 equiv. of CSA. A competition experiment between TBAB and CSA (ratio: 1.5/1) indicates co-encapsulation of both species (no free guest signals in the ¹H NMR) rather than replacement of TBAB by CSA.

Table 1: Influence of CSA on the hexamer **XI**-catalyzed intramolecular hydroalkoxylation of alcohol **142**.



entry	XI	CSA	TBAB	time	conv.
1	10 mol%	–	–	3.5 d	100%
2	10 mol%	–	15 mol%	3.5 d	7%
3	10 mol%	10 mol%	–	1 d	100%
4	10 mol%	10 mol%	15 mol%	1 d	68%
5	10 mol%	10 mol%	30 mol%	1 d	15%

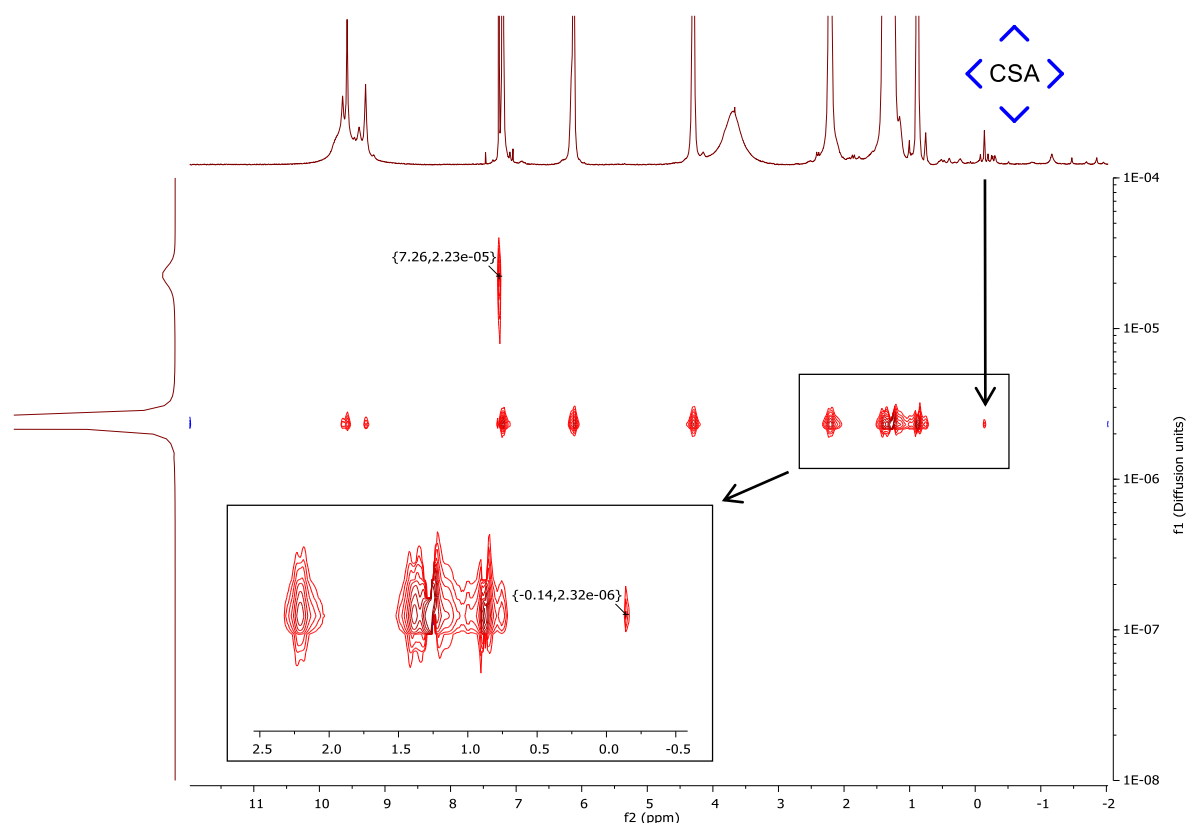
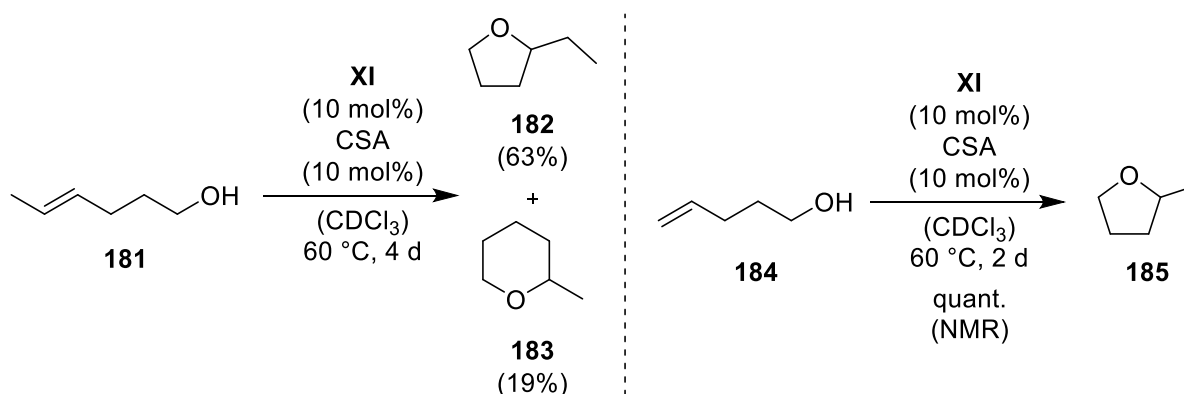


Figure 8: DOSY spectrum of hexamer **XI** (3.3 mM) with CSA (3.3 mM). The diffusion coefficients are given in cm^2/s .

The improved catalytic system was subsequently employed in reactions that proved difficult before (Scheme 46). At elevated temperature, substrates bearing di- or monosubstituted double bonds (**181** and **184**) underwent efficient cyclization to the corresponding cyclic ethers (**185** and **182/183**). It should be noted that at elevated temperature hexamer **XI** also yields small amounts of cyclic ether in the absence of CSA.



Scheme 46: Improved substrate scope utilizing 10 mol% of CSA as a co-catalyst (GC-based yields, not response factor-corrected).

In addition, the influence of CSA on the monoterpene cyclization was tested utilizing nerol (**19**) as the substrate. The reaction showed a significantly increased rate in the presence of 10 mol%

of CSA. However, the same products were formed as in the presence of the unmodified hexamer **XI**. The rigid structure of CSA favors the controlled modification of the cavity space, but its volume is too small to influence the conformation of the substrate within the cavity. The possible uptake of multiple CSA molecules into one cavity further restricts its use in controlled cavity modification. Nevertheless, the influence of CSA on the product distribution of the monoterpene cyclization has to be investigated more closely. Furthermore, it was so far not possible to prove that CSA is co-encapsulated with the substrate and that the protonation occurs within the cavity. Encapsulation of CSA was also attempted with the catalytically inactive pyrogallol[4]arene hexamer **XII**. However, even after short heating of a mixture containing 0.5 equiv. of CSA, no encapsulation was detectable in the ^1H NMR spectrum. An attempt to enforce encapsulation in an open flask via the melting approach published by *Purse et al.* failed due to decomposition of monomer **55b**.^{100a}

Irradiation of a supramolecular architecture represents an alternative, noninvasive method to modulate or enable its catalytic activity. Photoirradiation of hosts has been utilized to induce reactions of encapsulated guest molecules.¹⁶¹ In those examples, the excited host transfers the absorbed energy onto the substrate within the cavity, which subsequently undergoes a photochemical reaction. The molecular properties of the resorcin[4]arene hexamer **XI** are dominated by its phenolic moieties. Irradiation of phenols can result in a phenomenon that is called photoacidity.¹⁶² Photoacids are generally defined as Brønsted acids that show a remarkable drop in their $\text{p}K_{\text{a}}$ upon excitation to their first excited singlet state (S_1). Strong photoacids like cyano-naphthols can display a $\Delta\text{p}K_{\text{a}}$ of up to -12 upon excitation.¹⁶³ Photoacidity has been shown to be highly dependent on the substitution pattern of the photoacid and on the utilized solvent.¹⁶⁴ A postulated, but still debated, mechanism states that excitation is accompanied with an increased electronic redistribution from the phenolic oxygen into the aromatic ring. This abstraction of electron density weakens the O–H bond and thereby facilitates the proton transfer step.¹⁶² The excitation process can also give rise to radicals via homolytic O–H bond cleavage. Application of photoacidity in synthetic chemistry is mainly limited by the short lifetime of the proton dissociation state. The cleaved proton has not enough time to move away from its counteranion and therefore is unable to catalyze a chemical reaction. However, certain photoacids have been successfully applied to catalysis, for example in the acid-catalyzed Fischer esterification of acetic acid with ethanol.¹⁶⁵

Intrigued by this physical phenomenon, the possibility to significantly increase the acidity of phenol-based assemblies via irradiation was probed. The investigation was initiated by recording the UV/VIS spectra of resorcin[4]arene hexamer **XI** and pyrogallol[4]arene hexamer **XII** (Figure 9). According to literature, the high dilution required for UV/VIS spectroscopy is still sufficient to provide a high degree of assembled hexamer.^{104,166} In contrast to hexamer **XII**, the UV/VIS spectrum of hexamer **XI** shows a defined local maximum at 287 nm. The spectrum of hexamer **XI** remained nearly unchanged in the presence of TBAB (1.5 equiv.). No changes or new absorption bands arising from host-guest interactions could be observed.

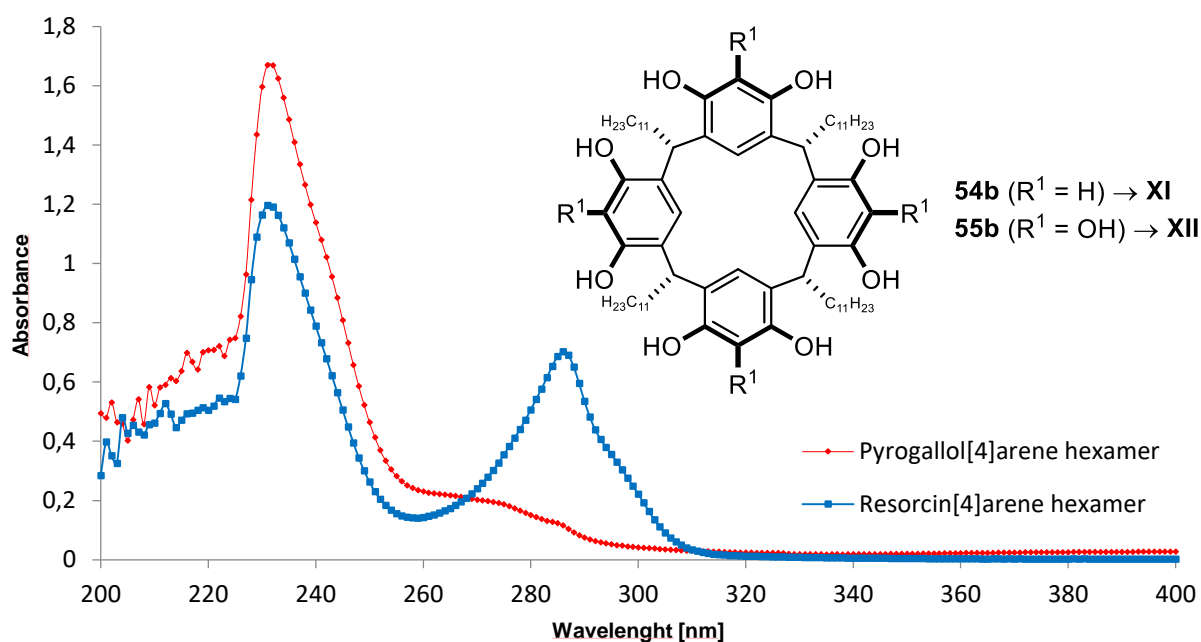
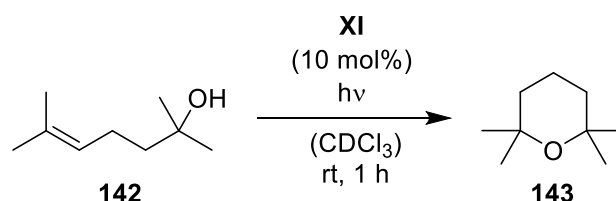


Figure 9: UV/VIS spectra of resorcin[4]arene hexamer **XI** (83 μ M) and pyrogallol[4]arene hexamer **XII** (83 μ M) in CDCl₃.

The stability of hexamer **XI** at 300 nm was indicated by comparison of the ¹H NMR spectra obtained before and after 1 h of irradiation. To study the influence of irradiation on the catalytic performance of hexamer **XI**, the intramolecular hydroalkoxylation of alcohol **142** was performed at different wavelengths. The stability of alcohol **142** in chloroform under irradiation is assumed, since in a control experiment the highly reactive nerol (**9**) remained sufficiently stable over an extended period at 300 nm (6% conversion after 1 h). As evident from Table 2, irradiation of the reaction mixture led to a strong acceleration of substrate conversion. In accordance with the recorded UV/VIS spectrum, the effect was most prominent at 254 nm and 300 nm. The acceleration at 350 nm and 366 nm, despite the lack of absorbance in this region, likely results from weak emission bands at 300 nm of the employed lamps. Although an acceleration of the conversion could be achieved via irradiation, the performed reactions

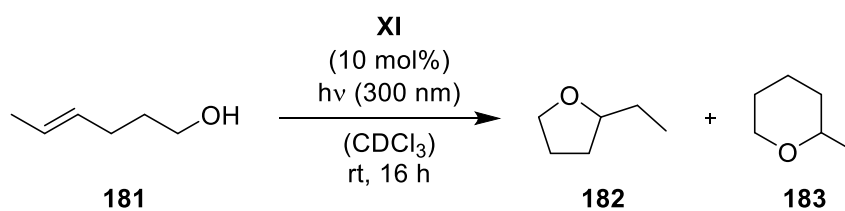
suffered from increased side reactions and reduced overall yields. The reduced selectivity is believed to partly arise from radical processes initiated by homolytic cleavage of the phenolic O–H bonds. This could also facilitate catalyst alkylation, which might explain the reduced total yield in entry 4 (see also Table 3).

Table 2: Influence of the wavelength on the hexamer **XI**-catalyzed cyclization of alcohol **142**; *(30 °C, 3.5 d); GC-based yields (response factor-corrected for product **143**); the reaction mixture turns reddish at 254 nm and 300 nm; sp = side products.



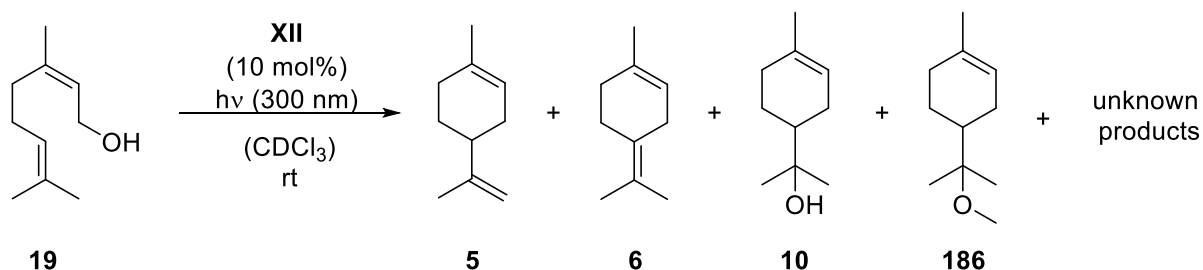
entry	nm [λ]	conv. [%]	yield [%] (ether)	yield [%] (sp)
1	–	1	–	–
2*	–	100	96	–
3	254	97	29	66
4	300	87	44	27
5	350	20	14	–
6	366	29	23	–

To gain further insight on the extent of the observed effect, the cyclization of hydroxy olefin **181** was investigated under irradiation. At room temperature, compound **181** shows no conversion in the presence of catalytic amounts of hexamer **XI**. To achieve the highest possible effect, irradiation was performed closest to the local absorption maximum at 300 nm. Indeed, after 16 h at room temperature, low amounts of cyclic ethers could be detected via GC analysis (Table 3, entry 1). GC analysis furthermore indicated – based on the observed retention time shift – significant formation of diol side products. However, significant conversion and traces of product could also be observed when the cavity was blocked by addition of 1.5 equiv. of a tetraalkylammonium guest. This result indicates a very strong increase of the phenol acidity under irradiation, which enables conversion on the outer surface, assuming the intactness of the assembly at 300 nm. Nevertheless, to harvest the advantages of supramolecular catalysis, the reaction is required to proceed within the cavity. A possible strategy to ascertain the presence of the hexameric structure under irradiation is the encapsulation of a catalyst by the host, which becomes inactive within the cavity. A shut down of the reaction would provide evidence that high energy photons do not cause disassembly of the structure.

Table 3: Conversion of hydroxy olefin **181** at room temperature under irradiation.

entry	TBAB (equiv.)	conv. [%]	yield [%] (ethers)	yield [%] (diols)
1	–	60	6	23
2	1.5	41	1	15

The effect of irradiation was also examined with pyrogallol[4]arene hexamer **XII** using nerol (**19**) as the substrate. In contrast to host **XI**, pyrogallol[4]arene hexamer **XII** is completely inactive in THT cyclizations. However, after 16 h of irradiation, several cyclic monoterpenes could be observed in the gas chromatogram of the reaction mixture (Table 4). The reaction was repeated in the presence of 1000 equiv. of methanol to inhibit the self-assembly process. Again, cyclic monoterpenes could be detected via GC analysis. This shows that the reaction does not rely on the presence of the hexameric assembly. Furthermore, cyclization could also be achieved with 1,2,3-trihydroxybenzene under irradiation. It is noteworthy that nerol is known to be able of unselective cyclization in solution due to its (*Z*)-configuration-derived reactivity. To conclude, photoacidity could be observed with the examined compounds. A useful application of the effect, however, could not be achieved due to the increased occurrence of side reactions and the uncontrollable background reaction. Yet, photochemical transformations within hexamer **XI** and **XII** are still underexplored and remain worthwhile to investigate.

Table 4: Influence of irradiation on the activity of the pyrogallol[4]arene hexamer **XII**.

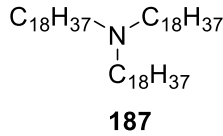
entry	conv. [%]	yield [%] (5)	yield [%] (6)	yield [%] (10)	yield [%] (186)	time	comment
1	78	18	9	18	–	16 h	–
2	86	14	-	10	35	18 h	+1000 equiv. MeOH

6.4 Elucidation: reasons for the catalytic inactivity of the pyrogallol[4]arene hexamer **XII**

The development of novel hydrogen bond-based catalysts for the THT cyclization requires a thorough understanding of the catalytically active system **XI**. To elucidate the responsible mechanisms for the catalytic activity, we compared the properties of hexamer **XI** with the properties of the closely related but catalytically inactive system **XII** (experiments mostly conducted by Qi Zhang).⁸⁸

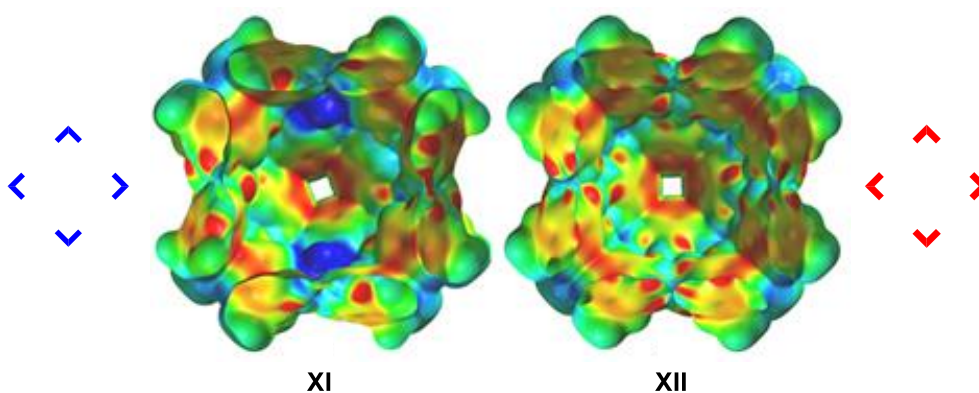
The proposed catalytic cycle of the THT cyclization within hexamer **XI** consists of four defined steps: uptake of the substrate, activation by protonation, cyclization via cation- π stabilized transition states and release of the product species. Hexamer **XII** is known to show a different uptake behavior than hexamer **XI**. Therefore, as a first step, an inability of substrate uptake had to be excluded. As evidenced by ^1H NMR and DOSY spectroscopy, hexamer **XII** is in fact capable of encapsulating the acyclic monoterpene nerol (**19**). For that reason, the catalytic inertness of hexamer **XII** had to be the result of a different characteristic. Next, we investigated a possible lack in cation- π stabilization, indicated by the inability of hexamer **XII** to encapsulate ammonium salts.⁹⁶ This inability is puzzling considering the reported encapsulation of tertiary amines by hexamer **XII**. We therefore reinvestigated the uptake of differently sized tertiary amines by hexamer **XII** and could show that the amines, in accordance with our previous findings for hexamer **XI**, are encapsulated in their protonated form. Furthermore, a decrease in degree of protonation and uptake could be observed for amines bearing longer alkyl chains, which is consistent with reduced cation- π interactions due to shielding of the cationic charge. This led to the conclusion that hexamer **XII** is also capable of stabilizing cations via cation- π interactions. This conclusion was further corroborated by DFT calculations, which attributed hexamer **XII** an even stronger cation stabilizing effect than hexamer **XI**. This made the inability of hexamer **XII** to encapsulate ammonium salts and the reported repulsion of an encapsulated amine after addition of a strong acid even more contradicting. We subsequently screened the uptake of differently sized ammonium salts by hexamer **XII** in chloroform solution to elucidate the molecular mechanisms behind this observed behavior (Table 5). Interestingly, the small ammonium ion Et_4NBr was found to be encapsulated to a considerable degree, but precipitation of a 2:1 host-guest complex prevented accurate quantification. But in accordance with the literature, the larger ammonium ions completely rejected encapsulation by **XII**.

Table 5: Encapsulation studies with hexamer **XI** and **XII** utilizing 1.0 equiv. of ammonium salt.

entry	ammonium salt	encapsulation degree of the cation by			
		XI	XII	XII , after addition of 187	
1	Et ₄ NBr	100%	nd*	nd*	 $\text{C}_{18}\text{H}_{37}-\text{N}-\text{C}_{18}\text{H}_{37}$ $\quad \quad \quad $ $\quad \quad \quad \text{C}_{18}\text{H}_{37}$ 187
2	<i>n</i> -Pr ₄ NBr	100%	4%	46%	
3	<i>n</i> -Bu ₄ NBr	100%	0%	30%	
4	<i>n</i> -Hex ₄ NBr	41%	0%	10%	

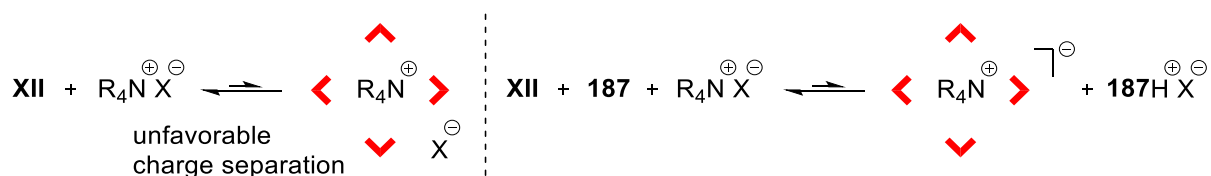
*precipitation occurred (2:1 complex)

An explanation for this behavior was found by closer inspection of the differences in the inner ESP surfaces of hexamer **XI** and **XII** (Figure 10). In contrast to hexamer **XII**, the inner surface of hexamer **XI** features areas of high potential (blue), which are evoked by the hydrogen atoms of the incorporated water molecules. We speculated that hydrogen bonding via these hydrogen atoms could stabilize the counteranions of the encapsulated ammonium salts in host **XI** and thereby explain its significantly higher affinity for ammonium salts. Interestingly, also DFT calculations confirmed a weaker binding of ammonium salts in hexamer **XII**, despite its higher stabilizing effect on cations. Intrigued by this finding, we investigated if anions are encapsulated at all by hexamer **XII**. For this purpose, we studied the encapsulation of the NMR active mesylate anion by adding EtPr₃N⁺MeSO₃⁻ to the solutions of each hexamer. Indeed, while hexamer **XI** showed uptake of the mesylate anion, no uptake was observed in the case of hexamer **XII**. Therefore, the low affinity of ammonium cations towards neutral **XII** might result from the required enthalpically unfavorable charge separation in chloroform.

**Figure 10:** Inner ESP surfaces of hexamer **XI** and **XII** (cross sections).⁸⁸

We speculated that the encapsulation problem might be overcome by addition of the amine base **187** (Table 5), which is sterically too hindered for encapsulation. Protonation of amine **187** on

the outer surface of hexamer **XII** would generate a negatively charged host structure, which could then encapsulate the ammonium cation without an overall charge separation, since the bromide ion would be saturated in solution by the protonated form of amine **187** (Scheme 47). Indeed, the uptake of ammonium cations by host **XII** could be significantly increased by addition of amine **187** (Table 5).



Scheme 47: Strategy utilized to increase the uptake of ammonium cations by hexamer **XII** in chloroform-*d*₁.

Having shown that hexamer **XII** is capable of cation stabilization, we shifted our focus on a possible lack of substrate activation via protonation to explain its catalytic inertness. The hydroxy functionality of the substrate is significantly less basic than the amine functionality and the acidity of hexamer **XII** might not be sufficient for the protonation step. The pK_a of hexamer **XII** was subsequently determined by measuring the deprotonation ratio in the presence of various amines of known pK_a . The thus measured pK_a of 9.5–10 is remarkably higher than that of hexamer **XI** ($pK_a \approx 5.5$ –6). Additional DFT calculations confirm the lower acidity of hexamer **XII** and indicate a decreased delocalization of the negative charge. The lower acidity might also be caused by multiple mesomeric destabilizations of the negative charge by the *ortho*-hydroxy substituents. This effect is also observed in 1,2-dihydroxybenzene ($pK_a = 9.48$),¹⁴⁵ which has a slightly higher pK_a than 1,3-dihydroxybenzene ($pK_a = 9.44$),¹⁴⁵ despite the possible stabilization of the anion via hydrogen bonding. Therefore, the inability of hexamer **XII** to activate the substrate via protonation is believed to be the reason behind its catalytic inertness. This lack in acidity cannot be overcome by simple addition of an acid co-catalyst, since the thus formed ion pair resists encapsulation due to the required, energetically unfavorable charge separation.

6.5 Derivatization: towards new hydrogen bond-based supramolecular catalysts

6.5.1 Inherently chiral mono-functionalized *C*-undecylcalix[4]resorcinarenes

In the biosynthesis of terpenes, cyclases transfer stereochemical information onto the prochiral olefinic carbons of the acyclic substrate.⁹ This induction of stereoinformation represents one of the key features of enzyme catalysis and remains so far unmatched by artificial enzyme mimics, although some progress has been made utilizing enantiopure assemblies.^{65,167} In order to perform the hexamer **XI**-catalyzed THT cyclizations in an enantioselective fashion, chiral optically active derivatives of the resorcin[4]arene hexamer have to be developed. Currently there are no reports of enantiopure hexameric assemblies related to structure **XI**. Although the resorcin[4]arene subunit **54b** is achiral, the self-assembled hexameric structure is in fact chiral. However, due to fast racemization in solution, no optically active product can be obtained. Therefore, enantioselective catalysis requires the synthesis of an inherently chiral resorcin[4]arene monomer. The synthesis of chiral, enantiopure resorcin[4]arene derivatives has been reported in literature, but no investigations regarding their self-assembling properties have been performed.¹⁶⁸ This mainly results from their insolubility in non-competitive solvents that allow hydrogen bond formation or from synthesis strategies that involve permanent protection of the phenolic moieties. In general, two major strategies can be envisioned to generate inherently chiral resorcin[4]arene building blocks that are in principle capable of self-assembly:

- 1) **Mono-(de)functionalization:** This strategy involves either the selective functionalization of one of the eight phenolic groups or the selective defunctionalization (removal) of a single phenolic group. Mono-functionalization requires the use of functional groups that are tolerated by the hydrogen bond network and still allow hexamer formation. Molecular modelling indicates that mono-alkylation as well as mono-acylation should be tolerated by the hexameric assembly. Mono-substitution of a phenolic group with a hydrogen bond donor/acceptor like a carboxylic acid or an amide could be feasible via transformation of the corresponding mono-triflate. The mono-triflate species should also allow access to the mono-defunctionalized derivative using deoxygenation methodologies. Functionalization with achiral electrophiles will result in the formation of both enantiomers, which have to be separated via chiral HPLC. Application of chiral, enantiopure electrophiles would not only facilitate the separation process by the formation of diastereoisomers but also increase the chance of chiral induction by installation of a second chiral element.

- 2) **Tetra-substitution:** An alternative strategy relies on creating axial chirality by substitution of four phenol moieties in an either clockwise or counterclockwise fashion.^{168c} This cyclochirality is in principle already present in the resorcin[4]arene monomer **54b**, created by the directional sense of the intramolecular hydrogen bond array.¹⁶⁹ The substituents need an incorporated hydrogen bond donor/acceptor motif, in order to compensate the loss of the phenol moieties and to allow for self-assembly (Figure 11).

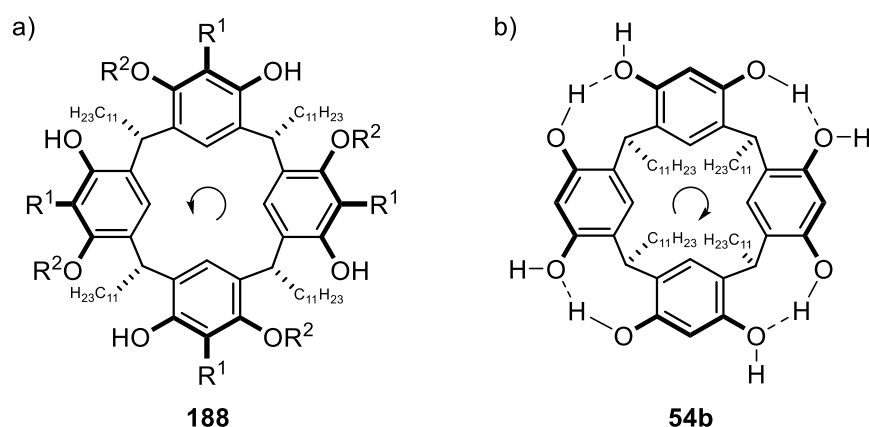
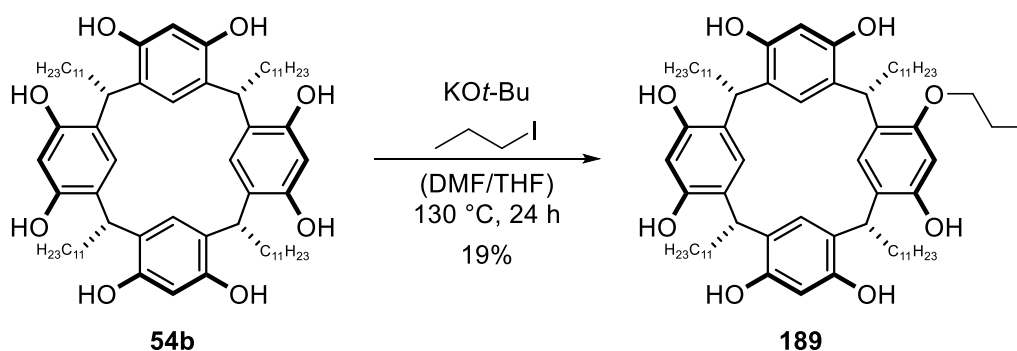


Figure 11: (a) General structure **188** of a C₄-symmetric chiral resorcin[4]arene; (b) one possibility of intramolecular hydrogen bonding in the resorcin[4]arene monomer.

In addition, chirality can also be installed at the alkyl chains (“feet”), but chiral induction is unlikely due to the distance to the reaction center. The following chapter summarizes attempts to achieve mono-functionalization of the resorcin[4]arene monomer **54b**.

Synthesis of a mono-alkylated resorcin[4]arene was described by *Dvořáková* and *Čajan* via selective defunctionalization of an octa-alkylated precursor.¹⁷⁰ However, utilizing a modified procedure of *Menger et al.*,^{168b} mono-propylation could be achieved by using 1.3 equiv. of electrophile and base (Scheme 48). The desired product **189** could be separated from the unreacted starting material and multi-alkylation products via column chromatography. Brownish impurities could be removed via a subsequent recrystallization from methanol. Removal of solvent residues was achieved under high vacuum at 55 °C overnight. In general, solvent molecules have a high tendency to stick to resorcin[4]arene derivatives, usually via hydrogen bonding interactions with the phenol moieties. Furthermore, some degree of product loss is believed to occur during extraction, given the poor phase-separation based on the tenside like character of C₁₁-resorcin[4]arenes.



Scheme 48: Mono-propylation of resorcin[4]arene **54b**.

The purity of the compound was confirmed by recording a ^1H NMR spectrum in acetone- d_6 , which inhibits the self-assembly process (Figure 12). The propyl residue is clearly visible and the integrals fit well to the desired product. The water signal can be seen at 2.92 ppm. The reduced integral of the phenolic OH-groups likely arises from hydrogen-deuterium exchange with acetone- d_6 . The origin of the singlet at 7.24 ppm is unclear, but it might represent a shifted phenolic OH-group, since it can be seen in every produced batch of this compound. Isolation of the desired product was further verified by HRMS measurement.

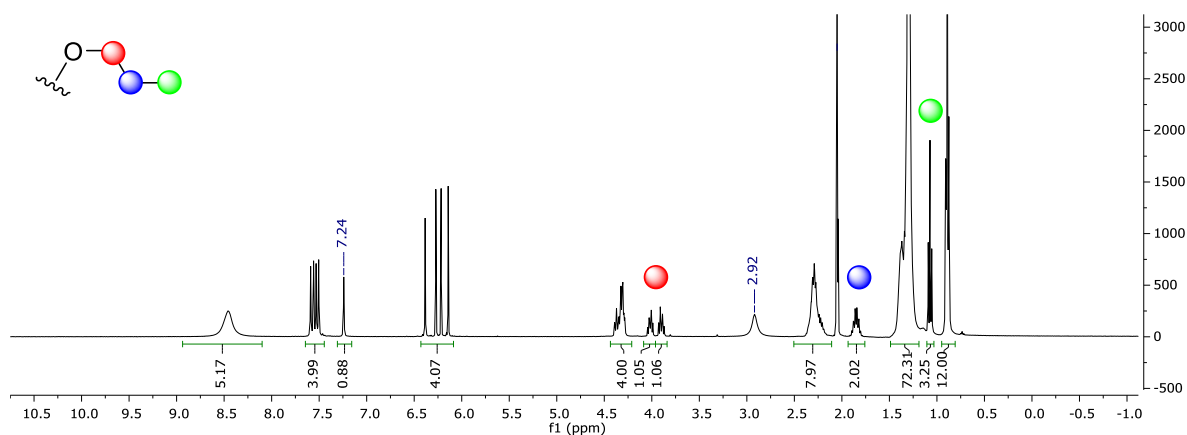


Figure 12: ^1H NMR spectrum of the mono-propylated resorcin[4]arene **189** in acetone- d_6 . For a reference ^1H NMR spectrum of compound **54b** in CDCl_3 , including assignment, see Figure 25b.

Efforts were subsequently directed towards the separation of the two enantiomers via chiral HPLC. Unfortunately, all in-house attempts to separate the enantiomers failed. The best separation was obtained externally by *Daicel* after intensive screening of columns and conditions (Figure 13). However, also in this case, no baseline separation could be achieved. Therefore, subsequent studies were performed with the racemic mixture. It has to be mentioned that the self-assembly process can be strongly influenced by the optical purity of the building block, as recently demonstrated by *Mastalerz et al.*⁸³

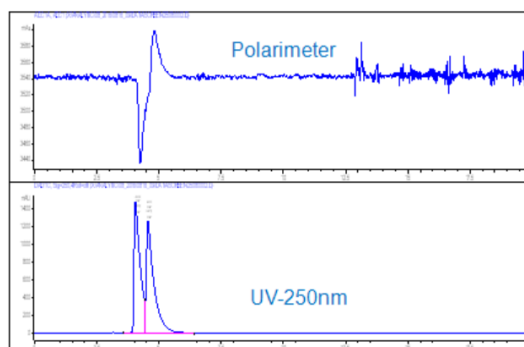


Figure 13: Best separation achieved for the enantiomers of compound **189** (CHIRALPAK® IF (250×4.6/5 μm); heptane/EtOH = 90/10; 1 mL/min; 25 °C)

The self-assembling properties of compound **189** were studied via NMR spectroscopy in deuterated chloroform. Figure 14a shows the ^1H NMR spectrum obtained after dissolving the compound in regular CDCl_3 after drying under high vacuum at 55 °C. The compound showed a high solubility, which usually indicates a sufficient water content for the self-assembly. The signals at around -0.5 ppm provide evidence that the propyl groups are partly directed into the cavity. In addition, the solution appears to contain a mixture of assemblies, which is to be expected considering the multitude of possible stereoisomers and regioisomers (orientation of the functionalized monomers towards each other). Interestingly, when the compound was dissolved in water-saturated chloroform, a more defined spectrum was obtained. The increase in order was also observed by a small change of the mean diffusion value from 0.21 to $0.20 \times 10^{-5} \text{ cm}^2\text{s}^{-1}$. According to modeling, water is believed to be still part of the assembly despite the introduced defects. It appears likely that the water content directly after drying was too low to ensure optimal self-assembly. The sample in water-saturated chloroform was monitored over an extended period to see if the equilibrium was already established. No change in the ^1H NMR and the diffusion value was detected over time and even after heating the sample to 50 °C, which indicates that equilibrium is reached rapidly. To further probe the formation of supramolecular assemblies, tetrabutylammonium bromide (1.5 equiv. relative to an assumed hexamer) was added to the solution of compound **189** in water-saturated chloroform. The appearance of broad signals between 0.50 and -2.50 ppm further corroborated the assumed self-assembly. Furthermore, no signals of free ammonium guest are visible in the spectrum.

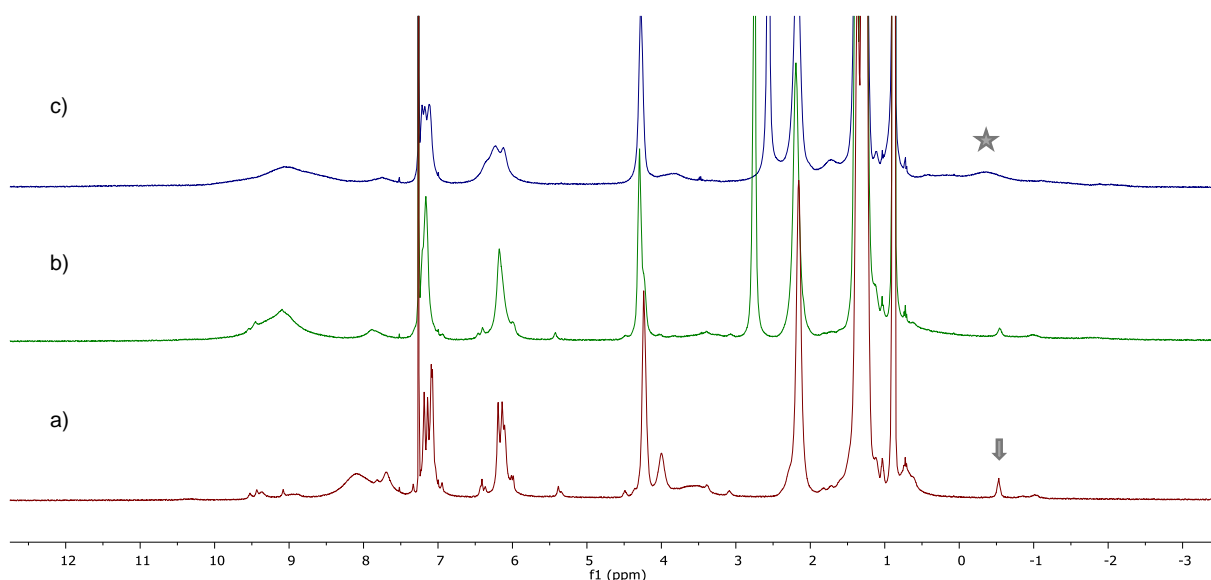


Figure 14: ¹H NMR spectrum of a solution of compound **189** in (a) regular CDCl₃ (supposed signals of inwards directed propyl groups marked with an arrow), (b) water-saturated CDCl₃ and (c) water-saturated CDCl₃ in the presence of 1.5 equiv. of TBAB (encapsulated TBAB marked with a star).

To test if the formed assemblies are still catalytically active in the THT cyclization, small scale reactions were performed with 10 equiv. of nerol (**19**), geraniol (**18**) and geranyl acetate (**138**) in regular CDCl₃ at 30 °C. It is noteworthy that attempts to increase the water content of compound **189** by equilibration in an open flask were not successful. Even after 2 d of open storage, the recorded ¹H NMR in regular CDCl₃ looked identical to that depicted in Figure 14a. In the case of nerol (**19**), after 7 d slow but significant conversion (55%) to α -terpineol (**10**) (16%), limonene (**5**) (10%), α -terpinene (**7**) (7%) and terpinolene (**6**) (6%) as the main products was observed. The product species were characterized by comparison with the internal GC retention time database. The slow reaction rate might result from the low equilibrium concentration of hexameric structures at the given water content, as indicated by the slightly higher diffusion value (see above). The experiment utilizing geraniol (**9**) as the starting material yielded only small amounts of linalool (**20**) (6%) after 7 d. No other products were formed in considerable amounts. Also when employing resorcin[4]arene hexamer **XI** as the catalyst, linalool (**20**) represents the initial main product in the cyclization of geraniol (**18**). Using geranyl acetate (**138**) as the substrate, only traces of product were observed, even after 7 d. The lower reactivity of geranyl acetate (**138**) compared to geraniol (**18**) is in accordance with previous findings.¹⁴ In parallel performed experiments in water-saturated, acid-free (filtered through basic alumina) CDCl₃ showed no conversion after 7 d. This is partly based on the negative influence of a high water content on the reaction rate, as observed before. Additionally, recent internal discoveries indicate a significantly higher influence of HCl traces (present in CDCl₃) on the reaction as previously assumed. HCl does not catalyze the reaction, as

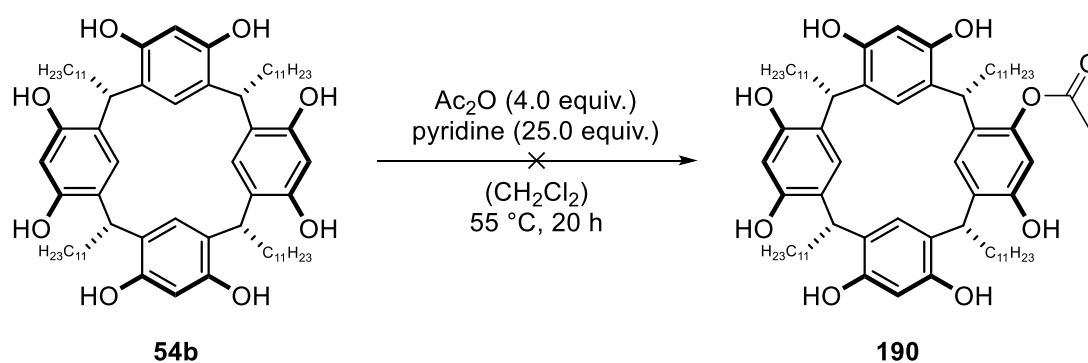
demonstrated by control experiments, but might be beneficial/essential for the substrate activation step.

The diminished reactivity observed in these preliminary experiments could also result from a change in the inner ESP surface or the acidity of the assembled structures. The inner ESP surface of the assemblies is unlikely to change significantly by alkylation of in total six phenolic OH-groups. However, the acidity could change due to the introduced defect into the hydrogen bond network. Unfortunately, application of the established pK_a determination method via protonation experiments with a series of amine bases is not possible in this case,¹¹⁴ due to extensive signal broadening and overlap in the presence of an amine base. This problem is also observed with other derivatives of **54b**, and therefore establishing an alternative method for the pK_a determination of the derivatives should be considered essential.¹⁷¹ Spectrophotometric methods that rely on the change of the UV/VIS spectrum of an indicator with known pK_a might represent possible alternatives.¹⁷²

To conclude, the ensemble of assemblies formed from compound **189** (= (**189**)₆) shows catalytic activity in the THT cyclization of nerol (**19**), but the activity is significantly reduced compared to the unfunctionalized hexamer **XI**. In the future, the experiments should be performed in water-saturated CDCl₃ with small amounts of added HCl. In addition, experiments have to be performed with an enantiopure mono-alkylated derivative in order to study the influence of inherent chirality on the enantioselectivity of the reaction. Since separation of the mono-alkylated enantiomers proved impossible, the mono-alkylation has to be repeated with an enantiopure alkylating agent. This would facilitate the separation and could improve the self-assembly process.^{83,168e} Enantiopure epoxides or cyclic carbonates might represent appropriate, commercially available electrophiles for this investigation. The feasibility of mono-alkylation of the resorcin[4]arene monomer via epoxide opening has already been demonstrated in the literature.¹⁷³

In addition to mono-alkylation, the mono-acetylation of building block **54b** was investigated. However, in contrast to the straightforward synthesis and isolation of product **189**, a successful mono-acetylation of **54b** could not be achieved in the course of this work. This is surprising, since peracetylation of **54b** is described in the literature and could be successfully reproduced.¹⁷⁴ Mono-acetylation is not described in the literature, but synthesis and HPLC-purification of the alternate (1,3,5,7) tetra-acetylated **54b** is described via a different route.^{168a}

A TLC-based optimization of the stoichiometry of acetic anhydride and pyridine led to the conditions depicted in Scheme 49. Under these conditions, mainly mono- and di-acetylated product was formed according to TLC analysis. However, the desired product **190** could not be isolated by purification via column chromatography. Decomposition on silica is unlikely, but cannot be completely ruled out and is supported by TLC analysis performed during the chromatographic operation. A lack of personal access to ESI-MS analysis at that time additionally complicated the evaluation of the progress.



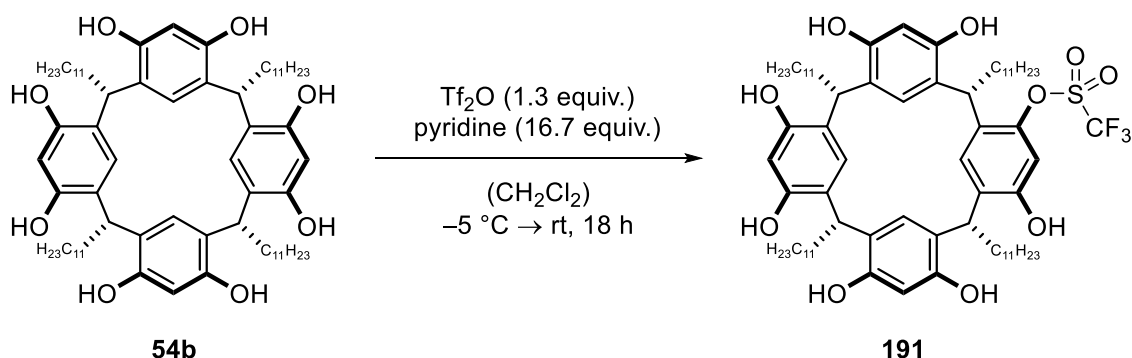
Scheme 49: Failed attempt to synthesize the mono-acetylated resorcin[4]arene **190**.

It is noteworthy that mono-acylated products might be prone to racemization via a shift of the residue from one phenolic OH-group to another. The possibility of such a transformation is implied by the literature.^{168e}

Only a few experiments were conducted regarding the mono-triflation of monomer **54b**. The resulting mono-triflate would be a useful starting point for palladium chemistry. No examples of mono-triflation of resorcin[4]arenes are reported in the literature, but the pertriflation of *n*-hexyl resorcin[4]arene and some tetra-triflation procedures are documented.^{168c,175} An example for a mono-sulfonylation of **54b** was reported by *Mattay et al.* utilizing enantiopure (*S*)-(+)-10-camphorsulfonyl chloride.^{168e}

The most promising result regarding mono-triflation was achieved when utilizing 1.3 equiv. of triflic anhydride and an excess of pyridine (Scheme 50). According to TLC analysis, the reaction yielded almost exclusively the mono-functionalized product aside from unreacted starting material. TLC analysis furthermore showed that the assumed product is stable under the applied work-up conditions. Half of the isolated crude product was subsequently subjected to column chromatography. The stability of the desired product on silica is unclear and the literature only reports on purification of the resorcin[4]arene triflates via recrystallization.

However, separation of the mono-functionalized product from the starting material via recrystallization is believed to be difficult due to similar solubility.



Scheme 50: Most promising reaction conditions for the mono-triflation of compound **54b**.

The separation proved challenging due to an almost co-eluting compound. The obtained ^1H NMR of the isolated compound in acetone- d_6 is depicted in Figure 15. Besides the low overall purity, significant amounts of pyridine are visible in the spectrum. However, the integrals fit quite well to the desired product structure and the splitting resembles the pattern obtained for the mono-alkylated product **189** (Figure 12). Except for a small impurity, the ^{19}F NMR of the isolated compound in acetone- d_6 shows a single peak at -75.1 ppm. This chemical shift is identical to the chemical shift reported for the octa-triflate derivative, however the literature data was obtained in deuterated chloroform. The phenolic OH-groups appear as a very broad signal with a center at around 8.50 ppm. The broadening is believed to result from the presence of pyridine. Due to the small amount of isolated material, no further analysis could be performed.

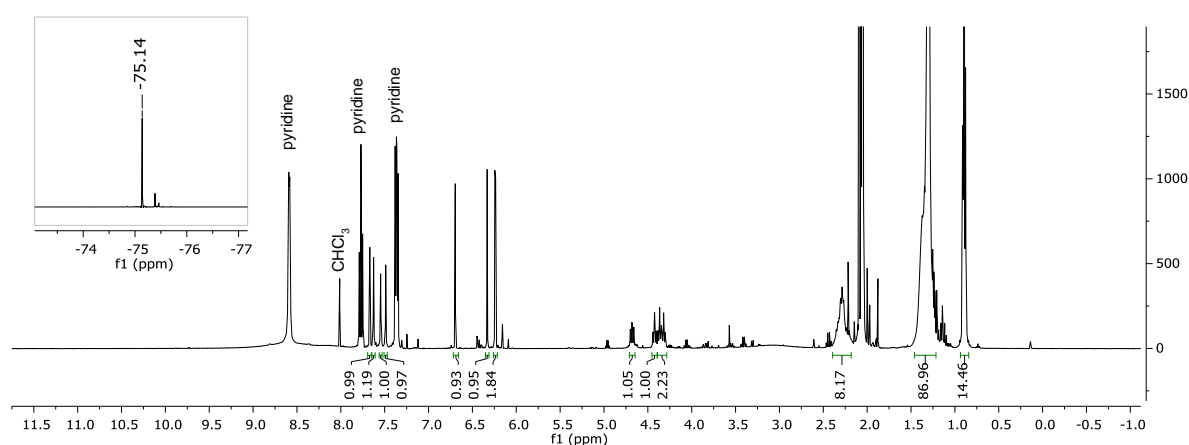


Figure 15: ^1H NMR spectrum in acetone- d_6 of the isolated compound after column chromatography; section of the ^{19}F NMR (top left corner).

The mass spectrum obtained from an LC-MS instrument could not corroborate isolation of the desired compound. However, as it was later discovered, resorcin[4]arene derivatives are best analyzed via direct injection to the mass spectrometer and appear to resist elution from an LC column. The stability of compound **191** under ESI-MS conditions is suggested by reported ESI-MS data for the octa-triflate derivative.

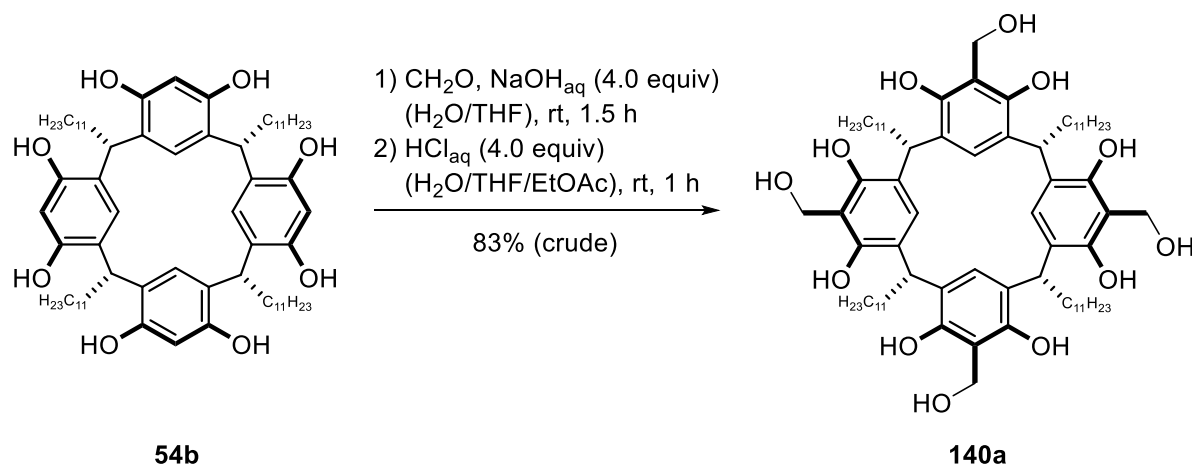
Overall, the data in hand suggests formation of the desired compound **191** under the depicted reaction conditions. Due to the problems encountered during chromatographic purification, future investigations should either attempt recrystallization or direct conversion of the crude material using palladium chemistry. However, the presence of multiple phenolic OH-groups is believed to hamper the palladium-catalyzed transformation due to competitive coordination to the catalyst. Palladium-catalyzed Buchwald-Hartwig amination and reductive deoxygenation is described for resorcin[4]arene triflates, but only in the presence of protected OH-groups.^{168c} If attempts to directly convert the crude material prove to be unsuccessful, *O*-selective permethylation¹⁷⁶ of the remaining OH-groups should be considered. An alternative, step-intensive, but robust strategy would consist of permethylation of **54b**,¹⁷⁶ selective mono-deprotection using BBr₃, triflation, transformation and finally global deprotection again with BBr₃. The advantage of this strategy would be that the reported literature conditions for the palladium-catalyzed step are likely to be also applicable in this case.

6.5.2 Achiral tetra-functionalized *C*-undecylcalix[4]resorcinarenes

6.5.2.1 Tetra-benzyl alcohol **140a** and tetra-aldehyde **140b**

In order to uncover the prerequisites for catalytic activity of hydrogen bond-based structures in the THT cyclization, the synthesis and investigation of achiral, tetra-*C*-functionalized derivatives of **54b** was attempted. According to molecular modelling, the subunits of the general structure **140** (Figure 7) should be capable of forming hexameric assemblies in solution. In contrast to the mono-*O*-functionalized derivatives, these subunits should yield a defined architecture instead of a complex mixture of assemblies. The primary goal of the investigation is to determine the p*K*_a ranges and calculate the inner ESP surfaces of catalytically active assemblies to gain valuable information for the construction of structurally novel catalysts. The investigation was initiated with the study of derivatives that were already reported in the literature with *i*-butyl “feet”. Due to their low solubility in apolar solvents, no studies regarding their self-assembling properties had been performed.

First efforts were directed at the synthesis of the tetra-hydroxymethylated compound **140a**. The procedure reported for the *i*-butyl analog by *Iwanek et al.* had to be modified to ensure complete dissolution of the starting material.¹⁷⁷ In contrast to its *i*-butyl analog, compound **54b** is not soluble in aqueous sodium hydroxide solution. This problem could be overcome by utilizing a 1:1 mixture of THF and aqueous sodium hydroxide. Besides modifying the solvent, the reaction was performed as reported (Scheme 51).



Scheme 51: Tetra-hydroxymethylation of subunit **54b**.

The reaction proceeds via alternate (1,3,5,7) deprotonation of four phenolic moieties. The regioselectivity of the deprotonation is based on the preservation of four hydrogen bonds (see Figure 11b). The thus activated benzene rings subsequently undergo a Friedel-Crafts reaction with formaldehyde. Protonation of the alcoholates then gives the final product.

Crude product **140a** was obtained in 83% yield after work-up. The obtained ¹H NMR spectrum in acetone-*d*₆ is depicted in Figure 16. Besides residues of ethyl acetate, which could not be removed even after prolonged drying under high vacuum at room temperature, no major impurities can be detected in the ¹H NMR spectrum. The successful introduction of four hydroxybenzyl moieties is indicated by the signal at 4.92 ppm, which represents the benzylic methylene groups, and by the signal at 5.48 ppm, which corresponds to the benzylic OH-groups. These chemical shifts are in excellent agreement with the data reported for the *i*-butyl analog. The integrals of the benzylic and phenolic OH-groups are smaller than theoretically expected due to hydrogen-deuterium exchange. The successful functionalization is further verified by ¹³C NMR analysis.

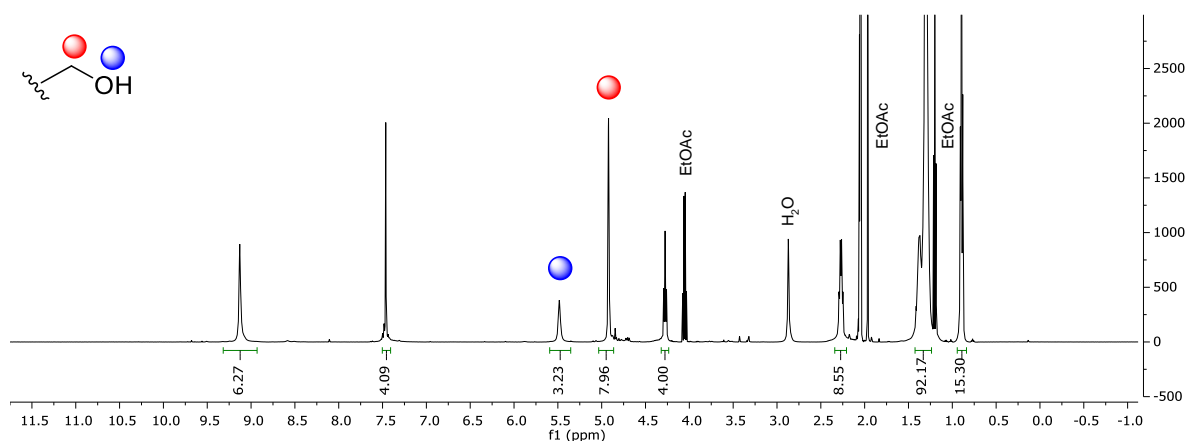
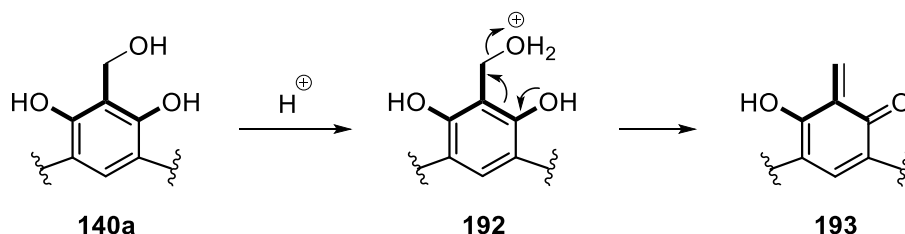


Figure 16: ^1H NMR spectrum of crude **140a** in acetone- d_6

No further purification was performed for the *i*-butyl analog. However, for the catalytic tests, a high purity of the employed catalyst is required. Therefore, a purification of compound **140a** via recrystallization was attempted. Surprisingly, compound **140a** displayed a very low solubility in common alcohols, which are the solvent of choice for the recrystallization of **54b** and **55b**. Since no other solvents provided sufficient solubility, recrystallization was attempted in *i*-propanol containing some drops of chloroform. However, the obtained ^1H NMR spectrum hints at decomposition, which is further confirmed by a change in color after recrystallization. In fact, the lability of the benzylic alcohol moiety was already reported by *Iwanek et al.* and utilized for the acid catalyzed substitution with alcohols. These reactions, as well as the assumed decomposition, proceed via the *o*-quinomethine intermediate **193**, which forms rapidly from the activated species **192** (Scheme 52). The *o*-quinomethine **193** acts as a strong Michael-acceptor for various nucleophiles.¹⁷⁷⁻¹⁷⁸ Recently *Iwanek* showed that heating of the *i*-butyl analog of **140a** was sufficient to create the *o*-quinomethine, which subsequently reacted in a hetero-Diels-Alder reaction with α -methylstyrene.¹⁷⁹



Scheme 52: Formation of the highly reactive *o*-quinomethine **193** from benzylic alcohol **140a**.

Purification was subsequently attempted using column chromatography. Again, TLC analysis indicated some degree of decomposition during the process. The ^1H NMR spectrum of the obtained material indicated only a very small increase in purity.

To study the self-assembly, a ^1H NMR spectrum of compound **140a** was recorded in deuterated chloroform. The spectrum depicted in Figure 17 shows extremely broad signals. However, it cannot be excluded that gentle heating of the sample in the intrinsically acidic chloroform already induced decomposition. Heating of the NMR sample is standardly performed when studying self-assembly processes in order to break up possible aggregates and facilitate the self-assembly process. Surprisingly, the DOSY experiment performed with this sample gave a diffusion value of $0.22 \times 10^{-5} \text{ cm}^2\text{s}^{-1}$, which is in good agreement with the value reported for the resorcin[4]arene hexamer **XI** ($0.24 \times 10^{-5} \text{ cm}^2\text{s}^{-1}$).¹⁸⁰ Nevertheless, the measurement should be repeated after complete removal of ethyl acetate and without heating of the sample.

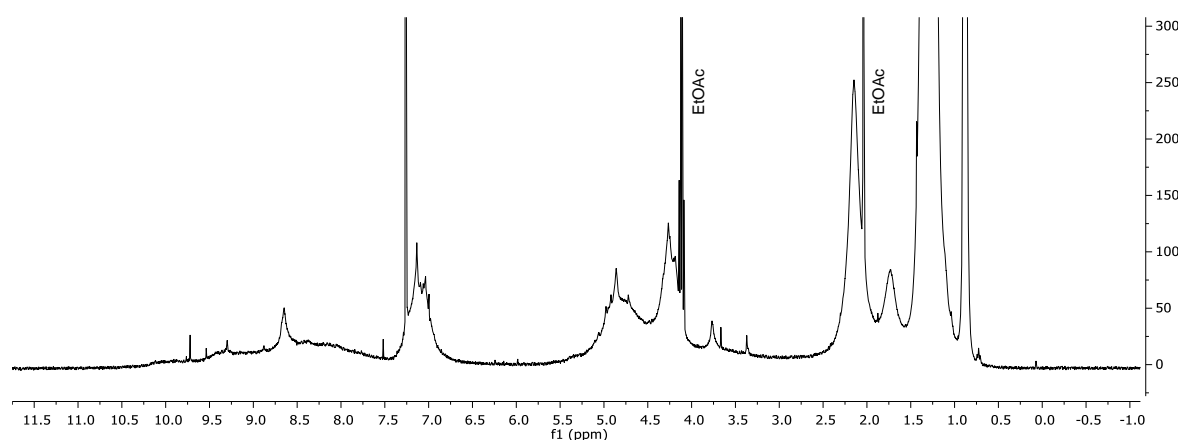
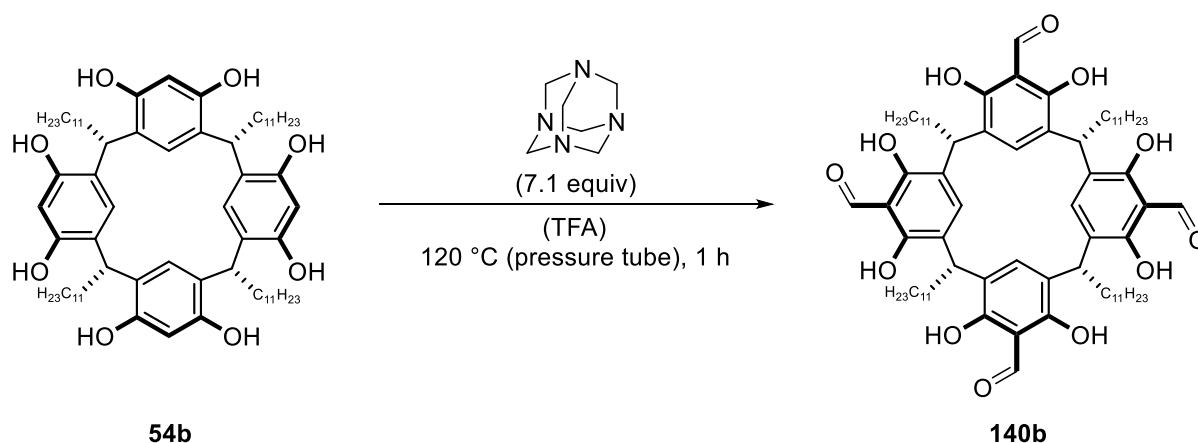


Figure 17: ^1H NMR spectrum of crude product **140a** in deuterated chloroform (contains 6 equiv. of EtOAc per theoretical hexamer).

To conclude, although some aspects should be reinvestigated, the problematic lability of subunit **140a** became apparent. Especially its sensitivity towards acids raises serious doubts about its possible application in acid catalysis.

A second derivative that was only studied with *i*-butyl “feet” is tetra-formyl resorcin[4]arene. The synthesis was achieved in 2013 by *Szumna et al.* utilizing a modified Duff formylation in neat trifluoroacetic acid.¹⁸¹ Purification of the crude product was achieved by washing with acetone. The reaction conditions could be adopted without change for the synthesis of tetra-aldehyde **140b**, since compound **54b** is soluble in neat TFA at high temperatures (Scheme 53). It is surprising that no cyclophane opening is observed under these harsh conditions, which would likely result in the formation of different stereoisomers (see Scheme 14). The crude product could be obtained in form of an orange, crystalline solid.



Scheme 53: Synthesis of tetra-aldehyde **140b** via a Duff reaction with hexamethylenetetramine (yield not determined).

The ^1H NMR spectrum of the crude reaction product indicated complete conversion of the starting material and successful formation of the desired structure. The already quite pure, crude product was subsequently subjected to solvent studies for recrystallization. Heating of small samples in ethanol or methanol resulted in a change in consistency and incomplete dissolution. TLC analysis indicated contamination with an apolar impurity. Attempts to remove this impurity via washing with pentane failed. Acetone and diethyl ether completely dissolved the product and could therefore not be used for washing. However, these solvents might be useful for purification via trituration. A small increase in purity was subsequently achieved using column chromatography. The product is apparently significantly less polar than the starting material due to complete intramolecular saturation of all hydrogen bond donors. Unfortunately, the only existing spectrum after purification was obtained in deuterated chloroform, which should in principle result in self-assembly of **140b** (Figure 18). Nevertheless, the relative integrals fit well to the structure of **140b**, but the presence of the apolar impurity is visible due to the deviation of the integrals in the aliphatic region from their theoretical values. Half of the phenolic OH-signals are significantly shifted downfield by intramolecular hydrogen bonding to the carbonyl oxygen atom, which is a strong hydrogen bond acceptor. The chemical shifts are in excellent agreement with the literature data, which was also obtained in deuterated chloroform. Interestingly, when the *i*-butyl analog was treated with primary amines, exclusive formation of the corresponding keto-enamine tautomer was detected.¹⁸¹

Since only a single experiment was dedicated to the study of the tetra-aldehyde **140b**, only very preliminary information can be provided. The NMR data suggests successful formation of the desired structure, but this has to be verified by a complete NMR analysis and ESI-MS measurements. The self-assembling properties have to be probed using DOSY spectroscopy.

However, the current purification problem has to be resolved. No conclusive statement can be made about the stability of the structure, but the conceivable reactivity towards nucleophilic alcohol substrates might pose a limitation to its application.

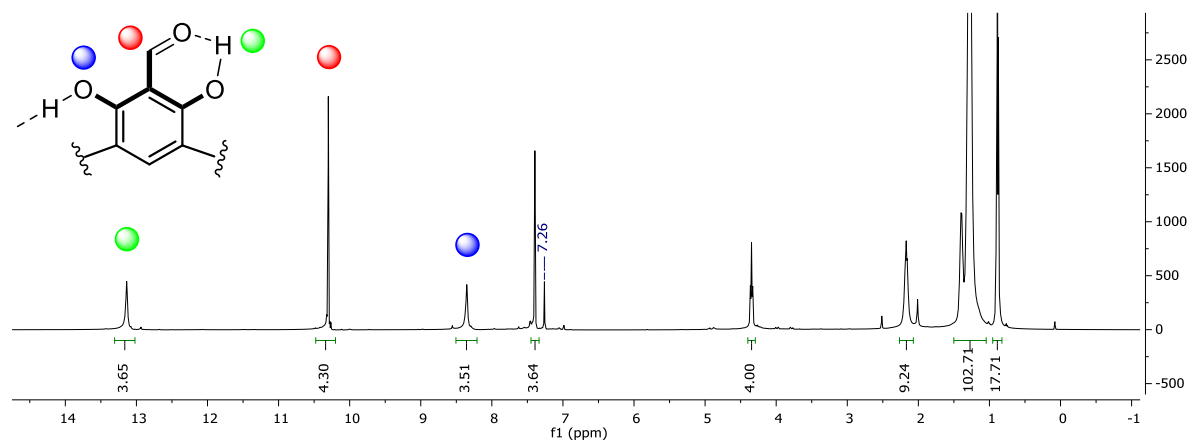
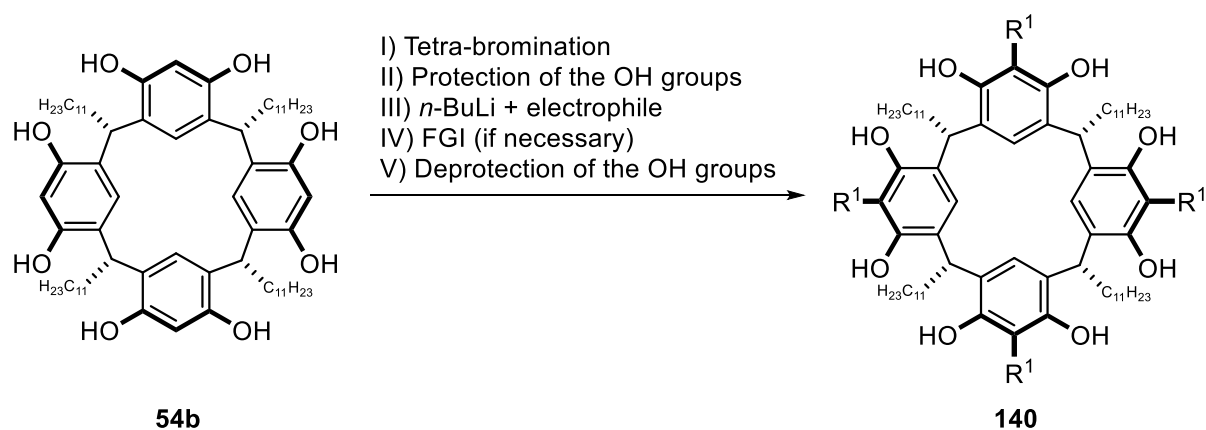


Figure 18: ^1H NMR spectrum of compound **140b** in deuterated chloroform.

6.5.2.2 Tetra-carboxylic acid **140c** and tetra-amide **140d**

Efforts were subsequently directed towards the synthesis of the tetra-carboxylic acid **140c** and the tetra-amide **140d**. Successful synthesis of a tetra-carboxy resorcin[4]arene bearing methyl “feet” was accomplished by *Schneider et al.* utilizing 2,6-dihydroxybenzoic acid instead of resorcinol in the condensation reaction with acetaldehyde.¹⁸² The key to the synthesis was to omit the external acid and to utilize the intrinsic acidity of the carboxylic acid to induce the condensation. The thus formed carboxylate increases the electron density of the aromatic ring and enables the Friedel-Crafts reaction. However, a mixture of the desired *rccc* and the undesired *rctt* stereoisomer was obtained, but apparently could be separated via repeated recrystallization. The formation of stereoisomers that are hard or impossible to separate represents a general limitation to the use of pre-functionalized resorcinols. Furthermore, the functionalization can also lead to an inhibition of the reaction, as it was demonstrated for 2,6-dihydroxybenzamide.¹⁸² Another conceivable short synthesis of tetra-carboxylic acid **140a** would involve treating the tetra-phenolate of **54b** with carbon dioxide (Kolbe-Schmitt reaction). However, usually very high pressure is required to achieve the desired carboxylation. Based on the apparently successful synthesis of tetra-aldehyde **140b**, also an oxidation strategy could be envisioned. However, one such attempt to oxidize tetra-aldehyde **140b** under Pinnick conditions failed to give an identifiable product. Nevertheless, the potential efficiency of this route calls for further investigations.

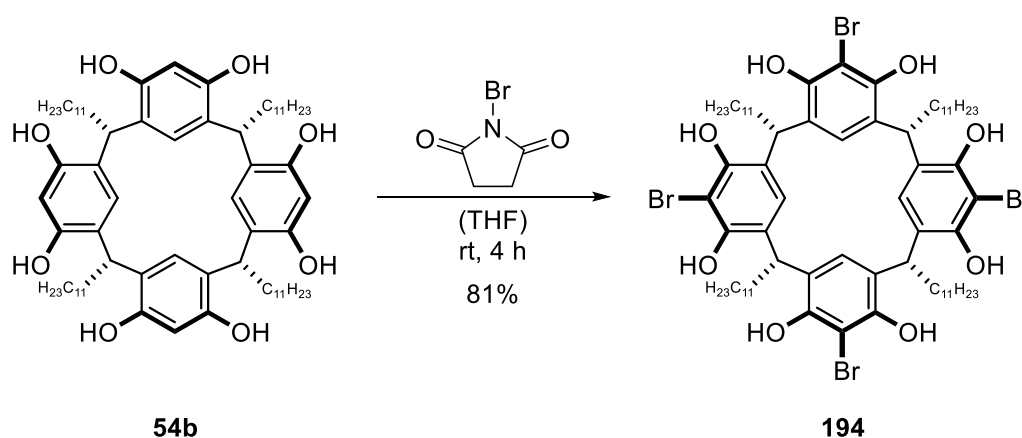
In order to overcome those problems and to establish a versatile route that would in principle allow access to different derivatives, a multi-step strategy was developed centered around a protected tetra-bromide as the key intermediate (Scheme 54). Application of non-permanent protecting groups for the phenolic OH-groups is underexplored in resorcin[4]arene chemistry. Research on cavitands for example is based on the permanent linking of the phenolic OH-groups via methylene bridges. Reversible protection of the OH-groups by peracetylation is possible, but not rational considering the following reaction conditions. TBS-protecting groups have been utilized to perform transformations at the “feet”,¹¹² but are not appropriate for reactions at the 2-position due to their steric demand. Considering the stability of the methylene bridges in cavitand chemistry under similar reaction conditions, the protection via methylation appeared suited. Furthermore, four examples of the dealkylation of resorcin[4]arene-based aryl methyl ethers were found in the literature.^{168a,183} Additionally, a wide range of reactants for the cleavage of aryl methyl ethers is available.¹⁸⁴ Boron tribromide is one of the most commonly applied reagents for this transformation. It was anticipated that pre-coordination to the carboxylic acid or amide functionality would facilitate the deprotection of the *ortho*-hydroxy groups. The use of MOM-protecting groups was avoided due to the possibility of cross-linking neighboring OH-groups. The protection was planned to follow the known,¹⁸⁵ initial bromination of the 2-positions. Subsequent introduction of the desired functional group was envisioned to occur via lithium-halogen exchange and addition of the respective electrophile, if necessary followed by a functional group interconversion (FGI). Final deprotection would then give the desired resorcin[4]arene derivative. Functionalization of the 2-positions can in principle be also performed via *ortho*-lithiation of the permethylated **54b**.¹⁷⁶ However, the bromide functionality additionally allows the use of conventional cross-coupling chemistry.



Scheme 54: General route for the functionalization of the 2-position of subunit **54b**.

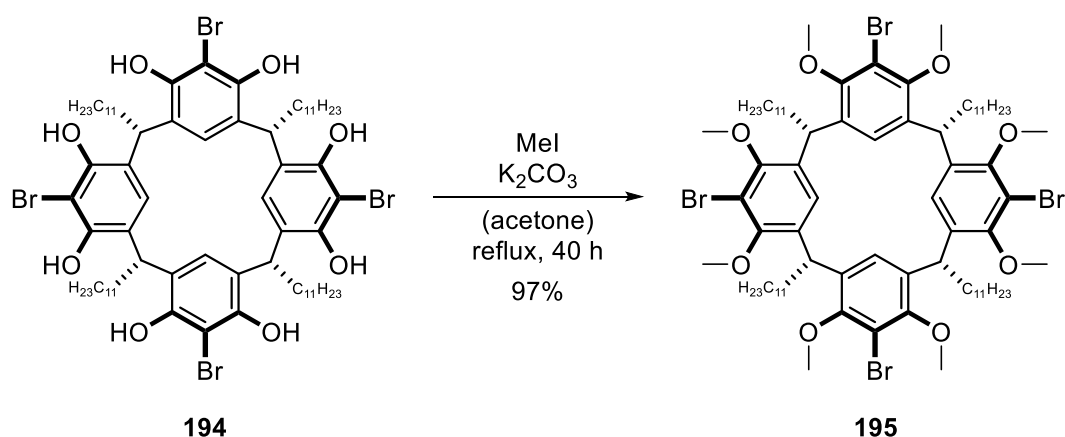
The depicted route also gives access to mono-, di- and tri-*C*-functionalized derivatives by selective removal of the corresponding equivalents of bromides prior to the functionalization step.^{171,186}

The work towards tetra-carboxylic acid **140c** started with a large scale synthesis of subunit **54b**. Utilizing the standard reaction conditions,¹⁵³ 129 g of the universal precursor **54b** could be obtained. A 50 g batch was subsequently subjected to bromination,¹⁸⁵ yielding the desired tetra-bromide **194** in 81% yield (Scheme 55). Purification was performed by suspending the crude product in boiling methanol, followed by hot filtration.



Scheme 55: Synthesis of tetra-bromide **194**.

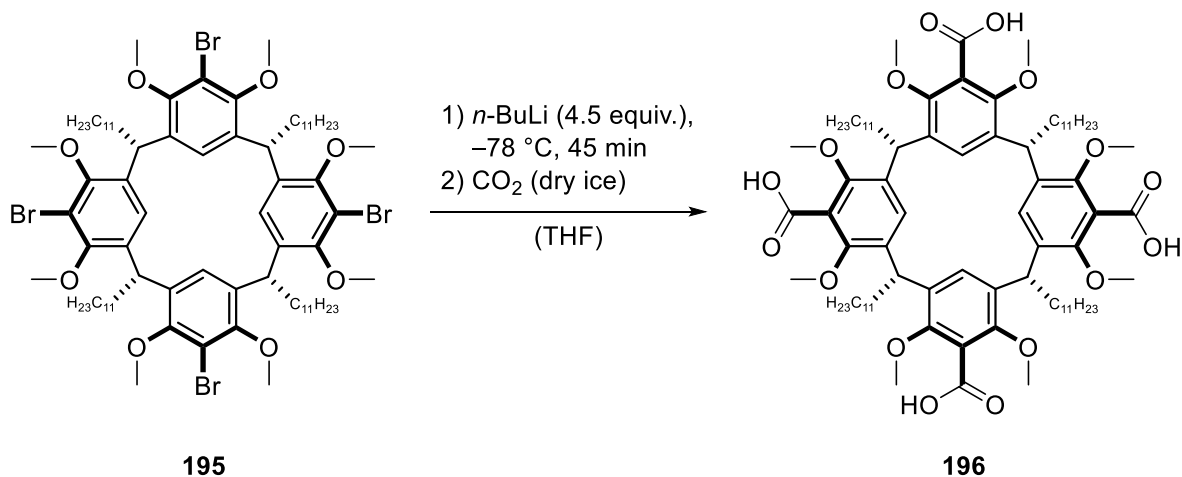
The permethylation of tetra-bromide **194** was achieved by using an excess of methyl iodide and potassium carbonate as the base (Scheme 56). After optimization of the reaction conditions, the methylation was performed with 50 g of tetra-bromide **194**. The protected product **195** was obtained in almost quantitative yield after purification by filtration through a plug of silica. After filtration, the compound contains an NMR-inactive, odorous yellow impurity, which can in principle be removed by additional recrystallization from methanol.¹⁷¹ However, recrystallization is not necessary for the following transformations. Performing the protection step after the bromination proved beneficial under the applied conditions, presumably by suppressing *C*-methylation side reactions.



Scheme 56: Permethylation of tetra-bromide **194**.

In literature concerning cavitands, the starting material for the lithium-halogen exchange is dried rigorously by repeated dissolution in anhydrous THF and subsequent evaporation of the solvent, and drying under high vacuum at elevated temperatures.¹⁸⁷ This process ensures complete removal of water and residues of organic solvents, especially dichloromethane, which is known to react with organometallic reagents like *n*-butyllithium. However, since the purification of **195** was performed with a mixture of inert pentane and diethyl ether, no such preparation was performed. The following reactions showed that the drying process is not necessary. Nevertheless, the yields might be improved by incorporating this procedure.

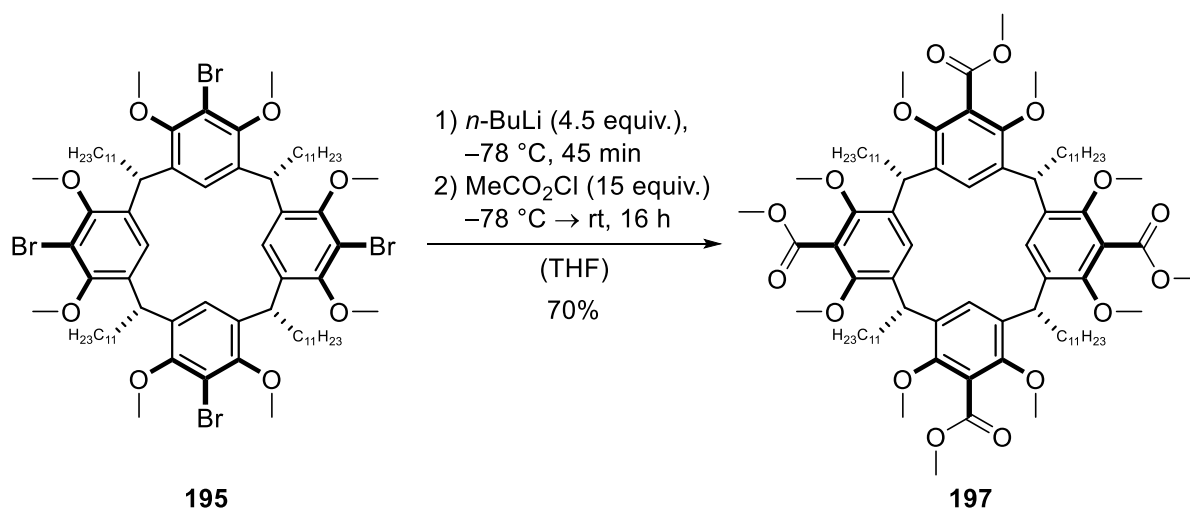
The metal-halogen exchange could be performed successfully with *tert*-butyllithium and *n*-butyllithium. Due to its less hazardous character, *n*-butyllithium was subsequently used for all the lithium-exchange reactions. The first attempt to introduce the carboxylic acid functionality aimed at quenching the organolithium species directly with carbon dioxide, in analogy to a published procedure (Scheme 57).¹⁸⁸



Scheme 57: Direct conversion of the tetra-bromide **195** to the tetra-carboxylic acid **196** (yield not determined).

Three different methods of carbon dioxide addition were investigated: 1) direct addition of dry ice into the reaction flask, 2) passing CO₂ gas into the solution via an inlet and 3) pouring the reaction mixture on crushed dry ice. Only after pouring on crushed dry ice, a promising NMR spectrum was obtained. ¹³C NMR analysis clearly proved successful introduction of a carboxylic acid functionality. The obtained ¹H NMR indicated the presence of several conformers, which is expected due to the loss of hydrogen bonding between the phenolic OH-groups. The relatively high energy barrier between the conformations (likely crown and boat) results in a slow exchange and therefore multiple sets of signals (see Figure 6). The complex NMR spectra obtained for the protected derivatives posed a general challenge. However, performing the NMR measurements at higher temperatures could in principle lead to a single, averaged set of signals and thereby simplify the analysis. Due to the complicated NMR spectra, ESI-MS measurements proved essential in the analysis of the performed derivatizations. Comparison of the ¹H NMR spectrum with data obtained at a later point showed that treatment with carbon dioxide indeed yielded the desired tetra-acid **196** in high selectivity without the formation of the mono-, di- or tri-functionalized product. Unfortunately, this reaction could not be reproduced under identical conditions.

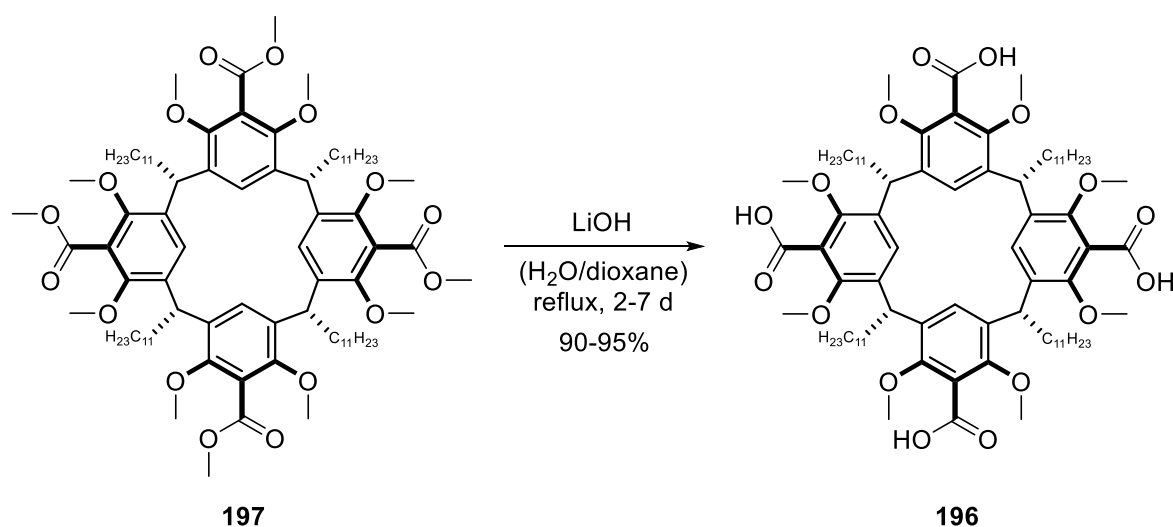
For this reason, the synthesis of compound **196** was attempted using a more robust two-step sequence, consisting of the introduction of carboxylic esters and subsequent hydrolysis. Using freshly titrated *n*-butyllithium, formation of tetra-ester **197** could be achieved in a reproducible fashion by employing methyl chloroformate as the electrophile (Scheme 58). Like in other reactions performed with the tetra-aryllithium species, a large excess of the electrophile proved beneficial. Purification was performed via column chromatography.



Scheme 58: Synthesis of tetra-ester **197** via lithium-halogen exchange.

It is noteworthy that under the applied concentration the fourfold lithium-halogen exchange is apparently accompanied by a sudden change in the viscosity of the solution. This visual indicator can be used to confirm the correct execution of the first reaction step. The structure of the alkoxycarbonylation product **197** was confirmed by ESI-MS and NMR analysis. Again ^1H NMR indicated the presence of multiple conformers.

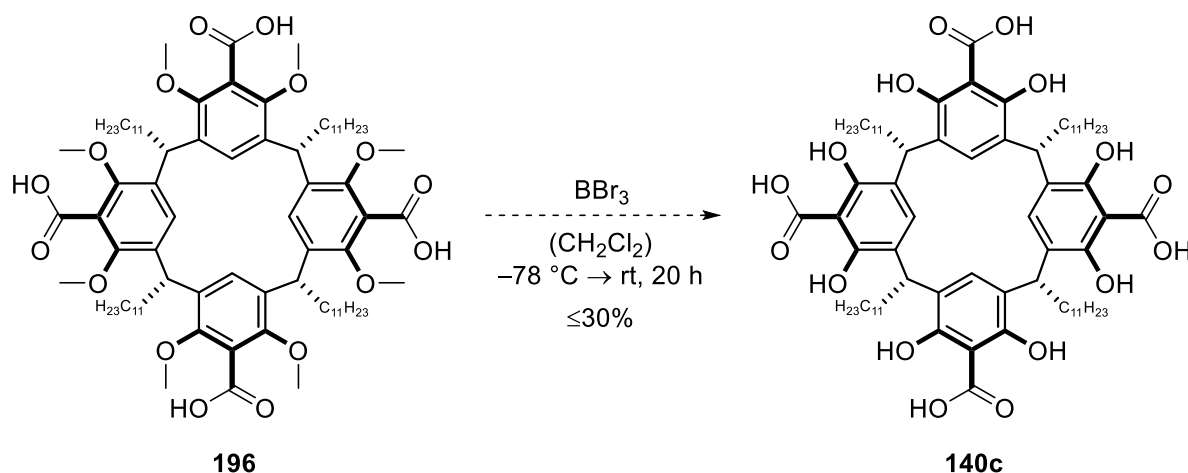
Surprisingly, the hydrolysis proved more difficult than the alkoxycarbonylation step. Several reagents and solvents had to be screened until a robust procedure was found. A high temperature as well as a long reaction time were found necessary to completely hydrolyze all ester units (Scheme 59). Formation of the desired product was confirmed by ESI-MS and NMR analysis. The crude product obtained by precipitation after evaporation of dioxane contained significant amounts of inorganic salt. Therefore, the crude product was taken up in THF, and filtered to remove the insoluble contaminations.¹⁸⁹ Due to the purity of the crude product, no further purification was performed. It is worthy to mention that the polarity of product **196** prevents the use of column chromatography in established eluent mixtures.



Scheme 59: Best reaction conditions for the hydrolysis of tetra-ester **197**.

With the protected tetra-acid **196** in hand, the focus was set on the dealkylation of the ether units utilizing boron tribromide (Scheme 60). Considering the potentially high water-solubility of product **140c**, a water-free work-up was devised. The reaction was quenched with methanol and the mixture was evaporated to dryness. The solid residue was subsequently recrystallized from methanol, which yielded white, pearly plates. The ESI mass spectrum of the plates only showed the desired product mass and the mass resulting from decarboxylation. The decarboxylation event is most likely evoked by the ESI-MS conditions and does not indicate an

impurity. The mass of the decarboxylated species can also be found in the mass spectra of the protected tetra-acid **197**.



Scheme 60: Attempted deprotection of tetra-acid **196** (standard conditions).

A subsequent attempt to reproduce the result in a larger scale, starting from a different batch of **196**, failed, yielding only insoluble material after recrystallization from methanol. Eventually, the result could be repeated using again another batch of **196**. The recorded NMR spectra as well as the ESI mass spectrum were consistent with the data obtained from the initially isolated material. In acetone- d_6 , multiple methine resonances indicate the presence of different conformations in slow exchange (Figure 19a). The integrals of the ^1H NMR spectrum support isolation of a tetra-functionalized resorcin[4]arene, although no hydroxy groups are visible. After complete removal of residual methanol under vacuum, the compound was dissolved in deuterated chloroform in order to investigate the self-assembly. The obtained ^1H NMR spectrum showed a significantly less complex signal pattern. However, the methine signal indicated an equilibrium of multiple species. In addition, the determined diffusion coefficient of $0.32 \times 10^{-5} \text{ cm}^2\text{s}^{-1}$ excluded formation of a hexameric assembly. It has to be noted that this value and the following diffusion values were determined using a non-calibrated pulse sequence. The reference diffusion value of hexameric species **XI** on this instrument is $0.19 \times 10^{-5} \text{ cm}^2\text{s}^{-1}$. In principle, a higher diffusion coefficient could also result from a smaller assembly. Indeed, molecular modelling indicates the possibility of a trimeric assembly of tetra-acid **140c** (Figure 20). Self-assembly was further probed by addition of tetrabutylammonium bromide, which acts as a high affinity guest for hexamer **XI**. In this case, no encapsulation was observed. This does not necessarily exclude the formation of an assembly, since hexamer **XII** likewise rejects the encapsulation of ammonium salts. However, also in the presence of an alcohol guest like nerol (**19**), no upfield-shifted resonances could be detected.

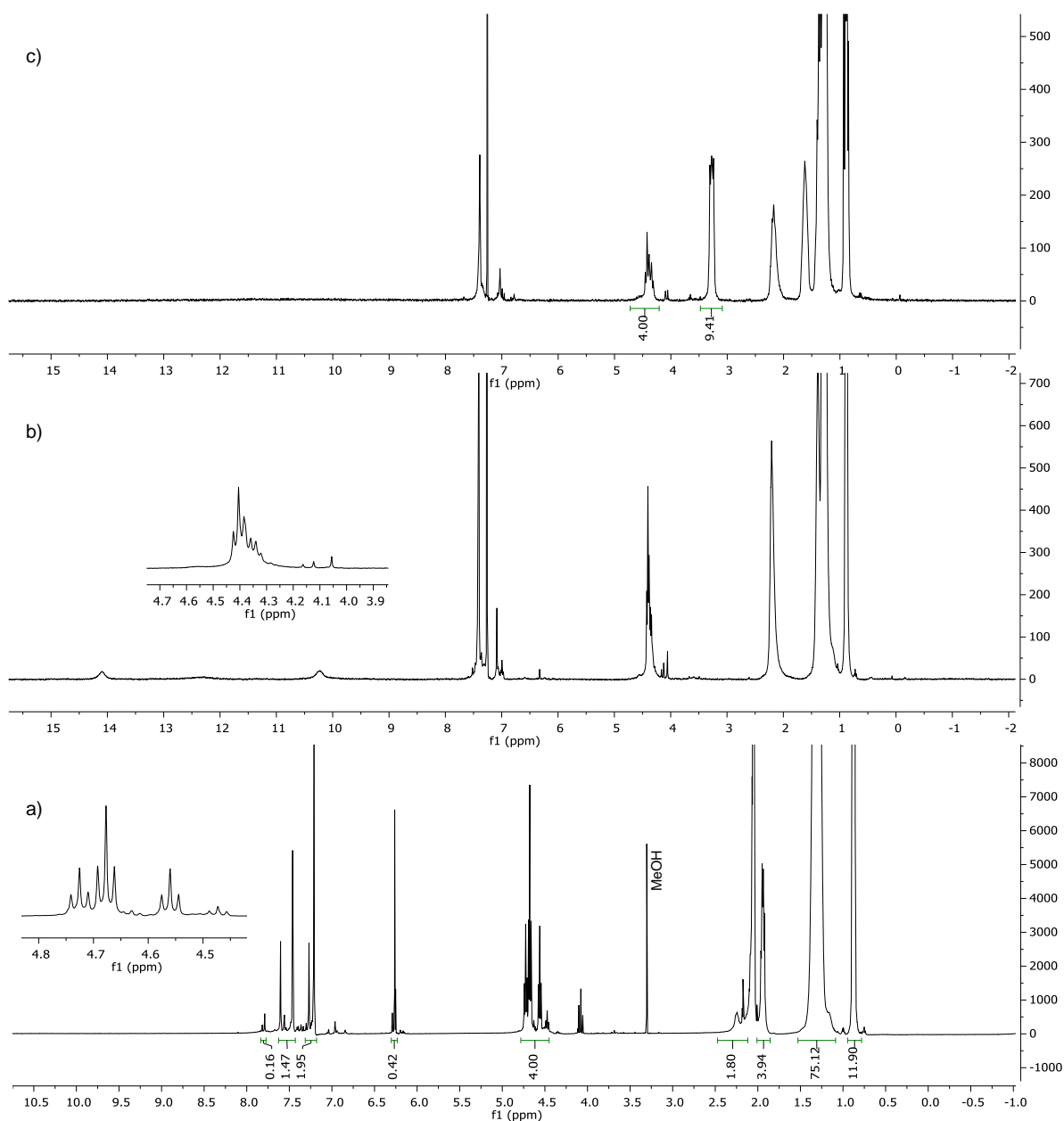


Figure 19: ^1H NMR spectra of the compound obtained after deprotection of **196**: (a) in acetone- d_6 , (b) in CDCl_3 and (c) in CDCl_3 in the presence of tetrabutylammonium bromide (~ 7 equiv. per expected hexamer).

The results gave rise to doubts about the nature of the isolated product. An initial assumption concerning stereoisomer formation via reversible macrocycle opening during recrystallization due to the high intrinsic acidity ($\text{p}K_a$ of 2,6-dihydroxybenzoic acid ≈ 1.2)¹⁴⁵ appears unlikely. The resorcin[4]arene subunit **54b** appears to be stable in TFA at 120 °C and also in the presence of CSA at 60 °C over a prolonged period (see chapters 6.5.2.1 and 6.3). Furthermore, the methyl “feet” analog was recrystallized without problems.¹⁸² Additionally, the introduced electron-withdrawing substituents should reduce the probability of protonation of the aromatic core. Attempts to obtain conclusive data before the recrystallization failed, probably due to the large amounts of boron impurity.

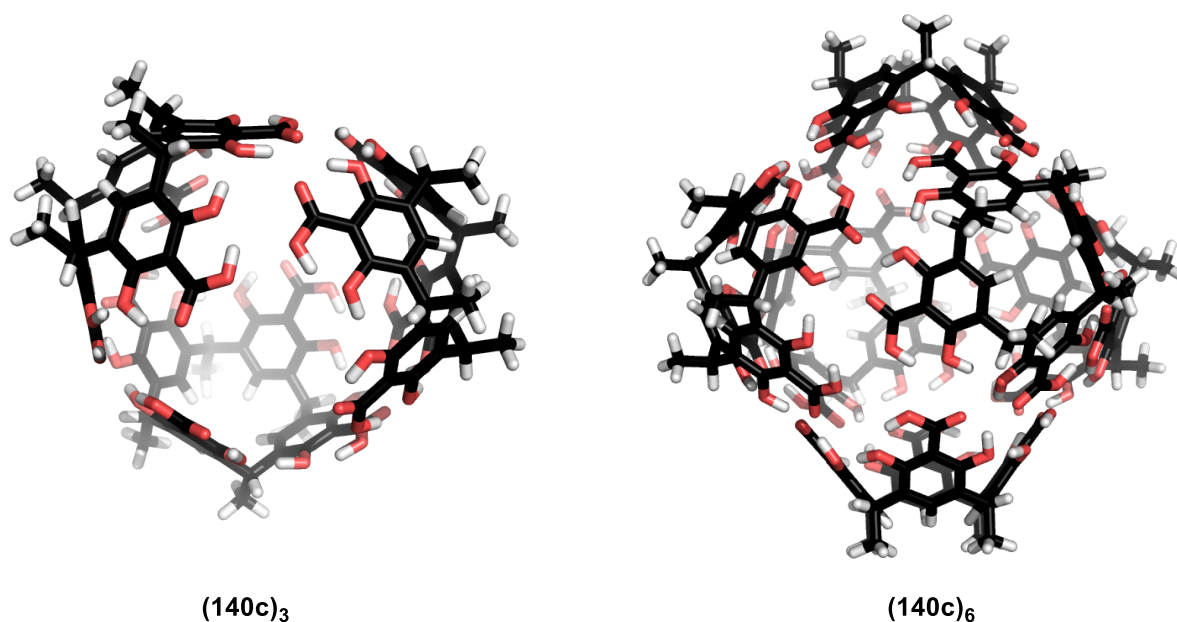


Figure 20: Molecular modelling of a trimeric (left) and a hexameric (right) assembly of tetra-carboxylic acid **140c** (optimized with methyl “feet”).

To overcome this problem, boron tribromide was substituted with trimethylsilyl iodide (TMSI), which can be removed easier. The reaction was performed in chloroform at 40 °C to facilitate the deprotection step. The NMR obtained after quenching with methanol is consistent with the data obtained previously after recrystallization. This further contradicts an undesired transformation during recrystallization. In addition, to exclude incomplete removal of boron species or uncleaved O-B bonds after recrystallization, the recrystallized material was treated with aqueous HCl and subsequently extracted with DCM. The obtained NMR spectra show no significant difference to the data obtained previously.

Additional studies were performed regarding a reversal of the last two reaction steps in the sequence towards **140c**. However, multiple attempts to deprotect the phenolic OH-groups of the tetra-ester **197** utilizing boron tribromide failed, despite a screening of reaction time, temperature and work-up conditions. Complete deprotection could be achieved in none of the attempts.

Overall, the studies regarding compound **140c** gave no conclusive result so far and the structure of the isolated material remains elusive. However, the established route to the protected tetra-acid **196** still bears some potential for accessing other possible derivatives. For example, treatment of compound **196** with diphenylphosphoryl azide (DPPA) could allow formation of a C-N bond *ortho* to both phenolic units (2-position),¹⁹⁰ which so far proved difficult to form

by applying standard nitration techniques (Figure 21a). The intermediary isocyanate formed in this Curtius rearrangement could also be trapped by an alcohol to yield a carbamate. An intramolecular version of this reaction with the deprotected tetra-acid **140c** would build up an oxazolone moiety (Figure 21b). Yet, C-N bond formation at this position is likely easier achievable using palladium chemistry and starting from the protected tetra-bromide **195**. A more intuitive use of compound **196** would be its transformation to the protected form of tetra-amide **140d** via the corresponding acid chloride.¹⁸⁹ However, this strategy for the synthesis of tetra-amide **140d** was abandoned after the discovery of a more direct route via the tetra-bromide **195**.

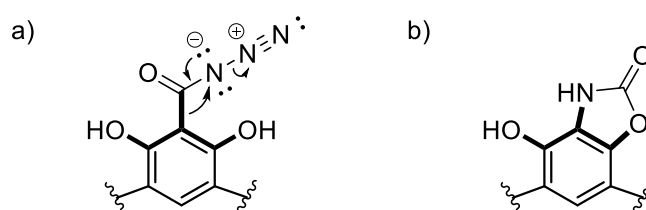
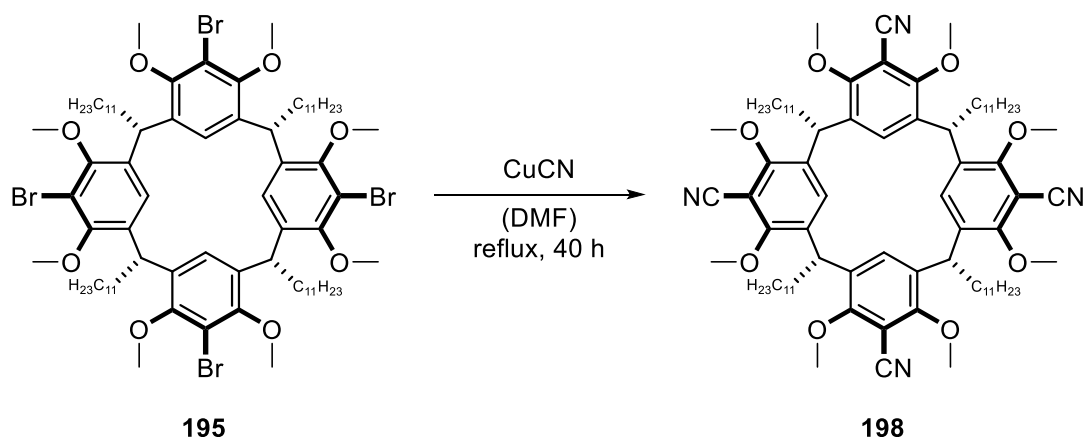


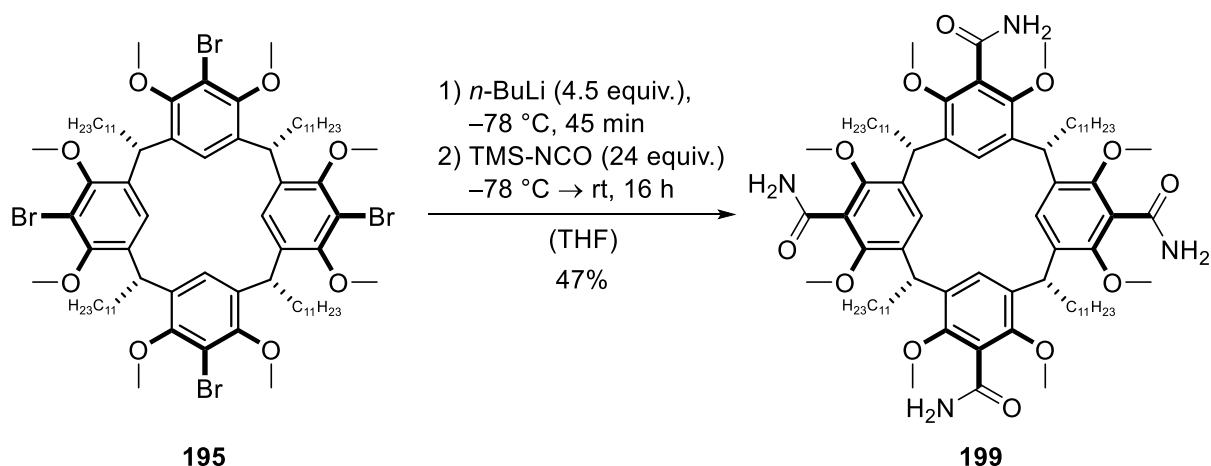
Figure 21: (a) Formation of a C-N bond in 2-position via a **140c**-derived acyl azide; (b) oxazolone motif, formed by intramolecular attack of a phenol unit on the intermediary isocyanate.

Work on the tetra-amide derivative **140d** began with the synthesis of tetra-nitrile **198**. It was envisioned that simple hydrolysis of the nitrile functionalities using hydrogen peroxide would yield the protected form of the corresponding tetra-amide **140d**. Furthermore, this route allowed to resort to a published procedure for the synthesis of the tridecyl “feet” analog of the tetra-nitrile compound.¹⁹¹ The synthesis is based on the treatment of tetra-bromide **195** with copper(I) cyanide in refluxing dimethylformamide (Scheme 61). This Rosenmund-von Braun reaction yielded the desired tetra-nitrile **198**, as indicated by NMR analysis of the crude reaction product. The synthesis and purification was subsequently optimized as part of an internal collaboration.¹⁷¹



Scheme 61: Synthesis of tetra-nitrile **198** via a Rosenmund-von Braun reaction.

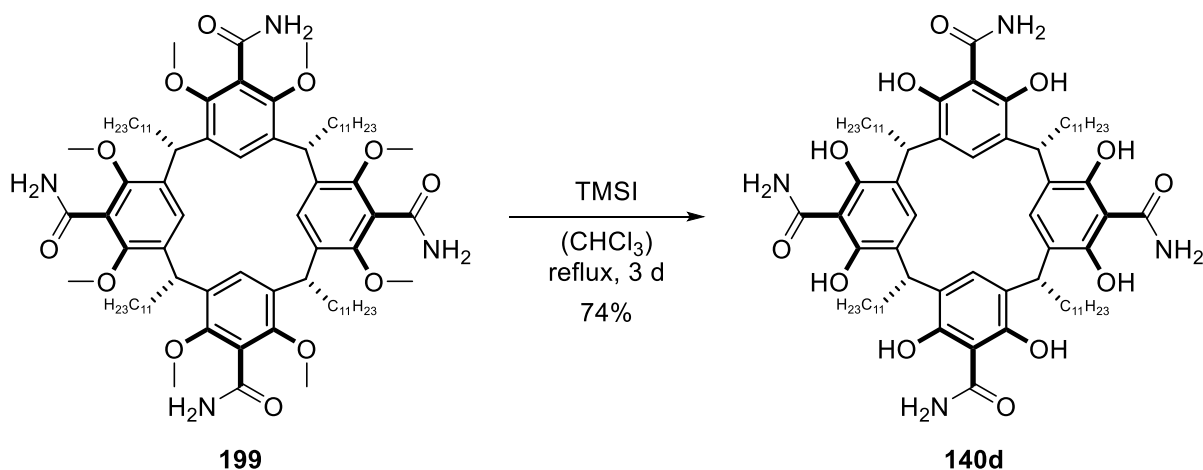
Despite significant efforts, a successful hydrolysis of the tetra-nitrile could not be achieved.¹⁷¹ Especially solubility issues might have played a major part in the failure of the hydrolysis. A subsequent study of the literature revealed the possibility to directly convert the tetra-bromide **195** to the protected tetra-amide **199** utilizing (trimethylsilyl)isocyanate (TMS-NCO) after lithium-halogen exchange. Surprisingly, the first attempt was already successful and yielded the desired tetra-amide **199**, although in poor yield and contaminated. Subsequent optimization of the work-up (extraction with DCM/*i*-PrOH = 4/1) and the chromatographic purification (dry load) led to the isolation of product **199** in 47% yield (Scheme 62). The corresponding tri-amide was isolated as a side product in 30% yield.



Scheme 62: Synthesis of the tetra-amide **199** utilizing TMS-NCO.

The product structure was verified by NMR analysis and ESI-MS. The obtained ¹H NMR spectrum is very defined and indicates fast exchange between the different possible conformations. Furthermore, the amide protons are clearly visible as two separate singlets due to the double bond character of the C-N bond.

The deprotection was subsequently investigated by employing a large excess of boron tribromide. The first attempt yielded a sparingly soluble powder after 24 hours at room temperature, which consisted of the desired product and large amounts of the mono- and dimethylated species according to ESI-MS analysis. This sort of incomplete deprotection was consistent with the experience made with other derivatives. It is believed that this problem results either from the steric bulk of the *in situ* formed O-BBr₂ units or from the intermolecular cross-linking of phenolic units via the boron atom.¹⁹² Since the steric hindrance increases as the reaction continues, the formation of the mono-methylated species as the main side product appears reasonable. Longer reaction times help to achieve complete deprotection, but some degree of decomposition appears to take place after several days, probably induced by traces of HBr formed by hydrolysis with residual water. The first complete deprotection according to ESI-MS analysis was achieved by performing the reaction in chloroform under reflux conditions. Surprisingly, the obtained product was poorly soluble in common organic solvents. The low solubility also caused an attempted recrystallization from methanol to fail. The ¹H NMR spectra in chloroform indicated formation of the desired product, but the weak intensity, broad peak shape and inconsistent integration suggested some kind of contamination. It was speculated that some N-B bonds might still be in place, and that those bonds were cleaved under the ESI-MS conditions, resulting in the correct m/z value. This cannot be completely ruled out, but appears unlikely since the B-N bond has a lower dissociation energy than the B-O bond.¹⁹³ Nevertheless, the rapid cleavage of the N-Si bond during work-up in the previous step inspired the use of TMSI in the deprotection of the tetra-amide **199**. Indeed, utilizing TMSI in chloroform under reflux conditions gave the desired product in 74% yield (Scheme 63). The work-up consisted of addition of aqueous HCl, evaporation of the organic solvent and filtration of the precipitated product. This modified work-up was introduced after realizing the initial overestimation of the water solubility of the deprotected derivatives. The product can be recrystallized from ethyl acetate. However, a subsequent scale-up proved again problematic regarding complete deprotection. The overall performance of the final deprotection step remains altogether unsatisfying and requires further investigation. Incomplete deprotection poses a less severe problem for derivatives that can be purified via column chromatography. Recent TLC studies indicate that it might be possible to purify compound **140d** via column chromatography using a very polar solvent mixture (DCM/acetone = 1/1).



Scheme 63: Successful deprotection of tetra-amide **199** utilizing TMSI.

The obtained ^1H NMR spectrum in acetone- d_6 shows very broad resonances and a low signal-to-noise ratio, partly because of the poor solubility of compound **140d** in acetone. However, the spectrum obtained in chloroform- d_1 strongly suggests formation of the desired structure, despite deviations of the integrals of acidic protons from the expected values (Figure 22). The good solubility in chloroform provides some evidence for self-assembly, since saturation of the polar functionalities via intermolecular interaction creates a more lipophilic structure. Another indication for self-assembly is the significantly downfield-shifted signal at 16.0 ppm, which is believed to correspond to the nitrogen-attached proton that is part of the amide dimer motif. The small shoulders of the amide protons are believed to rather represent a structural property than an impurity. Furthermore, DOSY experiments gave values ranging between $0.19 \times 10^{-5} \text{ cm}^2\text{s}^{-1}$ and $0.22 \times 10^{-5} \text{ cm}^2\text{s}^{-1}$, which is in good agreement with the value obtained for the hexameric assembly **XI** ($0.19 \times 10^{-5} \text{ cm}^2\text{s}^{-1}$). Preliminary tests indicate that the assumed host structure is incapable of encapsulating amines and ammonium salts. However, the material is believed to still contain minor impurities and therefore an improved purification protocol is required for detailed investigation. According to modelling, the hexameric structure formed by **140d**, depicted in Figure 23, is hold together only by the amide dimer motifs. Intrigued by the potentially minor influence of the OH-groups on the self-assembly, the capability of the OH-protected precursor **199** to self-assemble was investigated. However, the obtained diffusion coefficient is significantly higher ($0.27 \times 10^{-5} \text{ cm}^2\text{s}^{-1}$) than the one obtained for **140d**, despite having an increased molecular weight. Additionally, no indication for tetrabutylammonium bromide encapsulation was observed. It appears reasonable that the OH-groups are required for enforcing the crown conformation. In addition, hydrogen bonding to the amide group might reduce the rotational freedom of the amide functionality and thereby strengthen the amide dimer motif. Alternatively, the steric repulsion between the methoxy groups might be sufficient to

prevent the self-assembly process. In this context, the idea of bridging the hydroxy groups with a methylene unit is highly intriguing, since bridging would provide the necessary crown conformation and the bridges would sterically be tolerated by the self-assembly process. Furthermore, this approach would significantly simplify the synthesis of the building block, since deprotection would no longer be required. The compound could also be purified by column chromatography, which ensures pure material for the study of its properties. This strategy has already been successfully employed in dynamic covalent chemistry using a methylene-bridged tetra-formyl cavitand and diamino linkers for imine bond formation.^{48,194}

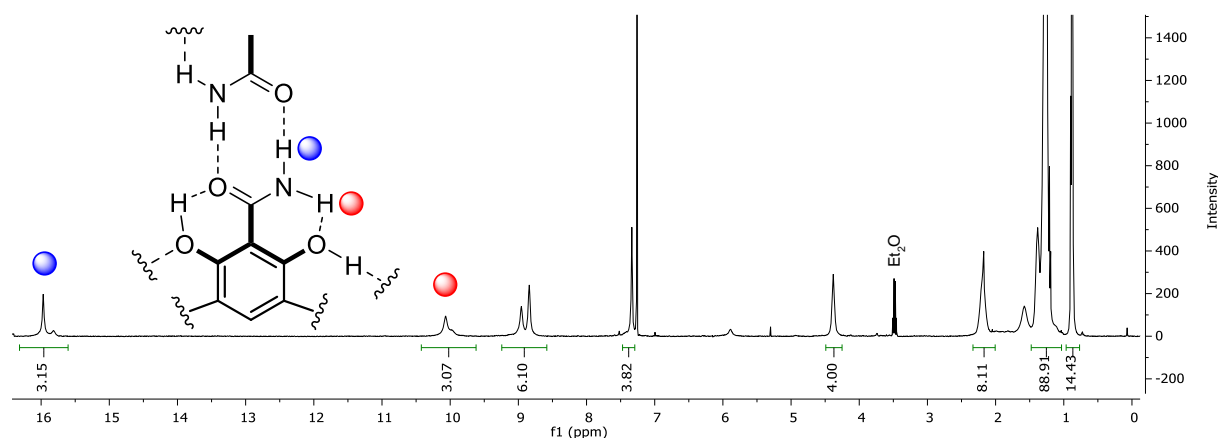


Figure 22: ¹H NMR spectrum of compound **140d** in chloroform-*d*₁ (contains traces of Et₂O).

The hexameric assembly of **140d** is significantly larger than the assembly of **54b**, and in addition features holes in the surface that could potentially be used as binding sites for subunits capable of hydrogen bonding. Intelligent design of the surface-binders could allow modification of the inner cavity space by inwards directed functionalities. Molecular modelling revealed carboxylic acid **200** as a suitable binder. However, the synthesis of the molecule as well as installation of the functionality L will likely be challenging. Furthermore, to ensure an inwards directed orientation of the functionality, two binders would have to be bridged via L. In addition, the influence on the existing hydrogen bond network might be more detrimental than suggested by molecular modeling. An alternative strategy that would leave the original hydrogen bond network of the phenolic OH-groups intact relies on the use of terephthalamide spacers. The spacers would insert between the amide dimer motifs and thereby significantly enlarge the assembly. Functionalization of the aromatic core of the terephthalamide could in principle allow functionalization of the cavity. This concept was probed by adding 12 equiv. of terephthalamide to a solution of 6 equiv. of subunit **140d** (3.3 mM) in chloroform-*d*₁. The experiment was hampered by the extremely low solubility of terephthalamide in chloroform-*d*₁, even in the presence of **140d**, sonication and heating to 50 °C. The ¹H NMR spectrum shows

very broad signals and might indicate some sort of uncontrolled interaction. The DOSY spectrum shows only a single entity with a diffusion coefficient of $0.17 \times 10^{-5} \text{ cm}^2\text{s}^{-1}$. However, this intriguing value is considered very questionable and should not be overestimated. The insertion of the spacers is entropically unfavored. This thermodynamic penalty could be overcome by designing a spacer that forms stronger hydrogen bonds with the amides than the amides with themselves.

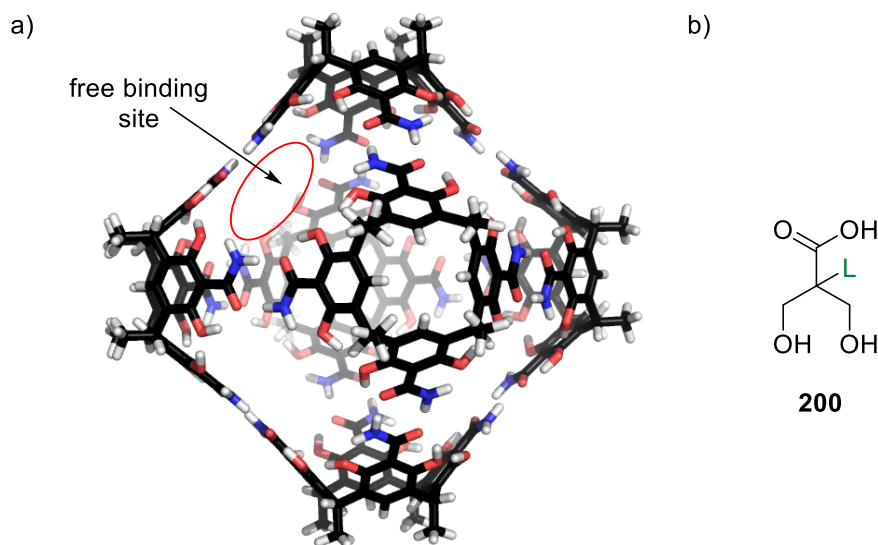


Figure 23: (a) Molecular model of the hexameric assembly of **140d** (one of the eight potential binding sites is highlighted); (b) potential surface-binder with functionality L to modify the cavity.

The catalytic activity of the hexameric assembly of **140d** has not yet been tested in THT cyclizations. It appears likely that the acidity of the assembly will not be sufficient to activate the acyclic substrates via protonation. In this case, external acids will have to be utilized to activate the substrate.

An essential requirement for a deeper understanding of the investigated assemblies is the elucidation of their structure via X-ray analysis. Unfortunately, the long aliphatic chains, which are installed to provide solubility, prevent crystallization of the assemblies due to their extremely high conformational freedom. Therefore, analogs of the derivatives bearing short alkyl chains have to be synthesized in order to obtain highly crystalline compounds. The resorcin[4]arene hexamer **XI** could be successfully crystallized utilizing methyl “feet”,⁸⁵ while the more stable pyrogallol[4]arene assembly **XII** could be crystallized using *i*-butyl “feet”.⁸⁶ Considering the required solubility of the synthetic intermediates in solvents compatible with the performed reactions, an adaptation of the established route was attempted with the *i*-butyl analog of resorcin[4]arene **54b**. Indeed, it was found that the established conditions can be

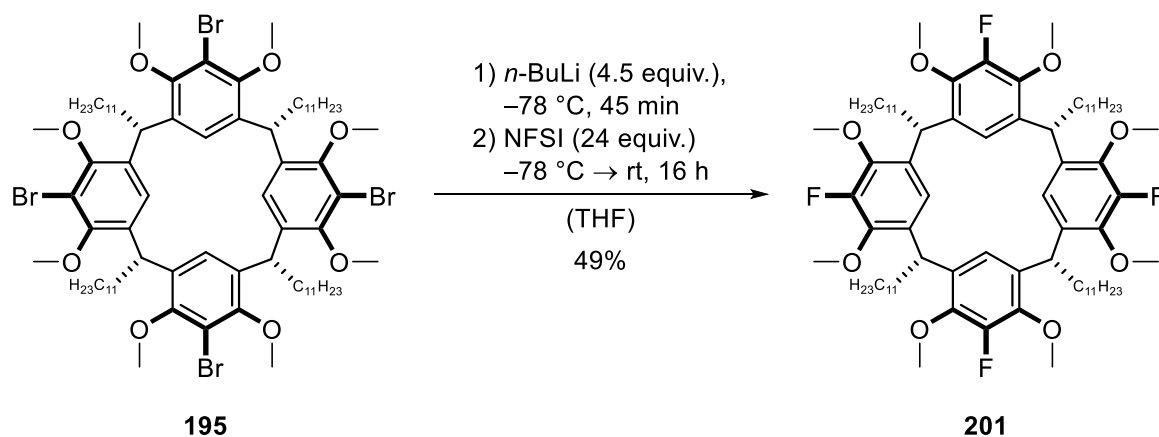
utilized for the reactions with the *i*-butyl analogs. Purification via column chromatography yielded the pure *i*-butyl analog of compound **199** (see experimental section). A preliminary deprotection experiment with boron tribromide also demonstrated the principle feasibility of the last reaction step. It is worthy to mention that synthesis and purification of the cavitand analog (methylene bridged OH-groups) of **140d** might be possible employing methyl “feet”, which would facilitate the crystallization.

Overall, this unprecedented amide derivative presents intriguing opportunities and future investigations are highly encouraged. As a side note, the deprotected tetra-amide **140d** could in principle be utilized for a one step transformation into a C₄-symmetric chiral oxazolone derivative via a iodosylbenzene-induced Hofmann rearrangement.¹⁹⁵

6.5.2.3 Tetra-fluoride **140e**

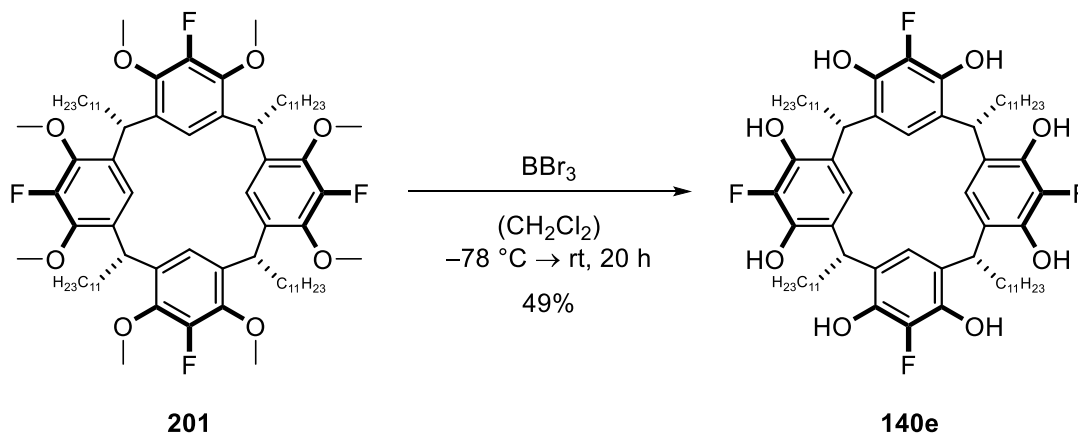
The subunits of the general structure **140** that have been discussed up to now feature substituents that are expected to replace the water molecules present in the original structure of the resorcin[4]arene hexamer **XI**. Indeed, even methyl substituents in 2-position are sterically too demanding to allow for self-assembly. According to molecular modelling, only fluorine substituents are small enough to allow for the formation of a hexameric assembly that still contains the original water molecules. Furthermore, fluorine substituents are expected to show a significant influence on the pK_a and the inner ESP surface of the assembly. Interestingly, there are no reports on fluoro derivatives of resorcin[4]arene **54b** or pyrogallol[4]arene **55b**, except a derivative of **54b** that bears fluorinated “feet” that bestow solubility in fluoruous solvents.¹⁵¹ Considering these aspects, the synthesis of tetra-fluoride **140e** was attempted utilizing the established route for derivatives.

Inspired by a report from *Knochel et al.* on the fluorination of aryl Grignards,¹⁹⁶ the introduction of the fluorides was studied by treating the *in situ* formed aryllithium species with *N*-fluorobenzenesulfonimide (NFSI). To our delight, already the first attempt yielded the desired product **201** in satisfying yield (Scheme 64). Formation of the desired structure was confirmed by ESI-MS and NMR analysis. After column chromatography, ¹⁹F NMR analysis showed a single resonance at –149 ppm in acetone-*d*₆. Byproducts of the reaction were the mono-, di- and tri-fluorinated species.



Scheme 64: Synthesis of the protected tetra-fluoride **201**.

Likewise, the deprotection with boron tribromide proceeded smoothly, yielding a mixture of the desired product and the mono-methylated species (Scheme 65). Fortunately, in this case, column chromatography could be applied to separate both compounds, resulting in highly pure material of product **140e**. The co-isolated mono-methylated species is inherently chiral, but obtained as a racemate. Separation of the mono-propylated resorcin[4]arene **189** via chiral HPLC has so far been unsuccessful (see chapter 6.5.1). Nevertheless, separation of the two enantiomers of the mono-methylated tetra-fluoride should be investigated.



Scheme 65: Deprotection of compound **201**.

After removal of the residual solvent under high vacuum at 55 °C, the material was no longer soluble in regular chloroform-*d*₁. However, the compound could be dissolved utilizing water-saturated chloroform-*d*₁, which provided first evidence that water is indeed part of the assembly. Furthermore, the observed downfield shift of the water signal in the ¹H NMR spectrum in chloroform-*d*₁ is consistent with the data obtained for hexamer **XI** and strongly indicates incorporation of water into the hydrogen bond network (Figure 25a). Since the incorporated water molecules are in fast exchange with the bulk water, only a single resonance is observed

for the water molecules in the ^1H NMR spectrum. In addition, the obtained diffusion coefficient in chloroform- d_1 perfectly matches the one obtained for the hexameric assembly **XI** ($0.19 \times 10^{-5} \text{ cm}^2\text{s}^{-1}$). Additional DOSY experiments are required to determine the exact amount of incorporated water molecules per hexamer.¹⁸⁰ Nevertheless, the similarity to hexamer **XI** suggests the incorporation of eight water molecules into the hexameric assembly (Figure 24).

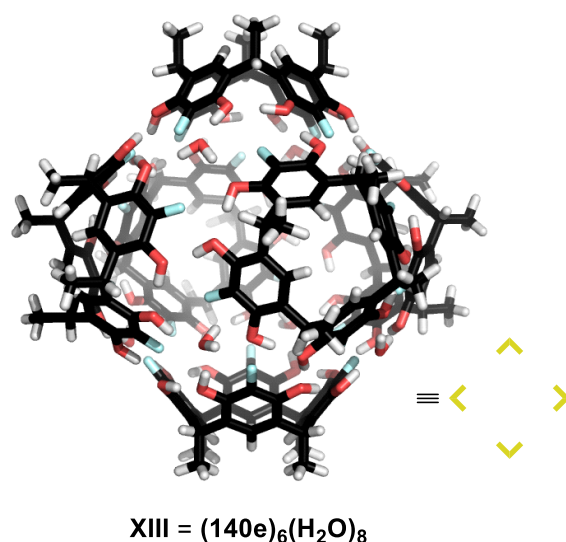


Figure 24: Model of the hexameric assembly **XIII** and its symbolic representation (with methyl “feet” for clarity; F = cyan).

A high water content reduces the reaction rate of THT cyclizations using hexamer **XI** as a catalyst. It is believed that the water molecules compete with the hydroxy group of the substrate for the protons of the catalyst. Therefore, the reactivity of hydrogen bond-based catalysts is investigated in regular, not water-saturated chloroform- d_1 . To enable the use of regular chloroform- d_1 , the water content of the material of **140e** was slowly increased by storage in an open flask. After two days of equilibration, integration of the ^1H NMR spectrum showed a water content of around 11 equiv. per hexamer after dissolution in regular chloroform- d_1 , which is suitable for reactivity studies (Figure 25a).

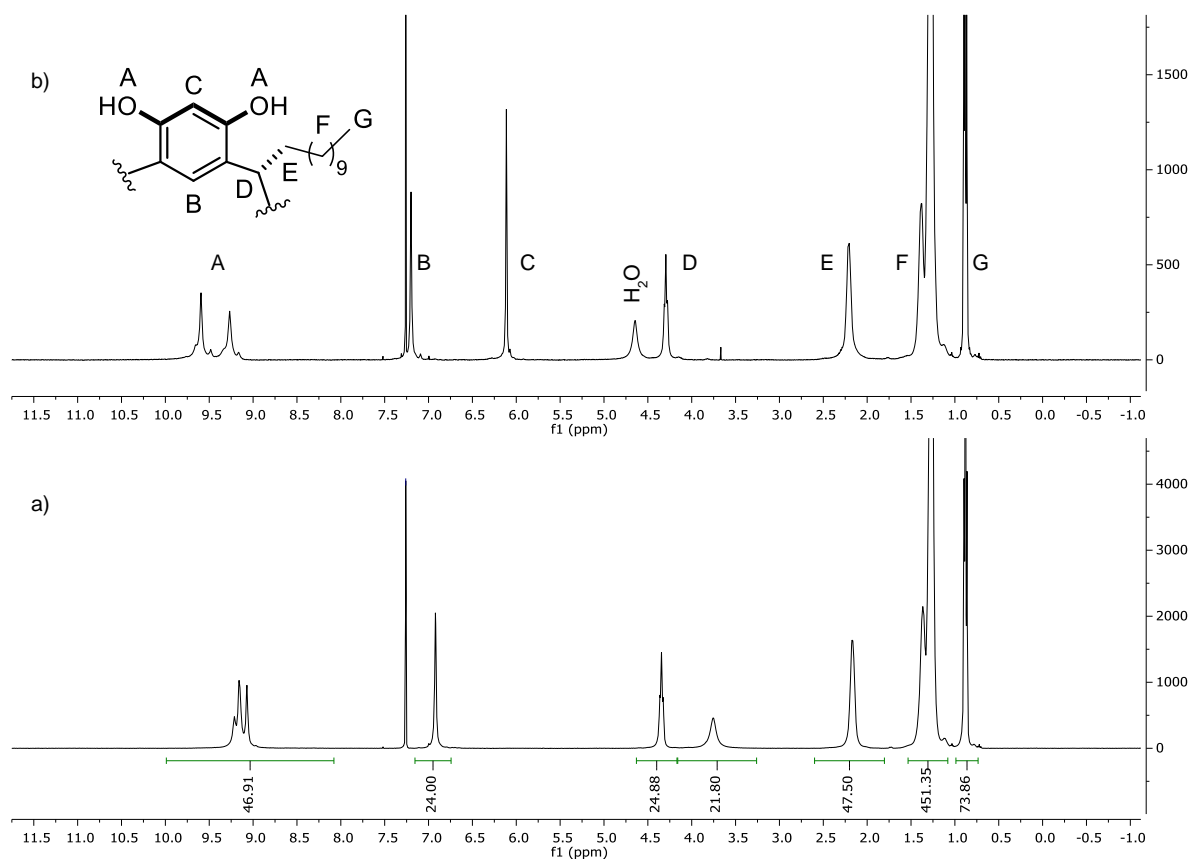


Figure 25: (a) ¹H NMR spectrum of **140e** in regular CDCl₃ (integration assuming hexamer formation; optimized water content; water signal at 3.75 ppm); (b) ¹H NMR spectrum of **54b** in regular CDCl₃, including signal assignment (reference).

The similarity between the structures **XI** and **XIII** stimulated the investigation of hetero-hexamer formation upon mixing of **54b** and **140e**. It has been demonstrated in the literature that macrocycle **54b** and **55a** self-assemble with complete self-recognition.¹⁹⁷ In that case, even after heating and a prolonged observation time, no hetero-hexamers were detected via DOSY NMR analysis. For the purpose of this study, hexamer **XI** (3.3 mM) and hexamer **XIII** (3.3 mM) were mixed in water-saturated chloroform-*d*₁ and the equilibration process was monitored via ¹H NMR analysis. The spectrum obtained directly after mixing resembles a mere superposition of the two individual ¹H NMR spectra (Figure 26). After storage at 30 °C for 43 h, the spectrum showed little difference except small changes in the phenolic OH-group pattern. However, after subsequently heating the same sample to 55 °C for 24 h, the obtained ¹H NMR spectrum clearly indicated some degree of scrambling. Besides the drastically changed pattern of the OH-groups, the splitting of the aromatic signal at 6.12 ppm provided strong evidence for the formation of hetero-hexamers. No further change in the appearance of the spectrum could be observed after additional heating, which indicated complete equilibration. Interestingly, the ¹H NMR spectrum of a mixture of hexamer **XII** and hexamer **XIII** remained a mere superposition, even after prolonged heating to 55 °C. In this case, the structural difference of the assemblies demands complete self-recognition. However, it has been reported that even without apparent changes in

the ^1H NMR spectrum hetero-hexamer formation can in some cases be detected via DOSY NMR.¹⁹⁷ Investigation of the self-recognition properties via DOSY NMR requires the use of molecules of different molecular weight. In this case, the molecular weight can be easily modified by changing the alkyl chains of the macrocycles. Therefore, to corroborate the obtained results regarding self-recognition, the experiments should be repeated with analogs of different molecular weight, for example with *i*-butyl resorcin[4]arene and compound **140e**.

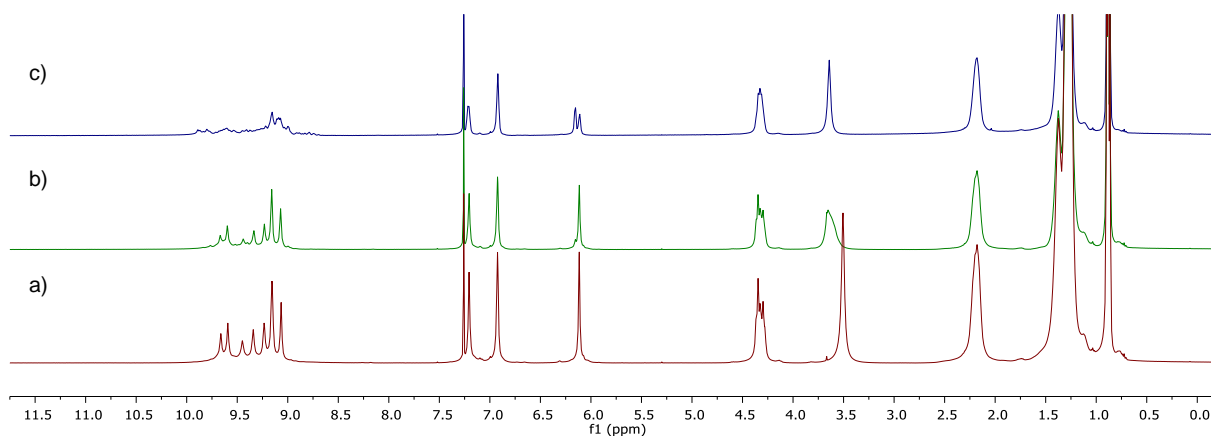


Figure 26: Self-sorting experiment: mixture of hexamer **XII** (3.3 mM) and **XIII** (3.3 mM) in $w\text{-CDCl}_3$ directly after mixing (a), after 43 h at 30 °C (b) and after heating to 55 °C for 24 h (c).

The investigation was continued by calculating the inner ESP surface of the hexameric assembly **XIII** using SPARTAN '16 at the AM1 level, which has been shown to produce reliable ESP surfaces.²⁹ The calculation is based on the structure obtained by adding fluorine atoms to the DFT-optimized structure of hexamer **XI**, followed by a molecular mechanics-based structure optimization (Figure 24). The ESP surface is considered to provide a qualitative indication of the potential strength of the cation- π interactions.²⁸ As shown in Figure 27, in the case of hexamer **XIII**, the area around the central aperture is of slightly lower potential (less red; less electron-rich) than in the case of hexamer **XI** or **XII**. Furthermore, the high-potential area surrounding the electron-poor (blue) hydrogen atoms of the water molecules is less pronounced than in hexamer **XI**. In addition, concentrated regions of low potential area can be assigned to the highly electronegative fluorine atoms. The results corroborate the expected inductive effect of the fluorine substituents on the ESP surface. Electron-density is pulled away from the aromatic core, which should result in weaker interactions with encapsulated cationic guest molecules.

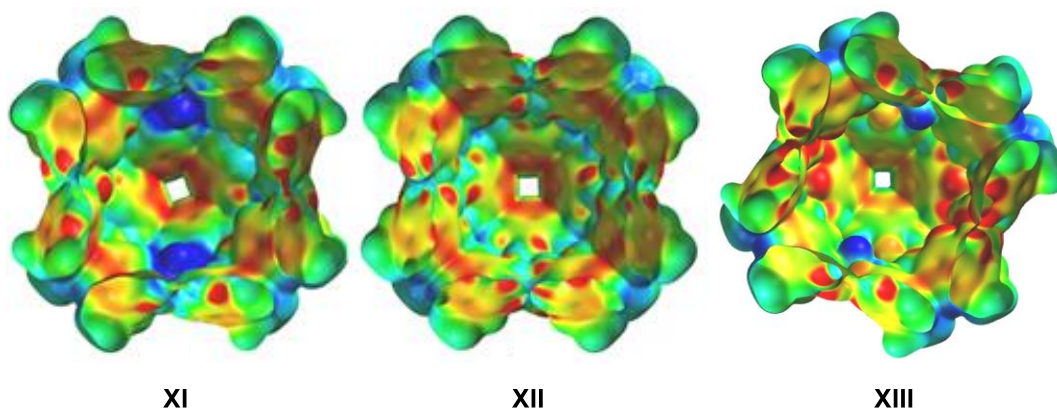


Figure 27: Comparison of the inner ESP surfaces of assemblies **XI**, **XII** and **XIII** (for details see experimental section).

In order to validate the theoretical data, encapsulation experiments with hexamer **XIII** were performed using triethylamine and tetrabutylammonium bromide. In both cases, good uptake was indicated by appearance of new upfield-shifted resonances and by integration of the signals of remaining free guest. Addition of 1.5 equiv. of tetrabutylammonium bromide to hexamer **XIII** resulted in the encapsulation of 0.91-0.96 equiv. in regular chloroform- d_1 , which is comparable to results obtained with hexamer **XI** in a parallel experiment. Unfortunately, signal overlap prevented determination of an exact value in the case of hexamer **XI**. Surprisingly, neither the presence of triethylamine nor tetrabutylammonium bromide led to a significant broadening of the hexamer signals, as observed with the original hexamer **XI**. Especially the new upfield-shifted resonances were significantly more defined than in the case of hexamer **XI**. This reproducible observation is exemplified for tetrabutylammonium bromide in Figure 28. The more defined signal pattern might indicate reduced interaction with the cavity walls and therefore less restricted tumbling of the encapsulated guest molecule. The reduced interaction might result from weaker cation- π interactions with the ammonium salt, which would be in good agreement with the theoretical data obtained from the ESP calculation (Figure 27).

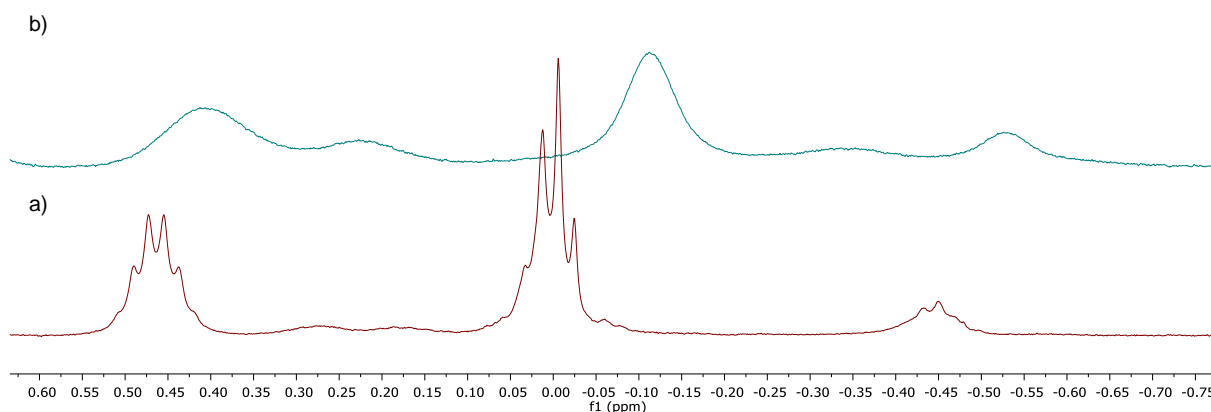


Figure 28: Interaction with a cationic guest: (a) hexamer **XIII** (3.3 mM) + TBAB (5.0 mM) in CDCl_3 ; (b) hexamer **XI** (3.3 mM) + TBAB (5.0 mM) in CDCl_3 .

According to our previous study with hexamer **XII** (chapter 6.4), encapsulation of an ammonium salt in chloroform- d_1 requires the co-encapsulation of the counteranion to avoid an energetically unfavorable charge separation. To probe this result with hexamer **XIII**, encapsulation of the NMR active mesylate anion was investigated by applying 1.0 equiv. of $\text{EtPr}_3\text{N}^+\text{MeSO}_3^-$. Surprisingly, the obtained ^1H NMR spectrum indicates encapsulation of the cationic component (signals between 0.60 and -1.60 ppm), while the mesylate functionality appears to reside outside the cavity (Figure 29). The slightly reduced integral of the mesylate anion (2.68 instead of 3.00) is believed to result from addition of less material than intended, due to the hygroscopic nature of the salt. This could in principle be verified by determination of the water content of $\text{EtPr}_3\text{N}^+\text{MeSO}_3^-$ via NMR analysis. Additionally, the encapsulation of the mesylate anion should be investigated using ^{13}C NMR spectroscopy. It is noteworthy that the signal of the mesylate anion displays a downfield shift in the presence of hexamer **XIII**, an effect, which is not observed in the case of pyrogallol[4]arene hexamer **XII**. However, further investigation via 2D NMR analysis is required, to undoubtedly assign the downfield-shifted signal to the mesylate anion. The cause for the apparent contradiction between good uptake of tetrabutylammonium bromide and repulsion of the mesylate anion remains to be investigated.

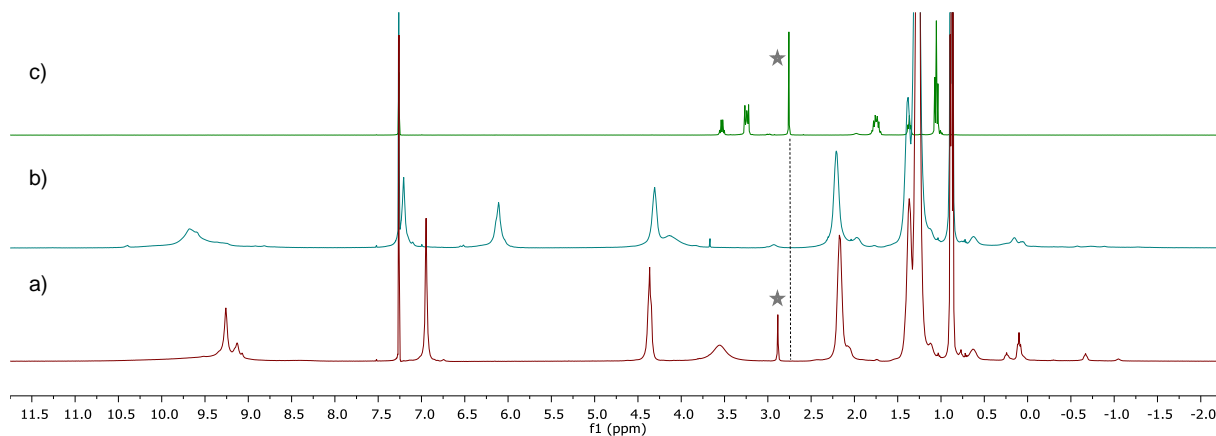


Figure 29: Anion binding studies in CDCl_3 : (a) hexamer **XIII** (3.3 mM) + $\text{EtPr}_3\text{N}^+\text{MeSO}_3^-$ (3.3 mM); (b) hexamer **XI** (3.3 mM) + $\text{EtPr}_3\text{N}^+\text{MeSO}_3^-$ (3.3 mM); (c) $\text{EtPr}_3\text{N}^+\text{MeSO}_3^-$ (3.3 mM) (signal of the anion MeSO_3^- marked with a star)

One of the primary goals of the investigation of derivatives concerns the determination of the pK_a values of their assemblies. Experience has shown that the NMR-based method utilized for the pK_a determination of hexamer **XI** can only be applied to highly symmetric assemblies. This is due to signal overlap in the case of less symmetric assemblies in the presence of an amine base, which prevents accurate integration of the signals. Fortunately, in the case of the highly symmetric assembly **XIII**, the established method, consisting of a series of deprotonation experiments with amines of varying basicity, could be successfully applied. The determined

pK_a value of approximately 6.5 renders hexamer **XIII** one order of magnitude less acidic than the resorcin[4]arene hexamer **XI** (for details see experimental section). The reduced acidity is surprising considering the influence of a fluorine substituent on the pK_a value of a regular phenol molecule (Figure 30).¹⁴⁵ The trend indicates that the inductive effect of the highly electronegative fluorine atom outweighs its countering mesomeric effect. One reason for the reduced acidity of **XIII** might be its weaker cation- π interactions with the ammonium ion after protonation, resulting in an energetically less stabilized product, which lowers the equilibrium concentration of protonated amine. Further investigations and detailed DFT calculations are necessary to completely understand the current data.

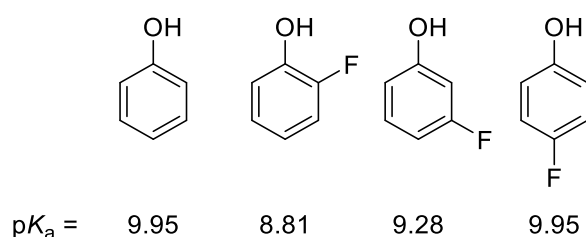


Figure 30: Influence of a fluorine substituent on the acidity of phenol.¹⁴⁵

Having shown that hexamer **XIII** is moderately acidic, the catalytic activity of the assembly in acetal hydrolysis and THT cyclizations was investigated. Addition of 10 equiv. of 1,1-diethoxyethane to a solution of **XIII** in water-saturated chloroform- d_1 (3.3 mM) resulted in only 5% conversion after 1 h at room temperature (42% after 16.5 h), compared to 85% conversion in the presence of hexamer **XI**. Addition of tetrabutylammonium bromide reduced the conversion rate by a factor of 10, which indicated that the reaction proceeds indeed within the cavity. Next, the catalytic activity in the THT cyclization of nerol (**19**), geraniol (**18**) and geranyl acetate (**138**) was investigated. The encapsulation of alcohol substrates by hexamer **XIII** was confirmed via ^1H NMR analysis for 3,7-dimethyl-1-octanol, which is the completely saturated analog of nerol (**19**) and geraniol (**18**). The saturated analog has been successfully utilized for NMR-based determination of the binding constant of terpene substrates in the case of hexamer **XI**. Unfortunately, attempts to determine the binding constant in the case of hexamer **XIII** failed, since the results obtained with trifluorotoluene as internal standard are not conclusive. However, the experiments clearly demonstrated that alcohol substrates are much weaker bound to the cavity than in the case of hexamer **XI**. This might result from weakening of the hydrogen bond to the incorporated water molecule by repulsion between the alcohol oxygen and the partially negative fluorine atom.

The result for the cyclization of nerol (**19**) in the presence of 10 mol% of hexamer **XIII** is depicted in Figure 31. The reaction proceeds extremely slowly and more than 17 days are required for full conversion of the starting material. Utilizing hexamer **XI**, full conversion of nerol (**19**) is achieved after only 10 h under otherwise identical reaction conditions.¹⁴ The conversion could be successfully inhibited by addition of 1.5 equiv. of tetrabutylammonium bromide, which indicated conversion within the cavity of **XIII**. The cyclic reaction products are obtained in very low yield and correspond to the products also observed with hexamer **XI**. Eucalyptol (not depicted in Figure 31), which is the main product (~40% yield) using hexamer **XI**, is obtained in less than 5% after 17 d at 30 °C. The difference in reaction rate cannot be attributed to a difference in water content, since the same trend is also observed in water-saturated chloroform. The reaction with geraniol proceeded even slower (57% conversion after 17 d) and yielded linalool as the main product in 11% and only traces of other cyclic monoterpenes. Only 42% of geranyl acetate (**138**) were consumed after 17 d and the reaction gave 5% of terpinolene as the main product.

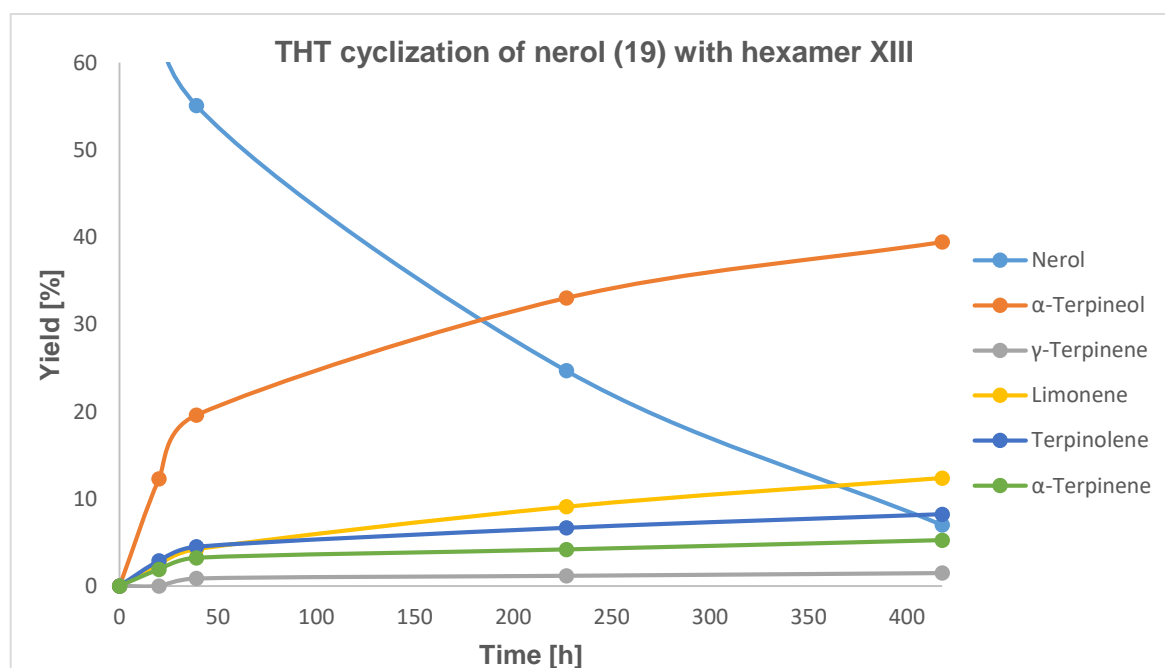
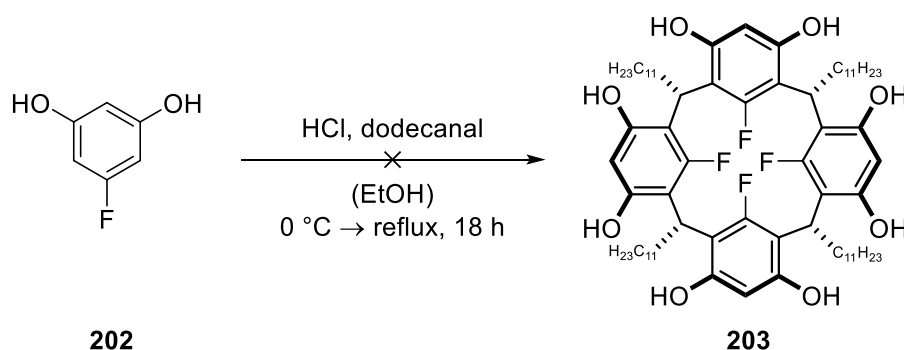


Figure 31: Hexamer **XIII** (10 mol%)-catalyzed THT cyclization of nerol (**19**) in regular chloroform-*d*₁ at 30 °C.

The elucidate the cause for the slow reaction, further kinetic investigations are required to determine the rate determining step of the hexamer **XIII**-catalyzed reaction. Internal studies have demonstrated that cleavage of the leaving group is the rate determining step in the hexamer **XI**-catalyzed THT cyclization in regular chloroform-*d*₁. However, also uptake of the substrate or activation of the substrate via protonation could be rate-determining in the case of hexamer **XIII**. To sum this up, hexamer **XIII** shows catalytic activity in the THT cyclization of

monoterpenes, but the activity is drastically reduced compared to the resorcin[4]arene hexamer **XI**.

Introduction of the fluorine substituents in 2-position (*ortho* to both phenolic OH-groups) was easily achieved via lithium-halogen exchange and subsequent addition of NFSI using the established route. However, introduction of the fluorine substituents in 5-position (*meta* to both phenolic OH-groups) was considered impossible after the initial macrocyclization step due to steric reasons. Although the 5-position is sterically crowded, molecular modelling indicates that the small fluorine substituents could be tolerated. The introduction was subsequently investigated by utilizing *meta*-fluororesorcinol (**202**), which could be readily synthesized by deprotection of the commercially available precursor in quantitative yield. Cyclization was attempted utilizing the established conditions for the synthesis of resorcin[4]arene **54b** (Scheme 66).¹⁵³ After complete addition of dodecanal, a solid chunk began to form upon heating of the reaction mixture. This can be considered an indication of irreversible polymerization. Protonation in *ortho*-position to the fluorine atom, which is necessary for depolymerization, is likely prevented by the strong inductive effect of the fluorine atom. Analysis of the formed solid was prevented by its complete insolubility in organic solvents, which further confirms the assumed polymerization.



Scheme 66: Unsuccessful attempt to synthesize derivative **203** by cyclization of *meta*-fluororesorcinol (**202**).

As a last point, it's worthy to mention that the established route could be successfully applied in a collaborative effort to the synthesis of hybrids between resorcin[4]arene **54b** and pyrogallol[4]arene **55b** (Figure 32).¹⁷¹ The number of hydroxy groups could be varied by selective debromination of the tetra-bromide **195** and subsequent conversion of the remaining bromides to hydroxy groups via rearrangement of the corresponding boronic acids in the presence of hydrogen peroxide.

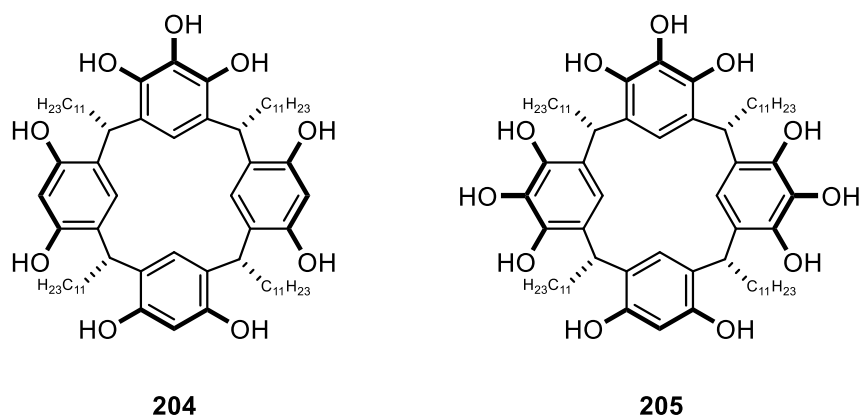


Figure 32: Successful preparation of the hybrid derivatives **204** and **205** utilizing the established synthetic route.¹⁷¹

7. Summary and outlook

The discovery of the Brønsted acid character of the resorcin[4]arene hexamer **XI** in 2013 triggered intensive investigation regarding its application in supramolecular acid catalysis. The unique aromatic microenvironment provided by the assembly was shown to efficiently stabilize cationic intermediates and transition states via cation- π interactions. The stabilization of cationic transition states by hexamer **XI** was successfully harnessed to catalyze the intramolecular hydroalkoxylation of encapsulated, unactivated hydroxy olefins under mild conditions. The preference of the cavity for smaller, flexible substrates was furthermore exploited to perform the reaction in a substrate selective fashion. The concept of using the resorcin[4]arene hexamer cavity as a reaction chamber was subsequently extended to a dehydrative cyclization-rearrangement cascade reaction. The extended delocalization of the negative charge could be utilized to perform some of the multistep reactions in a non-stop fashion without the detection of intermediates. The scope of the reaction was studied in detail for the first time. In addition, the study led to the discovery of an unprecedented cyclobutanone formation through an intramolecular 1,5-hydride transfer within the cavity of hexamer **XI**. Furthermore, first preliminary experiments were conducted regarding hexamer **XI**-catalyzed Friedel-Crafts alkylations. The principle feasibility of performing intermolecular Friedel-Crafts alkylations within the cavity was successfully demonstrated. A first experiment targeting selective oligomerization within the cavity was performed, but further investigation is required to assess the potential of this process. The extensive studies regarding application of hexamer **XI** revealed several intrinsic limitations of the current system. A limitation of catalyst **XI** discovered during the intramolecular hydroalkoxylation project was the inability to convert substrates requiring the formation of intermediary secondary cations. To overcome this limitation, the application of a high affinity acid co-catalyst was studied. Camphorsulfonic acid

was revealed to bind strongly to the cavity and to enable the intramolecular hydroalkoxylation of substrates bearing mono- and disubstituted double bonds. The co-encapsulation of substrate and camphorsulfonic acid could not be conclusively clarified and remains to be investigated. As an alternative, unconventional approach to increase the acidity of the catalyst, the photoacidity of the polyphenolic structure was investigated. Indeed, photoacidity could be utilized to accelerate and enable transformations in the presence of hexamer **XI**, but the reactions suffered from severe side reactions probably caused by homolytic cleavage of the phenolic OH-groups and a too low pK_a of the catalyst.

Despite the intensive practical research with hexamer **XI**, the fundamental requirements for the catalytic activity of this assembly and hydrogen bond-based structures in general remained elusive. Especially with the long-term goal of controlling THT cyclizations in supramolecular enzyme mimics in mind, efforts were directed towards increasing the understanding of the current system. The closely related, catalytically inert pyrogallol[4]arene hexamer **XII** was identified as a suitable target to study the molecular mechanisms responsible for catalytic activity. The study could show that the inactivity in the THT cyclization of monoterpenes resulted from a lack in acidity of the assembly. More importantly, the inability of pyrogallol[4]arene hexamer **XII** to encapsulate counteranions was revealed, which explained the failed attempts to activate the system by using an acid co-catalyst. This discovery is of prime importance, especially considering the design of novel catalyst that do not feature intrinsic acidity.

The research on catalytic prerequisites of hydrogen bond-based structures was further advanced by synthesizing lipophilic derivatives of the resorcin[4]arene monomer **54b** that were expected to self-assemble in solution. With the intention to study the catalytic activity of the formed assemblies, several derivatizations were performed, guided by indications obtained by molecular modelling. In this process, some of the originally selected targets for catalysis were shown to suffer intrinsic disadvantages. For instance, the tetra-benzyl alcohol derivative **140a** was demonstrated to be limited by the acid sensitivity of the newly introduced functionality. Also some data indicated that tetra-aldehyde **140b** might be unstable in the presence of nucleophilic substrates. To access more advanced derivatives, a versatile route was established centered around the protected tetra-bromide **195**. Relying on this strategy, the synthesis of tetra-carboxylic acid **140c** was attempted. Although the material obtained in this process could not be conclusively identified as **140c**, ESI-MS data supports isolation of the desired structure. The

route could be successfully applied to synthesize tetra-amide **140d**, which self-assembles via amide-dimer motifs. This alternative mode of connectivity is unprecedented in resorcin[4]arene chemistry and in principle enables further functionalization of the phenolic OH-groups. Additionally, introduction of fluorine substituents could be achieved for the first time in 2-position utilizing NFSI after lithium-halogen exchange, which led to the straightforward synthesis of the tetra-fluoro derivative **140e**. Detailed studies revealed the capability of **140e** to self-assemble to a resorcin[4]arene-like hexamer featuring incorporated water molecules. The pK_a value of the assembly could be determined in a series of deprotonation experiments to be approximately 6.5, which renders the newly developed hexamer about one order of magnitude less acidic than the original resorcin[4]arene hexamer **XI**. Evidence was provided that the drop in acidity is based on reduced cation- π interactions after protonation of the amine. In addition, preliminary data suggested that anions might not be encapsulated by the cavity of the formed hexamer **XIII**, but further analysis is required for clarification of this observation. Self-recognition of resorcin[4]arene **54b** and subunit **140e** could be overcome at higher temperatures, yielding a scrambled mixture of hetero-hexamers in solution. Finally, the catalytic activity of hexamer **XIII** in the THT cyclization of monoterpenes could be demonstrated. However, the catalytic activity was found to be drastically reduced in comparison to the resorcin[4]arene hexamer **XI**. In a joint effort, the developed synthetic route could be furthermore extended to the synthesis of hybrid subunits (**204** and **205**) featuring an uneven number of phenolic OH-groups.

First steps into the direction of an inherently chiral, enantiopure resorcin[4]arene hexamer catalyst were taken by successful mono-propylation of the resorcin[4]arene **54b**. The experiments performed suggested that the propyl group is tolerated by the hydrogen bond network and that hexamer formation is still possible. However, despite significant efforts, the two enantiomers of the obtained racemate were shown to be inseparable via chiral HPLC using different columns and eluent mixtures. In addition, some progress regarding mono-triflation could be reported. The mono-triflate could allow subsequent palladium chemistry for further functionalization, including mono-defunctionalization.

Despite some significant progress, several basic issues need to be resolved in the future. A reliable, NMR-independent method for the pK_a determination of the phenol-based assemblies has to be developed. Furthermore, ITC measurements have to be integrated into the research to provide a more universally applicable method for the determination of thermodynamic

parameters. In parallel, alternative methods for the determination of binding constants, like fluorophore displacement,¹⁹⁸ have to be investigated. Moreover, the role of HCl traces in the resorcin[4]arene hexamer-catalyzed THT cyclization has to be elucidated.

Research on resorcin[4]arene derivatives is only just beginning, and different aspects have to be considered in future investigations. The synthesis of the highly intriguing tetra-amide **140d** is flawed by the unreliable deprotection step utilizing boron tribromide. A protecting-group free synthesis based on an attack of ammonia or ammonia equivalent (phthalimide) on an intermediary *o*-quinomethine, followed by oxidation of the resulting benzyl amine could prove beneficial. Furthermore, the properties of the assembly formed by **140d** have to be investigated in detail. In this context, also different solvents have to be investigated to factor in the increased cavity size and to achieve an optimum packing coefficient. Additional studies are also required in the case of the assembly formed by tetra-fluoride **140e**, including stability towards polar additives, determination of the binding constants of substrate analogs, determination of kinetic parameters and sophisticated DFT calculations. Regarding the enantiopure resorcin[4]arene hexamer catalyst, mono-functionalizations with chiral, optically active electrophiles have to be performed in order to facilitate isolation of enantiopure material. Of prime importance is also the structure verification of the formed assemblies via X-ray crystallographic analysis. This will require synthesis and crystallization of derivatives bearing short alkyl groups (Me, *i*-Bu).

Based on the current results, the synthesis of two additional derivatives should be considered (Figure 33). First, the cavitand-like tetra-amide **206** is believed to provide significant advantages over subunit **140d**. The synthesis can in principle be accomplished in three reliable steps from resorcin[4]arene **54b**. Additionally, the uncontrollable deprotection step could be avoided. Self-assembly would be achieved via amide-dimerization, while bridging of the phenolic OH-groups would enforce the desired crown conformation. Catalytic activity could be achieved by addition of an external acid or functionalization of the methylene bridges. A second derivative that might be worth to investigate is tetra-thio pyrogallol[4]arene **207**. The thiol substituents could result in an increased acidity of an assumed assembly due to less severe mesomeric destabilization. At the same time, the electron-rich surface of the cavity would be maintained. Introduction of the thiol groups is believed to be possible via treating the protected tetra-aryl lithium species with elemental sulfur.¹⁹⁹ If self-assembly is prevented by introduction of the thiol groups, the building block could in principle still find application in a disulfide-based dynamic combinatorial library.

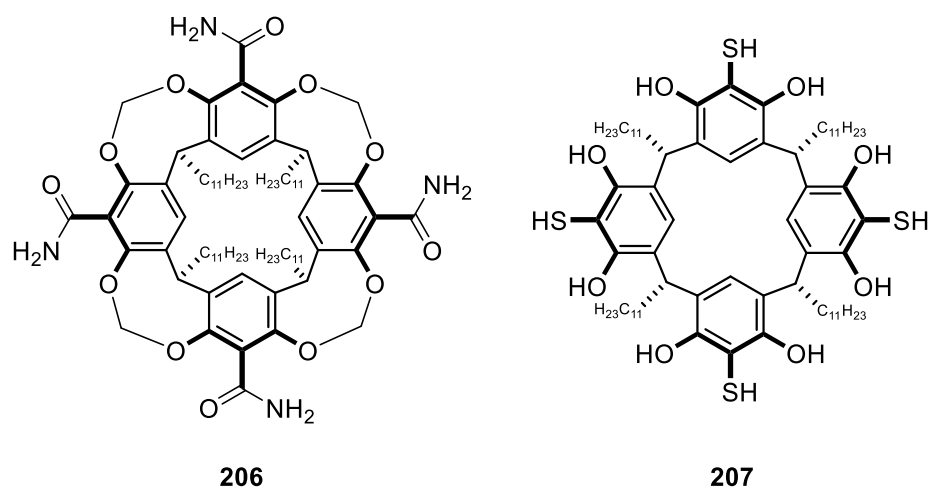


Figure 33: Possible derivatives of prospective investigations.

Another fundamental aspect that has to be investigated in prospective studies is the controlled modification of the cavity space. This could either be achieved by tightly bound co-guests or by inwards directed functionalities incorporated into the subunits. Studies on the pyrogallol[4]arene hexamer **XII** have shown that anion binding might be the key to supramolecular acid catalysis utilizing acid co-catalysts. Anion binding within the cavity might be favored by installing halogen atoms into the subunits that point into the cavity and facilitate anion binding via halogen bonding.²⁰⁰ The advantage over classical hydrogen bonding would be the non-nucleophilic character of the inwards directed halogen functionalities, which would not interfere with the cationic cascade reaction within the self-assembled reaction-chamber.

8. Experimental section

8.1 General information

Experimental:

Reactions were carried out under an atmosphere of argon unless otherwise indicated. Analytical thin-layer chromatography (TLC) was performed on Merck silica gel 60 F₂₅₄ glass-baked plates, which were analyzed under UV light ($\lambda = 254$ nm) or after exposure to standard staining reagents (basic KMnO₄, iodine or CAM: cerium ammonium molybdate). Solutions of *n*-butyllithium in hexanes were titrated at 0 °C in THF against menthol with 1,10-phenanthroline as indicator. All NMR experiments were performed on three Bruker Avance III NMR spectrometers operating at 250 MHz, 400 MHz and 500 MHz proton frequency. The instruments were equipped with a direct observe 5-mm BBFO smart probe or an indirect 5-mm BBI probe (500 MHz). The experiments were performed at 295 K and 298 K (500 MHz) and the temperature was calibrated using a methanol standard showing accuracy within +/- 0.2 K. Chemical shifts of ¹H NMR, ¹³C NMR and ¹⁹F NMR are given in ppm. The proton signal of the deuterated solvent was used as reference: CDCl₃ $\delta(^1\text{H}) = 7.26$ ppm, $\delta(^{13}\text{C}) = 77.16$ ppm; (CD₃)₂SO $\delta(^1\text{H}) = 2.50$ ppm, $\delta(^{13}\text{C}) = 39.52$ ppm; (CD₃)₂CO $\delta(^1\text{H}) = 2.05$ ppm, $\delta(^{13}\text{C}) = 206.26$ ppm. For ¹⁹F NMR, a drop of CFC1₃ ($\delta(^{19}\text{F}) = 0.00$ ppm) was added to the sample as internal standard. Coupling constants (*J*) are reported in Hertz (Hz). Standard abbreviations indicating multiplicity were used as follows: s (singlet), bs (broad singlet), d (doublet), t (triplet), m (multiplet). DOSY NMR measurements were performed utilizing standard NMR tubes. GC analyses for the Friedel-Crafts alkylation and the modulation studies were done on an Agilent GC6890 instrument equipped with a FID detector and a HP-5 capillary column (length = 29.5 m). Hydrogen was used as the carrier gas and the constant-flow mode (flow rate = 1.8 mL min⁻¹) with a split ratio of 1:20 was used. The following temperature-program was used: 60 °C for 3 min, 15 °C min⁻¹ to 250 °C, and 250 °C for 5 min. GC analyses for all other experiments were done on a Shimadzu GC-2010 Plus instrument equipped with a FID detector and a Rtx-5 capillary column (length = 30.0 m). Hydrogen was used as the carrier gas and the constant-flow mode (flow rate = 40 mL min⁻¹) with a split ratio of 1:20 was used. The following temperature-program was used: 60 °C for 1 min, 15 °C min⁻¹ to 250 °C, and 250 °C for 5 min. Direct injection mass spectrometry using the electrospray ionization (ESI) technique was performed on an esquire 3000 plus instrument by Shimadzu. High-resolution mass spectra were obtained using the ESI technique on a Bruker maXis 4G mass spectrometer. Centrifugation was

performed using a VWR MiniStar silverline. Infrared (IR) spectra were measured on a Bruker ALPHA IR spectrometer (ATR, attenuated total reflection). UV/VIS measurements were carried out using a Perkin Elmer Lambda 35 spectrometer. Irradiation experiments were conducted in a RPR-100 photochemical reactor by Rayonet equipped with 16 fluorescence lamps (RPR-2537 Å ($\lambda = 254$ nm), RPR-3000 Å ($\lambda = 300$ nm), RPR-3500 Å ($\lambda = 350$ nm), Philips black light blue 8 W ($\lambda = 366$ nm)). The reaction mixtures were irradiated in Duran tubes (300 nm, 350 nm, 366 nm) or quartz tubes (254 nm). The reactor was cooled with an internal fan. For the photoreactions, no degassing of the solvents was performed due to the S₁ character of the investigated photoacidity.

Chemicals:

THF was processed by a Pure Solv solvent purification system prior to use. All other solvents used for synthesis were purchased from Sigma-Aldrich and Acros Organics with the highest commercially available purity and employed without further treatment. For work-up and column chromatography ethyl acetate, dichloromethane and methanol were purchased from VWR in HPLC-grade purity. Pentane and diethyl ether were purchased in technical grade and distilled prior to use. CDCl₃ (99.8%) was purchased from Deutero GmbH and Sigma-Aldrich. All employed reagents were purchased from commercial distributors (Sigma-Aldrich, Acros Organics, Fluka, Alfa Aesar, VWR) and used without further purification. Resorcin[4]arene **54b**,¹⁵³ pyrogallol[4]arene **55b**⁸⁸ and *C-iso*-butylcalix[4]resorcinarene²⁰¹ were synthesized according to published procedures.

Details regarding experiments with the supramolecular catalysts:

Transfer of liquids with a volume ranging from 1 to 10 μ L or from 10 to 100 μ L was performed with a Microman M1 pipette (Gilson, systematic error: 1.40% - 1.60%) equipped with 10 μ L or 100 μ L pipette tips respectively. For reactions with the supramolecular catalysts, only glass pipettes and syringes with stainless steel cannula from Unimed were used in the preparation to prevent contamination with silicone grease, which is visible at 0.07 ppm in the ¹H NMR spectrum. The weighing of tetrabutylammonium bromide and substrates with unknown density for the preparation of stock solutions and density determinations was performed using a M3P Sartorius microbalance.

Molecular modelling:

Molecular modelling was performed using Spartan '16 (Wavefunction, Irvine, CA, 2016, Version 1.0.0). All modelled structures were based on the DFT-optimized structures of hexamer **XI** and **XII**.⁸⁸ The ESP surface of hexamer **XIII** was calculated at the AM1 level. The potential energy values displayed in Figure 10 and 27 range from +104.6 kJ mol⁻¹ (25 kcal mol⁻¹) to -104.6 kJ mol⁻¹ (-25 kcal mol⁻¹). The red color indicates a value equal to or larger than the maximum in negative potential. The blue color indicates a value equal to or larger than the maximum in positive potential. Rendering of the obtained models was performed with the software PyMOL (Schrödinger, LLC, 2014, Version 1.7.6.0).

Experimental details regarding the intramolecular hydroalkoxylation¹⁵³ (chapter 6.1.1), the cyclodehydration-rearrangement cascade reaction¹⁵⁴ (chapter 6.1.2) and the pyrogallol[4]arene studies⁸⁸ (chapter 6.4) can be found in the corresponding supporting information.

8.2 General procedures for hexamer studies

8.2.1 General procedure for catalytic tests with hexamer **XI**:

C-Undecylcalix[4]resorcinarene (**54b**) (11.0 mg, 9.95 μmol, 6.0 eq.) was weighed directly into a GC vial. After addition of CDCl₃ (0.50 mL), the mixture was gently heated with a heat gun under agitation to ensure complete homogeneity. To this solution, *n*-decane (internal standard) (2.59 μL, 13.3 μmol, 8.0 eq.) and the substrate (16.6 μmol, 10.0 eq.) were added successively in one portion and the mixture was immediately sampled after 30 s of vigorous agitation. The small sample (approximately 10 μL) was diluted with *n*-hexane (0.1 mL) containing 0.08% (v/v) DMSO – the addition of *n*-hexane containing DMSO results in termination of the reaction in this sample and precipitation of the catalyst (protects the GC instrument) – centrifuged, decanted and subjected to GC analysis (initial sample). The GC vial was kept at the given temperature (±1 °C) using a thermostated heating block made from alumina. The progress of the reaction was monitored via GC analysis. For NMR analysis, the sample was transferred into a NMR tube using a glass pipette.

For the preliminary Friedel-Crafts alkylation experiments (chapter 6.2), GC-based yields were calculated assuming a response factor (RF) of 1.0 for starting material and product relative to

n-decane as internal standard (IS). Conversions and yields were then calculated by employing the following equations (8.1 – 8.5).

$$n(\text{sm})_0 = \frac{(A_{\text{sm}})_0}{\text{RF}_{\text{sm}} \cdot (A_{\text{IS}})_0} = x \quad (8.1)$$

$$n(\text{sm})_n = \frac{(A_{\text{sm}})_n}{\text{RF}_{\text{sm}} \cdot (A_{\text{IS}})_n} = y \quad (8.2)$$

$$n(\text{p})_n = \frac{(A_{\text{p}})_n}{\text{RF}_{\text{p}} \cdot (A_{\text{IS}})_n} = z \quad (8.3)$$

$$\text{conversion}(\text{sm}) = \left(\frac{x - y}{x} \right) \cdot 100\% \quad (8.4)$$

$$\text{yield}(\text{p}) = \left(\frac{z}{x} \right) \cdot 100\% \quad (8.5)$$

$n(\text{sm})_n$ = amount of starting material in the *n*-th measurement; $(A_{\text{sm}})_0$ = area of starting material in the initial measurement; $(A_{\text{IS}})_0$ = area of internal standard in the initial measurement; $(A_{\text{sm}})_n$ = area of starting material in the *n*-th measurement; $(A_{\text{IS}})_n$ = area of internal standard in the *n*-th measurement; $(A_{\text{p}})_n$ = area of product in the *n*-th measurement; RF_{sm} = response factor of starting material; RF_{p} = response factor of product.

NMR-based yields were calculated by utilizing hexamer **XI** as an internal standard. For this purpose, an integral value of a hexamer **XI** resonance was normalized to the expected value (methine group = 24H, *o*-aromatic proton = 24H or CH₂ group next to the methine group = 48H). The integral of a product resonance was then compared to the expected value assuming complete and selective conversion of 10.0 eq. of substrate to the corresponding product.

8.2.2 General procedure for the control experiments with inhibitor Bu₄NBr:

Stock solutions of Bu₄NBr were prepared in a concentration of 62.3 mM in CDCl₃.

C-Undecylcalix[4]resorcinarene (**54b**) (11.0 mg, 9.95 μmol, 6.0 eq.) was weighed directly into a GC vial. After addition of CDCl₃ (0.46 mL), the mixture was gently heated with a heat gun under agitation to ensure complete homogeneity. Subsequently an aliquot of a Bu₄NBr (2.49 μmol, 1.5 eq.) stock solution in CDCl₃ was added to give a total volume of 0.50 mL. Under agitation the sample was subsequently heated using a heat gun to ensure complete uptake of the inhibitor. After allowing the solution to cool to rt, *n*-decane (internal standard) (2.59 μL,

13.3 μmol , 8.0 eq.) and the substrate (16.58 μmol , 10.0 eq.) were added in one portion and the mixture was immediately sampled. The GC vial was kept at the given temperature (± 1 $^{\circ}\text{C}$) using a thermostated heating block made from alumina. The reaction was monitored by GC analysis. The background conversions were calculated by employing the equations above (8.1, 8.2, 8.4).

8.2.3 General procedure for the modulation experiments with camphorsulfonic acid:

Stock solutions of camphorsulfonic acid were prepared in a concentration of 11.1 mM in CDCl_3 .

C-Undecylcalix[4]resorcinarene (**54b**) (11.0 mg, 9.95 μmol , 6.0 eq.) was weighed directly into a GC vial. After addition of CDCl_3 (0.35 mL), the mixture was gently heated with a heat gun under agitation to ensure complete homogeneity. Subsequently an aliquot of a camphorsulfonic acid (1.66 μmol , 1.0 eq.) stock solution in CDCl_3 was added to give a total volume of 0.50 mL. Under agitation the sample was subsequently heated using a heat gun to ensure complete uptake of the co-catalyst. After allowing the solution to cool to rt, *n*-decane (internal standard) (2.59 μL , 13.3 μmol , 8.0 eq.) and the substrate (16.58 μmol , 10.0 eq.) were added in one portion and the mixture was immediately sampled. The GC vial was kept at the given temperature (± 1 $^{\circ}\text{C}$) using a thermostated heating block made from alumina. The reaction was monitored by GC analysis. The conversions and yields were then calculated by employing the equations above (8.1 – 8.5).

8.2.4 General procedure for the modulation experiments using photoacidity:

The reactions were performed analogously to the standard procedure (8.2.1). However, the reaction scale was tripled to ensure a higher surface for photon absorption and a reduced amount of internal standard (4.0 eq.) was used. The reactions were monitored via GC analysis. The conversions and yields were then calculated by employing the equations above (8.1 – 8.5). For the reaction with substrate **143** and nerol (**19**), the previously determined response factors were used.^{14,153}

8.2.5 General procedure for the THT cyclizations with hexamer **XIII** and (**189**)₆:

The reactions were performed analogously to the standard procedures (8.2.1, 8.2.2). However, a reduced amount of internal standard (4.0 eq.) was used. In order to precisely calculate the conversions and yields of the THT cyclizations, GC-response factors to *n*-decane as internal

standard were utilized, which had been determined previously (Table 6).¹⁴ The values were validated for the new instrument that was used for the experiments.¹⁷¹

Table 6: GC-response factors to *n*-decane for acyclic and cyclic monoterpenes.

compound	RF
nerol (19)	0.90
geraniol (18)	0.91
geranyl acetate (138)	1.15
α -terpineol (10)	0.97
eucalyptol (11)	0.90
terpinolene (6)	0.94
limonene (5)	0.97
α -terpinene (7)	0.94
linalool (20)	0.86
γ -terpinene (8)	0.99

8.2.6 Acetal hydrolysis with hexamer **XIII**:

Water-saturated CDCl_3 (w- CDCl_3) was prepared by filtration of CDCl_3 (20 mL) through basic aluminum oxide 60 active (5 mL, activity stage I), adding distilled water (0.10 mL) and mixing the sample by agitation. After letting the mixture equilibrate for 30 minutes, the CDCl_3 -phase was directly used for the experiments.

Compound **140e** (11.7 mg, 9.95 μmol , 6.0 eq.) was weighed directly into a GC vial. After addition of w- CDCl_3 (0.50 mL), the mixture was gently heated with a heat gun under agitation to ensure complete homogeneity. The mixture was then transferred into a NMR tube. Next, 1,1-diethoxyethane (2.38 μL , 16.6 μmol , 10.0 eq.) was added in one portion and the mixture was immediately subjected to NMR spectroscopy to determine the initial ratio between substrate and hexamer **XIII** (internal standard). Following the acquisition of the ^1H NMR spectrum, the NMR tube was kept at room temperature. The reaction was monitored by NMR analysis (Figure 34). The conversions were calculated by employing the equations above and the following equations (8.6 - 8.7).

$$n(\text{sm})_0 = \frac{(I_{\text{sm}})_0}{(I_{\text{sm}})_{0,\text{exp}}} = x \quad (8.6)$$

$$n(\text{sm})_n = \frac{(I_{\text{sm}})_n}{(I_{\text{sm}})_{0,\text{exp}}} = y \quad (8.7)$$

$n(\text{sm})_0$ = amount of starting material in the initial measurement; $(I_{\text{sm}})_0$ = integral of a characteristic starting material resonance in the initial measurement, after normalizing an integral value of a hexamer **XIII** resonance (methine group = 24H); $(I_{\text{sm}})_{0,\text{exp}}$ = expected integral of the corresponding resonance assuming 10.0 eq. of starting material; $(I_{\text{sm}})_n$ = integral of a characteristic starting material resonance in the n-th measurement, after normalizing an integral value of a hexamer **XIII** resonance.

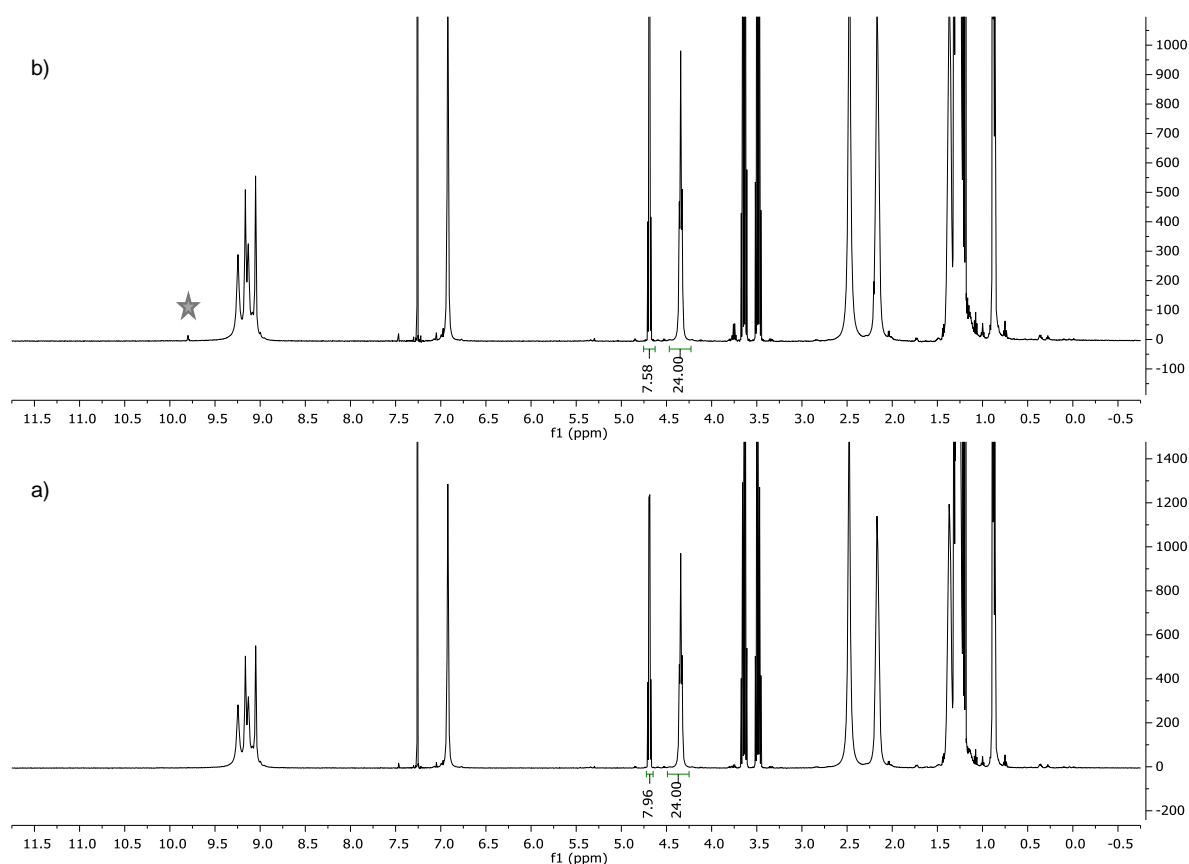


Figure 34: Acetal hydrolysis with hexamer **XIII** in CDCl₃: (a) ¹H NMR directly after substrate addition; (b) ¹H NMR after 1 h at rt (aldehydic proton marked with a star).

Control experiment in the presence of Bu₄NBr: compound **140e** (11.7 mg, 9.95 μmol, 6.0 eq.) was weighed directly into a GC vial. After addition of w-CDCl₃ (0.46 mL), the mixture was gently heated with a heat gun under agitation to ensure complete homogeneity. Subsequently an aliquot of a Bu₄NBr (2.49 μmol, 1.5 eq.) stock solution in w-CDCl₃ was added to give a total

volume of 0.50 mL. The mixture was then transferred into a NMR tube. The reaction itself was performed and analyzed as described above.

8.2.7 Encapsulation studies with hexamer **XIII** and (**189**)₆:

Compound **140e** (11.7 mg, 9.95 μmol , 6.0 eq.) was weighed directly into a GC vial. After addition of CDCl_3 (0.46 mL), the mixture was gently heated with a heat gun under agitation to ensure complete homogeneity. Subsequently an aliquot of a Bu_4NBr (2.49 μmol , 1.5 eq.) stock solution in CDCl_3 was added to give a total volume of 0.50 mL. The mixture was then transferred into a NMR tube and kept at 30 °C for 30 min. The sample was then subjected to NMR analysis (Figure 28).

The encapsulation of Bu_4NBr by the ensemble of hexamers formed by compound **189** was studied analogously. However, *w*- CDCl_3 was used instead of regular CDCl_3 , in order to ensure correct formation of the hexamers (Figure 14).

Compound **140e** (11.7 mg, 9.95 μmol , 6.0 eq.) was weighed directly into a GC vial. After addition of CDCl_3 (0.46 mL), the mixture was gently heated with a heat gun under agitation to ensure complete homogeneity. Subsequently an aliquot of a $\text{EtPr}_3\text{N}^+\text{MeSO}_3^-$ (1.66 μmol , 1.0 eq.) stock solution in CDCl_3 (41.5 mM) was added to give a total volume of 0.50 mL. The mixture was then transferred into a NMR tube and kept at 30 °C for 30 min. The sample was then subjected to ^1H NMR analysis (Figure 29). The encapsulation study was performed analogously in parallel with compound **54b**.

8.2.8 Self-recognition studies with compounds **140e** and **54b**:

Compound **140e** (11.7 mg, 9.95 μmol , 6.0 eq.) was weighed directly into a GC vial. After addition of *w*- CDCl_3 (0.25 mL), the mixture was gently heated with a heat gun under agitation to ensure complete homogeneity. The same procedure was performed in parallel with compound **54b** (11.0 mg, 9.95 μmol , 6.0 eq.) using a second GC vial. The two solutions were subsequently combined in a NMR tube and immediately subjected to ^1H NMR analysis. The sample was then kept at the given temperature (± 1 °C) using a thermostated heating block made from alumina. The progress of the equilibration process was monitored via NMR analysis (Figure 26). A second experiment using **55b** instead of **54b** was performed analogously.

8.2.9 Determination of the pK_a value of hexamer **XIII**:

Compound **140e** (11.7 mg, 9.95 μmol , 6.0 eq.) was weighed directly into a NMR tube. After addition of $w\text{-CDCl}_3$ (prepared as described above) (0.46 mL), the mixture was gently heated with a heat gun under agitation to ensure complete homogeneity. Next, 20 μL of a tetraethylsilane (internal standard) (1.69 μmol , 1.0 eq.) stock solution in $w\text{-CDCl}_3$ (84.6 mM) were added and the mixture was subjected to ^1H NMR analysis to determine the initial ratio between internal standard and hexamer **XIII**. Subsequently 20 μL of an amine (0.83 μmol , 0.5 eq.) stock solution in $w\text{-CDCl}_3$ (41.5 mM) were added, the mixture was agitated and then kept at 30 $^\circ\text{C}$ for 30 min. Following, a ^1H NMR of the sample was measured to determine the protonation ratio via integration (Figure 35-37). The pK_a value was subsequently calculated using the equations presented in Figure 38.

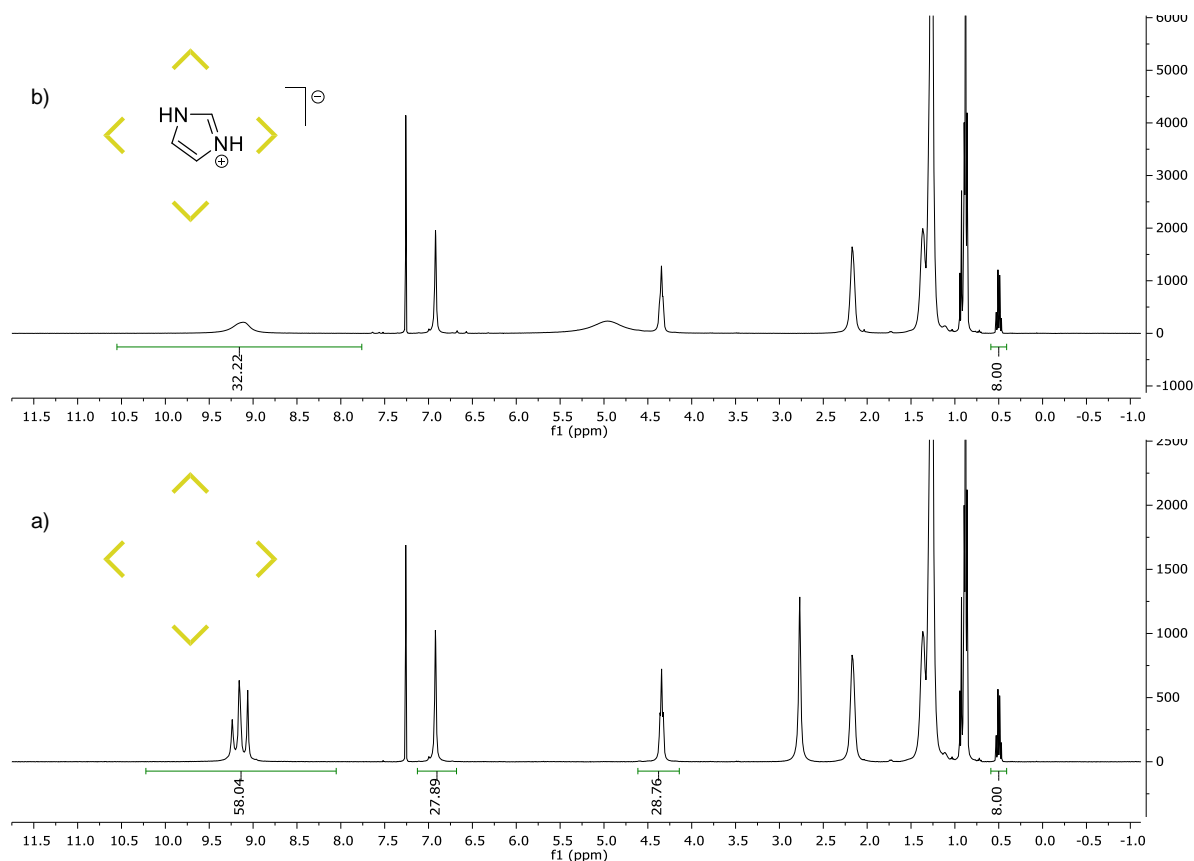


Figure 35: Protonation studies with imidazole: (a) **XIII** (3.3 mM); (b) **XIII** (3.3 mM) + imidazole (1.66 mM); 89% of added imidazole was protonated by **XIII** as indicated by the integral of the remaining phenolic protons.

8. Experimental section

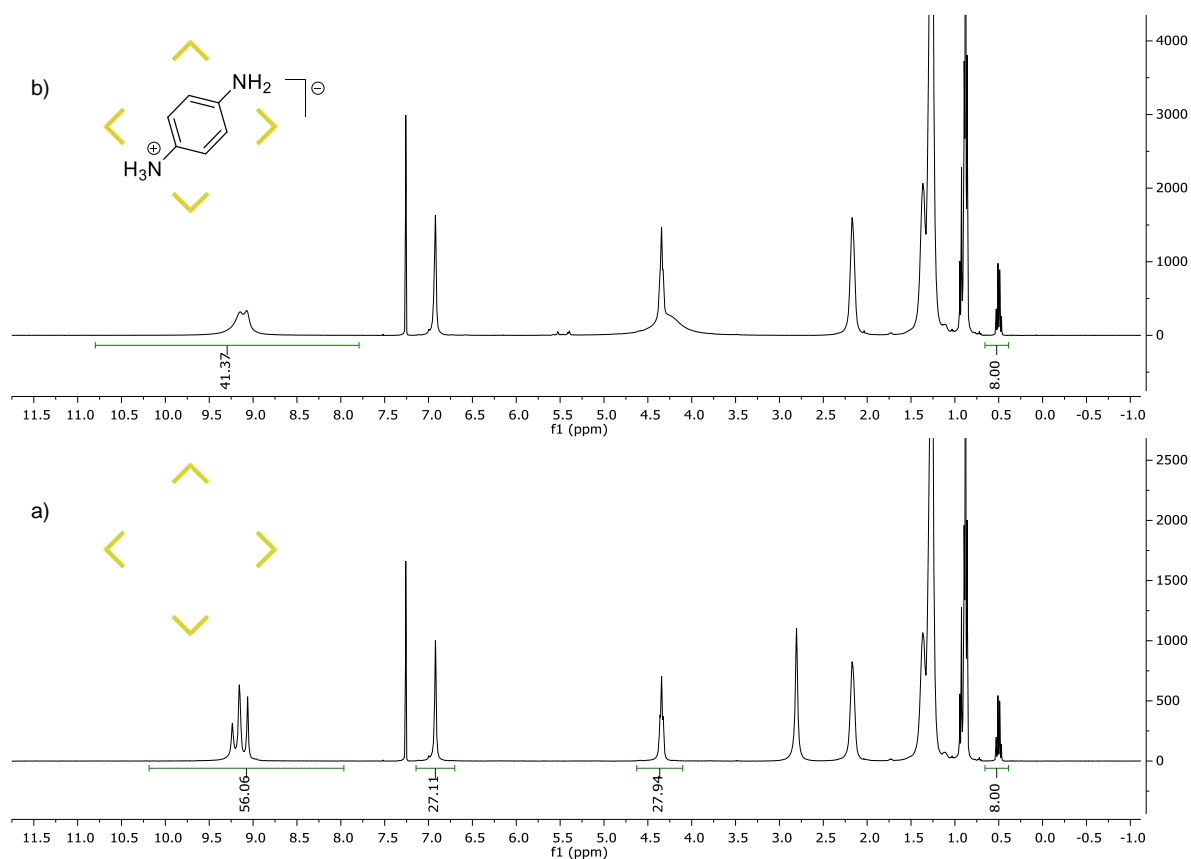


Figure 36: Protonation studies with *p*-phenylenediamine: (a) **XIII** (3.3 mM); (b) **XIII** (3.3 mM) + *p*-phenylenediamine (1.66 mM); 52% of added *p*-phenylenediamine was protonated by **XIII** as indicated by the integral of the remaining phenolic protons.

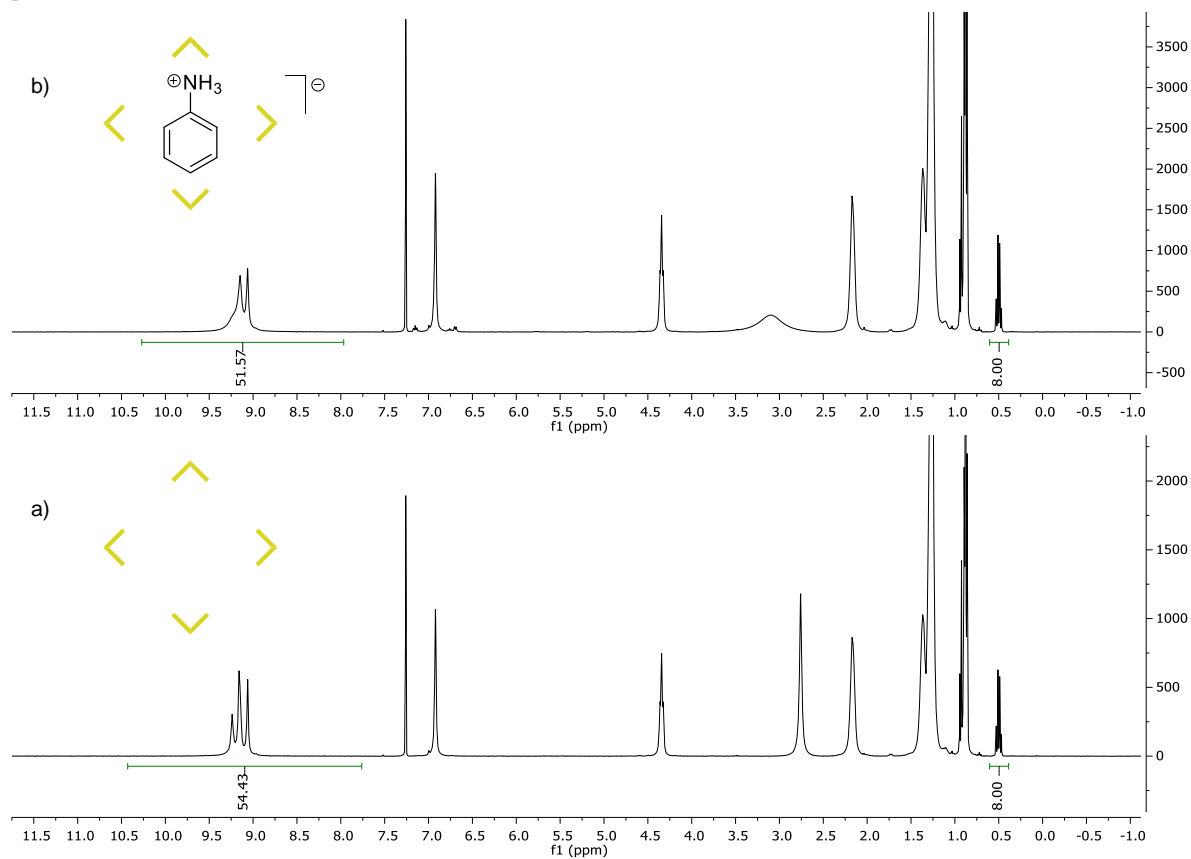


Figure 37: Protonation studies with aniline: (a) **XIII** (3.3 mM); (b) **XIII** (3.3 mM) + aniline (1.66 mM); 10% of added aniline was protonated by **XIII** as indicated by the integral of the remaining phenolic protons.

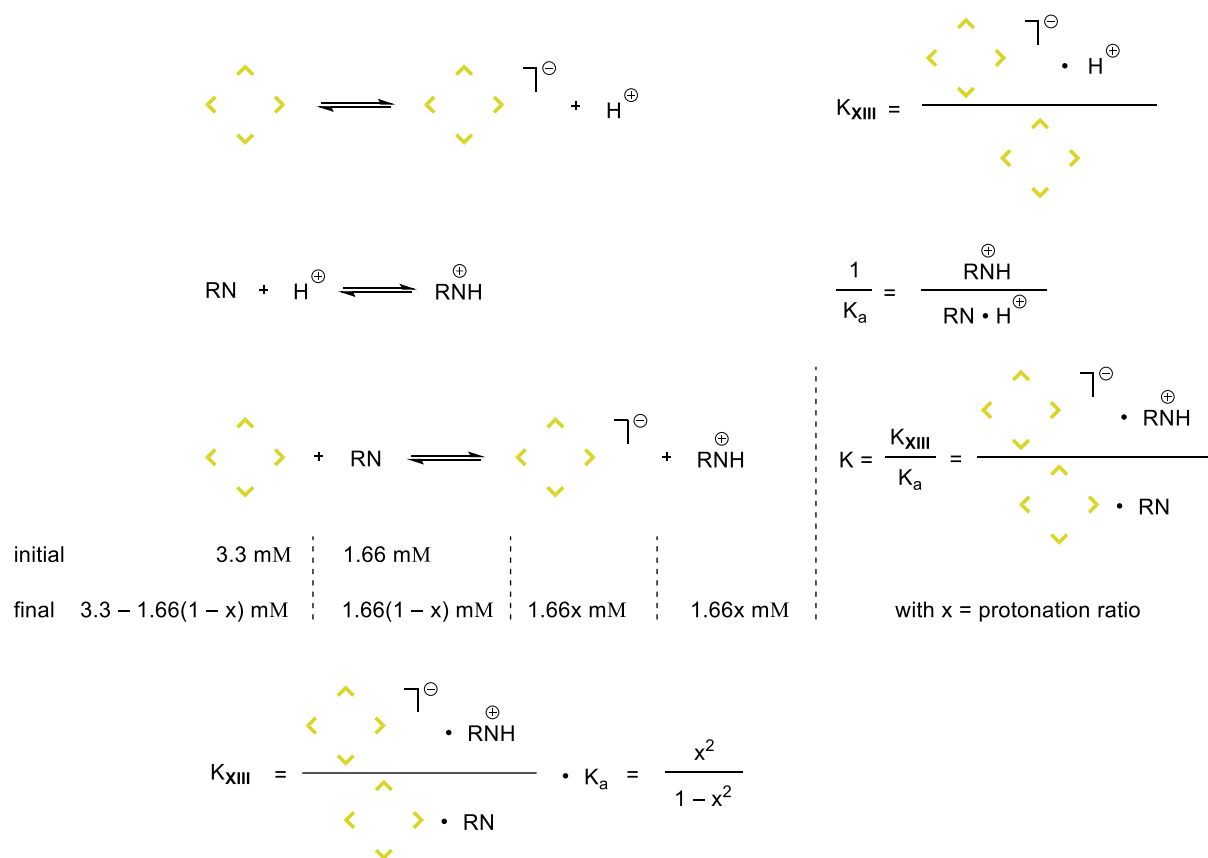


Figure 38: Equations used for the calculation of the pK_a value of hexamer **XIII**.

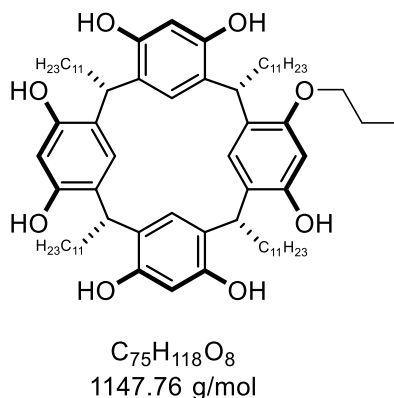
In case of imidazole, $K_a = 10^{-7.0}$, $x = 89\%$, $\rightarrow pK_{XIII} = 6.4$

In case of *p*-phenylenediamine, $K_a = 10^{-6.1}$, $x = 52\%$, $\rightarrow pK_{XIII} = 6.5$

In case of aniline, $K_a = 10^{-4.6}$, $x = 10\%$, $\rightarrow pK_{XIII} = 6.6$

$\rightarrow \emptyset = 6.5$

8.3 Synthetic procedures

7⁶-Propoxy-2,4,6,8-tetraundecyl-1,3,5,7(1,3)-tetrabenzenacyclooctaphane-14,16,34,36,54,56,74-heptaol (189)

To a stirred solution of *C*-undecylcalix[4]resorcinarene (**54b**) (10.0 g, 9.05 mmol, 1.0 eq.) in a mixture of anhydrous DMF (50 mL) and anhydrous THF (25 mL) was added potassium *tert*-butoxide (1.32 g, 11.8 mmol, 1.3 eq.) at rt. The red solution was subsequently refluxed for 45 min at 130 °C. After cooling to rt, *n*-propyl iodide (1.15 mL, 11.8 mmol, 1.3 eq.) was added rapidly and the reaction mixture was stirred at 130 °C for 18 h. The reaction was quenched at rt by addition of water and the crude product was extracted with Et₂O (3 × 100 mL). The combined organic phases were washed with water (5 × 100 mL), dried over Na₂SO₄, filtered and concentrated under vacuum. Purification by flash column chromatography (CH₂Cl₂/MeCN = 7/2 → 7/4) yielded ether **189** as a beige solid. Subsequent recrystallization from methanol, followed by drying under high vacuum at 55 °C overnight gave the pure product (2.00 g, 1.74 mmol, 19%) as a white powder.

¹H NMR (400 MHz, acetone-*d*₆): δ [ppm] = 8.68 – 8.20 (m, 6H, Ar-OH), 7.59 (s, 1H), 7.55 (s, 1H), 7.53 (s, 1H), 7.50 (s, 1H), 7.24 (s, 1H), 6.39 (s, 1H), 6.28 (s, 1H), 6.22 (s, 1H), 6.15 (s, 1H), 4.43 – 4.24 (m, 4H, 4 × -(CH)- (methine)), 4.06 – 3.85 (m, 2H, -O(CH₂)-), 2.43 – 2.13 (m, 8H, 4 × -(CH₂)(CH₂)₉CH₃), 1.93 – 1.77 (m, 2H, -O(CH₂)(CH₂)-), 1.52 – 1.13 (m, 72H, 4 × -(CH₂)(CH₂)₉CH₃), 1.07 (t, *J* = 7.4 Hz, 3H, O(CH₂)₂CH₃), 0.89 (t, *J* = 7.0 Hz, 12H, 4 × -(CH₂)(CH₂)₉CH₃).

¹³C NMR (101 MHz, acetone-*d*₆): δ [ppm] = 154.1, 153.9, 153.0, 153.0, 152.6, 152.6, 152.4, 126.5, 126.2, 126.0, 125.8, 125.4, 125.2, 125.1, 125.0, 124.9, 124.8, 124.5, 103.8, 103.7, 103.5, 101.1, 71.4, 34.9, 34.5, 34.4, 34.3, 34.3, 33.9, 32.7, 30.6, 30.6, 30.5, 30.5, 30.4, 30.2, 29.8, 29.1,

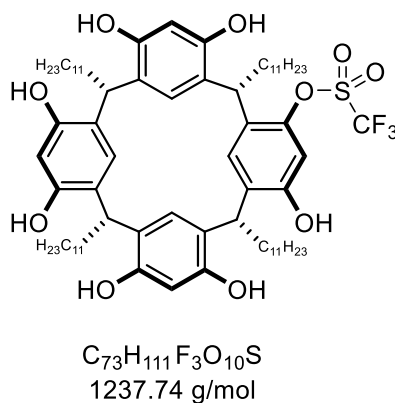
29.0, 28.9, 23.4, 23.1, 14.4, 10.8. (The number of signals deviates from the theoretical value due to signal overlap).

HRMS (ESI): calcd for $C_{75}H_{117}O_8^-$ [(M - H) $^-$]: 1145.8754, found: 1145.8770.

IR (ATR): $\tilde{\nu}$ [cm^{-1}] = 3286 (m), 2921 (vs), 2852 (s), 1619 (w), 1497 (m), 1465 (m), 1442 (m), 1291 (m), 1234 (m), 1159 (m), 1088 (m), 962 (w), 902 (w), 840 (m), 721 (m), 606 (m), 519 (m).

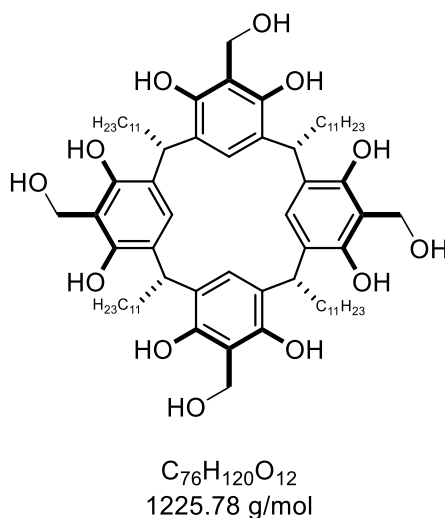
TLC: R_f = 0.51 ($CHCl_3/MeCN$ = 5/3 (4 mL) + one drop of AcOH) [CAM].

1⁶,3⁴,3⁶,5⁴,5⁶,7⁴,7⁶-Heptahydroxy-2,4,6,8-tetraundecyl-1,3,5,7(1,3)-tetrabenzenacyclo-octaphane-1⁴-yl trifluoromethanesulfonate (191)



To a stirred solution of *C*-undecylcalix[4]resorcinarene (**54b**) (250 mg, 226 μ mol, 1.0 eq.) in anhydrous DCM (3.0 mL) was added pyridine (0.30 mL, 3.78 mmol, 16.7 eq.) at rt. After cooling to -5 $^{\circ}C$, 0.20 mL of a trifluoromethanesulfonic anhydride (49.5 μ L, 294 μ mol, 1.3 eq.) stock solution in anhydrous DCM (0.59 M) were added dropwise and the reaction mixture was allowed to warm to rt over 20 h. The reaction was subsequently quenched by addition of 1 M aqueous HCl. The crude product was extracted with DCM (3 \times 30 mL) and washed successively with water and brine. The combined organic phases were dried over Na_2SO_4 , filtered and concentrated under vacuum. Purification was attempted via flash column chromatography ($CHCl_3/MeCN$ = 7/3). The 1H NMR spectrum of the collected fraction is depicted in Figure 15. Due to the low purity of the isolated material, no reliable analytical data can be provided.

1⁵,3⁵,5⁵,7⁵-Tetrakis(hydroxymethyl)-2,4,6,8-tetraundecyl-1,3,5,7(1,3)-tetrabenzenacyclo-octaphan-1⁴,1⁶,3⁴,3⁶,5⁴,5⁶,7⁴,7⁶-octaol (140a)



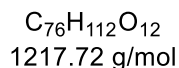
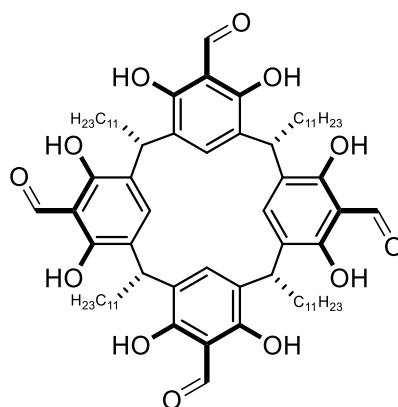
To a stirred solution of *C*-undecylcalix[4]resorcinarene (**54b**) (1.00 g, 904 μ mol, 1.0 eq.) in THF (2.8 mL) was added 2 M aqueous NaOH (2.80 mL) at rt. The dark red slurry was subsequently treated dropwise with 37% aqueous formaldehyde (505 μ l, 6.78 mmol, 7.5 eq.) and stirring was continued for 100 min at rt. The reaction mixture was then poured into EtOAc (60 mL) and the precipitated solid was redissolved by addition of 1 M aqueous HCl (5.60 mL). After stirring the biphasic mixture for 1 h at rt, the organic phase was separated and the aqueous phase was extracted with EtOAc (3 \times 100 mL). The combined organic phases were washed successively with water and brine. After drying over MgSO₄ for 24 h and filtration, the solvent was removed under vacuum to yield the crude product (919 mg, 750 μ mol, 83%) as a light brown solid.

¹H NMR (500 MHz, acetone-*d*₆): δ [ppm] = 9.30 – 9.00 (m, 6H, 6 \times Ar-OH), 7.46 (s, 4H, 4 \times Ar-H), 5.57 – 5.40 (bs, 3H, 3 \times -(CH₂)OH), 4.92 (bs, 8H, 4 \times -(CH₂)OH), 4.28 (t, *J* = 7.9 Hz, 4H, 4 \times -(CH)- (methine)), 2.35 – 2.20 (m, 8H, 4 \times -(CH₂)(CH₂)₉CH₃), 1.44 – 1.23 (m, 72H, 4 \times -(CH₂)(CH₂)₉CH₃), 0.89 (t, *J* = 7.0 Hz, 12H, 4 \times -(CH₂)(CH₂)₉CH₃). (H-D exchange is responsible for the diminished integral of the OH-groups).

¹³C NMR (101 MHz, acetone-*d*₆): δ [ppm] = 150.8, 125.2, 123.8, 112.2, 60.3, 34.3, 34.2, 32.7, 30.6, 30.6, 30.5, 30.2, 23.4, 14.4. (The number of signals deviates from the theoretical value due to signal overlap).

The obtained analytical data is in good agreement with the data reported for the *i*-butyl analog.¹⁷⁷

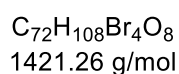
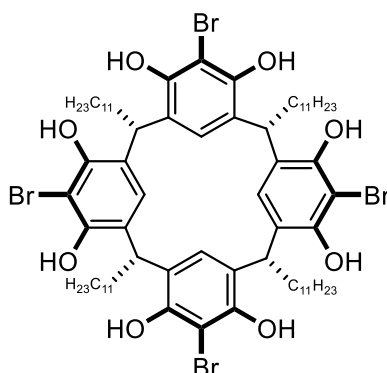
1⁴,1⁶,3⁴,3⁶,5⁴,5⁶,7⁴,7⁶-Octahydroxy-2,4,6,8-tetraundecyl-1,3,5,7(1,3)-tetrabenzenacyclo-octaphane-1⁵,3⁵,5⁵,7⁵-tetracarbaldehyde (140b)



C-Undecylcalix[4]resorcinarene (**54b**) (885 mg, 800 μmol , 1.0 eq.) and urotropine (799 mg, 5.70 mmol, 7.1 eq.) were put in a 40 mL pressure tube. Trifluoroacetic acid (5.0 mL) was added and the tube was shaken until the solid was dispersed in the liquid. The tube was then sealed and stirred for 1 h at 120 °C. After cooling to rt, the black solution was poured into a mixture of CHCl_3 (25 mL) and 1 M aqueous HCl (25 mL). The biphasic mixture was subsequently stirred vigorously overnight. The organic phase was separated and the aqueous phase was extracted with CHCl_3 ($3 \times 100 \text{ mL}$). The combined organic phases were dried over MgSO_4 , filtered and concentrated under vacuum. A small sample of the orange crude product was subjected to column chromatography ($\text{CHCl}_3/\text{MeCN} = 1/1$). The ^1H NMR of the purified material is depicted in Figure 18.

^1H NMR (500 MHz, CDCl_3): δ [ppm] = 13.1 (bs, 4H, $4 \times \text{Ar-OH}$), 10.3 (s, 4H, $4 \times \text{Ar-CHO}$), 8.35 (bs, 4H, $4 \times \text{Ar-OH}$), 7.39 (bs, 4H, $4 \times \text{Ar-H}$), 4.35 (t, $J = 7.8 \text{ Hz}$, 4H, $4 \times \text{-(CH)}$ (methine)), 2.27 – 2.07 (m, 8H, $4 \times \text{-(CH}_2\text{)(CH}_2\text{)}_9\text{CH}_3$), 1.50 – 1.05 (m, 72H, $4 \times \text{-(CH}_2\text{)(CH}_2\text{)}_9\text{CH}_3$), 0.89 (t, $J = 6.8 \text{ Hz}$, 12H, $4 \times \text{-(CH}_2\text{)(CH}_2\text{)}_9\text{CH}_3$).

Due to the remaining apolar impurities, no further analytical data is provided. However, the ^1H NMR data is in good agreement with the data reported for the *i*-butyl analog.¹⁸¹

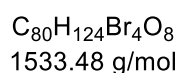
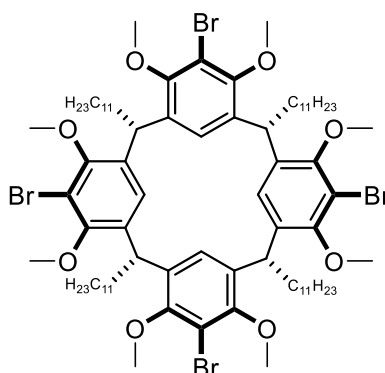
1⁵,3⁵,5⁵,7⁵-Tetrabromo-2,4,6,8-tetraundecyl-1,3,5,7(1,3)-tetrabenzenacyclooctaphan-1⁴,1⁶,3⁴,3⁶,5⁴,5⁶,7⁴,7⁶-octaol (194)

C-Undecylcalix[4]resorcinarene (**54b**) (50 g, 45.2 mmol, 1.0 eq.) was dissolved in anhydrous THF (450 mL) and the flask was wrapped in aluminum foil. *N*-Bromosuccinimide (32.5 g, 181 mmol, 4.0 eq.) was added portionwise over 15 min and the mixture was subsequently stirred for 4 h at rt. After removal of the solvent under vacuum, the residue was suspended in boiling methanol (750 mL) for 40 min, followed by hot filtration. The crude product was washed with methanol and dried under vacuum. The obtained white solid (52.0 g, 36.6 mmol, 81%) was used without further purification in the next step.

¹H NMR (400 MHz, acetone-*d*₆): δ [ppm] = 8.28 (bs, 5H, 5 × Ar-OH), 7.62 (s, 4H, 4 × Ar-H), 4.45 (t, *J* = 7.8 Hz, 4H, 4 × -(CH)- (methine)), 2.37 – 2.24 (m, 8H, 4 × -(CH₂)(CH₂)₉CH₃), 1.44 – 1.18 (m, 72H, 4 × -(CH₂)(CH₂)₉CH₃), 0.89 (t, *J* = 7.1 Hz, 12H, 4 × -(CH₂)(CH₂)₉CH₃). (H-D exchange is responsible for the diminished integral of the OH-groups).

The spectroscopic data matches the data reported in the literature.¹⁸⁵

1⁵,3⁵,5⁵,7⁵-Tetrabromo-1⁴,1⁶,3⁴,3⁶,5⁴,5⁶,7⁴,7⁶-octamethoxy-2,4,6,8-tetraundecyl-1,3,5,7(1,3)-tetrabenzenacyclooctaphane (195)

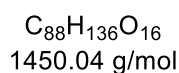
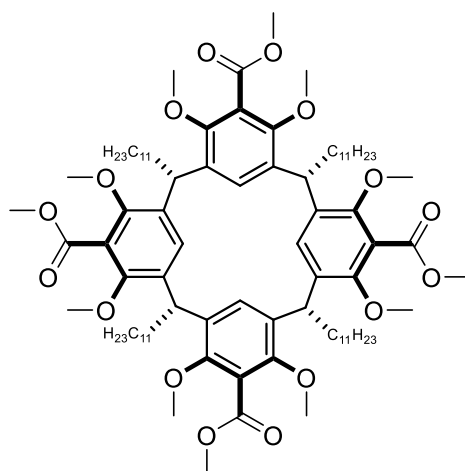


To a solution of tetra-bromide **194** (50.0 g, 35.2 mmol, 1.0 eq.) in anhydrous acetone (610 mL) was added potassium carbonate (58.9 g, 426 mmol, 12.1 eq.) and the resulting purple suspension was stirred for 40 min at rt before adding methyl iodide (99.6 mL, 1.58 mol, 45.0 eq.). The suspension was subsequently refluxed for 40 h. After cooling to rt, the solvent was removed under vacuum. The residue was taken up in DCM and water and the organic phase was separated. The aqueous phase was extracted with DCM (2 × 300 mL). The combined organic phases were dried over Na₂SO₄, filtered and concentrated under vacuum. Purification by flash column chromatography (pentane/Et₂O = 10/1) yielded product **195** (52.3 g, 34.1 mmol, 97%) as a yellow powder.

¹H NMR (400 MHz, CDCl₃): δ [ppm] = 6.53 (bs, 4H, 4 × Ar-H), 4.46 (t, J = 7.3 Hz, 4H, 4 × -(CH)- (methine)), 3.66 (bs, 24H, 24 × -O(CH₃)) 1.95 – 1.74 (m, 8H, 4 × -(CH₂)(CH₂)₉CH₃), 1.44 – 1.12 (m, 72H, 4 × -(CH₂)(CH₂)₉CH₃), 0.87 (t, J = 7.1 Hz, 12H, 4 × -(CH₂)(CH₂)₉CH₃).

TLC: R_f = 0.67 (pentane/EtOAc = 10/1) [CAM].

The spectroscopic data matches the data reported in the literature.²⁰²

Tetramethyl 1⁴,1⁶,3⁴,3⁶,5⁴,5⁶,7⁴,7⁶-octamethoxy-2,4,6,8-tetraundecyl-1,3,5,7(1,3)-tetraben-zenacyclooctaphane-1⁵,3⁵,5⁵,7⁵-tetracarboxylate (197)

Tetra-bromide **195** (9.00 g, 5.87 mmol, 1.0 eq.) was dissolved in anhydrous THF (450 mL) and the solution was cooled to $-78\text{ }^{\circ}\text{C}$. Freshly titrated *n*-butyllithium (2.0 M in hexanes, 13.2 mL, 26.4 mmol, 4.5 eq.) was added rapidly and the turbid mixture was stirred for 45 min at $-78\text{ }^{\circ}\text{C}$ (side note: sometimes additional THF had to be added to enable stirring of the viscous solution). After dropwise addition of methyl chloroformate (6.82 mL, 88.1 mmol, 15.0 eq.), stirring at $-78\text{ }^{\circ}\text{C}$ was continued for 2.5 h before allowing the solution to warm to rt overnight. The reaction was subsequently quenched by the addition of methanol and the solvent was removed under vacuum. The residue was taken up in DCM and water and the organic phase was separated. The aqueous phase was extracted with DCM ($3 \times 150\text{ mL}$) and the combined organic phases were, dried over Na_2SO_4 , filtered and concentrated under vacuum. The organic mixture was purified via flash column chromatography (pentane/EtOAc = 3/1 \rightarrow 2/1) to give tetra-ester **197** (5.96 g, 4.11 mmol, 70%) as a white solid.

$^1\text{H NMR}$ (400 MHz, acetone- d_6): δ [ppm] = 7.28 (s, 0.3H, Ar-*H*), 7.15 (s, 0.3H, Ar-*H*), 7.00 (s, 2.4H, Ar-*H*), 6.53 (s, 0.6H, Ar-*H*), 6.49 (s, 0.4H, Ar-*H*), 4.62 – 4.42 (m, 4H, 4 \times -(CH)-(methine)), 3.96 – 3.82 (m, 15H, -O(CH₃)), 3.64 (s, 17H, -O(CH₃)), 3.23 (s, 2H, -O(CH₃)), 2.02 – 1.69 (m, 8H, 4 \times -(CH₂)(CH₂)₉CH₃), 1.50 – 1.12 (m, 72H, 4 \times -(CH₂)(CH₂)₉CH₃), 0.94 – 0.82 (m, 12H, 4 \times -(CH₂)(CH₂)₉CH₃).

The integrals not amounting to full protons result from the different conformations present in solution. The error associated with integration gave a diminished total methoxy integral.

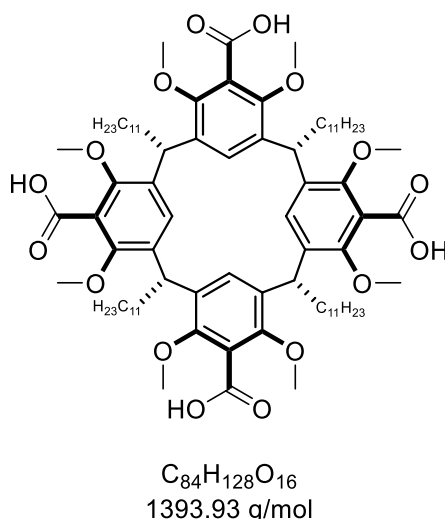
^{13}C NMR (101 MHz, acetone- d_6): δ [ppm] = 167.7, 154.9, 133.8, 128.9, 124.0, 62.3, 52.6, 37.5, 36.2, 32.7, 30.5 – 29.1, 23.4, 14.4. (The number of signals deviates from the theoretical value due to signal overlap).

HRMS (ESI): calcd for $\text{C}_{88}\text{H}_{136}\text{NaO}_{16}^+$ [(M + Na) $^+$]: 1471.9721, found: 1471.9703.

IR (ATR): $\tilde{\nu}$ [cm^{-1}] = 2918 (vs), 2850 (s), 1727 (vs), 1578 (m), 1504 (s), 1467 (s), 1434 (m), 1421 (m), 1269 (s), 1236 (s), 1194 (s), 1144 (s), 1114 (s), 1093 (s), 1005 (s), 898 (w), 824 (w), 753 (w), 721 (w), 647 (w), 584 (w), 525 (w), 417 (w).

TLC: R_f = 0.68 (pentane/EtOAc = 2/1) [CAM].

$1^4,1^6,3^4,3^6,5^4,5^6,7^4,7^6$ -Octamethoxy- $2,4,6,8$ -tetraundecyl- $1,3,5,7(1,3)$ -tetrabenzenacyclo-octaphane- $1^5,3^5,5^5,7^5$ -tetracarboxylic acid (196**)**



To tetra-ester **197** (4.91 g, 3.39 mmol, 1.0 eq.) was added 1,4-dioxane (177 mL) and the mixture was stirred until complete dissolution. After addition of saturated aqueous LiOH (177 mL), the mixture was refluxed for 7 d (caution: extensive foaming). The suspension was subsequently acidified by addition of concentrated aqueous HCl at 0 °C, until a pH of ~2 was reached. The suspension was dispersed via sonication and then filtered and washed successively with cold 2 M aqueous HCl and water. The residue was taken up in THF (250 mL) and sonicated. After drying over MgSO_4 , the suspension was filtered and concentrated under vacuum. Product **196** (4.39 g, 3.14 mmol, 93%) could be obtained as an off-white powder after drying under high vacuum overnight.

^1H NMR (400 MHz, $\text{DMSO-}d_6$): δ [ppm] = 13.1 (bs, 3H, Ar-COOH), 7.11 – 6.86 (m, 3H, Ar-H), 6.52 – 6.31 (m, 1H, Ar-H), 4.53 – 4.28 (m, 4H, $4 \times$ -(CH)- (methine)), 3.77 – 3.17 (m, 24H, -O(CH₃)), 2.02 – 1.53 (m, 8H, $4 \times$ -(CH₂)(CH₂)₉CH₃), 1.36 – 0.98 (m, 72H, $4 \times$ -(CH₂)(CH₂)₉CH₃), 0.84 – 0.75 (m, 12H, $4 \times$ -(CH₂)(CH₂)₉CH₃). (H-D exchange is responsible for the diminished integral of the OH-groups).

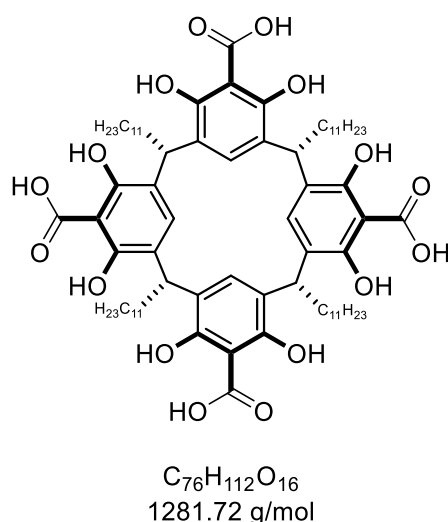
The complex signal pattern in the ^1H NMR is caused by different conformations present in solution.

^{13}C NMR (101 MHz, $\text{DMSO-}d_6$): δ [ppm] = 167.5, 152.8, 132.4, 124.4, 99.5, 61.6, 31.3, 29.3, 29.1, 29.1, 28.8, 22.1, 13.9 (The number of signals deviates from the theoretical value due to signal overlap).

HRMS (ESI): calcd for $\text{C}_{83}\text{H}_{127}\text{O}_{14}^-$ [(M – CO₂H)⁻]: 1347.9231, found: 1347.9249.

IR (ATR): $\tilde{\nu}$ [cm^{-1}] = 3300 – 2500 (w, Ar-COOH), 2920 (s), 2851 (s), 1702 (s), 1579 (m), 1469 (s), 1422 (s), 1387 (w), 1290 (s), 1272 (s), 1233 (s), 1190 (w), 1164 (s), 1117 (w), 1093 (s), 1034 (s), 1005 (s), 905 (w), 884 (w), 826 (w), 720 (w), 665 (w), 632 (w), 548 (w), 524 (w).

1⁴,1⁶,3⁴,3⁶,5⁴,5⁶,7⁴,7⁶-Octahydroxy-2,4,6,8-tetraundecyl-1,3,5,7(1,3)-tetrabenzenacyclo-octaphane-1⁵,3⁵,5⁵,7⁵-tetracarboxylic acid (140c)



To a turbid solution of tetra-acid **196** (90.0 mg, 64.6 μmol , 1.0 eq.) in anhydrous DCM (3.2 mL) was added boron tribromide (1 M in DCM, 1.29 mL, 1.29 mmol, 20.0 eq.) at -78 °C. After stirring for 1 h at -78 °C, the mixture was allowed to warm to rt overnight. The reaction was

subsequently quenched by addition of methanol and the resulting mixture was concentrated under vacuum. The residue was recrystallized from methanol, which presumably yielded product **140c** (25.0 mg, 19.5 μmol , 30%) in form of pearly plates.

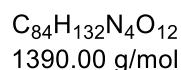
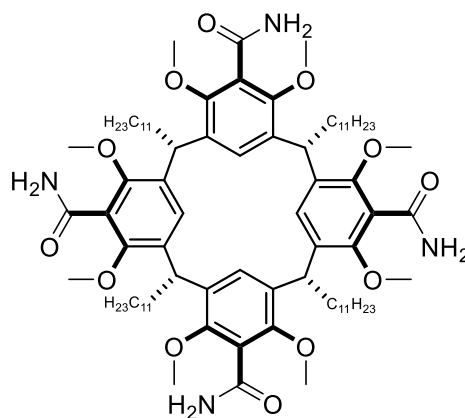
$^1\text{H NMR}$ (250 MHz, acetone- d_6): δ [ppm] = 7.63 (s, 0.2H, Ar-*H*), 7.50 (s, 0.6H, Ar-*H*), 7.30 (s, 0.2H, Ar-*H*), 7.22 (s, 2.3H, Ar-*H*), 6.26 (s, 0.4H, Ar-*H*), 4.76 – 4.46 (m, 4H, 4 \times -(CH)-(methine)), 2.13 – 1.85 (m, 8H, 4 \times -(CH₂)(CH₂)₉CH₃), 1.46 – 1.17 (m, 72H, 4 \times -(CH₂)(CH₂)₉CH₃), 0.95 – 0.80 (m, 12H, 4 \times -(CH₂)(CH₂)₉CH₃).

The integrals not amounting to full protons result from the different conformations present in solution.

MS (ESI): calcd for C₇₅H₁₁₁O₁₄⁻ [(M – CO₂H)⁻]: 1235.80, found: 1235.68.

The structure of the isolated material could not be conclusively verified. Therefore, only preliminary analytical data is provided. For further discussion, see chapter 6.5.2.2.

1⁴,1⁶,3⁴,3⁶,5⁴,5⁶,7⁴,7⁶-Octamethoxy-2,4,6,8-tetraundecyl-1,3,5,7(1,3)-tetrabenzenacyclo-octaphane-1⁵,3⁵,5⁵,7⁵-tetracarboxamide (199)



A solution of permethylated tetra-bromide **195** (600 mg, 391 μmol , 1.0 eq.) in THF (30 mL) was cooled to -78 °C. Freshly titrated *n*-butyllithium (2.39 M in hexanes, 0.74 mL, 1.76 mmol, 4.5 eq.) was added rapidly. The mixture was stirred for 45 min at -78 °C before (trimethylsilyl)isocyanate (1.26 mL, 9.38 mmol, 24.0 eq.) was added rapidly. The solution was

kept at $-78\text{ }^{\circ}\text{C}$ for 15 min. The reaction mixture was then allowed to warm to rt and stirring was continued for 16 h. The reaction was subsequently quenched by the addition of water and the solvent was removed under vacuum. The residue was taken up in a mixture of DCM and *iso*-propanol (4/1) and brine. The organic phase was separated and the aqueous phase was extracted with a mixture of DCM and *iso*-propanol (4/1, $3 \times 100\text{ mL}$). The combined organic phases were washed with saturated aqueous NaHCO_3 , dried over MgSO_4 , filtered and concentrated. Column chromatography (dry load, DCM/MeOH = 10/1 \rightarrow 5/1) of the crude product yielded the protected tetra-amide **199** (254 mg, 183 μmol , 47 %) as a white solid.

^1H NMR (400 MHz, $\text{DMSO-}d_6$): δ [ppm] = 7.65 (s, 4H, $-(\text{CO})\text{NH}_2$), 7.55 (s, 4H, $-(\text{CO})\text{NH}_2$), 6.69 (s, 4H, $4 \times \text{Ar-}H$), 4.35 (t, $J = 7.2\text{ Hz}$, 4H, $4 \times -(\text{CH})-$ (methine)), 3.58 (s, 24H, $8 \times -\text{O}(\text{CH}_3)$), 1.93 – 1.63 (m, 8H, $4 \times -(\text{CH}_2)(\text{CH}_2)_9\text{CH}_3$), 1.50 – 0.98 (m, 72H, $4 \times -(\text{CH}_2)(\text{CH}_2)_9\text{CH}_3$), 0.94 – 0.71 (m, 12H, $4 \times -(\text{CH}_2)(\text{CH}_2)_9\text{CH}_3$).

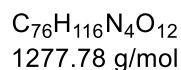
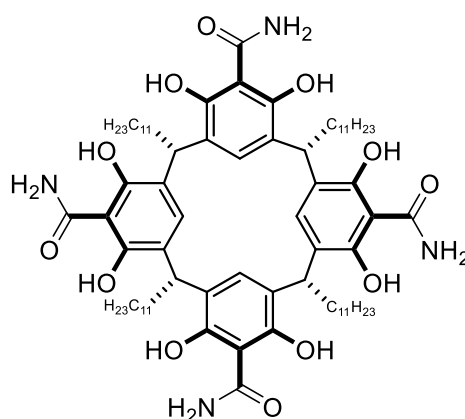
^{13}C NMR (101 MHz, $\text{DMSO-}d_6$): δ [ppm] = 187.2, 167.7, 152.8, 127.3, 106.4, 61.5, 31.3, 29.4, 29.3, 29.2, 29.2, 29.1, 28.7, 22.1, 13.9. (The number of signals deviates from the theoretical value due to signal overlap).

HRMS (ESI): calcd for $\text{C}_{84}\text{H}_{132}\text{N}_4\text{NaO}_{12}^+$ [(M + Na) $^+$]: 1411.9734, found: 1411.9730.

IR (ATR): $\tilde{\nu}$ [cm^{-1}] = 3491 (w), 3184 (w), 2919 (s), 2850 (m), 1661 (vs), 1468 (m), 1420 (m), 1373 (m), 1288 (m), 1091 (m), 1004 (m), 722 (w).

TLC: $R_f = 0.29$ (DCM/MeOH = 10/1) [CAM].

1⁴,1⁶,3⁴,3⁶,5⁴,5⁶,7⁴,7⁶-Octahydroxy-2,4,6,8-tetraundecyl-1,3,5,7(1,3)-tetrabenzenacyclo-octaphane-1⁵,3⁵,5⁵,7⁵-tetracarboxamide (140d)



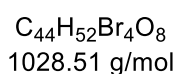
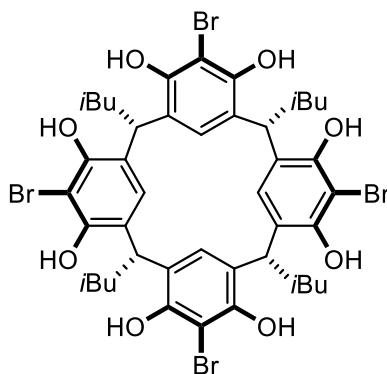
To a solution of the protected tetra-amide **199** (300 mg, 216 μ mol, 1.0 eq.) in $CHCl_3$ (10 mL) was added trimethylsilyl iodide (617 μ L, 4.32 mmol, 20.0 eq.) at rt. The mixture was subsequently refluxed for 3 d. The reaction was quenched at 0 °C with 2 M aqueous HCl and the solvent was removed under vacuum. The residue was suspended in water and filtered. The crude product was purified by recrystallization from ethyl acetate to give compound **140d** (204 mg, 160 μ mol, 74%) as a white solid.

¹H NMR (400 MHz, $CDCl_3$): δ [ppm] = 16.0 (s, 24H, $-(CO)NH_2$), 10.07 (bs, 24H, $-(CO)NH_2$), 9.16 – 8.62 (m, 48H, Ar-OH), 7.34 (s, 24H, Ar-H), 4.38 (t, $J = 7.8$ Hz, 24H, $-(CH)-$ (methine)), 2.37 – 2.02 (m, 48H, $-(CH_2)(CH_2)_9CH_3$), 1.54 – 1.10 (m, 432H, $-(CH_2)(CH_2)_9CH_3$), 0.89 (t, $J = 6.7$ Hz, 72H, $-(CH_2)(CH_2)_9CH_3$). (Integration based on assumed hexamer formation in $CDCl_3$).

¹³C NMR (101 MHz, $CDCl_3$): δ [ppm] = 174.5, 157.2, 153.0, 124.7, 103.1, 32.1, 29.9, 29.6, 28.1, 22.9, 14.3. (The number of signals deviates from the theoretical value due to signal overlap).

HRMS (ESI): calcd for $C_{76}H_{115}N_4O_{12}^-$ [(M – H)⁻]: 1275.8517, found: 1275.8520.

IR (ATR): $\tilde{\nu}$ [cm^{-1}] = 3426 (w), 3202 (w), 2921 (vs), 2852 (m), 1650 (m), 1596 (vs), 1452 (vs), 1234 (m), 1098 (w), 811 (w), 720 (w).

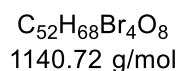
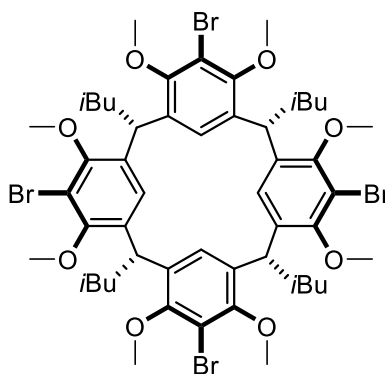
1⁵,3⁵,5⁵,7⁵-Tetrabromo-2,4,6,8-tetraisobutyl-1,3,5,7(1,3)-tetrabenzenacyclooctaphan-1⁴,1⁶,3⁴,3⁶,5⁴,5⁶,7⁴,7⁶-octaol (208)

C-iso-Butylcalix[4]resorcinarene – synthesized according to a published procedure²⁰¹ - (8.00 g, 11.2 mmol, 1.0 eq.) was dissolved in 2-butanone (112 mL) and the flask was wrapped in aluminum foil. *N*-Bromosuccinimide (19.4 g, 108 mmol, 9.7 eq.) was added portionwise over 10 min at 0 °C and the mixture was subsequently stirred for 23 h at rt under an argon atmosphere. After removal of the solvent under vacuum, the residue was suspended in methanol under sonication, filtered and washed with methanol. The obtained white solid (6.14 g, 5.97 mmol, 53%) was dried under vacuum and used without further purification in the next step.

¹H NMR (400 MHz, DMSO-*d*₆): δ [ppm] = 9.16 (s, 8H, 8 × Ar-OH), 7.35 (s, 4H, 4 × Ar-H), 4.49 (t, J = 7.8 Hz, 4H, 4 × -(CH)- (methine)), 2.12 – 1.99 (m, 8H, 4 × -(CH₂)(CH)(CH₃)₂), 1.40 – 1.27 (m, 4H, 4 × -(CH₂)(CH)(CH₃)₂), 0.91 (d, J = 6.6 Hz, 24H, 4 × -(CH₂)(CH)(CH₃)₂).

The spectroscopic data matches the data reported in the literature.²⁰³

1⁵,3⁵,5⁵,7⁵-Tetrabromo-2,4,6,8-tetraisobutyl-1⁴,1⁶,3⁴,3⁶,5⁴,5⁶,7⁴,7⁶-octamethoxy-1,3,5,7(1,3)-tetrabenzenacyclooctaphane (209)



To a suspension of tetra-bromide **208** (6.14 g, 5.97 mmol, 1.0 eq.) in anhydrous acetone (140 mL) was added potassium carbonate (13.4 g, 96.9 mmol, 16.2 eq.) and the resulting purple suspension was stirred for 30 min at rt before adding methyl iodide (15.1 mL, 240 mol, 40.2 eq.). The suspension was subsequently refluxed for 47 h. After cooling to rt, the solvent was removed under vacuum. The residue was taken up in DCM and water and the organic phase was separated. Next, the aqueous phase was extracted with DCM (2 × 100 mL). The combined organic phases were dried over Na₂SO₄, filtered and concentrated under vacuum. Purification by flash column chromatography (pentane/Et₂O = 10/1 → 1/1) yielded product **209** (4.29 g, 3.76 mmol, 63%) as a yellow powder.

¹H NMR (400 MHz, CDCl₃): δ [ppm] = 6.51 (bs, 4H, 4 × Ar-H), 4.59 (t, *J* = 7.4 Hz, 4H, 4 × -(CH)- (methine)), 3.69 (bs, 24H, 8 × -O(CH₃)), 1.88 – 1.64 (m, 8H, 4 × -(CH₂)(CH)(CH₃)₂), 1.63 – 1.49 (m, 4H, 4 × -(CH₂)(CH)(CH₃)₂), 0.94 (d, *J* = 6.5 Hz, 24H, 4 × -(CH₂)(CH)(CH₃)₂).

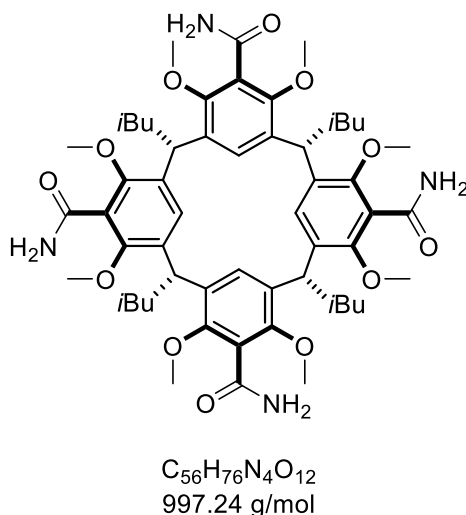
¹³C NMR (101 MHz, CDCl₃): δ [ppm] = 154.5, 125.9, 113.3, 60.7, 44.0, 36.5, 26.0, 22.7. (The number of signals deviates from the theoretical value due to signal overlap).

HRMS (ESI): calcd for C₅₂H₆₈Br₄NaO₈⁺ [(M + Na)⁺]: 1159.1540, found: 1159.1544.

IR (ATR): $\tilde{\nu}$ [cm⁻¹] = 2951 (m), 2866 (w), 1593 (w), 1469 (s), 1417 (s), 1395 (m), 1385 (m), 1367 (m), 1340 (m), 1295 (m), 1229 (m), 1213 (m), 1190 (m), 1168 (m), 1129 (m), 1086 (m), 1044 (m), 1000 (vs), 982 (m), 914 (m), 903 (w), 851 (w), 828 (w), 799 (w), 784 (w), 751 (w), 726 (w), 656 (w), 632 (w), 589 (w), 569 (m), 531 (m), 492 (m), 440 (w), 409 (w).

TLC: $R_f = 0.38$ (pentane/DCM = 1/1) [CAM].

2,4,6,8-Tetraisobutyl-1⁴,1⁶,3⁴,3⁶,5⁴,5⁶,7⁴,7⁶-octamethoxy-1,3,5,7(1,3)-tetrabenzenacyclo-octaphane-1⁵,3⁵,5⁵,7⁵-tetracarboxamide (210)



A solution of permethylated tetra-bromide **209** (2.00 g, 1.75 mmol, 1.0 eq.) in THF (134 mL) was cooled to $-78\text{ }^\circ\text{C}$. Freshly titrated *n*-butyllithium (2.03 M in hexanes, 3.88 mL, 7.88 mmol, 4.5 eq.) was added rapidly, followed by additional THF (20 mL) to ensure stirring of the viscous solution. The mixture was stirred for 45 min at $-78\text{ }^\circ\text{C}$ before (trimethylsilyl)isocyanate (5.63 mL, 42.0 mmol, 24.0 eq.) was added rapidly. The solution was kept at $-78\text{ }^\circ\text{C}$ for 15 min. The reaction mixture was then allowed to warm to rt and stirring was continued for 14 h. The reaction was subsequently quenched by the addition of water and the solvent was removed under vacuum. The residue was taken up in a mixture of DCM and *iso*-propanol (4/1) and brine. The organic phase was separated and the aqueous phase was extracted with a mixture of DCM and *iso*-propanol (4/1, $3 \times 100\text{ mL}$). The combined organic phases were washed with saturated aqueous NaHCO_3 , dried over MgSO_4 , filtered and concentrated. Column chromatography (dry load, DCM/MeOH = 10/1 \rightarrow 5/1) of the crude product yielded the protected tetra-amide **210** (254 mg, 183 μmol , 47 %) as a white solid.

¹H NMR (400 MHz, $\text{DMSO-}d_6$): δ [ppm] = 7.70 (s, 4H, $-(\text{CO})\text{NH}_2$), 7.59 (s, 4H, $-(\text{CO})\text{NH}_2$), 6.63 (bs, 4H, $4 \times \text{Ar-H}$), 4.48 (t, $J = 7.4\text{ Hz}$, 4H, $4 \times -(\text{CH})-$ (methine)), 3.60 (s, 24H, $8 \times -\text{O}(\text{CH}_3)$), 1.81 – 1.57 (m, 8H, $4 \times -(\text{CH}_2)(\text{CH})(\text{CH}_3)_2$), 1.54 – 1.35 (m, 4H, $4 \times -(\text{CH}_2)(\text{CH})(\text{CH}_3)_2$), 0.90 (d, $J = 6.4\text{ Hz}$, 24H, $4 \times -(\text{CH}_2)(\text{CH})(\text{CH}_3)_2$).

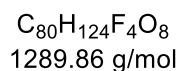
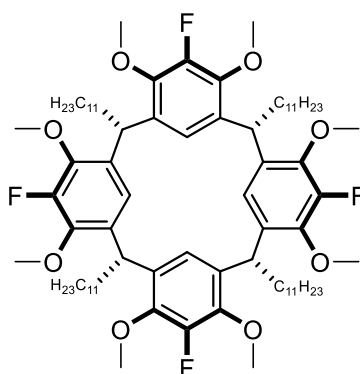
^{13}C NMR (101 MHz, DMSO- d_6): δ [ppm] = 167.7, 152.7, 127.4, 126.3, 61.5, 43.9, 34.2, 25.5, 22.4. (The number of signals deviates from the theoretical value due to signal overlap).

HRMS (ESI): calcd for $\text{C}_{56}\text{H}_{75}\text{N}_4\text{O}_{12}^-$ [(M - H) $^-$]: 995.5387, found: 995.5383.

IR (ATR): $\tilde{\nu}$ [cm^{-1}] = 3487 (w), 3365 (m), 3290 (m), 3171 (m), 2954 (m), 2868 (vs), 1663 (m), 1629 (m), 1579 (m), 1467 (m), 1418 (m), 1380 (m), 1366 (m), 1341 (m), 1323 (m), 1292 (m), 1227 (m), 1214 (m), 1187 (m), 1172 (m), 1130 (m), 1089 (s), 1048 (m), 1003 (s), 923 (m), 903 (m), 811 (m), 774 (m), 759 (m), 667 (m), 635 (m), 622 (m), 595 (m), 567 (m), 526 (m), 478 (m), 442 (m).

TLC: R_f = 0.46 (DCM/MeOH = 5/1 (3 mL) + one drop of AcOH) [CAM].

1⁵,3⁵,5⁵,7⁵-Tetrafluoro-1⁴,1⁶,3⁴,3⁶,5⁴,5⁶,7⁴,7⁶-octamethoxy-2,4,6,8-tetraundecyl-1,3,5,7(1,3)-tetrabenzenacyclooctaphane (201)



A solution of permethylated tetra-bromide **195** (200 mg, 130 μmol , 1.0 eq.) in THF (10 mL) was cooled to -78 $^\circ\text{C}$. Freshly titrated *n*-butyllithium (2.5 M in hexanes, 0.23 mL, 585 μmol , 4.5 eq.) was added rapidly. The mixture was stirred for 45 min at -78 $^\circ\text{C}$ before a solution of *N*-fluorobenzenesulfonimide (1.26 mL, 9.38 mmol, 24.0 eq.) in THF (4.0 mL) was added dropwise. The solution was stirred at -78 $^\circ\text{C}$ for 2 h. The mixture was then allowed to warm to rt over 30 min. The reaction was subsequently quenched by the addition of saturated aqueous NH_4Cl and the solvent was removed under vacuum. The residue was taken up in a mixture of DCM and water. The organic phase was separated and the aqueous phase was extracted with DCM (2 \times 50 mL). The combined organic phases were dried over Na_2SO_4 , filtered and

concentrated. Purification via column chromatography (pentane/EtOAc = 40/1 → 10/1) yielded the protected tetra-fluoride **201** (82.0 mg, 63.6 μmol, 49 %) as a white solid (side note: a solution of the product in pentane/EtOAc can be decanted from the insoluble NFSI side product).

¹H NMR (400 MHz, acetone-*d*₆): δ [ppm] = 6.56 (s, 4H, 4 × Ar-*H*), 4.54 (t, *J* = 7.4 Hz, 4H, 4 × -(*CH*)- (methine)), 3.71 (s, 24H, 8 × -O(*CH*₃)), 1.95 – 1.73 (m, 8H, 4 × -(*CH*₂)(*CH*₂)₉CH₃), 1.46 – 1.15 (m, 72H, 4 × -(*CH*₂)(*CH*₂)₉CH₃), 0.95 – 0.79 (m, 12H, 4 × -(*CH*₂)(*CH*₂)₉CH₃).

¹³C NMR (101 MHz, acetone-*d*₆): δ [ppm] = 151.6, 149.1, 145.4, 145.3, 133.9, 120.9, 120.8, 61.2, 61.2, 37.2, 35.8, 32.7, 30.6 – 28.8, 23.4, 14.4. (The number of signals deviates from the theoretical value due to signal overlap).

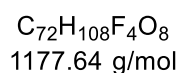
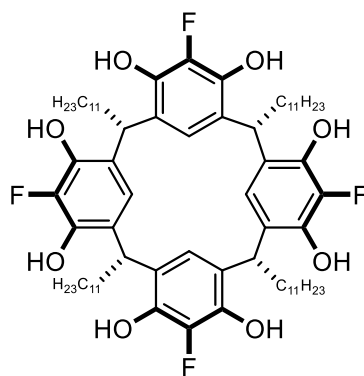
¹⁹F NMR (376 MHz, acetone-*d*₆): δ [ppm] = -147.9.

HRMS (ESI): calcd for C₈₀H₁₂₄F₄NaO₈⁺ [(M + Na)⁺]: 1311.9125, found: 1311.9115.

IR (ATR): $\tilde{\nu}$ [cm⁻¹] = 2917 (vs), 2849 (vs), 1490 (s), 1462 (vs), 1426 (vs), 1365 (w), 1318 (vs), 1238 (m), 1194 (m), 1122 (m), 1097 (s), 1056 (w), 1034 (w), 1010 (vs), 952 (m), 930 (m), 890 (w), 866 (w), 791 (w), 777 (w), 720 (w), 698 (w), 666 (w), 640 (w), 613 (w), 589 (w), 543 (w).

TLC: *R*_f = 0.81 (pentane/EtOAc = 10/1) [CAM].

1⁵,3⁵,5⁵,7⁵-Tetrafluoro-2,4,6,8-tetraundecyl-1,3,5,7(1,3)-tetrabenzenacyclooctaphan-1⁴,1⁶,3⁴,3⁶,5⁴,5⁶,7⁴,7⁶-octaol (140e)



To a solution of tetra-fluoride **201** (916 mg, 710 μmol , 1.0 eq.) in anhydrous DCM (35 mL) was added boron tribromide (1 M in DCM, 17.8 mL, 17.8 mmol, 25.0 eq.) at $-78\text{ }^\circ\text{C}$. After stirring for 1 h at $-78\text{ }^\circ\text{C}$, the mixture was allowed to warm to rt overnight. Since TLC analysis indicated incomplete conversion, the mixture was again cooled to $-78\text{ }^\circ\text{C}$ and treated with boron tribromide (1 M in DCM, 3.56 mL, 3.56 mmol, 5 eq.). The solution was subsequently stirred for 30 min at $-78\text{ }^\circ\text{C}$ and then for 14 h at rt. The reaction was subsequently quenched by addition of 2 M aqueous HCl at $0\text{ }^\circ\text{C}$ and the resulting mixture was concentrated under vacuum. The aqueous suspension was filtered after sonication and the residue was washed with water. The brown solid was subjected to column chromatography (DCM/MeOH = 25/1 \rightarrow 10/1), which yielded product **140e** (410 mg, 348 μmol , 49%) as a light brown powder.

^1H NMR (400 MHz, acetone- d_6): δ [ppm] = 8.56 (s, 8H, $8 \times \text{Ar-OH}$), 7.41 – 7.26 (m, 4H, $4 \times \text{Ar-H}$), 4.44 (t, $J = 7.9\text{ Hz}$, 4H, $4 \times \text{-(CH)-}$ (methine)), 2.42 – 2.13 (m, 8H, $4 \times \text{-(CH}_2\text{)(CH}_2\text{)}_9\text{CH}_3$), 1.52 – 1.10 (m, 72H, $4 \times \text{-(CH}_2\text{)(CH}_2\text{)}_9\text{CH}_3$), 0.98 – 0.81 (m, 12H, $4 \times \text{-(CH}_2\text{)(CH}_2\text{)}_9\text{CH}_3$).

^{13}C NMR (101 MHz, acetone- d_6): δ [ppm] = 143.1, 140.8, 140.8, 140.7, 126.2, 119.2, 119.1, 34.6, 34.4, 32.7, 30.6 – 28.9, 23.4, 14.4. (The number of signals deviates from the theoretical value due to signal overlap).

^{19}F NMR (376 MHz, acetone- d_6): δ [ppm] = -157.8 .

HRMS (ESI): calcd for $\text{C}_{72}\text{H}_{107}\text{F}_4\text{O}_8^-$ [(M – H) $^-$]: 1175.7908, found: 1175.7912.

IR (ATR): $\tilde{\nu}$ [cm^{-1}] = 3293 (m), 2921 (vs), 2852 (s), 2048 (w), 2021 (s), 1979 (s), 1633 (m), 1492 (s), 1466 (m), 1406 (m), 1319 (s), 1206 (m), 1117 (m), 1097 (m), 972 (m), 934 (w), 872 (w), 776 (m), 721 (m), 609 (m), 583 (m), 500 (m), 450 (m), 412 (m).

TLC: $R_f = 0.43$ (DCM/MeOH = 10/1) [CAM].

9. Index of abbreviations

A \supset B	B encapsulated within A
Ac	acetyl
AM1	Austin Model 1
BDSB	bromodiethylsulfonium bromopentachloroantimonate
BINAP	2,2'-bis(diphenylphosphino)-1,1'-binaphthyl
Bn	benzyl
bpy	2,2'-bipyridine
Bu	butyl
cat.	catalyst
CSA	camphorsulfonic acid
DCM	dichloromethane
DFT	density functional theory
DME	1,2-dimethoxyethane
DMF	dimethylformamide
DMSO	dimethyl sulfoxide
DOSY	diffusion ordered spectroscopy
DPPA	diphenylphosphoryl azide
E1	unimolecular elimination
ee	enantiomeric excess
equiv.	equivalents
er	enantiomeric ratio
ESI-MS	electrospray ionization mass spectrometry
ESP	electrostatic potential
Et	ethyl
FGI	functional group interconversion
FRET	fluorescence resonance energy transfer
GC	gas chromatography
HB	hydrogen bond
Hex	hexyl
HPLC	high-performance liquid chromatography
HS	host structure
HTT cyclization	head-to-tail terpene cyclization

ITC	isothermal titration calorimetry
LBA	Lewis acid-assisted Brønsted acid
LC-MS	liquid chromatography mass spectrometry
MALDI-TOF	matrix-assisted laser desorption/ionization time-of-flight
Me	methyl
MOM	methoxymethyl
MS	mass spectrometry/molecular sieve
M _x L _y	metal _x ligand _y
NFSI	<i>N</i> -fluorobenzenesulfonimide
NHC	<i>N</i> -heterocyclic carbene
NIS	<i>N</i> -iodosuccinimide
NMR	nuclear magnetic resonance
PBA	pyrene butyric acid
Ph	phenyl
PP	diphosphate
Pr	propyl
TBAB	tetrabutylammonium bromide
TBME	<i>tert</i> -butyl methyl ether
Tf	triflate
TFA	trifluoroacetic acid
THF	tetrahydrofuran
THT cyclization	tail-to-head terpene cyclization
TLC	thin-layer chromatography
TMS	trimethylsilyl
TMSI	trimethylsilyl iodide
TMS-NCO	(trimethylsilyl)isocyanate
Tris	tris(hydroxymethyl)aminomethane
S ₁	first excited singlet state
S _N 1/2	unimolecular/bimolecular nucleophilic substitution
sp	side products
UV/VIS	ultraviolet/visible
w-C ₆ D ₆	water-saturated C ₆ D ₆
w-CDCl ₃	water-saturated CDCl ₃
XB	halogen bond

10. References

- [1] Lehn, J.-M. *Angew. Chem. Int. Ed.* **1990**, *29*, 1304.
- [2] Lehn, J.-M. *Science* **2002**, *295*, 2400.
- [3] Lehn, J.-M. *Proc. Natl. Acad. Sci. U.S.A.* **2002**, *99*, 4763.
- [4] Bissantz, C.; Kuhn, B.; Stahl, M. *J. Med. Chem.* **2010**, *53*, 5061.
- [5] Garcia-Viloca, M.; Gao, J.; Karplus, M.; Truhlar, D. G. *Science* **2004**, *303*, 186.
- [6] Zhang, X.; Houk, K. N. *Acc. Chem. Res.* **2005**, *38*, 379.
- [7] Ringe, D.; Petsko, G. A. *Science* **2008**, *320*, 1428.
- [8] Wolfenden, R.; Snider, M. J. *Acc. Chem. Res.* **2001**, *34*, 938.
- [9] Dickschat, J. S. *Nat. Prod. Rep.* **2011**, *28*, 1917.
- [10] Kingston, D. G. I. *J. Nat. Prod.* **2000**, *63*, 726.
- [11] Paddon, C. J.; Westfall, P. J.; Pitera, D. J.; Benjamin, K.; Fisher, K.; McPhee, D.; Leavell, M. D.; Tai, A.; Main, A.; Eng, D.; Polichuk, D. R.; Teoh, K. H.; Reed, D. W.; Treynor, T.; Lenihan, J.; Jiang, H.; Fleck, M.; Bajad, S.; Dang, G.; Dengrove, D.; Diola, D.; Dorin, G.; Ellens, K. W.; Fickes, S.; Galazzo, J.; Gaucher, S. P.; Geistlinger, T.; Henry, R.; Hepp, M.; Horning, T.; Iqbal, T.; Kizer, L.; Lieu, B.; Melis, D.; Moss, N.; Regentin, R.; Secrest, S.; Tsuruta, H.; Vazquez, R.; Westblade, L. F.; Xu, L.; Yu, M.; Zhang, Y.; Zhao, L.; Lievens, J.; Covello, P. S.; Keasling, J. D.; Reiling, K. K.; Renninger, N. S.; Newman, J. D. *Nature* **2013**, *496*, 528.
- [12] Christianson, D. W. *Chem. Rev.* **2006**, *106*, 3412.
- [13] Pronin, S. V.; Shenvi, R. A. *Nat. Chem.* **2012**, *4*, 915.
- [14] Zhang, Q.; Tiefenbacher, K. *Nat. Chem.* **2015**, *7*, 197.
- [15] (a) Stork, G.; Burgstahler, A. W. *J. Am. Chem. Soc.* **1955**, *77*, 5068; (b) Eschenmoser, A.; Ruzicka, L.; Jeger, O.; Arigoni, D. *Helv. Chim. Acta* **1955**, *38*, 1890.
- [16] (a) Ishihara, K.; Nakamura, S.; Yamamoto, H. *J. Am. Chem. Soc.* **1999**, *121*, 4906; (b) Ungarean, C. N.; Southgate, E. H.; Sarlah, D. *Org. Biomol. Chem.* **2016**, *14*, 5454.
- [17] (a) Mullen, C. A.; Gagné, M. R. *J. Am. Chem. Soc.* **2007**, *129*, 11880; (b) Mullen, C. A.; Campbell, A. N.; Gagné, M. R. *Angew. Chem. Int. Ed.* **2008**, *47*, 6011.
- [18] Cochrane, N. A.; Nguyen, H.; Gagne, M. R. *J. Am. Chem. Soc.* **2013**, *135*, 628.
- [19] (a) Sethofer, S. G.; Mayer, T.; Toste, F. D. *J. Am. Chem. Soc.* **2010**, *132*, 8276; (b) Schafroth, M. A.; Sarlah, D.; Krautwald, S.; Carreira, E. M. *J. Am. Chem. Soc.* **2012**, *134*, 20276.
- [20] Sakakura, A.; Ukai, A.; Ishihara, K. *Nature* **2007**, *445*, 900.

- [21] Snyder, S. A.; Treitler, D. S.; Brucks, A. P. *J. Am. Chem. Soc.* **2010**, *132*, 14303.
- [22] Rendler, S.; MacMillan, D. W. C. *J. Am. Chem. Soc.* **2010**, *132*, 5027.
- [23] Beeson, T. D.; Mastracchio, A.; Hong, J.-B.; Ashton, K.; MacMillan, D. W. C. *Science* **2007**, *316*, 582.
- [24] Knowles, R. R.; Lin, S.; Jacobsen, E. N. *J. Am. Chem. Soc.* **2010**, *132*, 5030.
- [25] Baunach, M.; Franke, J.; Hertweck, C. *Angew. Chem. Int. Ed.* **2015**, *54*, 2604.
- [26] (a) Schneider, H.-J. *Angew. Chem. Int. Ed.* **2009**, *48*, 3924; (b) Persch, E.; Dumele, O.; Diederich, F. *Angew. Chem. Int. Ed.* **2015**, *54*, 3290.
- [27] (a) Pedersen, C. J. *J. Am. Chem. Soc.* **1967**, *89*, 7017; (b) Cram, D. J.; Kaneda, T.; Helgeson, R. C.; Brown, S. B.; Knobler, C. B.; Maverick, E.; Trueblood, K. N. *J. Am. Chem. Soc.* **1985**, *107*, 3645; (c) Lehn, J. M.; Pine, S. H.; Watanabe, E.; Willard, A. K. *J. Am. Chem. Soc.* **1977**, *99*, 6766.
- [28] Dougherty, D. A. *Acc. Chem. Res.* **2013**, *46*, 885.
- [29] Mecozzi, S.; West, A. P.; Dougherty, D. A. *Proc. Natl. Acad. Sci. U.S.A.* **1996**, *93*, 10566.
- [30] Tsuzuki, S.; Honda, K.; Uchimar, T.; Mikami, M.; Tanabe, K. *J. Am. Chem. Soc.* **2002**, *124*, 104.
- [31] Dawson, R. E.; Hennig, A.; Weimann, D. P.; Emery, D.; Ravikumar, V.; Montenegro, J.; Takeuchi, T.; Gabutti, S.; Mayor, M.; Mareda, J.; Schalley, C. A.; Matile, S. *Nat. Chem.* **2010**, *2*, 533.
- [32] Mecozzi, S.; Rebek, J. J. *Chem. Eur. J.* **1998**, *4*, 1016.
- [33] Rablen, P. R.; Lockman, J. W.; Jorgensen, W. L. *J. Phys. Chem. A* **1998**, *102*, 3782.
- [34] Rozas, I.; Alkorta, I.; Elguero, J. *J. Phys. Chem. A* **1998**, *102*, 9925.
- [35] Quioco, F. A. *Pure Appl. Chem.* **1989**, *61*.
- [36] Murray, T. J.; Zimmerman, S. C. *J. Am. Chem. Soc.* **1992**, *114*, 4010.
- [37] Dumele, O.; Wu, D.; Trapp, N.; Goroff, N.; Diederich, F. *Org. Lett.* **2014**, *16*, 4722.
- [38] (a) Ringer, A. L.; Senenko, A.; Sherrill, C. D. *Protein Sci.* **2007**, *16*, 2216; (b) Paulini, R.; Müller, K.; Diederich, F. *Angew. Chem. Int. Ed.* **2005**, *44*, 1788.
- [39] Breslow, R. *Science* **1982**, *218*, 532.
- [40] Mackay, L. G.; Wylie, R. S.; Sanders, J. K. M. *J. Am. Chem. Soc.* **1994**, *116*, 3141.
- [41] Cram, D. J.; Katz, H. E.; Dicker, I. B. *J. Am. Chem. Soc.* **1984**, *106*, 4987.
- [42] Mattei, P.; Diederich, F. *Helv. Chim. Acta* **1997**, *80*, 1555.
- [43] Mock, W. L.; Irra, T. A.; Wepsiec, J. P.; Manimaran, T. L. *J. Org. Chem.* **1983**, *48*, 3619.

- [44] Masseroni, D.; Mosca, S.; Mower, M. P.; Blackmond, D. G.; Rebek, J. *Angew. Chem. Int. Ed.* **2016**, *55*, 8290.
- [45] Shi, Q.; Masseroni, D.; Rebek, J. *J. Am. Chem. Soc.* **2016**.
- [46] Shi, Q.; Mower, M. P.; Blackmond, D. G.; Rebek, J. *Proc. Natl. Acad. Sci. U.S.A.* **2016**, *113*, 9199.
- [47] Vriezema, D. M.; Comellas Aragonès, M.; Elemans, J. A. A. W.; Cornelissen, J. J. L. M.; Rowan, A. E.; Nolte, R. J. M. *Chem. Rev.* **2005**, *105*, 1445.
- [48] Liu, X.; Liu, Y.; Li, G.; Warmuth, R. *Angew. Chem. Int. Ed.* **2006**, *118*, 915.
- [49] Sun, J.; Patrick, B. O.; Sherman, J. C. *Tetrahedron* **2009**, *65*, 7296.
- [50] Brachvogel, R.-C.; Hampel, F.; von Delius, M. *Nat. Commun.* **2015**, *6*.
- [51] Tamaki, K.; Ishigami, A.; Tanaka, Y.; Yamanaka, M.; Kobayashi, K. *Chem. Eur. J.* **2015**, *21*, 13714.
- [52] Brown, C. J.; Toste, F. D.; Bergman, R. G.; Raymond, K. N. *Chem. Rev.* **2015**, *115*, 3012.
- [53] Hof, F.; Craig, S. L.; Nuckolls, C.; Rebek, J. J. *Angew. Chem. Int. Ed.* **2002**, *41*, 1488.
- [54] Jordan, J. H.; Gibb, B. C. *Chem. Soc. Rev.* **2015**, *44*, 547.
- [55] Oshovsky, G. V.; Reinhoudt, D. N.; Verboom, W. *J. Am. Chem. Soc.* **2006**, *128*, 5270.
- [56] (a) Dumele, O.; Trapp, N.; Diederich, F. *Angew. Chem. Int. Ed.* **2015**, *54*, 12339; (b) Dumele, O.; Schreib, B.; Warzok, U.; Trapp, N.; Schalley, C. A.; Diederich, F. *Angew. Chem. Int. Ed.* **2017**, *56*, 1152.
- [57] Fujita, D.; Ueda, Y.; Sato, S.; Mizuno, N.; Kumasaka, T.; Fujita, M. *Nature* **2016**, *540*, 563.
- [58] Fujita, M.; Oguro, D.; Miyazawa, M.; Oka, H.; Yamaguchi, K.; Ogura, K. *Nature* **1995**, *378*, 469.
- [59] Murase, T.; Peschard, S.; Horiuchi, S.; Nishioka, Y.; Fujita, M. *Supramol. Chem.* **2011**, *23*, 199.
- [60] Schmidt, A.; Casini, A.; Kühn, F. E. *Coord. Chem. Rev.* **2014**, *275*, 19.
- [61] Han, M.; Michel, R.; He, B.; Chen, Y.-S.; Stalke, D.; John, M.; Clever, G. H. *Angew. Chem. Int. Ed.* **2013**, *52*, 1319.
- [62] Yamashina, M.; Sei, Y.; Akita, M.; Yoshizawa, M. *Nat. Commun.* **2014**, *5*, 4662.
- [63] Caulder, D. L.; Powers, R. E.; Parac, T. N.; Raymond, K. N. *Angew. Chem. Int. Ed.* **1998**, *37*, 1840.
- [64] Davis, A. V.; Raymond, K. N. *J. Am. Chem. Soc.* **2005**, *127*, 7912.

- [65] Zhao, C.; Sun, Q.-F.; Hart-Cooper, W. M.; DiPasquale, A. G.; Toste, F. D.; Bergman, R. G.; Raymond, K. N. *J. Am. Chem. Soc.* **2013**, *135*, 18802.
- [66] Sgarlata, C.; Mugridge, J. S.; Pluth, M. D.; Tiedemann, B. E. F.; Zito, V.; Arena, G.; Raymond, K. N. *J. Am. Chem. Soc.* **2010**, *132*, 1005.
- [67] Mal, P.; Schultz, D.; Beyeh, K.; Rissanen, K.; Nitschke, J. R. *Angew. Chem. Int. Ed.* **2008**, *47*, 8297.
- [68] Smulders, M. M. J.; Zarra, S.; Nitschke, J. R. *J. Am. Chem. Soc.* **2013**, *135*, 7039.
- [69] Bolliger, J. L.; Belenguer, A. M.; Nitschke, J. R. *Angew. Chem. Int. Ed.* **2013**, *52*, 7958.
- [70] (a) Tidmarsh, I. S.; Faust, T. B.; Adams, H.; Harding, L. P.; Russo, L.; Clegg, W.; Ward, M. D. *J. Am. Chem. Soc.* **2008**, *130*, 15167; (b) Whitehead, M.; Turega, S.; Stephenson, A.; Hunter, C. A.; Ward, M. D. *Chem. Sci.* **2013**, *4*, 2744.
- [71] Cullen, W.; Turega, S.; Hunter, C. A.; Ward, M. D. *Chem. Sci.* **2015**, *6*, 2790.
- [72] (a) Cullen, W.; Thomas, K. A.; Hunter, C. A.; Ward, M. D. *Chem. Sci.* **2015**, *6*, 4025; (b) Cullen, W.; Turega, S.; Hunter, C. A.; Ward, M. D. *Chem. Sci.* **2015**, *6*, 625.
- [73] Slagt, V. F.; Reek, J. N. H.; Kamer, P. C. J.; van Leeuwen, P. W. N. M. *Angew. Chem. Int. Ed.* **2001**, *40*, 4271.
- [74] Bocokić, V.; Kalkan, A.; Lutz, M.; Spek, A. L.; Gryko, D. T.; Reek, J. N. H. *Nat. Commun.* **2013**, *4*.
- [75] Wang, Q. Q.; Gonell, S.; Leenders, S. H.; Durr, M.; Ivanovic-Burmazovic, I.; Reek, J. N. *Nat. Chem.* **2016**, *8*, 225.
- [76] Gibb, C. L. D.; Gibb, B. C. *J. Am. Chem. Soc.* **2006**, *128*, 16498.
- [77] Kaanumalle, L. S.; Gibb, C. L. D.; Gibb, B. C.; Ramamurthy, V. *J. Am. Chem. Soc.* **2004**, *126*, 14366.
- [78] Meissner, R. S.; Rebek, J.; de Mendoza, J. *Science* **1995**, *270*, 1485.
- [79] Kang, J.; Rebek, J. *Nature* **1996**, *382*, 239.
- [80] Heinz, T.; Rudkevich, D. M.; Rebek, J. *Nature* **1998**, *394*, 764.
- [81] (a) Palmer, L. C.; Rebek, J. *J. Org. Biomol. Chem.* **2004**, *2*, 3051; (b) Pluth, M. D.; Raymond, K. N. *Chem. Soc. Rev.* **2007**, *36*, 161.
- [82] Catti, L.; Zhang, Q.; Tiefenbacher, K. *Chem. Eur. J.* **2016**, *22*, 9060.
- [83] Beaudoin, D.; Rominger, F.; Mastalerz, M. *Angew. Chem. Int. Ed.* **2016**, *55*, 15599.
- [84] (a) Liu, X.; Weinert, Z. J.; Sharafi, M.; Liao, C.; Li, J.; Schneebeli, S. T. *Angew. Chem. Int. Ed.* **2015**, *54*, 12772; (b) Mastalerz, M. *Angew. Chem. Int. Ed.* **2016**, *55*, 45.
- [85] MacGillivray, L. R.; Atwood, J. L. *Nature* **1997**, *389*, 469.

- [86] Gerkensmeier, T.; Iwanek, W.; Agena, C.; Fröhlich, R.; Kotila, S.; Näther, C.; Mattay, J. *Eur. J. Org. Chem.* **1999**, 1999, 2257.
- [87] Palmer, L. C.; Rebek, J. *Org. Lett.* **2005**, 7, 787.
- [88] Zhang, Q.; Catti, L.; Kaila, V. R. I.; Tiefenbacher, K. *Chem. Sci.* **2017**, 8, 1653.
- [89] Tunstad, L. M.; Tucker, J. A.; Dalcanale, E.; Weiser, J.; Bryant, J. A.; Sherman, J. C.; Helgeson, R. C.; Knobler, C. B.; Cram, D. J. *J. Org. Chem.* **1989**, 54, 1305.
- [90] Weinelt, F.; Schneider, H. J. *J. Org. Chem.* **1991**, 56, 5527.
- [91] Timmerman, P.; Verboom, W.; Reinhoudt, D. N. *Tetrahedron* **1996**, 52, 2663.
- [92] Moll, H. E.; Semeril, D.; Matt, D.; Youinou, M.-T.; Toupet, L. *Org. Biomol. Chem.* **2009**, 7, 495.
- [93] Avram, L.; Cohen, Y.; Rebek Jr, J. *Chem. Commun.* **2011**, 47, 5368.
- [94] Jiang, W.; Ajami, D.; Rebek, J. *J. Am. Chem. Soc.* **2012**, 134, 8070.
- [95] Yamanaka, M.; Shivanyuk, A.; Rebek, J. *J. Am. Chem. Soc.* **2004**, 126, 2939.
- [96] Avram, L.; Cohen, Y. *J. Am. Chem. Soc.* **2003**, 125, 16180.
- [97] Yariv-Shoushan, S.; Cohen, Y. *Org. Lett.* **2016**, 18, 936.
- [98] Cohen, Y.; Slovak, S.; Avram, L. *Hydrogen Bond Hexameric Capsules: Structures, Host-Guest Interactions, Guest Affinities, and Catalysis*. In *Calixarenes and Beyond*; Neri, P., Sessler, J. L., Wang, M.-X., Eds.; Springer International Publishing: Cham, **2016**, 811.
- [99] Avram, L.; Goldbourt, A.; Cohen, Y. *Angew. Chem. Int. Ed.* **2016**, 55, 904.
- [100] (a) Kvasnica, M.; Chapin, J. C.; Purse, B. W. *Angew. Chem. Int. Ed.* **2011**, 123, 2292; (b) Chapin, J. C.; Kvasnica, M.; Purse, B. W. *J. Am. Chem. Soc.* **2012**, 134, 15000.
- [101] Dalgarno, S. J.; Tucker, S. A.; Bassil, D. B.; Atwood, J. L. *Science* **2005**, 309, 2037.
- [102] Slovak, S.; Cohen, Y. *Chem. Eur. J.* **2012**, 18, 8515.
- [103] Evan-Salem, T.; Baruch, I.; Avram, L.; Cohen, Y.; Palmer, L. C.; Rebek, J. *Proc. Natl. Acad. Sci. U.S.A.* **2006**, 103, 12296.
- [104] Horiuchi, S.; Tanaka, H.; Sakuda, E.; Arikawa, Y.; Umakoshi, K. *Chem. Eur. J.* **2016**, 22, 17533.
- [105] Mileo, E.; Yi, S.; Bhattacharya, P.; Kaifer, A. E. *Angew. Chem. Int. Ed.* **2009**, 48, 5337.
- [106] Swaminathan Iyer, K.; Norret, M.; Dalgarno, S. J.; Atwood, J. L.; Raston, C. L. *Angew. Chem. Int. Ed.* **2008**, 47, 6362.
- [107] Cohen, Y.; Avram, L.; Frish, L. *Angew. Chem. Int. Ed.* **2005**, 44, 520.
- [108] Avram, L.; Cohen, Y. *J. Am. Chem. Soc.* **2002**, 124, 15148.
- [109] Ugono, O.; Holman, K. T. *Chem. Commun.* **2006**, 2144.

- [110] Avram, L.; Cohen, Y. *Org. Lett.* **2008**, *10*, 1505.
- [111] Slovak, S.; Cohen, Y. *Supramol. Chem.* **2010**, *22*, 803.
- [112] Barrett, E. S.; Dale, T. J.; Rebek, J. *J. Am. Chem. Soc.* **2007**, *129*, 3818.
- [113] Ajami, D.; Schramm, M. P.; Volonterio, A.; Rebek, J. *Angew. Chem. Int. Ed.* **2007**, *46*, 242.
- [114] Zhang, Q.; Tiefenbacher, K. *J. Am. Chem. Soc.* **2013**, *135*, 16213.
- [115] Zhang, L.; Sonaglia, L.; Stacey, J.; Lautens, M. *Org. Lett.* **2013**, *15*, 2128.
- [116] (a) Catti, L.; Zhang, Q.; Tiefenbacher, K. *Synthesis* **2016**, *48*, 313; (b) Catti, L.; Bräuer, T. M.; Zhang, Q.; Tiefenbacher, K. *Chimia* **2016**, *70*, 810.
- [117] Yoshizawa, M.; Klosterman, J. K.; Fujita, M. *Angew. Chem. Int. Ed.* **2009**, *48*, 3418.
- [118] Hastings, C. J.; Pluth, M. D.; Bergman, R. G.; Raymond, K. N. *J. Am. Chem. Soc.* **2010**, *132*, 6938.
- [119] Murase, T.; Nishijima, Y.; Fujita, M. *J. Am. Chem. Soc.* **2012**, *134*, 162.
- [120] Yoshizawa, M.; Tamura, M.; Fujita, M. *Science* **2006**, *312*, 251.
- [121] Fiedler, D.; Bergman, R. G.; Raymond, K. N. *Angew. Chem. Int. Ed.* **2004**, *43*, 6748.
- [122] Hastings, C. J.; Fiedler, D.; Bergman, R. G.; Raymond, K. N. *J. Am. Chem. Soc.* **2008**, *130*, 10977.
- [123] Pluth, M. D.; Bergman, R. G.; Raymond, K. N. *Science* **2007**, *316*, 85.
- [124] Pluth, M. D.; Bergman, R. G.; Raymond, K. N. *Angew. Chem. Int. Ed.* **2007**, *46*, 8587.
- [125] Hastings, C. J.; Bergman, R. G.; Raymond, K. N. *Chem. Eur. J.* **2014**, *20*, 3966.
- [126] Hart-Cooper, W. M.; Clary, K. N.; Toste, F. D.; Bergman, R. G.; Raymond, K. N. *J. Am. Chem. Soc.* **2012**, *134*, 17873.
- [127] Kaphan, D. M.; Toste, F. D.; Bergman, R. G.; Raymond, K. N. *J. Am. Chem. Soc.* **2015**, *137*, 9202.
- [128] Zhao, C.; Toste, F. D.; Raymond, K. N.; Bergman, R. G. *J. Am. Chem. Soc.* **2014**, *136*, 14409.
- [129] Wang, Z. J.; Clary, K. N.; Bergman, R. G.; Raymond, K. N.; Toste, F. D. *Nat. Chem.* **2013**, *5*, 100.
- [130] Wang, Z. J.; Brown, C. J.; Bergman, R. G.; Raymond, K. N.; Toste, F. D. *J. Am. Chem. Soc.* **2011**, *133*, 7358.
- [131] (a) Kaphan, D. M.; Levin, M. D.; Bergman, R. G.; Raymond, K. N.; Toste, F. D. *Science* **2015**, *350*, 1235; (b) Levin, M. D.; Kaphan, D. M.; Hong, C. M.; Bergman, R. G.; Raymond, K. N.; Toste, F. D. *J. Am. Chem. Soc.* **2016**, *138*, 9682.

- [132] Salles, A. G., Jr.; Zarra, S.; Turner, R. M.; Nitschke, J. R. *J. Am. Chem. Soc.* **2013**, *135*, 19143.
- [133] Cullen, W.; Misuraca, M. C.; Hunter, C. A.; Williams, N. H.; Ward, M. D. *Nat. Chem.* **2016**, *8*, 231.
- [134] Kuil, M.; Soltner, T.; van Leeuwen, P. W. N. M.; Reek, J. N. H. *J. Am. Chem. Soc.* **2006**, *128*, 11344.
- [135] Gadzikwa, T.; Bellini, R.; Dekker, H. L.; Reek, J. N. H. *J. Am. Chem. Soc.* **2012**, *134*, 2860.
- [136] Kaanumalle, L. S.; Gibb, C. L. D.; Gibb, B. C.; Ramamurthy, V. *Org. Biomol. Chem.* **2007**, *5*, 236.
- [137] Kang, J.; Santamaría, J.; Hilmersson, G.; Rebek, J. *J. Am. Chem. Soc.* **1998**, *120*, 7389.
- [138] Chen, J.; Rebek, J. *Org. Lett.* **2002**, *4*, 327.
- [139] Cavarzan, A.; Scarso, A.; Sgarbossa, P.; Strukul, G.; Reek, J. N. H. *J. Am. Chem. Soc.* **2011**, *133*, 2848.
- [140] Cavarzan, A.; Reek, J. N. H.; Trentin, F.; Scarso, A.; Strukul, G. *Catal. Sci. Tech.* **2013**, *3*, 2898.
- [141] Jans, A. C.; Gomez-Suarez, A.; Nolan, S. P.; Reek, J. N. *Chem. Eur. J.* **2016**, *22*, 14836.
- [142] Bianchini, G.; Scarso, A.; Sorella, G. L.; Strukul, G. *Chem. Commun.* **2012**, *48*, 12082.
- [143] Bianchini, G.; Sorella, G. L.; Canever, N.; Scarso, A.; Strukul, G. *Chem. Commun.* **2013**, *49*, 5322.
- [144] Giust, S.; La Sorella, G.; Sporni, L.; Fabris, F.; Strukul, G.; Scarso, A. *Asian J. Org. Chem.* **2015**, *4*, 217.
- [145] Jencks, W. P.; Regenstein, J. *Ionization constants of acids and bases*. In *Handbook of Biochemistry and Molecular Biology, Physical Chemical Data*; CRC Press: Cleveland, **1976**, Vol. 1, 305.
- [146] La Sorella, G.; Sporni, L.; Strukul, G.; Scarso, A. *ChemCatChem* **2015**, *7*, 291.
- [147] Giust, S.; La Sorella, G.; Sporni, L.; Strukul, G.; Scarso, A. *Chem. Commun.* **2015**, *51*, 1658.
- [148] Caneva, T.; Sporni, L.; Strukul, G.; Scarso, A. *RSC Adv.* **2016**, *6*, 83505.
- [149] La Sorella, G.; Sporni, L.; Ballester, P.; Strukul, G.; Scarso, A. *Catal. Sci. Tech.* **2016**, *6*, 6031.
- [150] La Sorella, G.; Sporni, L.; Strukul, G.; Scarso, A. *Adv. Synth. Catal.* **2016**, *358*, 3443.
- [151] Shimizu, S.; Usui, A.; Sugai, M.; Suematsu, Y.; Shirakawa, S.; Ichikawa, H. *Eur. J. Org. Chem.* **2013**, *2013*, 4734.

- [152] Bräuer, T. M.; Zhang, Q.; Tiefenbacher, K. *Angew. Chem. Int. Ed.* **2016**, *55*, 7698.
- [153] Catti, L.; Tiefenbacher, K. *Chem. Commun.* **2015**, *51*, 892.
- [154] Catti, L.; Pöthig, A.; Tiefenbacher, K. *Adv. Synth. Catal.* **2017**, in press, DOI: 10.1002/adsc.201601363.
- [155] Böhm, P. *Studies towards the formation of cyclobutanones via a hydride transfer ring expansion cascade reaction*, Bachelor's Thesis, Technical University of Munich, Department of Chemistry, **2016**.
- [156] Calloway, N. O. *Chem. Rev.* **1935**, *17*, 327.
- [157] Rueping, M.; Nachtsheim, B. J. *Beilstein J. Org. Chem.* **2010**, *6*, 6.
- [158] Niggemann, M.; Meel, M. J. *Angew. Chem. Int. Ed.* **2010**, *49*, 3684.
- [159] Richter, M. *Nat. Prod. Rep.* **2013**, *30*, 1324.
- [160] Cardellini, F.; Germani, R.; Cardinali, G.; Corte, L.; Roscini, L.; Spreti, N.; Tiecco, M. *RSC Adv.* **2015**, *5*, 31772.
- [161] (a) Furutani, Y.; Kandori, H.; Kawano, M.; Nakabayashi, K.; Yoshizawa, M.; Fujita, M. *J. Am. Chem. Soc.* **2009**, *131*, 4764; (b) Jagadesan, P.; Mondal, B.; Parthasarathy, A.; Rao, V. J.; Ramamurthy, V. *Org. Lett.* **2013**, *15*, 1326; (c) Dalton, D. M.; Ellis, S. R.; Nichols, E. M.; Mathies, R. A.; Toste, F. D.; Bergman, R. G.; Raymond, K. N. *J. Am. Chem. Soc.* **2015**, *137*, 10128.
- [162] Tolbert, L. M.; Solntsev, K. M. *Acc. Chem. Res.* **2002**, *35*, 19.
- [163] Prémont-Schwarz, M.; Barak, T.; Pines, D.; Nibbering, E. T. J.; Pines, E. *J. Phys. Chem. B* **2013**, *117*, 4594.
- [164] (a) Szczepanik, B. *J. Mol. Struct.* **2015**, *1099*, 209; (b) Bekçioğlu, G.; Hoffmann, F.; Sebastiani, D. *J. Phys. Chem. A* **2015**, *119*, 9244.
- [165] Shi, Z.; Peng, P.; Strohecker, D.; Liao, Y. *J. Am. Chem. Soc.* **2011**, *133*, 14699.
- [166] Barrett, E. S.; Dale, T. J.; Rebek, J. *J. Am. Chem. Soc.* **2008**, *130*, 2344.
- [167] Brown, C. J.; Bergman, R. G.; Raymond, K. N. *J. Am. Chem. Soc.* **2009**, *131*, 17530.
- [168] (a) Wiegmann, S.; Mattay, J. *Org. Lett.* **2011**, *13*, 3226; (b) Menger, F. M.; Bian, J.; Sizova, E.; Martinson, D. E.; Seredyuk, V. A. *Org. Lett.* **2004**, *6*, 261; (c) Page, P. C. B.; Bygrave, T. R.; Chan, Y.; Heaney, H.; McKee, V. *Eur. J. Org. Chem.* **2011**, *2011*, 3016; (d) Klaes, M.; Agena, C.; Köhler, M.; Inoue, M.; Wada, T.; Inoue, Y.; Mattay, J. *Eur. J. Org. Chem.* **2003**, *2003*, 1404; (e) Agena, C.; Wolff, C.; Mattay, J. *Eur. J. Org. Chem.* **2001**, *2001*, 2977.
- [169] Rudkevich, D. M. *Chem. Eur. J.* **2000**, *6*, 2679.

- [170] Dvořáková, H.; Štursa, J.; Čajan, M.; Moravcová, J. *Eur. J. Org. Chem.* **2006**, 2006, 4519.
- [171] Merget, S. *Synthesis of Resorcin[4]arene Derivatives and the Study of their Supramolecular Properties*, Master`s Thesis, Technical University of Munich, Department of Chemistry, **2017**.
- [172] Christ, P.; Lindsay, A. G.; Vormittag, S. S.; Neudörfl, J.-M.; Berkessel, A.; O'Donoghue, A. C. *Chem. Eur. J.* **2011**, *17*, 8524.
- [173] Tan, H. M.; Soh, S. F.; Zhao, J.; Yong, E. L.; Gong, Y. *Chirality* **2011**, *23*, E91.
- [174] Aoyama, Y.; Tanaka, Y.; Sugahara, S. *J. Am. Chem. Soc.* **1989**, *111*, 5397.
- [175] (a) Bartenstein, J. E.; Lucas, N. T. *Supramol. Chem.* **2012**, *24*, 618; (b) Serkova, O. S.; Burikhina, A. V.; Vasyanina, L. K.; Kuprina, O. S.; Maslennikova, V. I.; Nifantiev, E. *E. Russ. J. Gen. Chem.* **2014**, *84*, 745.
- [176] Ngodwana, L.; Kleinhans, D. J.; Smuts, A.-J.; van Otterlo, W. A. L.; Arnott, G. E. *RSC Adv.* **2013**, *3*, 3873.
- [177] Iwanek, W.; Stefańska, K. *Tetrahedron Lett.* **2015**, *56*, 1496.
- [178] Iwanek, W.; Stefańska, K.; Szumna, A.; Wierzbicki, M. *Tetrahedron* **2016**, *72*, 142.
- [179] Iwanek, W.; Stefanska, K.; Szumna, A.; Wierzbicki, M. *RSC Adv.* **2016**, *6*, 13027.
- [180] Avram, L.; Cohen, Y. *Org. Lett.* **2002**, *4*, 4365.
- [181] Grajda, M.; Wierzbicki, M.; Cmoch, P.; Szumna, A. *J. Org. Chem.* **2013**, *78*, 11597.
- [182] Schneider, U.; Schneider, H.-J. *Chem. Ber.* **1994**, *127*, 2455.
- [183] (a) Tan, S.-D.; Chen, W.-H.; Satake, A.; Wang, B.; Xu, Z.-L.; Kobuke, Y. *Org. Biomol. Chem.* **2004**, *2*, 2719; (b) Li, D.; Yamagishi, T.-a.; Nakamoto, Y. *J. Net. Polym. Jpn.* **2002**, *23*, 134; (c) Della Sala, P.; Gaeta, C.; Navarra, W.; Talotta, C.; De Rosa, M.; Brancatelli, G.; Geremia, S.; Capitelli, F.; Neri, P. *J. Org. Chem.* **2016**, *81*, 5726.
- [184] (a) Weissman, S. A.; Zewge, D. *Tetrahedron* **2005**, *61*, 7833; (b) Ranu, B. C.; Bhar, S. *Org. Prep. Proced. Int.* **1996**, *28*, 371.
- [185] Pietraszkiewicz, M.; Prus, P.; Pietraszkiewicz, O. *Tetrahedron* **2004**, *60*, 10747.
- [186] Irwin, J. L.; Sherburn, M. S. *J. Org. Chem.* **2000**, *65*, 602.
- [187] Hass, O.; Schierholt, A.; Jordan, M.; Lützen, A. *Synthesis* **2006**, 2006, 519.
- [188] Moran, J. R.; Karbach, S.; Cram, D. J. *J. Am. Chem. Soc.* **1982**, *104*, 5826.
- [189] Park, Y. S.; Paek, K. *Org. Lett.* **2008**, *10*, 4867.
- [190] Borrero, N. V.; Bai, F.; Perez, C.; Duong, B. Q.; Rocca, J. R.; Jin, S.; Huigens Iii, R. W. *Org. Biomol. Chem.* **2014**, *12*, 881.

- [191] Chen, W.-H.; Nishikawa, M.; Tan, S.-D.; Yamamura, M.; Satake, A.; Kobuke, Y. *Chem. Commun.* **2004**, 872.
- [192] Kosak, T. M.; Conrad, H. A.; Korich, A. L.; Lord, R. L. *Eur. J. Org. Chem.* **2015**, 2015, 7460.
- [193] Darwent, B. d. *Bond Dissociation Energies in Simple Molecules*; U.S. Dept. of Commerce, National Bureau of Standards: Washington, D.C, **1970**.
- [194] Liu, X.; Warmuth, R. *Nat. Protoc.* **2007**, 2, 1288.
- [195] Liu, P.; Wang, Z.; Hu, X. *Eur. J. Org. Chem.* **2012**, 2012, 1994.
- [196] Yamada, S.; Gavryushin, A.; Knochel, P. *Angew. Chem. Int. Ed.* **2010**, 49, 2215.
- [197] Avram, L.; Cohen, Y. *J. Am. Chem. Soc.* **2004**, 126, 11556.
- [198] Turega, S.; Cullen, W.; Whitehead, M.; Hunter, C. A.; Ward, M. D. *J. Am. Chem. Soc.* **2014**, 136, 8475.
- [199] Abreu, Ana S.; Silva, Natália O.; Ferreira, Paula M. T.; Queiroz, M.-João R. P. *Eur. J. Org. Chem.* **2003**, 2003, 1537.
- [200] (a) Langton, M. J.; Robinson, S. W.; Marques, I.; Félix, V.; Beer, P. D. *Nat. Chem.* **2014**, 6, 1039; (b) Brown, A.; Beer, P. D. *Chem. Commun.* **2016**, 52, 8645.
- [201] Miao, S.; Adams, R. D.; Guo, D.-S.; Zhang, Q.-F. *J. Mol. Struct.* **2003**, 659, 119.
- [202] Stoll, I.; Mix, A.; Rozhenko, A. B.; Neumann, B.; Stammeler, H.-G.; Mattay, J. *Tetrahedron* **2008**, 64, 3813.
- [203] Turunen, L.; Warzok, U.; Puttreddy, R.; Beyeh, N. K.; Schalley, C. A.; Rissanen, K. *Angew. Chem. Int. Ed.* **2016**, 55, 14033.

11. Bibliographic data of complete publications

This chapter provides the bibliographic details of the publications summarized in chapters 6.1 and 6.4 of this thesis to facilitate the retrieval of the complete manuscripts and supporting information. In addition, the bibliographic details for the authored publications are listed, which were used as the foundation of chapters 3 and 4.

Intramolecular hydroalkoxylation catalyzed inside a self-assembled cavity of an enzyme-like host structure

Lorenzo Catti and Konrad Tiefenbacher*

Department of Chemistry, Technical University of Munich, Lichtenbergstraße 4, D-85747 Garching, Germany

E-mail: konrad.tiefenbacher@unibas.ch

Originally published in: *Chem. Commun.* **2015**, 51, 892 – 894.

DOI: 10.1039/c4cc08211g

Hyperlink: <http://pubs.rsc.org/en/Content/ArticleLanding/2015/CC/c4cc08211g#!divAbstract>

Host-catalyzed cyclodehydration-rearrangement cascade reaction of unsaturated tertiary alcohols

Lorenzo Catti,^[a] Alexander Pöthig^[b] and Konrad Tiefenbacher^{[a,c]*}

[a] Department of Chemistry, University of Basel, St. Johannis-Ring 19, CH-4056 Basel, Switzerland

[b] Catalysis Research Center, Technical University of Munich, Ernst-Otto-Fischer-Straße 1, D-85748 Garching, Germany

[c] Department of Biosystems Science and Engineering, ETH Zürich, Mattenstrasse 26, CH-4058 Basel, Switzerland

E-mail: konrad.tiefenbacher@unibas.ch

Originally published in: *Adv. Synth. Catal.* **2017**, in press.

DOI: 10.1002/adsc.201601363

Hyperlink: –

To catalyze or not to catalyze: elucidation of the subtle differences between the hexameric capsules of pyrogallolarene and resorcinarene

Qi Zhang,^[a] Lorenzo Catti,^[a] Ville R. I. Kaila^[b] and Konrad Tiefenbacher^{[a,c]*}

[a] Department of Chemistry, University of Basel, St. Johannis-Ring 19, CH-4056 Basel, Switzerland

[b] Department of Chemistry, Technical University of Munich, Lichtenbergstraße 4, D-85747 Garching, Germany

[c] Department of Biosystems Science and Engineering, ETH Zürich, Mattenstrasse 26, CH-4058 Basel, Switzerland

E-mail: konrad.tiefenbacher@unibas.ch

Originally published in: *Chem. Sci.* **2017**, 8, 1653 – 1657.

DOI: 10.1039/c6sc04565k

Hyperlink: <http://pubs.rsc.org/en/content/articlelanding/2017/sc/c6sc04565k#!divAbstract>

Self-assembled supramolecular structures as catalysts for reactions involving cationic transition states

Lorenzo Catti, Qi Zhang and Konrad Tiefenbacher*

Department of Chemistry, Technical University of Munich, Lichtenbergstraße 4, D-85747 Garching, Germany

E-mail: konrad.tiefenbacher@unibas.ch

Originally published in: *Synthesis* **2016**, 48, 313 – 328.

DOI: 10.1055/s-0035-1560362

Hyperlink: <https://www.thieme-connect.com/products/ejournals/abstract/10.1055/s-0035-1560362?lang=de>

Advantages of catalysis in self-assembled molecular capsules

Lorenzo Catti, Qi Zhang and Konrad Tiefenbacher*

Department of Chemistry, Technical University of Munich, Lichtenbergstraße 4, D-85747 Garching, Germany

E-mail: konrad.tiefenbacher@unibas.ch

Originally published in: *Chem. Eur. J.* **2016**, 22, 9060 – 9066.

DOI: 10.1002/chem.201600726

Hyperlink: <http://onlinelibrary.wiley.com/doi/10.1002/chem.201600726/full>

Exploring catalysis inside self-assembled supramolecular containers

Lorenzo Catti,^[a] Thomas M. Bräuer,^[a] Qi Zhang^[a] and Konrad Tiefenbacher^{[a,b]*}

[a] Department of Chemistry, University of Basel, St. Johannis-Ring 19, CH-4056 Basel, Switzerland

[b] Department of Biosystems Science and Engineering, ETH Zürich, Mattenstrasse 26, CH-4058 Basel, Switzerland

E-mail: konrad.tiefenbacher@unibas.ch

Originally published in: *Chimia* **2016**, *70*, 810 – 814.

DOI: 10.2533/chimia.2016.810

Hyperlink:

<http://www.ingentaconnect.com/contentone/scs/chimia/2016/00000070/00000011/art00010>

12. Reprint permissions and reprints

12.1 The Royal Society of Chemistry

The manuscript published in *Chemical Communications*¹⁵³ was reproduced with permission (**open access**) of The Royal Society of Chemistry.

Intramolecular hydroalkoxylation catalyzed inside a self-assembled cavity of an enzyme-like host structure

L. Catti and K. Tiefenbacher, *Chem. Commun.*, 2015, **51**, 892

DOI: 10.1039/C4CC08211G

This article is licensed under a [Creative Commons Attribution-NonCommercial 3.0 Unported Licence](#). Material from this article can be used in other publications provided that the correct acknowledgement is given with the reproduced material and it is not used for commercial purposes.

Scheme 13 is partly reproduced from reference⁸⁸ with permission (**open access**) of The Royal Society of Chemistry.

To catalyze or not to catalyze: elucidation of the subtle differences between the hexameric capsules of pyrogallolarene and resorcinarene

Q. Zhang, L. Catti, V. R. I. Kaila and K. Tiefenbacher, *Chem. Sci.*, 2017, **8**, 1653

DOI: 10.1039/C6SC04565K

This article is licensed under a [Creative Commons Attribution-NonCommercial 3.0 Unported Licence](#). Material from this article can be used in other publications provided that the correct acknowledgement is given with the reproduced material and it is not used for commercial purposes.

12.2 John Wiley and Sons

The manuscript published in *Advanced Synthesis and Catalysis*¹⁵⁴ was reproduced with permission of John Wiley and Sons. The reprinted version represents the accepted version of the manuscript, since a more advanced version was not available at the time of writing. The reprinted version therefore does not represent the final version of the publication. Because the supporting information is not yet available online, a reprint of the supporting information is attached as well.

**WG: Advanced Synthesis & Catalysis - Decision on Manuscript ID
adsc.201601363.R1 (permission for reprint)**

Rights DE [RIGHTS-and-LICENCES@wiley-vch.de]

Gesendet: Montag, 30. Januar 2017 12:48

An: Lorenzo Catti

Cc: Rights DE [RIGHTS-and-LICENCES@wiley-vch.de]

Dear Lorenzo Catti,

We hereby grant permission for the requested use expected that due credit is given to the original source.

If material appears within our work with credit to another source, authorisation from that source must be obtained.

Credit must include the following components:

- Journals: Author(s) Name(s): Title of the Article. Name of the Journal. Publication year. Volume. Page(s). Copyright Wiley-VCH Verlag GmbH & Co. KGaA. Reproduced with permission.

If you also wish to publish your thesis in electronic format, you may use the article according to the Copyright transfer agreement:

3. Final Published Version.

Wiley-VCH hereby licenses back to the Contributor the following rights with respect to the final published version of the Contribution:

a. [...]

b. Re-use in other publications. The right to re-use the final Contribution or parts thereof for any publication authored or edited by the Contributor (excluding journal articles) where such re-used material constitutes less than half of the total material in such publication. In such case, any modifications should be accurately noted.

Kind regards

Heike Weller
Rights Manager
Rights & Licenses

Wiley-VCH Verlag GmbH & Co. KGaA
Boschstraße 12
69469 Weinheim
Germany
www.wiley-vch.de

T +(49) 6201 606-585

F +(49) 6201 606-332

rightsDE@wiley.com

Scheme 11 is partly reproduced from reference⁸³ with permission of John Wiley and Sons.

**JOHN WILEY AND SONS LICENSE
TERMS AND CONDITIONS**

Jan 12, 2017

This Agreement between Lorenzo Catti ("You") and John Wiley and Sons ("John Wiley and Sons") consists of your license details and the terms and conditions provided by John Wiley and Sons and Copyright Clearance Center.

License Number	4023011434947
License date	Jan 06, 2017
Licensed Content Publisher	John Wiley and Sons
Licensed Content Publication	Angewandte Chemie International Edition
Licensed Content Title	Chirality-Assisted Synthesis of a Very Large Octameric Hydrogen-Bonded Capsule
Licensed Content Author	Daniel Beaudoin, Frank Rominger, Michael Mastalerz
Licensed Content Date	Nov 10, 2016
Licensed Content Pages	5
Type of use	Dissertation/Thesis
Requestor type	University/Academic
Format	Print and electronic
Portion	Figure/table
Number of figures/tables	1
Original Wiley figure/table number(s)	Figure 1
Will you be translating?	No
Title of your thesis / dissertation	Application and Development of Resorcin[4]arene-Based Supramolecular Catalysts
Expected completion date	Feb 2017
Expected size (number of pages)	100
Requestor Location	Lorenzo Catti Stöberstrasse 5, 4055 Basel
	Basel, 4055 Switzerland Attn: Lorenzo Catti
Publisher Tax ID	EU826007151
Billing Type	Invoice
Billing Address	Lorenzo Catti Stöberstrasse 5, 4055 Basel
	Basel, Switzerland 4055 Attn: Lorenzo Catti
Total	0.00 CHF
Terms and Conditions	

Scheme 11 is partly reproduced from reference⁸² with permission of John Wiley and Sons.

**JOHN WILEY AND SONS LICENSE
TERMS AND CONDITIONS**

Jan 12, 2017

This Agreement between Lorenzo Catti ("You") and John Wiley and Sons ("John Wiley and Sons") consists of your license details and the terms and conditions provided by John Wiley and Sons and Copyright Clearance Center.

License Number	4026611288974
License date	Jan 12, 2017
Licensed Content Publisher	John Wiley and Sons
Licensed Content Publication	Chemistry - A European Journal
Licensed Content Title	Advantages of Catalysis in Self-Assembled Molecular Capsules
Licensed Content Author	Lorenzo Catti, Qi Zhang, Konrad Tiefenbacher
Licensed Content Date	May 6, 2016
Licensed Content Pages	7
Type of use	Dissertation/Thesis
Requestor type	Author of this Wiley article
Format	Print and electronic
Portion	Full article
Will you be translating?	No
Title of your thesis / dissertation	Application and Development of Resorcin[4]arene-Based Supramolecular Catalysts
Expected completion date	Feb 2017
Expected size (number of pages)	100
Requestor Location	Lorenzo Catti Stöberstrasse 5, 4055 Basel Basel, 4055 Switzerland Attn: Lorenzo Catti
Publisher Tax ID	EU826007151
Billing Type	Invoice
Billing Address	Lorenzo Catti Stöberstrasse 5, 4055 Basel Basel, Switzerland 4055 Attn: Lorenzo Catti
Total	0.00 CHF
Terms and Conditions	



Cite this: *Chem. Commun.*, 2015, 51, 892

Received 16th October 2014,
Accepted 20th November 2014

DOI: 10.1039/c4cc08211g

www.rsc.org/chemcomm

Intramolecular hydroalkoxylation catalyzed inside a self-assembled cavity of an enzyme-like host structure†

L. Catti and K. Tiefenbacher*

Self-assembled resorcin[4]arene hexamer catalyzes the intramolecular hydroalkoxylation of unsaturated alcohols to the corresponding cyclic ethers under mild conditions. The mode of catalysis and encapsulation-based substrate selectivity of the host efficiently mimic the basic principle of operation observed in enzymes.

Supramolecular catalysis aims to mimic the functions of enzymes without copying the complexity of their evolutionarily derived three-dimensional structure. Key features of enzyme catalysis comprise the selection of suitable substrates inside a hydrophobic reaction pocket, the altering of substrate orientation and/or conformation and the stabilization of the transition state of the reaction.¹ In the last two decades, research in the field of supramolecular chemistry has led to the preparation of a variety of self-assembled hosts bearing an internal cavity, which provides a defined chemical environment distinct from the bulk solvent.^{1,2} Application of a subset of noncovalently self-assembled structures to catalysis was successfully investigated by several groups.^{1,2d,f,3} However, the use of hydrogen bond-based assemblies in catalysis is limited to only five examples reported in literature.^{3f,4}

The resorcin[4]arene hexamer **I** (Fig. 1) represents one of the largest hydrogen bond-based self-assembled hosts and has been studied intensively due to its ready accessibility.⁵ It spontaneously forms in apolar solvents like chloroform and benzene from six resorcin[4]arene units **1**, which are easily prepared in multigram scale in a single step. In addition to the six monomer units, eight water molecules participate in the formation of the hexamer,⁶ which explains the excessive use of water-saturated solvents in resorcin[4]arene chemistry.^{2a,7} The capsule-like structure, held together by 60 hydrogen bonds, forms an octahedral-shaped cavity of about 1375 Å³.^{5a} In chloroform solution, this cavity is occupied by six solvent molecules in the absence of suitable guests.⁸ Due to extended cation-π interactions with the aromatic cavity, positive

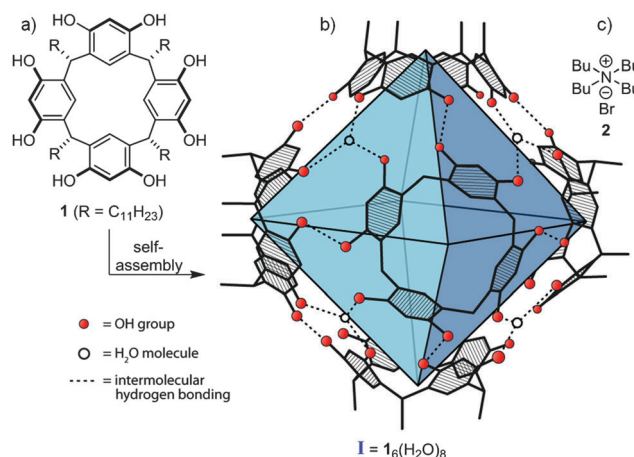


Fig. 1 (a) Structure of resorcin[4]arene **1**; (b) schematic representation of the hexameric resorcin[4]arene capsule **I**, emphasizing the octahedral cavity space (blue); alkyl groups have been omitted for clarity; (c) competitive inhibitor tetrabutylammonium bromide (Bu_4NBr) (**2**).

charged compounds like quaternary ammonium ions (*e.g.* **2**) display a high affinity for the capsule interior.⁹ Other suitable guests like alcohols and carboxylic acids rely on their ability to form hydrogen bonds with the hexameric host and, depending on their size, are coencapsulated with residual solvent molecules.^{7,10} Besides the capability of reversible guest encapsulation, the resorcin[4]arene hexamer acts as relatively strong phenol-based Brønsted acid ($\text{p}K_{\text{a}} \approx 5.5\text{--}6$), as recently reported by our group,^{3f} making it an appropriate choice for the study of enzyme-like acid catalysis.

Being aware of the good uptake of certain alcohol molecules,^{10b} we set out to explore the potential use of **I** as an acid catalyst in the intramolecular hydroalkoxylation of unactivated hydroxy olefins. Intramolecular hydroalkoxylation offers a direct, atom-economical access to cyclic ethers, which represent important core structures frequently found in polyether antibiotics, marine macrocycles and flavor compounds.¹¹ Although the cationic intramolecular hydroalkoxylation of unsaturated alcohols has been reported to be catalyzed by strong Brønsted acids like triflic acid (TfOH),¹²

Department Chemie, Technische Universität München, Lichtenbergstraße 4, D-85747 Garching, Germany. E-mail: konrad.tiefenbacher@tum.de

† Electronic supplementary information (ESI) available: Experimental details, characterization data and NMR spectra. See DOI: 10.1039/c4cc08211g



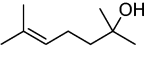
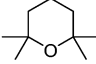
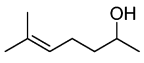
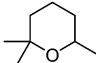
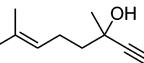
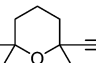
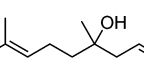
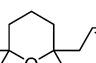
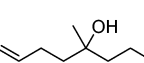
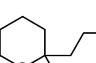
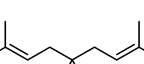
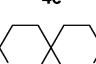
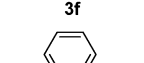
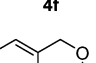
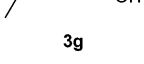

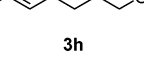
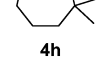
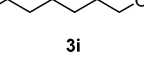
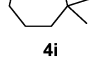
poor functional group compatibility, acid induced side reactions and the overall harsh reaction conditions limit the scope of these protocols. The application of weaker acids on the other hand often requires the use of over-stoichiometric amounts.¹³ Alternative catalytic approaches include the utilization of Lewis super-acids like $\text{Al}(\text{OTf})_3$ ¹⁴ and $\text{Ca}(\text{NTf}_2)_2$,¹⁵ transition metals,¹⁶ zeolites¹⁷ and Amberlyst H-15.¹⁸ In the context of supramolecular catalysis, Bergman, Raymond and Toste investigated the intramolecular hydroalkoxylation of activated hydroxy olefins inside a supramolecular host using an encapsulated gold catalyst.¹⁹

We began our investigation by adding 10 equiv. of hydroxy olefin **3a** (Table 1) to a solution of **I** (1 equiv.) in water-saturated CDCl_3 (3.3 mM). The appearance of new upfield-shifted signals

in the region of 0.5 to -0.6 ppm in the ^1H NMR spectrum of the reaction mixture, caused by the anisotropy of the capsule walls, indicated encapsulation of substrate **3a**. Reaction monitoring *via* NMR spectroscopy and GC and finally isolation confirmed selective conversion to cyclic ether **4a**. A subsequent optimization of the reaction conditions revealed the influence of water content and substrate concentration on the reaction rate. Reducing the water content of the reaction mixture from 30 equiv. to 11 equiv. of water per hexamer **I** (determined *via* ^1H NMR spectroscopy) by utilizing regular CDCl_3 instead of water-saturated CDCl_3 resulted in a significant increase in the reaction rate. It seems likely that the water molecules compete with the substrate for the protons of the catalyst. High substrate concentration on the other hand lead to a drastic decrease of the reaction rate, since the hydroxyl group of the substrate can interact with the monomer units and thereby reduce the equilibrium concentration of operational catalyst.⁹ Applying the optimized conditions, full conversion of substrate **3a** was achieved after about 3.5 d at 30 °C. In a control experiment, a small excess of the high affinity guest Bu_4NBr (**2**) (1.5 equiv.) was added to the catalyst solution prior to substrate addition. When catalyst **I** was blocked in this manner, the hydroalkoxylation of alcohol **3a** was efficiently slowed down, giving only a weak background conversion of 7%. A second control experiment without added catalyst was performed to rule out a background reaction catalyzed by trace amounts of HCl/DCl , potentially formed by photodegradation of CDCl_3 . In this case, no detectable conversion was observed after 7 d. These results demonstrated that a catalytic conversion is indeed possible with **I** and that the reaction takes place inside the cavity after initial protonation of the substrate. The observed catalytic effect imparted by hexamer **I** is believed to result from the stabilization of cationic intermediates and transitions states by cation- π interactions with the aromatic cavity. The catalytic cycle is finally completed by release of the cyclic ether, which does not bind strongly to the cavity.

In order to evaluate the scope of the hexamer **I**-catalyzed intramolecular hydroalkoxylation, we next investigated the formation of differently substituted tetrahydropyran and oxepane derivatives as summarized in Table 1. In general, the reactions proceeded to completion in 0.7 to 6 d at 30 °C using a 10 mol% catalyst loading. Conversion of γ,δ -unsaturated monoalcohols gave the corresponding tetrahydropyran derivatives in good yields (Table 1, entries 1–4). When employing substrates bearing two hydroxyl groups, full conversion was achieved within 16 h, owing to the high affinity of diols to the capsule interior (Table 1, entries 5 and 6). In the case of substrate **3g**, a reduced yield was obtained, presumably due to an oligomerization side reaction, as implied by broad signals in the ^1H NMR spectrum. Meanwhile, the formation of oxepane **4h** proceeded in good yield. However, when a terminal olefin was used, the reaction proceeded much slower with GC indicating intermediary formation of the corresponding trisubstituted and hydrated olefin (Table 1, entry 9). The spirobicyclic ether **4j** was obtained in 63%. The reduced yield is based on an equilibrium between starting material and cyclization product, as proven by subjecting the isolated ether to standard reaction conditions. All performed hydroalkoxylation occurred with Markovnikov selectivity. Furthermore, all substrates were tested with Bu_4NBr (**2**)-inhibited catalyst, giving only a weak background reaction in each case (Table 1). Catalyst **I** was also

Table 1 Intramolecular hydroalkoxylation of unactivated hydroxy olefins^a

Entry	Substrate	Product	Background conv. ^b (%)	Yield ^b (%) (Time (d))
1			7 ^c	96 ^c (3.5)
2			8	98 (1.5)
3			3	91 (1.8)
4			8	84 (3.4)
5			6	88 (0.7)
6			8	93 (0.7)
7			6	45 (5.5)
8			4	94 (1.9)
9			10	91 (5.0)
10			4	63 (5.0)

^a Reaction conditions: hydroxy olefin (33 mM), catalyst **I** (3.3 mM), CDCl_3 , 30 °C, 0.7–6 d. ^b Determined *via* ^1H NMR. ^c Determined *via* GC (response factor-corrected).



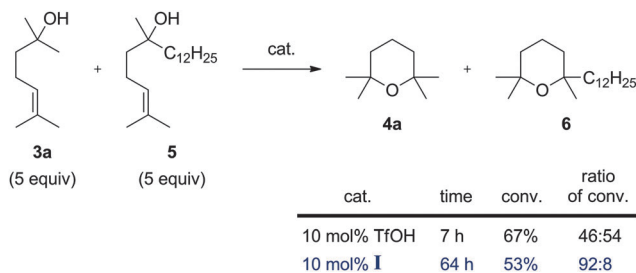


Fig. 2 Substrate selectivity imposed by hexamer **I**.

successfully applied for the synthesis of tetrahydrofuran derivatives. However, in those cases, an increased background reaction was observed, caused by the high reactivity of the employed starting materials. On the other hand, substrates that would require the formation of an intermediary secondary cation showed no reactivity under the reaction conditions (see ESI,[†] chapter 10).

After having demonstrated the applicability of hexamer **I** as a catalyst in intramolecular hydroalkoxylation, we next tried to explore the possibility of selectively converting one hydroxy olefin in the presence of another. Indeed, when adding a mixture of **3a** and **5** (5 equiv. each; Fig. 2) to a solution of **I** (1 equiv.) in CDCl_3 (3.3 mM), the reaction proceeded in a highly selective fashion: After 64 h, the small substrate was almost completely converted (98%), while the large analogue showed only 8% conversion. This corresponds to a 92:8 ratio of conversion. The slow transformation of the large hydroxy olefin **5** can be explained by its decreased uptake. This observation correlates to previous findings regarding the hydrolysis rate of acetals utilizing hexamer **I**.^{3f} As a control experiment, capsule **I** was replaced with 10 mol% of TfOH ($\text{p}K_{\text{a}} = -12$; in water),²⁰ since use of 10 mol% of a weaker reagent like acetic acid ($\text{p}K_{\text{a}} = 4.8$; in water)²⁰ did not provide any conversion in the case of substrate **3b** after 3 d. As expected, conversion to the cyclic ethers **4a** and **6** proceeded unselectively and less cleanly, resulting in 61% conversion of **3a** and 72% conversion of **5** after 7 h (ratio of 46:54). This experiment successfully demonstrated the selectivity imposed by hexamer **I** in a reaction that is very hard to control in bulk solution.

We herein presented the application of hexameric capsule **I** as a catalyst in the intramolecular hydroalkoxylation of unactivated hydroxy olefins under mild conditions. Evidence was provided that the reactions proceed inside the self-assembled cavity upon encapsulation of the substrate. These findings were successfully translated into substrate selectivity when a mixture of differently sized olefins was employed. Thus, the unique properties of hexamer **I**, including its large internal cavity, its acidic nature and its ability to undergo strong cation- π interactions were efficiently utilized to mimic basic properties of enzyme catalysis.

This project was supported by the ‘‘Bayerische Akademie der Wissenschaften’’ (Junges Kolleg), ‘‘Fonds der Chemischen Industrie’’ (Sachkostenzuschuss), the TUM Junior Fellow Fund and the ‘‘Dr-Ing. Leonhard-Lorenz-Stiftung’’. The help of MSc Johannes Richers with graphical design is greatly acknowledged.

Furthermore, we thank Dr Thomas Magauer and MSc Klaus Speck for help with HRMS measurements.

Notes and references

- (a) T. S. Koblenz, J. Wassenaar and J. N. H. Reek, *Chem. Soc. Rev.*, 2008, **37**, 247–262; (b) M. J. Wiester, P. A. Ulmann and C. A. Mirkin, *Angew. Chem., Int. Ed.*, 2011, **50**, 114–137; (c) M. Raynal, P. Ballester, A. Vidal-Ferran and P. W. N. M. van Leeuwen, *Chem. Soc. Rev.*, 2014, **43**, 1734–1787.
- (a) F. Hof, S. L. Craig, C. Nuckolls and J. J. Rebek, *Angew. Chem., Int. Ed.*, 2002, **41**, 1488–1508; (b) L. C. Palmer and J. J. Rebek, *Org. Biomol. Chem.*, 2004, **2**, 3051–3059; (c) J. Rebek, *Acc. Chem. Res.*, 2009, **42**, 1660–1668; (d) M. Yoshizawa, J. K. Klosterman and M. Fujita, *Angew. Chem., Int. Ed.*, 2009, **48**, 3418–3438; (e) D. Ajami and J. Rebek, *Acc. Chem. Res.*, 2012, **46**, 990–999; (f) S. Zarra, D. M. Wood, D. A. Roberts and J. R. Nitschke, *Chem. Soc. Rev.*, 2014, DOI: 10.1039/C4CS00165F; (g) J. H. Jordan and B. C. Gibb, *Chem. Soc. Rev.*, 2014, DOI: 10.1039/C4CS00191E.
- For recent examples, see: (a) V. Bocokic, A. Kalkan, M. Lutz, A. L. Speck, D. T. Gryko and J. N. H. Reek, *Nat. Commun.*, 2013, **4**, 2670, DOI: 10.1038/ncomms3670; (b) P. Dydio, R. J. Detz and J. N. H. Reek, *J. Am. Chem. Soc.*, 2013, **135**, 10817–10828; (c) A. G. Salles, S. Zarra, R. M. Turner and J. R. Nitschke, *J. Am. Chem. Soc.*, 2013, **135**, 19143–19146; (d) Z. J. Wang, K. N. Clary, R. G. Bergman, K. N. Raymond and F. D. Toste, *Nat. Chem.*, 2013, **5**, 100–103; (e) C. Zhao, Q.-F. Sun, W. M. Hart-Cooper, A. G. DiPasquale, F. D. Toste, R. G. Bergman and K. N. Raymond, *J. Am. Chem. Soc.*, 2013, **135**, 18802–18805; (f) Q. Zhang and K. Tiefenbacher, *J. Am. Chem. Soc.*, 2013, **135**, 16213–16219; (g) P. Jagadesan, B. Mondal, A. Parthasarathy, V. J. Rao and V. Ramamurthy, *Org. Lett.*, 2013, **15**, 1326–1329; (h) R. Kulasekharan, M. V. S. N. Maddipatla, A. Parthasarathy and V. Ramamurthy, *J. Org. Chem.*, 2013, **78**, 942–949.
- (a) J. Kang, J. Santamaria, G. Hilmersson and J. Rebek, *J. Am. Chem. Soc.*, 1998, **120**, 7389–7390; (b) A. Cavarzan, A. Scarso, P. Sgarbossa, G. Strukul and J. N. H. Reek, *J. Am. Chem. Soc.*, 2011, **133**, 2848–2851; (c) G. Bianchini, G. La Sorella, N. Canever, A. Scarso and G. Strukul, *Chem. Commun.*, 2013, **49**, 5322–5324; (d) S. Shimizu, A. Usui, M. Sugai, Y. Suematsu, S. Shirakawa and H. Ichikawa, *Eur. J. Org. Chem.*, 2013, 4734–4737.
- (a) L. R. MacGillivray and J. L. Atwood, *Nature*, 1997, **389**, 469–472; (b) L. Avram, Y. Cohen and J. Rebek, *Chem. Commun.*, 2011, **47**, 5368–5375.
- L. Avram and Y. Cohen, *Org. Lett.*, 2002, **4**, 4365–4368.
- T. Evan-Salem, I. Baruch, L. Avram, Y. Cohen, L. C. Palmer and J. Rebek, *Proc. Natl. Acad. Sci. U. S. A.*, 2006, **103**, 12296–12300.
- A. Shivanyuk and J. Rebek, *J. Am. Chem. Soc.*, 2003, **125**, 3432–3433.
- L. Avram and Y. Cohen, *J. Am. Chem. Soc.*, 2004, **126**, 11556–11563.
- (a) L. Avram and Y. Cohen, *J. Am. Chem. Soc.*, 2002, **124**, 15148–15149; (b) S. Slovak and Y. Cohen, *Chem. – Eur. J.*, 2012, **18**, 8515–8520.
- M. C. Elliott and E. Williams, *J. Chem. Soc., Perkin Trans. 1*, 2001, 2303–2340.
- D. C. Rosenfeld, S. Shekhar, A. Takemiya, M. Utsunomiya and J. F. Hartwig, *Org. Lett.*, 2006, **8**, 4179–4182.
- (a) G. Carr and D. Whittaker, *J. Chem. Soc., Perkin Trans. 2*, 1989, 359–366; (b) P. J. Linares-Palomino, S. A. Salido, J. n. Altarejos and A. Sánchez, *Tetrahedron Lett.*, 2003, **44**, 6651–6655.
- L. Coulombel, M. Rajzmann, J.-M. Pons, S. Olivero and E. Duñach, *Chem. – Eur. J.*, 2006, **12**, 6356–6365.
- A. Kena Diba, J.-M. Begouin and M. Niggemann, *Tetrahedron Lett.*, 2012, **53**, 6629–6632.
- H. Qian, X. Han and R. A. Widenhoefer, *J. Am. Chem. Soc.*, 2004, **126**, 9536–9537.
- E. Pérez-Mayoral, I. Matos, P. Nachtigall, M. Polozij, I. Fonseca, D. Vitvarová-Procházková and J. Čejka, *ChemSusChem*, 2013, **6**, 1021–1030.
- S. A. Singh, S. Kabiraj, R. P. Khandare, S. P. Nalawade, K. B. Upar and S. V. Bhat, *Synth. Commun.*, 2009, **40**, 74–80.
- Z. J. Wang, C. J. Brown, R. G. Bergman, K. N. Raymond and F. D. Toste, *J. Am. Chem. Soc.*, 2011, **133**, 7358–7360.
- E. Raamat, K. Kaupmees, G. Ovsjannikov, A. Trummal, A. Kütt, J. Saamat, I. Koppel, I. Kaljurand, L. Lipping, T. Rodima, V. Pihl, I. A. Koppel and I. Leito, *J. Phys. Org. Chem.*, 2013, **26**, 162–170.

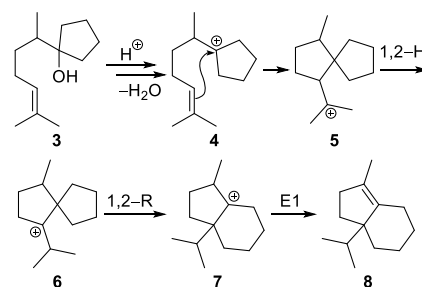


A hydrophobic cavity of about 1400 Å³ is formed by the hexameric resorcin[4]arene structure **I**, which self-assembles in apolar solvents like chloroform from six resorcin[4]arene units **1** and eight water molecules (Figure 1).^[7] The resorcin[4]arene unit **1** can be easily prepared in multigram scale in a single step, starting from 1,3-dihydroxybenzene. The octahedral-shaped assembly is held together by a network of 60 hydrogen bonds and is capable of reversible guest encapsulation *via* a proposed pentameric intermediate.^[8] Cationic species like quaternary ammonium ions (e.g. **2**) show a high affinity towards the capsule interior due to strong cation- π interactions with the aromatic cavity walls.^[9] Additionally, also compounds capable of hydrogen bonding, like carboxylic acids and alcohols, are known to be encapsulated well within the capsule interior.^[10] Depending on the size of the guest molecule, residual solvent molecules are coencapsulated to reach an optimum packing coefficient of approximately 0.55.^[11] The hexameric assembly has been furthermore shown by our group to act as a mild phenol-based Brønsted acid ($pK_a \sim 5.5-6$), capable of activating suitable substrates by protonation.^[12] The extended delocalization of the negative charge renders the deprotonated capsule a non-nucleophilic counter ion, which allows for the study of cationic cascade reactions. Yet the application of hexamer **I** as an acid catalyst is still limited.^[12-13]

As part of our ongoing investigation of hexamer **I**-catalyzed cationic cyclizations, we became aware of an early report of the Epstein group regarding a selective cyclodehydration-rearrangement cascade reaction of hydroxy olefin **3** (Scheme 1). The report describes the use of a sevenfold excess of trifluoroacetic acid (TFA) ($pK_a = 0.2$) to induce the depicted reaction.^[14] Indeed, similar cyclorearrangements have also been shown to require an excess of Brønsted acid and in most cases also require an excess of Lewis acid.^[15] Catalytic approaches to related reactions are limited to the use of expensive transition metal catalysts.^[16] We therefore decided to probe if the reaction of substrate **3** can be rendered catalytic by exploiting the unique microenvironment provided by the supramolecular hexamer **I**. Furthermore, prompted by the report of only two substrates, we set out to investigate the scope and limitations of this cationic cascade reaction.

The reaction sequence starts with an initial protonation of the hydroxy group, followed by dehydration to yield cationic intermediate **4** (Scheme 1). Subsequent 5-*exo* olefin cyclization results in cationic species **5**, which is related to the protosterol cation observed in the biosynthesis of lanosterol.^[17] Next, a 1,2-hydride shift generates the thermodynamically more stable^[18] endocyclic cation **6**. According to a detailed DFT study by Vreck, the formation of intermediate **6** represents the rate determining step of the overall reaction cascade.^[18] The spiro-type cation **6** then undergoes a Wagner–Meerwein ring expansion to give intermediate **7**, which eliminates to yield annulated

cyclopentene **8** as the final product of the cyclorearrangement.



Scheme 1. Mechanism of the cyclodehydration-rearrangement cascade reaction of hydroxy olefin **3**.^[18]

Results and Discussion

We started our investigation by adding cyclopentyl alcohol **3** to a solution of 10 mol% of hexamer **I** in CDCl₃. Shortly after mixing, new upfield-shifted resonances in the region of 0.5 to -0.6 ppm could be observed in the ¹H NMR spectrum of the reaction mixture (Figure 2). The observed upfield-shift, caused by the aromatic anisotropy of the cavity walls, indicated successful encapsulation of the alcohol substrate. In addition, the diffusion coefficient of those resonances matched the diffusion coefficient of the hexameric assembly, which further corroborated successful uptake of the substrate (see ESI Figure S3). A quantification of encapsulated guest *via* integration of the upfield-shifted resonances, however, could not be performed due to the reactivity of the guest and the unknown correlation between shifted and original resonances. In contrast to our previous studies,^[12, 13b, 13c] the reaction temperature was raised to 50 °C in order to facilitate the dehydration process. Furthermore, literature data suggests an acceleration of guest encapsulation at elevated temperatures.^[8, 19] According to GC analysis, complete consumption of the starting material was achieved after 2 h. The initially formed product mixture, consisting of the desired product and the two non-cyclized dehydration products (see ESI chapter 15), slowly equilibrated over 4 d to give the desired bicyclic structure **8** as the main product in 81% yield (Table 1). The slow equilibration process via reprotonation can be attributed to the low affinity of the dehydrated side products towards the capsule interior. The weak binding of the dehydrated products results from their inability to form hydrogen bonds and successfully prevents product inhibition, a problem often encountered in supramolecular catalysis.^[5a, 20] The applied catalyst loading is based on one of our previous studies,^[13b] which revealed a negative effect of high hydroxy olefin concentration on the overall reaction rate. This negative effect is believed to arise from the interaction of the hydroxyl group of the

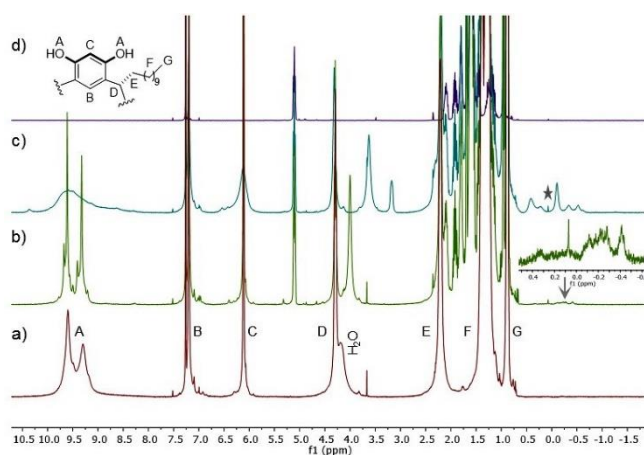


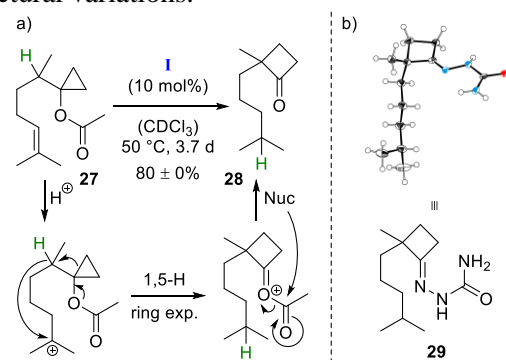
Figure 2. ^1H NMR spectra in CDCl_3 of (a) hexamer **I** (3.3 mM); (b) hexamer **I** (3.3 mM) and substrate **3** (33 mM), 10 min after mixing (area between 0.5 and -0.6 ppm enlarged); (c) hexamer **I** (3.3 mM), Bu_4NBr (**2**) (5.0 mM) and substrate **3** (33 mM); (d) substrate **3** (33 mM) (silicone grease marked with an asterisk).

substrate with the monomer units, which reduces the equilibrium concentration of operational catalyst.^[21] Additionally, a low initial water content of the reaction mixture was found beneficial for the reaction rate. It appears likely that excess water molecules compete with the alcohol substrate for the protons of the hexamer.^[13b] When the cavity was blocked by addition of the high affinity guest Bu_4NBr (**2**) (1.5 equiv), the yield of cyclopentene **8** was reduced to 7% after 4 d under otherwise identical reaction conditions. This control experiment provided first evidence that the reaction proceeds within the cavity of the hexameric assembly. It is noteworthy, that encapsulation of Bu_4NBr (**2**) has been shown to increase the acidity of hexamer **I**.^[13c] This further enhances the quality of the performed control experiment. When the reaction was repeated in the presence of methanol, which disrupts the hydrogen-bonding network and leads to dissociation of hexamer **I**, no formation of product **8** could be observed. This excludes substrate activation by simple hydrogen bonding from the phenolic units. In addition, when hexamer **I** was replaced by 10 mol% of TFA, only 5% of product were formed after 4 d at 50°C , although the acidity of TFA is about five orders of magnitude higher than that of **I**. This significant difference is likely to result from the stabilization of cationic intermediates and transition states *via* cation- π interactions in the cavity of hexamer **I**, as it has been observed in other reactions.^[22]

Next, we investigated the formation of product **8** starting from hydroxy olefin **9**, the only other substrate reported by Epstein *et al.*^[14] The structure of substrate **9** requires a hydride shift after protonation and cleavage of water or a deprotonation-reprotonation sequence of an intermediary formed alkene prior to cyclization. Similar to exocyclic cation **5**, the initial hydride shift lowers the energy of the system by locating the positive charge within the ring, as indicated by DFT calculations.^[18] Indeed, treatment of

substrate **9** with hexamer **I** for 3 d yielded product **8** in 75% yield. Reaction monitoring *via* GC furthermore excludes substantial deprotonation, favoring a 1,2-hydride shift mechanism. After having proven the applicability of hexamer **I** as a catalyst, the tolerance of the reaction sequence towards β -residue variation was probed utilizing substrate **10**. In this case, the desired product **11** was formed in moderate yield. Additionally, no significant amounts of electrophilic aromatic substitution products could be observed. When the β -residue was completely omitted, the reaction still proceeded, yielding annulated cyclopentene **13** in good yield from hydroxy olefin **12**. Following this, we investigated the influence of the substituents geminal to the hydroxy group. An initial attempt, utilizing a cyclobutyl analogon of substrate **3**, failed to give a selective transformation, probably due to the complex mesomeric nature of the cyclobutyl cation.^[23] Also a cyclopropyl analogon of substrates **3** failed to undergo the desired rearrangement process, apparently forming the corresponding cyclic ether instead. Employing substrate **14**, which features two ethyl groups, restored the desired reactivity, giving cyclopentene **15** in moderate yield. The corresponding methyl substrate **16** performed even better, despite the reduced migratory aptitude of methyl groups.^[24] In this case, the desired product **17** was formed together with a cyclohexene side product, which is assumed to result from an intramolecular proton transfer step (see ESI Scheme S7).^[25] Derivative **18**, which requires a 1,2-hydride shift after protonation and cleavage of water, gave a reduced yield of product **17**, due to increased formation of the cyclohexene side product. In both cases, only traces of an acyclic diene intermediate could be detected during reaction monitoring. Additionally, no substantial amounts of other intermediates could be observed, which indicates a ‘non-stop’ reaction mechanism. This can to some extent be attributed to the high stabilization of the generated phenolate anion. The negative charge can freely shift through the entire hydrogen bond network *via* proton migration, resulting in high stabilization and therefore low nucleophilicity. Changing the β -residue led to substrates **19** and **21**, which cyclized in satisfactory yields to the corresponding cyclopentenes **20** and **22**. To showcase a possible derivatization of the obtained cyclopentenes and further confirm the rearranged structure, the crude mixture of product **20** was subjected to catalytic Sharpless alkene cleavage conditions,^[26] giving the corresponding diketone in 56% isolated yield over two steps (see ESI chapter 8). An attempt to induce polycycle formation, by employing a substrate carrying a second homoprenyl group in the β -position, failed, resulting only in unselective conversion of the starting material (see ESI chapter 12). Subsequent investigation of alcohol **23** illustrated the influence of the β -methyl group on the 1,2-methyl migration. The expected product **24** was formed in only 45% yield, together with 32% of a cyclopentene that was formed by direct elimination after the 1,2-hydride shift. A prolonged reaction time did not lead to an increased formation of product **24** by

unselective or did not undergo hydride transfer. This highlights the sensitivity of hydride transfers towards structural variations.

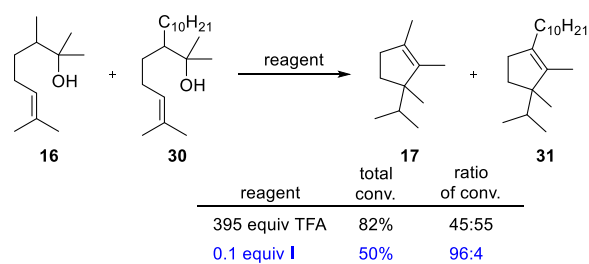


Scheme 2. (a) Mechanism of the cyclobutanone formation; (b) crystalline derivative of the formed cyclobutanone.

After having investigated the scope and limitations of the catalyzed cascade reaction, the possibility of substrate-selective conversion using hexamer **I** was explored in a competition experiment utilizing substrate **16** and its large derivative **30**. For this purpose, a mixture of **16** and **30** (5 equiv each; Scheme 3) was added to a solution of catalyst **I** (1 equiv) in CDCl₃ (3.3 mM) and the reaction was monitored *via* GC. In accordance with previous findings,^[12] the reaction proceeded highly selectively in favor of the smaller substrate due to its more efficient encapsulation. After 3 h, the small substrate showed almost complete conversion (95%), while substrate **30** remained nearly untouched by the catalyst (4%). This corresponds to a 96:4 ratio of conversion (see ESI chapter 11). In contrast, when the reaction was performed with an excess of TFA, no significant differentiation of the two substrates could be observed. As a result, the ratio of conversion changed to 45:55 (73% conversion of **16** and 91% conversion of **30**). This size-selectivity^[29] achieved with catalyst **I** marks a conceptual advantage of encapsulation-based supramolecular catalysis,^[4] which can be utilized for multicatalyst tandem reactions^[30] and working with complex substrate mixtures. The observation furthermore provides strong evidence that the reaction indeed proceeds within the cavity of the supramolecular assembly.

Conclusion

In conclusion, we herein presented the efficient catalysis of a cyclodehydration-rearrangement cascade reaction utilizing supramolecular assembly **I**. A reaction which so far was only observed with excess of a strong Brønsted acid. The scope and limitations of this reaction sequence were investigated in detail for the first time by systematic variation of the substitution pattern of the starting material. In this process, several highly substituted



Scheme 3. Selectivities observed with TFA (−5 °C, 10 s (CH₂Cl₂)) and catalyst **I** (50 °C, 3 h (CDCl₃)) in a competition experiment towards cyclopentenes **17** and **31**.

cyclopentenes could be obtained in moderate to good yield. Additionally, substrate-selectivity could be achieved starting from a mixture of differently sized hydroxy olefins. Thus, the reaction was shown to proceed within the cavity of the hexamer after encapsulation of the substrate. The cationic intermediates and transition states of the reaction are believed to be stabilized *via* cation– π interactions with the surrounding cavity walls. In addition, this study led to the discovery of an unprecedented cyclobutanone formation through an intramolecular 1,5-hydride transfer within the cavity of **I**. Altogether, this study further corroborates the important role of supramolecular structures in the long term goal of controlling cationic olefin cyclizations in an enzymatic fashion. This future goal will require the rational modification of the capsule interior to induce selective interactions between the catalyst and the encapsulated substrate.

Experimental Section

General Information

¹H and ¹³C NMR spectra were recorded at 300 MHz, 400 MHz or 500 MHz, using a Bruker AVHD 300, AVHD 400 and AVHD 500 spectrometer respectively. Chemical shifts of ¹H NMR and ¹³C NMR (measured at 298 K) are given in ppm by using CHCl₃ and CDCl₃ as references (7.26 ppm and 77.16 ppm respectively). GC analyses were done on an Agilent GC6890 instrument equipped with a FID detector and a HP-5 capillary column (length = 29.5 m). Hydrogen was used as the carrier gas and the constant-flow mode (flow rate = 1.8 mL min^{−1}) with a split ratio of 1:20 was used. Analytical thin-layer chromatography (TLC) was performed on Merck silica gel 60 F₂₅₄ glass-baked plates, which were analyzed after exposure to standard staining reagents. All chemicals were used without further purification. CDCl₃ was purchased from Deutero GmbH and Sigma Aldrich and used as received.

Catalyst, Substrates and Products

Resorcin[4]arene **1** was synthesized according to modified literature procedures.^[31] After dissolving **1** (11.0 mg) in

CDCl₃ (0.50 mL), a water content of 9-10 eq. H₂O/hexamer **1** was determined *via* integration of the ¹H NMR spectrum. The employed substrates were synthesized according to the procedures reported in the Supporting Information. All cyclodehydration-rearrangement products were isolated and purified using AgNO₃-coated silica, prepared according to Cert *et al.*^[32] Full characterization data and copies of relevant spectra of all new products, as well as X-ray crystallographic analysis data of compound **29**^[33] are provided in the Supporting Information.

Catalytic Studies

An aliquot of a stock solution containing 11.0 mg C-undecylcalix[4]resorcinarene (**1**) (9.95 μmol, 6.0 eq.) was transferred to a GC vial. Next CDCl₃ was added to adjust an overall CDCl₃ volume of 0.50 mL. To this solution, *n*-decane (internal standard) (2.59 μL, 13.3 μmol, 8.0 eq.) and the substrate (16.6 μmol, 10.0 eq.) were added successively in one portion and the mixture was immediately sampled after 30 s of vigorous agitation. The small sample (approximately 10 μL) was diluted with *n*-hexane (0.1 mL) containing 0.08% (v/v) DMSO, centrifuged, decanted and subjected to GC analysis (initial sample). The GC vial was kept at 50 °C (±1 °C) using a thermostated heating block made from alumina. Based on preliminary studies regarding reaction time optimization, a second sample (final sample) was taken after a given time frame. All substrates were tested in triplicate. In order to precisely calculate the conversion and yield, GC-response factors to *n*-decane as internal standard (IS) were determined for the investigated substrates and their corresponding products.

Control Experiments with Inhibitor 2

To a solution of C-undecylcalix[4]resorcinarene (**1**) (11.0 mg, 9.95 μmol, 6.0 eq.) in CDCl₃ (0.46 mL), 40 μL of Bu₄NBr (**2**) (2.49 μmol, 1.5 eq.) stock solution in CDCl₃ (62.3 mm) were added. Next, the sample was heated using a heat gun to ensure complete uptake of the inhibitor. After allowing the solution to cool to rt, *n*-decane (internal standard) (2.59 μL, 13.3 μmol, 8.0 eq.) and the substrate (16.6 μmol, 10.0 eq.) were added and the reaction was subsequently monitored as described above.

Acknowledgements

This project was supported by funding from the Swiss National Science Foundation as part of the NCCR Molecular Systems Engineering and the Bayerische Akademie der Wissenschaften (Junges Kolleg). We thank PD Dr. Daniel Häussinger for help with NMR-DOSY-measurements.

References

[1] a) M. D. Pluth, R. G. Bergman, K. N. Raymond, *Acc. Chem. Res.* **2009**, *42*, 1650-1659; b) M. Yoshizawa, M. Fujita, *Bull. Chem. Soc. Jpn.* **2010**, *83*, 609-618; c) T. K. Ronson, S. Zarra, S. P. Black, J. R. Nitschke, *Chem. Commun.* **2013**, *49*, 2476-2490; d) M. Han, D. M. Engelhard, G. H. Clever, *Chem. Soc. Rev.* **2014**, *43*, 1848-1860; e) S. H. A.

M. Leenders, R. Gramage-Doria, B. de Bruin, J. N. H. Reek, *Chem. Soc. Rev.* **2015**, *44*, 433-448.
 [2] a) J. Rebek, *Acc. Chem. Res.* **2009**, *42*, 1660-1668; b) D. Ajami, J. Rebek, *Acc. Chem. Res.* **2013**, *46*, 990-999; c) D. Ajami, L. Liu, J. Rebek Jr, *Chem. Soc. Rev.* **2015**, *44*, 490-499.
 [3] J. H. Jordan, B. C. Gibb, *Chem. Soc. Rev.* **2015**, *44*, 547-585.
 [4] L. Catti, Q. Zhang, K. Tiefenbacher, *Chem. Eur. J.* **2016**, *22*, 9060-9066.
 [5] For reviews see: a) M. Yoshizawa, J. K. Klosterman, M. Fujita, *Angew. Chem. Int. Ed.* **2009**, *48*, 3418-3438; b) J. Meeuwissen, J. N. H. Reek, *Nat. Chem.* **2010**, *2*, 615-621; c) L. Marchetti, M. Levine, *ACS Catal.* **2011**, *1*, 1090-1118; d) M. J. Wiester, P. A. Ulmann, C. A. Mirkin, *Angew. Chem. Int. Ed.* **2011**, *50*, 114-137; e) M. Raynal, P. Ballester, A. Vidal-Ferran, P. W. N. M. van Leeuwen, *Chem. Soc. Rev.* **2014**, *43*, 1734-1787; f) C. J. Brown, F. D. Toste, R. G. Bergman, K. N. Raymond, *Chem. Rev.* **2015**, *115*, 3012-3035; g) S. Zarra, D. M. Wood, D. A. Roberts, J. R. Nitschke, *Chem. Soc. Rev.* **2015**, *44*, 419-432; h) L. Catti, Q. Zhang, K. Tiefenbacher, *Synthesis* **2016**, *48*, 313-328.
 [6] D. A. Dougherty, *Acc. Chem. Res.* **2013**, *46*, 885-893.
 [7] a) L. R. MacGillivray, J. L. Atwood, *Nature* **1997**, *389*, 469-472; b) L. Avram, Y. Cohen, *Org. Lett.* **2002**, *4*, 4365-4368; c) L. Avram, Y. Cohen, J. Rebek Jr, *Chem. Commun.* **2011**, *47*, 5368-5375.
 [8] M. Yamanaka, A. Shivanyuk, J. Rebek, *J. Am. Chem. Soc.* **2004**, *126*, 2939-2943.
 [9] a) A. Shivanyuk, J. Rebek, *Proc. Natl. Acad. Sci. U.S.A.* **2001**, *98*, 7662-7665; b) L. Avram, Y. Cohen, *J. Am. Chem. Soc.* **2002**, *124*, 15148-15149.
 [10] S. Slovak, Y. Cohen, *Chem. Eur. J.* **2012**, *18*, 8515-8520.
 [11] S. Mecozzi, J. J. Rebek, *Chem. Eur. J.* **1998**, *4*, 1016-1022.
 [12] Q. Zhang, K. Tiefenbacher, *J. Am. Chem. Soc.* **2013**, *135*, 16213-16219.
 [13] a) G. Bianchini, G. L. Sorella, N. Canever, A. Scarso, G. Strukul, *Chem. Commun.* **2013**, *49*, 5322-5324; b) L. Catti, K. Tiefenbacher, *Chem. Commun.* **2015**, *51*, 892-894; c) Q. Zhang, K. Tiefenbacher, *Nat. Chem.* **2015**, *7*, 197-202; d) T. Caneva, L. Sperti, G. Strukul, A. Scarso, *RSC Adv.* **2016**, *6*, 83505-83509.
 [14] W. W. Epstein, J. R. Grua, D. Gregonis, *J. Org. Chem.* **1982**, *47*, 1128-1131.
 [15] a) J. Amupitan, A. Santos, J. K. Sutherland, *J. Chem. Soc., Chem. Commun.* **1980**, 399-400; b) B. B. Snider, M. Karras, R. T. Price, D. J. Rodini, *J. Org. Chem.* **1982**, *47*, 4538-4545; c) M. Nishizawa, H. Takao, Y. Iwamoto, H. Yamada, H. Imagawa, *Synlett* **1998**, *1998*, 76-78; d) H. Takao, A. Wakabayashi, K. Takahashi, H. Imagawa, T. Sugihara, M. Nishizawa, *Tetrahedron Lett.* **2004**, *45*, 1079-1082.

- [16] a) J. G. Sokol, C. S. Korapala, P. S. White, J. J. Becker, M. R. Gagné, *Angew. Chem. Int. Ed.* **2011**, *50*, 5658-5661; b) M. J. Geier, M. R. Gagné, *J. Am. Chem. Soc.* **2014**, *136*, 3032-3035.
- [17] a) B. A. Hess, *J. Am. Chem. Soc.* **2002**, *124*, 10286-10287; b) B. A. Hess, *Org. Lett.* **2003**, *5*, 165-167.
- [18] V. Vrcek, *Int. J. Quantum Chem.* **2007**, *107*, 1772-1781.
- [19] E. S. Barrett, T. J. Dale, J. Rebek, *J. Am. Chem. Soc.* **2008**, *130*, 2344-2350.
- [20] T. S. Koblenz, J. Wassenaar, J. N. H. Reek, *Chem. Soc. Rev.* **2008**, *37*, 247-262.
- [21] L. Avram, Y. Cohen, *J. Am. Chem. Soc.* **2004**, *126*, 11556-11563.
- [22] For a recent example see: G. La Sorella, L. Sporni, G. Strukul, A. Scarso, *Adv. Synth. Catal.* **2016**, *358*, 3443-3449.
- [23] a) G. A. Olah, C. L. Jeuell, D. P. Kelly, R. D. Porter, *J. Am. Chem. Soc.* **1972**, *94*, 146-156; b) R. A. Moss, F. Zheng, L. A. Johnson, R. R. Sauers, *J. Phys. Org. Chem.* **2001**, *14*, 400-406.
- [24] R. Brückner, in: *Organic Mechanisms: Reactions, Stereochemistry and Synthesis* (Ed.: M. Harmata), Springer, Berlin, Heidelberg, **2010**, chapter 14.
- [25] Y. J. Hong, D. J. Tantillo, *J. Am. Chem. Soc.* **2015**, *137*, 4134-4140.
- [26] P. H. J. Carlsen, T. Katsuki, V. S. Martin, K. B. Sharpless, *J. Org. Chem.* **1981**, *46*, 3936-3938.
- [27] Q. Zhang, L. Catti, V. R. I. Kaila, K. Tiefenbacher, *Chem. Sci.* **2017**, DOI: 10.1039/c6sc04565k.
- [28] a) B. Peng, N. Maulide, *Chem. Eur. J.* **2013**, *19*, 13274-13287; b) M. C. Haibach, D. Seidel, *Angew. Chem. Int. Ed.* **2014**, *53*, 5010-5036.
- [29] See for instance: a) J. Kang, G. Hilmersson, J. Santamaría, J. Rebek, *J. Am. Chem. Soc.* **1998**, *120*, 3650-3656; b) M. D. Pluth, R. G. Bergman, K. N. Raymond, *Science* **2007**, *316*, 85-88; c) S. Giust, G. La Sorella, L. Sporni, G. Strukul, A. Scarso, *Chem. Commun.* **2015**, *51*, 1658-1661.
- [30] A. G. Salles, Jr., S. Zarra, R. M. Turner, J. R. Nitschke, *J. Am. Chem. Soc.* **2013**, *135*, 19143-19146.
- [31] a) L. M. Tunstad, J. A. Tucker, E. Dalcanale, J. Weiser, J. A. Bryant, J. C. Sherman, R. C. Helgeson, C. B. Knobler, D. J. Cram, *J. Org. Chem.* **1989**, *54*, 1305-1312; b) I. Elidrisi, S. Negin, P. V. Bhatt, T. Govender, H. G. Kruger, G. W. Gokel, G. E. M. Maguire, *Org. Biomol. Chem.* **2011**, *9*, 4498-4506.
- [32] A. Cert, W. Moreda, *J. Chromatogr. A* **1998**, *823*, 291-297.
- [33] CCDC-1520534 contains the supplementary crystallographic data for this paper. These data can be obtained free of charge from The Cambridge Crystallographic Data Centre via www.ccdc.cam.ac.uk/data_request/cif.

Electronic Supporting Information

Host-Catalyzed Cyclodehydration-Rearrangement Cascade Reaction of Unsaturated Tertiary Alcohols

Lorenzo Catti,^[a] Alexander Pöthig^[b] and Konrad Tiefenbacher*^[a,c]

^[a]*Department of Chemistry, University of Basel, St. Johannis-Ring 19, CH-4056 Basel,
Switzerland*

^[b]*Catalysis Research Center, Technical University of Munich, Ernst-Otto-Fischer-Straße 1,
D-85748 Garching, Germany*

^[c]*Department of Biosystems Science and Engineering, ETH Zürich, Mattenstrasse 26, CH-
4058 Basel, Switzerland*

*Correspondence to: konrad.tiefenbacher@unibas.ch / tkonrad@ethz.ch

Index

1. General information	3
2. Synthesis of <i>C</i> -undecylcalix[4]resorcinarene (1)	5
3. Substrate syntheses	6
4. Determination of substrate densities	28
5. Cyclization-rearrangement: determination of yields	29
6. Synthesis of a GC reference compound	33
7. Large scale isolation of rearranged cyclodehydration products	34
8. Product derivatization	43
9. Intramolecular 1,5-hydride transfer	44
10. Control experiments	48
11. Competition experiment	51
12. Substrates yielding no defined main product	53
13. Influence of a β -dimethyl group on product selectivity	55
14. Confirmation of substrate uptake by DOSY NMR	55
15. Elucidation of the initially formed side products in the cyclization of 3	55
16. SC-XRD determination of compound 29	59
17. References	61
18. NMR spectra	62

1. General information

Experimental: Reactions were carried out under an atmosphere of argon unless otherwise indicated. Analytical thin-layer chromatography (TLC) was performed on Merck silica gel 60 F₂₅₄ glass-baked plates, which were analyzed after exposure to standard staining reagents (basic KMnO₄, iodine or CAM: cerium ammonium molybdate). TLC plates coated with AgNO₃ were prepared according to Fitjer *et al.*^[1] by dipping the TLC plates for 10 s into a solution of AgNO₃ (1.91 g) in a mixture of MeOH (13.3 mL) and water (6.7 mL) and drying for 1 h at 118 °C in an oven. ¹H NMR spectra were recorded at 300 MHz, 400 MHz or 500 MHz, using a Bruker AVHD 300, AVHD 400 and AVHD 500 spectrometer respectively. ¹³C NMR spectra were recorded at 75 MHz, 101 MHz or 126 MHz on a Bruker AVHD 300, AVHD 400 and AVHD 500 spectrometer respectively. Chemical shifts of ¹H NMR and ¹³C NMR (measured at 298 K) are given in ppm by using CHCl₃ and CDCl₃ as references (7.26 ppm and 77.16 ppm respectively). Coupling constants (*J*) are reported in Hertz (Hz). Standard abbreviations indicating multiplicity were used as follows: s (singlet), bs (broad singlet), d (doublet), dd (doublet of doublets), t (triplet), m (multiplet). GC analyses were done on an Agilent GC6890 instrument equipped with a FID detector and a HP-5 capillary column (length = 29.5 m). Hydrogen was used as the carrier gas and the constant-flow mode (flow rate = 1.8 mL min⁻¹) with a split ratio of 1:20 was used. The following temperature-program was used: 60 °C for 3 min, 15 °C min⁻¹ to 250 °C, and 250 °C for 5 min. GC analyses for the 1,5-hydride transfer reaction were done on a Shimadzu GC-2010 Plus instrument equipped with a FID detector and a Rtx-5 capillary column (length = 30.0 m). Hydrogen was used as the carrier gas and the constant-flow mode (flow rate = 40 mL min⁻¹) with a split ratio of 1:20 was used. The following temperature-program was used: 60 °C for 1 min, 15 °C min⁻¹ to 250 °C, and 250 °C for 5 min. Infrared spectra were recorded on a JASCO FT/IR-4100 spectrometer. High-resolution mass spectra were obtained using the electron impact ionization (EI) technique on a Finnigan MAT 8200 mass spectrometer and the electrospray ionization (ESI) technique on a Bruker maXis 4G mass spectrometer. Centrifugation was performed using a VWR MiniStar silverline. The X-ray intensity data were measured on a Bruker D8 Venture TXS system equipped with a Helios optic monochromator and a Mo TXS rotating anode ($\lambda = 0.71073 \text{ \AA}$) (see section 14).

Sources of chemicals: Anhydrous CH₂Cl₂, Et₂O and THF were taken from a solvent drying system (MBraun SPS-800). THF was further dried by distillation from sodium/benzophenone under argon atmosphere. CDCl₃ (99.8%) was purchased from Deutero GmbH and Sigma-Aldrich. Anhydrous ethanol, silver nitrate, cyclopropyl methyl ketone, benzyl bromide, 2,6-

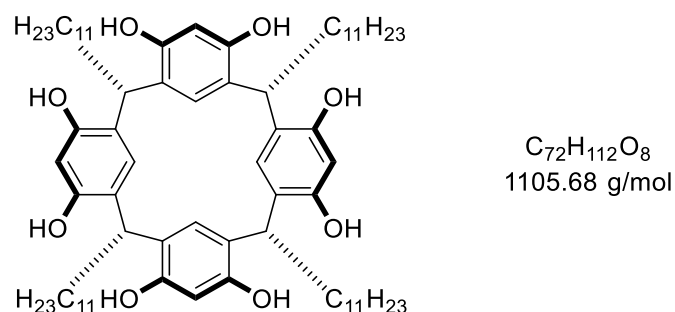
dimethyl-5-heptenal, methylmagnesium chloride solution in THF, methylmagnesium bromide solution in Et₂O, ethylmagnesium chloride solution in THF, ruthenium(III) chloride hydrate, carbon tetrachloride, 1-decanol, titanium(IV) isopropoxide, acetyl chloride, potassium *tert*-butoxide, 2-bromobenzaldehyde, semicarbazide hydrochloride, pyridinium chlorochromate, anhydrous pyridine, dodecanal, Celite and sodium chlorite were purchased from Sigma-Aldrich. Methyl phenylacetate was purchased from TCI. Silica gel (0.040-0.063 mm, 230-400 mesh ASTM), 2-methyl-2-butene, dimethyl malonate and sodium hydride (60% suspension in paraffin oil) were purchased from Merck. Magnesium sulfate and iodine were purchased from AppliChem. Potassium carbonate, sodium sulfate, magnesium, sodium iodide, sodium chloride, monosodium phosphate and ammonium chloride were purchased from Grüssing. Sodium hydroxide was purchased from Fisher Scientific. Hydrochloric acid (37%) (*TraceSELECT*), propylene oxide and *n*-decane were purchased from Fluka. Resorcinol, trifluoroacetic acid and 6-methylhept-5-en-2-one were purchased from Alfa Aesar. *n*-Hexane (HPLC grade), anhydrous acetone, 4Å molecular sieve, sodium acetate, sodium bicarbonate, *tert*-butanol, copper(II) sulfate pentahydrate, lithium chloride and methanol (HPLC grade) were purchased from VWR. Isopropyltriphenylphosphonium iodide, ethyl acetoacetate, cyclopentyl bromide, isopropylmagnesium chloride solution in THF, anhydrous *N,N*-dimethylformamide, *n*-butyllithium solution in hexanes, anhydrous dimethyl sulfoxide, cyclobutanone, anhydrous acetonitrile, methyl iodide, 1,4-dibromobutane, sodium periodate, diisopropylamine, methyllithium solution in Et₂O and tetrabutylammonium bromide were purchased from Acros Organics. H₂SO₄ was purchased from BHM Chemikalienhandel. Pentane, Et₂O and EtOAc were purchased from Brenntag and distilled prior to use. Chemicals were used without further purification, unless stated otherwise.

General: Transfer of liquids with a volume ranging from 1 to 10 µL or from 10 to 100 µL was performed with a Microman M1 pipette (Gilson, systematic error: 1.40% - 1.60%) equipped with 10 µL or 100 µL pipette tips respectively. For reactions with catalyst **I**, only glass pipettes and syringes with stainless steel cannula from Unimed were used in the preparation to prevent contamination with silicone grease, which is visible at 0.07 ppm in the ¹H NMR spectrum. The weighing of tetrabutylammonium bromide and substrates with unknown density for the preparation of stock solutions and density determinations was performed using a M3P Sartorius microbalance.

AgNO₃ column chromatography: AgNO₃-coated silica was prepared according to Cert *et al.*^[2] For this purpose silica gel 60 (120 g) was heated in an oven for 3 h at 118 °C. The activated

silica gel was subsequently transferred into a 500 mL round bottom flask wrapped in aluminum foil and allowed to cool to rt under vacuum. A solution of AgNO₃ (12.0 g) in water (28 mL) was then added in portions while shaking from time to time. After complete addition, the flask was sealed with a stopper and shaken vigorously for 20 s. To complete homogenization, the flask was rotated for 30 min under atmospheric pressure and rt. The in this manner prepared silica gel, coated with 10% (w/w) AgNO₃, was stored in a stoppered flask in the dark for subsequent use. Columns filled with AgNO₃-coated silica were wrapped in aluminum foil for protection from light.

2. Synthesis of *C*-undecylcalix[4]resorcinarene (1)

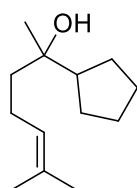


Resorcin[4]arene **1** was synthesized according to modified literature procedures.^[3] To a stirred solution of absolute ethanol (54 mL) and 37% aqueous HCl (18 mL), resorcinol (14.2 g, 129 mmol, 1.0 eq.) was added. After complete dissolution and cooling to 0 °C, a solution of dodecanal (29.9 mL, 129 mmol, 1.0 eq.) in absolute ethanol (37 mL) was added dropwise into the reaction mixture over the course of 40 min. The resulting solution was allowed to warm to rt and subsequently refluxed at 100 °C for 18 h. The dark red solution was then allowed to cool to rt whereby a yellow precipitate formed. The precipitate was dispersed in cold methanol, filtered and subsequently washed with cold methanol until the washings were light yellow (3 × 40 mL). The solid was then crystallized twice from methanol (45 mL and 14 mL respectively). The crystalline material was dried under reduced pressure (16 mbar) at 55 °C using a rotary evaporator. The drying process was continued under high vacuum at 55 °C until the residual methanol was completely removed. In order to raise the water content to a satisfactory level by equilibration, the solid was stored in an open flask at rt until ¹H NMR indicated sufficient uptake of water (38 h). Compound **1** (22.1 g, 20.0 mmol, 62%) was finally obtained as a yellowish powder. After dissolving **1** (11.0 mg) in CDCl₃ (0.50 mL), a water content of 9-10 eq. H₂O/hexamer **I** was determined via integration of the ¹H NMR spectrum. The spectroscopic data matched those reported in the literature.^[4]

General remark: If the water content is too low, a gel like mixture is obtained upon addition of CDCl_3 , because a minimum of eight water molecules per hexamer is required for self-assembly. On the contrary, if the water content is too high, a significant decrease in reaction rate is observed.^[5]

3. Substrate syntheses

2-Cyclopentyl-6-methylhept-5-en-2-ol (**9**)



$\text{C}_{13}\text{H}_{24}\text{O}$
196.33 g/mol

To cyclopentylmagnesium bromide (0.85 M in THF, 10.0 mL, 8.50 mmol, 1.3 eq.) – prepared from cyclopentyl bromide (1.63 mL, 15.2 mmol) by reaction with magnesium (555 mg, 22.8 mmol) in anhydrous THF (15.2 mL) containing a crystal of iodine – at 0 °C was slowly added 6-methylhept-5-en-2-one (0.93 mL, 6.34 mmol, 1.0 eq.). The ice bath was subsequently removed, and the solution was allowed to warm towards rt over a period of 2.5 h. The reaction was quenched with saturated aqueous NH_4Cl and extracted with Et_2O (3×30 mL). The combined organic phases were washed with brine (1×30 mL), dried over Na_2SO_4 , filtered and concentrated under vacuum. Purification via flash column chromatography (pentane/ Et_2O = 10/1 \rightarrow 2/1) afforded product **9** (141 mg, 721 μmol , 11%) as a colorless oil.

^1H NMR (300 MHz, CDCl_3): δ [ppm] = 5.17 - 5.09 (m, 1H), 2.12 - 2.00 (m, 2H), 1.99 - 1.88 (m, 1H), 1.69 (s, 3H), 1.66 - 1.30 (m, 11H), 1.62 (s, 3H), 1.14 (s, 3H).

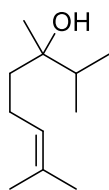
^{13}C NMR (75 MHz, CDCl_3): δ [ppm] = 131.8, 124.8, 74.2, 49.6, 41.4, 27.3, 26.7, 26.1, 26.1, 25.9, 24.6, 22.8, 17.8.

HRMS (EI): calcd for $\text{C}_{13}\text{H}_{22}^+$ [(M-H₂O)⁺]: 178.1716, found: 178.1716.

IR (ATR): $\tilde{\nu}$ [cm^{-1}] = 3443, 2951, 2867, 1450, 1375, 1340, 1265, 1174, 1111, 1078, 929, 832.

TLC: R_f = 0.23 (pentane/ Et_2O = 10/1) [KMnO_4].

2,3,7-Trimethyloct-6-en-3-ol (**18**)



$C_{11}H_{22}O$
170.30 g/mol

To a stirred solution of 6-methylhept-5-en-2-one (2.36 mL, 16.0 mmol, 1.0 eq.) in anhydrous THF (60 mL) at $-10\text{ }^{\circ}\text{C}$ was added isopropylmagnesium chloride (2.0 M in THF, 12.0 mL, 24.0 mmol, 1.5 eq.) dropwise. After 1 h of stirring at $0\text{ }^{\circ}\text{C}$, the reaction was quenched by addition of saturated aqueous NH_4Cl . The crude product was subsequently extracted with Et_2O ($3 \times 30\text{ mL}$) and washed with brine. The combined organic phases were dried over Na_2SO_4 , filtered and concentrated under vacuum. After flash column chromatography (pentane/ $\text{Et}_2\text{O} = 10/1$), alcohol **18** (323 mg, 1.90 mmol, 12%) was obtained as a colorless oil.

$^1\text{H NMR}$ (400 MHz, CDCl_3): δ [ppm] = 5.17 - 5.10 (m, 1H), 2.10 - 2.00 (m, 2H), 1.75 - 1.67 (m, 1H), 1.69 (s, 3H), 1.63 (s, 3H), 1.51 - 1.41 (m, 2H), 1.39 (bs, 1H), 1.10 (s, 3H), 0.93 (d, $J = 6.9\text{ Hz}$, 3H), 0.89 (d, $J = 6.9\text{ Hz}$, 3H).

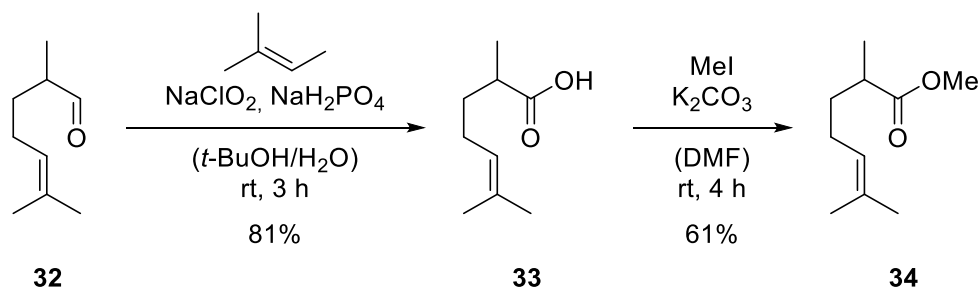
$^{13}\text{C NMR}$ (101 MHz, CDCl_3): δ [ppm] = 131.7, 124.7, 74.8, 39.5, 36.9, 25.7, 23.0, 22.2, 17.7, 17.6, 17.0.

HRMS (EI): calcd for $\text{C}_{11}\text{H}_{20}^+$ [(M-H $_2\text{O}$) $^+$]: 152.1560, found: 152.1561.

IR (ATR): $\tilde{\nu}$ [cm^{-1}] = 3450, 2966, 2927, 2878, 1451, 1375, 1312, 1264, 1181, 1117, 1088, 1006, 936, 914, 873, 831.

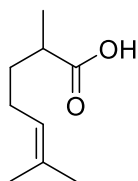
TLC: $R_f = 0.79$ (pentane/ $\text{Et}_2\text{O} = 2/1$) [KMnO_4].

Synthesis of ester **34**:



Scheme S1. Synthesis of ester **34**.

2,6-Dimethylhept-5-enoic acid (**33**)



C₉H₁₆O₂
156.23 g/mol

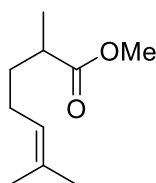
To a solution of 2,6-dimethylhept-5-enal (**32**) (24.7 mL, 150 mmol, 1.0 eq.) in *t*-BuOH (285 mL) and water (57 mL) were successively added 90% 2-methylbut-2-ene (58.7 mL, 499 mmol, 3.3 eq.) and NaH₂PO₄ (21.6 g, 180 mmol, 1.2 eq.) at rt. After complete dissolution, 80% NaClO₂ (32.0 g, 353 mmol, 2.4 eq.) was added in multiple portions and the reaction mixture was stirred over night at rt. Subsequently a pH of 9 was adjusted by addition of 2 M NaOH, followed by removal of *t*-BuOH under vacuum. The aqueous residue was washed with pentane (2 × 350 mL), adjusted to pH 3 by addition of 2 M HCl and extracted with EtOAc (4 × 350 mL). The combined organic phases were washed with brine, dried over Na₂SO₄, filtered and concentrated under vacuum. The crude product **33** was used without further purification in the next step as shown in scheme S1.

¹H NMR (500 MHz, CDCl₃): δ [ppm] = 5.11 - 5.06 (m, 1H), 2.52 - 2.43 (m, 1H), 2.06 - 1.99 (m, 2H), 1.77 - 1.70 (m, 1H), 1.68 (s, 3H), 1.60 (s, 3H), 1.50 - 1.41 (m, 1H), 1.18 (d, *J* = 7.0 Hz, 3H).

TLC: *R*_f = 0.50 (pentane/Et₂O = 2/1) [KMnO₄].

The spectroscopic data matched those reported in the literature.^[6]

Methyl 2,6-dimethylhept-5-enoate (**34**)



C₁₀H₁₈O₂
170.25 g/mol

To a stirred solution of crude carboxylic acid **33** (19.1 g, 122 mmol, 1.0 eq.) in anhydrous DMF (133 mL) was added K₂CO₃ (54.3 g, 393 mmol, 3.2 eq.) at rt. The suspension was slowly treated with MeI (26.7 mL, 430 mmol, 3.5 eq.) and stirred over night at rt. After addition of water (130 mL), the crude product was extracted with Et₂O (3 × 200 mL) and successively washed with water and brine. The combined organic phases were dried over MgSO₄, filtered and

concentrated under vacuum. Subsequent distillation under vacuum yielded ester **34** (13.5 g, 79.3 mmol, 65%) as a colorless oil.

¹H NMR (500 MHz, CDCl₃): δ [ppm] = 5.10 - 5.04 (m, 1H), 3.66 (s, 3H), 2.49 - 2.40 (m, 1H), 2.01 - 1.93 (m, 2H), 1.75 - 1.69 (m, 1H), 1.68 (s, 3H), 1.59 (s, 3H), 1.47 - 1.38 (m, 1H), 1.14 (d, $J = 7.0$ Hz, 3H).

b.p.: 65-70 °C (8 Torr).

TLC: $R_f = 0.74$ (pentane/Et₂O = 10/1) [KMnO₄].

The spectroscopic data matched those reported in the literature.^[6]

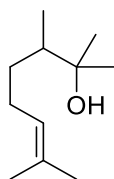
General procedure for the addition of methyl and ethyl Grignard reagents to methyl esters and ketones:

A commercially obtained solution of the corresponding Grignard reagent (2.5-3.3 eq.) was diluted with anhydrous THF (~0.2 M) and cooled to 0 °C. After dropwise addition of a solution of the electrophile (1.0 eq.) in anhydrous THF (~0.3 M), the reaction mixture was stirred at rt until TLC indicated complete consumption of the starting material. The reaction was carefully quenched with saturated aqueous NH₄Cl and extracted with Et₂O (3 ×). The combined organic phases were dried over Na₂SO₄, filtered and concentrated under vacuum. The crude product was subsequently purified via flash column chromatography (pentane/Et₂O).

General procedure for cyclopentation of methyl esters:

Magnesium (6.7 eq.) was suspended in anhydrous THF (0.44 M) and cooled to 0 °C. After dropwise addition of 1,4-dibromobutane (3.3 eq.), the reaction mixture was allowed to warm towards rt over the course of 1 h. The turbid suspension was subsequently cooled to 0 °C and slowly treated with a solution of the ester (1.0 eq.) in anhydrous THF (0.25 M). The mixture was stirred at rt until TLC indicated complete consumption of the starting material. The reaction was carefully quenched with saturated aqueous NH₄Cl at 0 °C and extracted with Et₂O (3 ×). The combined organic phases were dried over Na₂SO₄, filtered and concentrated under vacuum. The crude product was subsequently purified via flash column chromatography (pentane/Et₂O).

2,3,7-Trimethyloct-6-en-2-ol (**16**)



C₁₁H₂₂O
170.30 g/mol

According to the general procedure for the addition of Grignard reagents, ester **34** (1.50 g, 8.81 mmol, 1.0 eq.) was added to methylmagnesium chloride (3.0 M in THF, 8.81 mL, 26.4 mmol, 3.0 eq.) and the mixture was stirred over night at rt. After flash column chromatography (pentane/Et₂O = 5/1), alcohol **16** (845 mg, 4.96 mmol, 56%) was obtained as a colorless oil.

¹H NMR (300 MHz, CDCl₃): δ [ppm] = 5.16 - 5.07 (m, 1H), 2.18 - 2.02 (m, 1H), 1.98 - 1.92 (m, 1H), 1.69 (s, 3H), 1.64 - 1.56 (m, 1H), 1.61 (s, 3H), 1.46 - 1.34 (m, 1H), 1.39 (bs, 1H), 1.16 (s, 3H), 1.15 (s, 3H), 1.08 - 0.96 (m, 1H), 0.92 (d, *J* = 7.0 Hz, 3H).

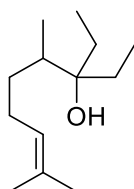
¹³C NMR (75 MHz, CDCl₃): δ [ppm] = 131.6, 124.8, 73.6, 44.0, 31.9, 27.1, 26.7, 26.5, 25.9, 17.8, 14.5.

HRMS (EI): calcd for C₁₁H₂₀⁺ [(M-H₂O)⁺]: 152.1560, found: 152.1567.

IR (ATR): $\tilde{\nu}$ [cm⁻¹] = 3380, 2967, 2926, 2876, 1452, 1375, 1306, 1216, 1164, 1138, 1103, 1081, 944, 912, 889, 866, 829.

TLC: *R*_f = 0.46 (pentane/Et₂O = 2/1) [KMnO₄].

3-Ethyl-4,8-dimethylnon-7-en-3-ol (**14**)



C₁₃H₂₆O
198.35 g/mol

According to the general procedure for the addition of Grignard reagents, ester **34** (500 mg, 2.94 mmol, 1.0 eq.) was added to ethylmagnesium chloride (2.0 M in THF, 3.67 mL, 7.34 mmol, 2.5 eq.) and the mixture was stirred over night at rt. After flash column chromatography (pentane/Et₂O = 10/1 → 5/1), alcohol **14** (336 mg, 1.70 mmol, 58%) was obtained as a colorless oil.

¹H NMR (400 MHz, CDCl₃): δ [ppm] = 5.15 - 5.09 (m, 1H), 2.16 - 2.04 (m, 1H), 1.95 - 1.83 (m, 1H), 1.69 (s, 3H), 1.61 (s, 3H), 1.59 - 1.40 (m, 6H), 1.32 (bs, 1H), 1.10 - 0.98 (m, 1H), 0.89 (d, $J = 7.4$ Hz, 3H), 0.86 (t, $J = 7.5$ Hz, 6H).

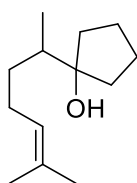
¹³C NMR (101 MHz, CDCl₃): δ [ppm] = 131.6, 124.9, 76.4, 38.9, 31.2, 28.2, 28.2, 26.8, 25.9, 17.8, 13.6, 7.6, 7.6.

HRMS (EI): calcd for C₁₃H₂₄⁺ [(M-H₂O)⁺]: 180.1873, found: 180.1881.

IR (ATR): $\tilde{\nu}$ [cm⁻¹] = 3486, 2928, 2881, 2860, 1457, 1377, 1320, 1302, 1260, 1154, 1126, 1040, 943, 923, 829.

TLC: $R_f = 0.67$ (pentane/Et₂O = 5/1) [KMnO₄].

1-(6-Methylhept-5-en-2-yl)cyclopentan-1-ol (**3**)



C₁₃H₂₄O
196.33 g/mol

According to the general procedure for cyclopentanation, methyl ester **34** (300 mg, 1.76 mmol, 1.0 eq.) was added to freshly prepared di-Grignard of 1,4-dibromobutane and the reaction mixture was stirred for 1 h at rt. Purification by flash column chromatography (pentane/Et₂O = 10/1) yielded alcohol **3** (314 mg, 1.60 mmol, 91%) as a colorless oil.

¹H NMR (400 MHz, CDCl₃): δ [ppm] = 5.14 - 5.08 (m, 1H), 2.16 - 2.04 (m, 1H), 1.97 - 1.87 (m, 1H), 1.84 - 1.74 (m, 2H), 1.69 (s, 3H), 1.66 - 1.52 (m, 7H), 1.61 (s, 3H), 1.48 - 1.41 (m, 1H), 1.34 (bs, 1H), 1.22 - 1.12 (m, 1H), 0.95 (d, $J = 6.8$ Hz, 3H).

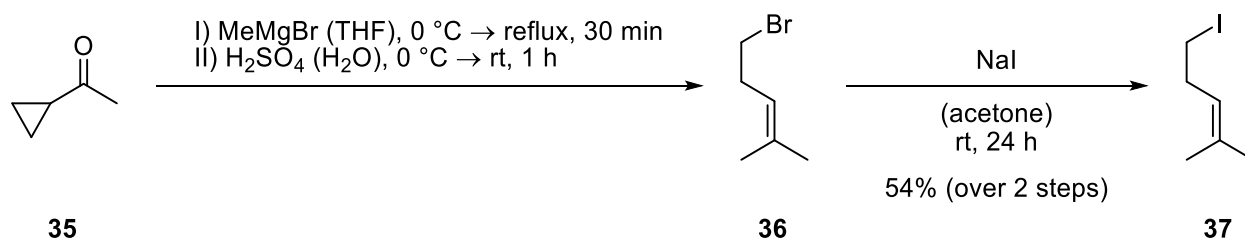
¹³C NMR (101 MHz, CDCl₃): δ [ppm] = 131.6, 124.9, 85.8, 42.1, 38.6, 38.5, 32.3, 26.4, 25.9, 24.2, 24.1, 17.8, 14.6.

HRMS (EI): calcd for C₁₃H₂₂⁺ [(M-H₂O)⁺]: 178.1716, found: 178.1719.

IR (ATR): $\tilde{\nu}$ [cm⁻¹] = 3403, 2963, 2929, 2871, 1450, 1376, 1323, 1185, 1132, 1056, 974, 948, 907, 828.

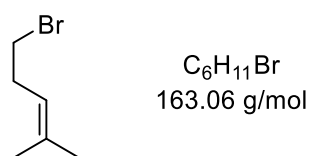
TLC: $R_f = 0.65$ (pentane/Et₂O = 2/1) [KMnO₄].

Synthesis of homoprenyl iodide (37):



Scheme S2. Synthesis of homoprenyl iodide (37).

Homoprenyl bromide (36)



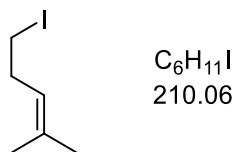
According to a modified literature procedure,^[7] a solution of methylmagnesium bromide (3.0 M in Et₂O, 38.4 mL, 115 mmol, 1.2 eq.) was slowly treated with a solution of cyclopropyl methyl ketone (35) (9.50 mL, 95.9 mmol, 1.0 eq.) in anhydrous THF (14 mL) under water bath cooling (caution: mixture tends to solidify upon fast addition). The reaction mixture was then refluxed for 30 min. After cooling to rt, the solution was slowly added to an ice bath cooled mixture of conc. H₂SO₄ (33 mL) and water (66 mL) at a rate to keep the internal temperature below 10 °C. The reaction mixture was subsequently stirred in the dark for 30 min at 0 °C. Stirring was then continued for 30 min at rt. The organic layer was separated and the aqueous phase was extracted with Et₂O (3 × 100 mL). The combined organic phases were washed with saturated aqueous NaHCO₃ and brine. After drying over Na₂SO₄ and filtration, the solvent was removed under vacuum. The crude product 36 was used without further purification in the next step as shown in scheme S2.

¹H NMR (300 MHz, CDCl₃): δ [ppm] = 5.17 - 5.08 (m, 1H), 3.34 (t, *J* = 7.3 Hz, 2H), 2.61 - 2.50 (m, 2H), 1.71 (s, 3H), 1.63 (s, 3H).

TLC: *R*_f = 0.54 (pentane) [KMnO₄].

The spectroscopic data matched those reported in the literature.^[8]

Homoprenyl iodide (**37**)



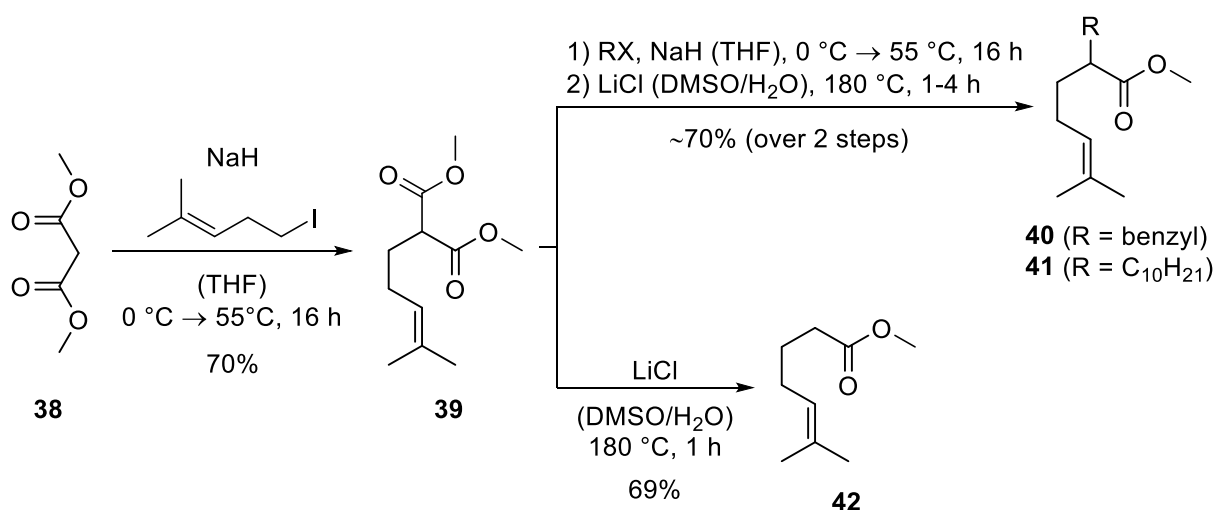
NaI (25.5 g, 170 mmol, 2.6 eq.) was dissolved in anhydrous acetone (100 mL) and the flask was wrapped in aluminum foil. Crude homoprenyl bromide (**36**) (10.8 g, 66.4 mmol, 1.0 eq.) was then added dropwise and the reaction mixture was stirred over night at rt. The suspension was subsequently concentrated under vacuum. The residue was diluted with water and extracted with Et₂O (3 × 60 mL). The combined organic phases were washed with brine, dried over Na₂SO₄, filtered and concentrated under vacuum. The crude product **37** (10.9 g, 52.0 mmol, 54% over 2 steps) was used without further purification in the next step as shown in scheme S3.

¹H NMR (400 MHz, CDCl₃): δ [ppm] = 5.13 - 5.06 (m, 1H), 3.11 (t, $J = 7.4$ Hz, 2H), 2.62 - 2.52 (m, 2H), 1.70 (s, 3H), 1.61 (s, 3H).

TLC: $R_f = 0.82$ (pentane) [KMnO₄].

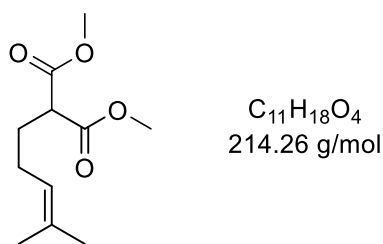
The spectroscopic data matched those reported in the literature.^[9]

Synthesis of methyl esters **40**, **41** and **42**:



Scheme S3. Synthesis of methyl esters **40**, **41** and **42**.

Dimethyl 2-(4-methylpent-3-en-1-yl)malonate (**39**)



To a suspension of NaH (60% suspension in paraffin oil, 668 mg, 27.9 mmol, 1.3 eq.) in anhydrous THF (200 mL) was added dimethyl malonate (**38**) (3.20 mL, 27.9 mmol, 1.3 eq.) dropwise at 0 °C. After 10 min of stirring at 0 °C, a solution of homoprenyl iodide (**37**) (4.50 g, 21.4 mmol, 1.0 eq.) in THF (100 mL) was slowly added and the reaction mixture was subsequently stirred for 16 h at 55 °C. The reaction was quenched by the addition of saturated aqueous NH_4Cl and extracted with Et_2O (3 × 150 mL). The combined organic phases were washed with brine, dried over Na_2SO_4 , filtered and concentrated under vacuum. The crude product was purified by flash column chromatography (pentane/ Et_2O = 5/1) to yield compound **39** (3.21 g, 15.0 mmol, 70%) as a colorless oil.

1H NMR (300 MHz, $CDCl_3$): δ [ppm] = 5.11 - 5.02 (m, 1H), 3.73 (s, 6H), 3.37 (t, J = 7.1 Hz, 1H), 2.08 - 1.88 (m, 4H), 1.69 (s, 3H), 1.57 (s, 3H).

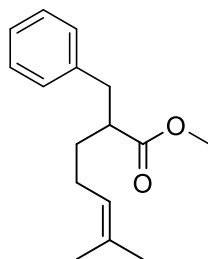
TLC: R_f = 0.46 (pentane/ Et_2O = 5/1) [$KMnO_4$].

The spectroscopic data matched those reported in the literature.^[10]

General procedure for Krapcho decarboxylation:

Malonate (1.0 eq.) was dissolved in a 40:1 mixture of DMSO and water (0.55 M). Anhydrous LiCl (3.1 eq.) was added and the reaction mixture was stirred for 1-4 h at 180 °C (caution: DMSO can decompose explosively at high temperatures). After cooling to rt and addition of water, the crude product was extracted with Et_2O (3 ×) and washed with water (5 ×). The combined organic phases were washed with brine, dried over Na_2SO_4 , filtered and concentrated under vacuum. The crude product was subsequently purified via flash column chromatography (pentane/ Et_2O).

Methyl 2-benzyl-6-methylhept-5-enoate (**40**)



C₁₆H₂₂O₂
246.35 g/mol

NaH (60% suspension in paraffin oil, 121 mg, 5.04 mmol, 1.2 eq.) was suspended in anhydrous THF (40 mL) and cooled to 0 °C. The suspension was slowly treated with malonate **39** (900 mg, 4.20 mmol, 1.0 eq.) and the reaction mixture was stirred for 30 min at rt. Benzyl bromide (624 μL, 5.25 mmol, 1.3 eq.) was added dropwise and the mixture was stirred for 16 h at 55 °C. The reaction was subsequently quenched by the addition of saturated aqueous NH₄Cl, and this mixture was extracted with Et₂O (3 × 30 mL) and washed with brine. The combined organic phases were dried over Na₂SO₄, filtered and concentrated under vacuum. The crude alkylation product (*R*_f = 0.46 (pentane/Et₂O = 5/1) [KMnO₄]) was used without further purification in the next step as shown in scheme S3.

According to the general procedure for Krapcho decarboxylation, crude benzylated malonate was treated with LiCl and the reaction mixture was stirred for 1 h at 180 °C. Purification by flash column chromatography (pentane/Et₂O = 20/1) afforded methyl ester **40** (751 mg, 3.05 mmol, 73% over 2 steps) as a colorless oil.

¹H NMR (400 MHz, CDCl₃): δ [ppm] = 7.30 - 7.12 (m, 5H), 5.08 - 5.00 (m, 1H), 3.59 (s, 3H), 2.93 (dd, *J* = 13.4 Hz, 8.2 Hz, 1H), 2.75 (dd, *J* = 13.4 Hz, 6.6 Hz, 1H), 2.71 - 2.63 (m, 1H), 2.05 - 1.88 (m, 2H), 1.75 - 1.65 (m, 1H), 1.67 (s, 3H), 1.57 (s, 3H), 1.55 - 1.46 (m, 1H).

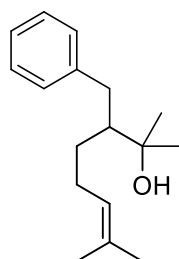
¹³C NMR (101 MHz, CDCl₃): δ [ppm] = 176.2, 139.5, 132.5, 129.9 (2C), 128.5 (2C), 126.4, 123.6, 51.5, 47.3, 38.7, 32.3, 26.0, 25.9, 17.8.

HRMS (EI): calcd for C₁₆H₂₂O₂⁺ [(M)⁺]: 246.1614, found: 246.1518.

IR (ATR): $\tilde{\nu}$ [cm⁻¹] = 3086, 3063, 3028, 2949, 2926, 2857, 1734, 1604, 1496, 1454, 1435, 1375, 1281, 1259, 1201, 1161, 1110, 1079, 1051, 1031, 984, 838, 745, 699.

TLC: *R*_f = 0.63 (pentane/Et₂O = 10/1) [KMnO₄].

3-Benzyl-2,7-dimethyloct-6-en-2-ol (21)



$C_{17}H_{26}O$
246.39 g/mol

According to the general procedure for the addition of Grignard reagents, ester **40** (150 mg, 609 μmol , 1.0 eq.) was added to methylmagnesium chloride (3.0 M in THF, 660 μL , 1.98 mmol, 3.3 eq.) and the mixture was stirred for 2 h at rt. After flash column chromatography (pentane/ Et_2O = 10/1 \rightarrow 5/1), alcohol **21** (75.4 mg, 306 μmol , 50%) was obtained as a colorless oil.

$^1\text{H NMR}$ (400 MHz, CDCl_3): δ [ppm] = 7.30 - 7.13 (m, 5H), 4.95 - 4.88 (m, 1H), 2.96 (dd, J = 13.8 Hz, 4.6 Hz, 1H), 2.40 (dd, J = 13.8 Hz, 8.7 Hz, 1H), 1.81 - 1.73 (m, 2H), 1.72 - 1.65 (m, 1H), 1.61 (s, 3H), 1.57 - 1.48 (m, 1H), 1.44 (s, 3H), 1.41 (bs, 1H), 1.28 - 1.20 (m, 1H), 1.24 (s, 3H), 1.23 (s, 3H).

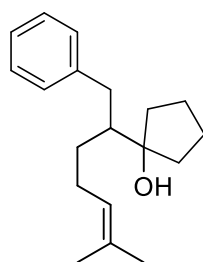
$^{13}\text{C NMR}$ (101 MHz, CDCl_3): δ [ppm] = 142.4, 131.6, 129.2 (2C), 128.4 (2C), 125.9, 124.7, 74.2, 51.3, 37.6, 31.2, 27.9, 27.9, 27.2, 25.8, 17.7.

HRMS (EI): calcd for $C_{17}H_{24}^+$ [(M-H₂O)⁺]: 228.1873, found: 228.1876.

IR (ATR): $\tilde{\nu}$ [cm^{-1}] = 3404, 3084, 3062, 3026, 2968, 2927, 2876, 1604, 1495, 1454, 1375, 1209, 1129, 1079, 1030, 933, 902, 828, 736, 698.

TLC: R_f = 0.07 (pentane/ Et_2O = 10/1) [KMnO_4].

1-(6-Methyl-1-phenylhept-5-en-2-yl)cyclopentan-1-ol (10)



$C_{19}H_{28}O$
272.43 g/mol

According to the general procedure for cyclopentanation, methyl ester **40** (300 mg, 1.22 mmol, 1.0 eq.) was added to freshly prepared di-Grignard of 1,4-dibromobutane and the reaction mixture was stirred for 1 h at rt. Purification by flash column chromatography (pentane/Et₂O = 10/1 → 5/1) yielded alcohol **10** (271 mg, 996 μmol, 82%) as a colorless oil.

¹H NMR (400 MHz, CDCl₃): δ [ppm] = 7.30 - 7.14 (m, 5H), 4.98 - 4.90 (m, 1H), 2.95 (dd, *J* = 13.9 Hz, 4.8 Hz, 1H), 2.56 (dd, *J* = 13.9 Hz, 8.5 Hz, 1H), 1.88 - 1.48 (m, 12H), 1.62 (s, 3H), 1.46 (s, 3H), 1.40 - 1.29 (m, 2H).

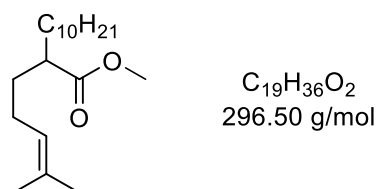
¹³C NMR (101 MHz, CDCl₃): δ [ppm] = 142.3, 131.6, 129.2 (2C), 128.4 (2C), 125.8, 124.8, 86.2, 49.4, 39.4, 39.0, 37.6, 31.2, 27.5, 25.8, 24.1, 23.9, 17.8.

HRMS (EI): calcd for C₁₉H₂₆⁺ [(M-H₂O)⁺]: 254.2029, found: 254.2038.

IR (ATR): $\tilde{\nu}$ [cm⁻¹] = 3461, 3084, 3062, 3026, 2960, 2927, 2871, 1604, 1495, 1453, 1375, 1325, 1272, 1179, 1109, 1066, 1030, 984, 908, 880, 828, 737, 699.

TLC: *R*_f = 0.26 (pentane/Et₂O = 5/1) [CAM].

Methyl 2-(4-methylpent-3-en-1-yl)dodecanoate (**41**)



NaH (60% suspension in paraffin oil, 101 mg, 4.20 mmol, 1.2 eq.) was suspended in anhydrous THF (34 mL) and cooled to 0 °C. The suspension was slowly treated with malonate **39** (750 mg, 3.50 mmol, 1.0 eq.) and the reaction mixture was stirred for 30 min at rt. Decyl iodide (1.17 g, 4.38 mmol, 1.3 eq.) – prepared according to a published procedure^[11] in one step from 1-decanol – was added dropwise and the mixture was stirred for 16 h at 55 °C. The reaction was subsequently quenched by the addition of saturated aqueous NH₄Cl, and this mixture was extracted with Et₂O (3 × 30 mL) and washed with brine. The combined organic phases were dried over Na₂SO₄, filtered and concentrated under vacuum. The crude alkylation product (*R*_f = 0.63 (pentane/Et₂O = 10/1) [KMnO₄]) was used without further purification in the next step as shown in scheme S3.

According to the general procedure for Krapcho decarboxylation, crude decylated malonate was treated with LiCl and the reaction mixture was stirred for 4 h at 180 °C. Purification by flash column chromatography (pentane/Et₂O = 50/1) afforded methyl ester **41** (728 mg, 2.45 mmol, 70% over 2 steps) as a colorless oil.

¹H NMR (400 MHz, CDCl₃): δ [ppm] = 5.10 - 5.03 (m, 1H), 3.67 (s, 3H), 2.39 - 2.30 (m, 1H), 1.99 - 1.90 (m, 2H), 1.70 - 1.54 (m, 2H), 1.68 (s, 3H), 1.58 (s, 3H), 1.50 - 1.40 (m, 2H), 1.29 - 1.22 (m, 16H), 0.89 (t, *J* = 6.6 Hz, 3H).

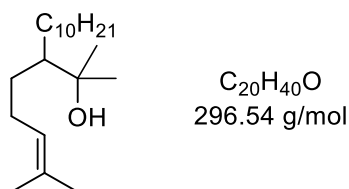
¹³C NMR (101 MHz, CDCl₃): δ [ppm] = 177.1, 132.3, 123.9, 51.4, 45.4, 32.6 (2C), 32.1, 29.8, 29.7, 29.7, 29.6, 29.5, 27.6, 26.1, 25.9, 22.8, 17.8, 14.2.

HRMS (EI): calcd for C₁₉H₃₆O₂⁺ [(M)⁺]: 296.2710, found: 296.2704.

IR (ATR): $\tilde{\nu}$ [cm⁻¹] = 2923, 2854, 1738, 1456, 1434, 1376, 1259, 1194, 1154, 983, 834, 722.

TLC: *R*_f = 0.38 (pentane/Et₂O = 50/1) [KMnO₄].

2-Methyl-3-(4-methylpent-3-en-1-yl)tridecan-2-ol (**30**)



According to the general procedure for the addition of Grignard reagents, ester **41** (350 mg, 1.18 mmol, 1.0 eq.) was added to methylmagnesium chloride (2.8 M in THF, 1.37 mL, 3.84 mmol, 3.3 eq.) and the mixture was stirred for 2 h at rt. After flash column chromatography (pentane/Et₂O = 10/1), alcohol **30** (184 mg, 620 μmol, 53%) was obtained as a colorless oil.

¹H NMR (400 MHz, CDCl₃): δ [ppm] = 5.16 - 5.09 (m, 1H), 2.14 - 1.92 (m, 2H), 1.69 (s, 3H), 1.61 (s, 3H), 1.56 - 1.08 (m, 22H), 1.17 (s, 6H), 0.88 (t, *J* = 6.6 Hz, 3H).

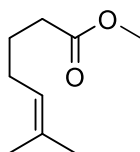
¹³C NMR (101 MHz, CDCl₃): δ [ppm] = 131.6, 125.1, 74.2, 49.5, 32.1, 31.5, 31.5, 30.5, 29.9, 29.8 (2C), 29.6, 29.5, 28.1, 27.5, 27.4, 25.9, 22.9, 17.9, 14.3.

HRMS (EI): calcd for C₂₀H₃₈⁺ [(M-H₂O)⁺]: 278.2968, found: 278.2970.

IR (ATR): $\tilde{\nu}$ [cm⁻¹] = 3388, 2960, 2923, 2853, 1466, 1376, 1137, 1109, 954, 899, 830, 720.

TLC: $R_f = 0.20$ (pentane/Et₂O = 10/1) [KMnO₄].

Methyl 6-methylhept-5-enoate (**42**)



C₉H₁₆O₂
156.23 g/mol

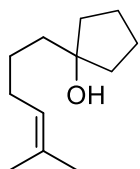
According to the general procedure for Krapcho decarboxylation, malonate **39** (850 mg, 3.97 mmol, 1.0 eq.) was treated with LiCl (518 mg, 12.2 mmol, 3.1 eq.) and the reaction mixture was stirred for 1 h at 180 °C. Purification by flash column chromatography (pentane/Et₂O = 50/1 → 20/1) afforded methyl ester **42** (429 mg, 2.75 mmol, 69%) as a colorless oil.

¹H NMR (400 MHz, CDCl₃): δ [ppm] = 5.12 - 5.05 (m, 1H), 3.66 (s, 3H), 2.30 (t, $J = 7.5$ Hz, 2H), 2.05 - 1.97 (m, 2H), 1.71 - 1.62 (m, 2H), 1.69 (s, 3H), 1.59 (s, 3H).

TLC: $R_f = 0.68$ (pentane/Et₂O = 10/1) [KMnO₄].

The spectroscopic data matched those reported in the literature.^[12]

1-(5-Methylhex-4-en-1-yl)cyclopentan-1-ol (**12**)



C₁₂H₂₂O
182.31 g/mol

According to the general procedure for cyclopentanation, methyl ester **42** (300 mg, 1.92 mmol, 1.0 eq.) was added to freshly prepared di-Grignard of 1,4-dibromobutane and the reaction mixture was stirred for 1 h at rt. Purification by flash column chromatography (pentane/Et₂O = 10/1) yielded alcohol **12** (300 mg, 1.65 mmol, 86%) as a colorless oil.

¹H NMR (400 MHz, CDCl₃): δ [ppm] = 5.17 - 5.08 (m, 1H), 2.05 - 1.94 (m, 2H), 1.86 - 1.73 (m, 2H), 1.71 - 1.52 (m, 8H), 1.69 (s, 3H), 1.60 (s, 3H), 1.51 - 1.38 (m, 2H), 1.29 (bs, 1H).

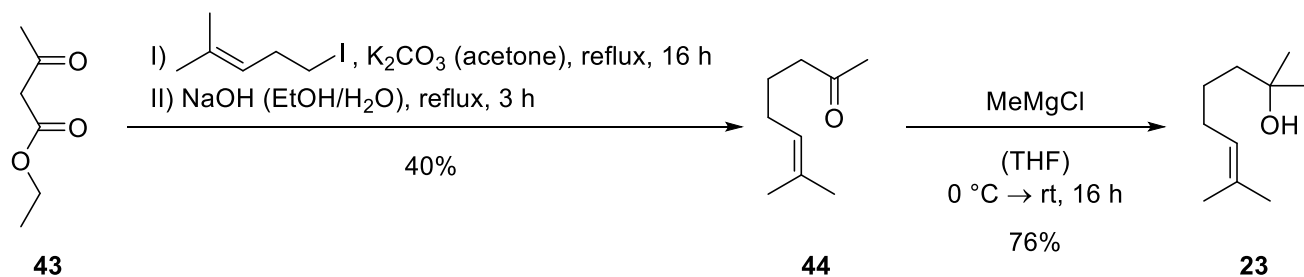
¹³C NMR (101 MHz, CDCl₃): δ [ppm] = 131.7, 124.7, 82.7, 41.3, 39.9 (2C), 28.6, 25.9, 25.2, 24.0 (2C), 17.9.

HRMS (ED): calcd for C₁₂H₂₀⁺ [(M-H₂O)⁺]: 164.1560, found: 164.1552.

IR (ATR): $\tilde{\nu}$ [cm^{-1}] = 3368, 2959, 2930, 2871, 1450, 1376, 1326, 1288, 1215, 1089, 1052, 983, 907, 833.

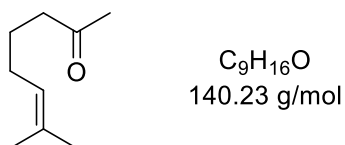
TLC: R_f = 0.62 (pentane/ Et_2O = 2/1) [KMnO_4].

Synthesis of alcohol **23**:



Scheme S4. Synthesis of substrate **23**.

7-Methyloct-6-en-2-one (**44**)



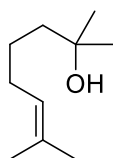
To a solution of ethyl acetoacetate (**43**) (989 μL , 7.83 mmol, 1.1 eq.) in anhydrous acetone (20 mL) were added anhydrous potassium carbonate (1.18 g, 8.56 mmol, 1.2 eq.) and homoprenyl iodide (**37**) (1.50, 7.14 mmol, 1.0 eq.). The reaction mixture was subsequently refluxed for 16 h. After cooling to rt, the solvent was removed under vacuum. The residue was then taken up in EtOH (15 mL) and treated with 10% aqueous NaOH (17 mL). After 3 h at reflux, the reaction mixture was allowed to cool to rt. The crude product was extracted with Et_2O (3×50 mL) and the combined organic phases were, dried over Na_2SO_4 , filtered and concentrated under vacuum. The organic mixture was purified via flash column chromatography (pentane/ Et_2O = 10/1) to give ketone **44** (400 mg, 2.86 mmol, 40%) as a colorless oil.

^1H NMR (300 MHz, CDCl_3): δ [ppm] = 5.12 - 5.04 (m, 1H), 2.41 (t, J = 7.4 Hz, 2H), 2.13 (s, 3H), 2.03 - 1.93 (m, 2H), 1.68 (s, 3H), 1.66 - 1.56 (m, 2H), 1.59 (s, 3H).

TLC: R_f = 0.27 (pentane/ Et_2O = 10/1) [KMnO_4].

The spectroscopic data matched those reported in the literature.^[13]

2,7-Dimethyloct-6-en-2-ol (**23**)



C₁₀H₂₀O
156.27 g/mol

According to the general procedure for the addition of Grignard reagents, ketone **44** (200 mg, 1.43 mmol, 1.0 eq.) was added to methylmagnesium chloride (3.0 M in THF, 1.55 mL, 4.64 mmol, 3.3 eq.) and the mixture was stirred over night at rt. After flash column chromatography (pentane/Et₂O = 5/1 → 2/1), alcohol **23** (169 mg, 1.08 mmol, 76%) was obtained as a colorless oil.

¹H NMR (400 MHz, CDCl₃): δ [ppm] = 5.15 - 5.08 (m, 1H), 2.03 - 1.94 (m, 2H), 1.69 (s, 3H), 1.60 (s, 3H), 1.50 - 1.31 (m, 5H), 1.21 (s, 6H).

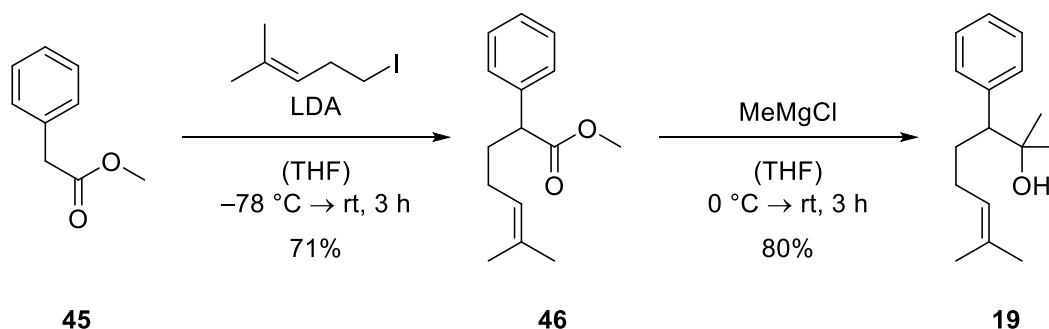
¹³C NMR (101 MHz, CDCl₃): δ [ppm] = 131.8, 124.7, 71.2, 43.7, 29.4 (2C), 28.6, 25.9, 24.8, 17.9.

HRMS (EI): calcd for C₁₀H₁₈⁺ [(M-H₂O)⁺]: 138.1403, found: 138.1386.

IR (ATR): $\tilde{\nu}$ [cm⁻¹] = 3361, 2967, 2932, 2862, 1451, 1376, 1365, 1317, 1300, 1220, 1189, 1147, 1099, 944, 907, 834.

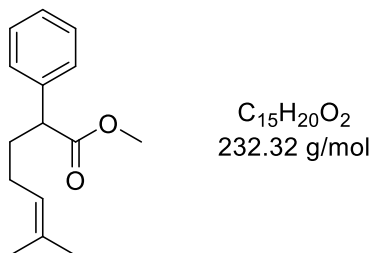
TLC: R_f = 0.46 (pentane/Et₂O = 2/1) [KMnO₄].

Synthesis of alcohol **19**:



Scheme S5. Synthesis of alcohol **19**.

Methyl 6-methyl-2-phenylhept-5-enoate (**46**)



Diisopropylamine (1.12 mL, 7.99 mmol, 1.2 eq.) was dissolved in anhydrous THF (20 mL) and cooled to -78 °C. To the solution was added *n*-butyllithium (2.5 M in hexanes, 2.93 mL, 7.32 mmol, 1.1 eq.) dropwise and the reaction mixture was stirred for 30 min at 0 °C. After cooling to -78 °C, a solution of ester **45** (935 μ L, 6.66 mmol, 1.0 eq.) was slowly added and stirring was continued for 1 h at -78 °C. Homoprenyl iodide (**37**) (2.10 g, 9.99 mmol, 1.5 eq.) was subsequently added dropwise and the mixture was stirred for 1 h at 0 °C. The solution was then allowed to warm to rt and stirred for 4 h. The reaction was quenched by the addition of saturated aqueous NH_4Cl , and this mixture was extracted with Et_2O (3×30 mL) and washed with brine. The combined organic phases were dried over Na_2SO_4 , filtered and concentrated under vacuum. Purification by flash column chromatography (pentane/ Et_2O = 70/1 \rightarrow 30/1) yielded ester **46** (1.10 g, 4.73 mmol, 71%) as a colorless oil.

1H NMR (400 MHz, $CDCl_3$): δ [ppm] = 7.34 - 7.22 (m, 5H), 5.12 - 5.05 (m, 1H), 3.65 (s, 3 H), 3.56 (t, J = 7.6 Hz, 1H), 2.17 - 2.07 (m, 1H), 1.98 - 1.89 (m, 2H), 1.86 - 1.75 (m, 1H), 1.68 (s, 3H), 1.52 (s, 3H).

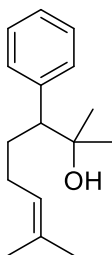
^{13}C NMR (101 MHz, $CDCl_3$): δ [ppm] = 174.7, 139.3, 132.8, 128.7 (2C), 128.1 (2C), 127.3, 123.4, 52.1, 51.1, 33.7, 26.0, 25.9, 17.8.

HRMS (ED): calcd for $C_{15}H_{20}O_2^+$ [(M) $^+$]: 232.1458, found: 232.1466.

IR (ATR): $\tilde{\nu}$ [cm^{-1}] = 3063, 3029, 2950, 2925, 2857, 1735, 1602, 1495, 1454, 1435, 1376, 1352, 1310, 1255, 1204, 1165, 1154, 1106, 1080, 1031, 773, 733, 699.

TLC: R_f = 0.63 (pentane/ Et_2O = 10/1) [$KMnO_4$].

2,7-Dimethyl-3-phenyloct-6-en-2-ol (**19**)



C₁₆H₂₄O
232.37 g/mol

According to the general procedure for the addition of Grignard reagents, ester **46** (1.10 g, 4.73 mmol, 1.0 eq.) was added to methylmagnesium chloride (3.0 M in THF, 5.13 mL, 15.4 mmol, 3.3 eq.) and the mixture was stirred for 3 h at rt. After flash column chromatography (pentane/Et₂O = 10/1), alcohol **19** (876 mg, 3.77 mmol, 80%) was obtained as a colorless oil.

¹H NMR (400 MHz, CDCl₃): δ [ppm] = 7.34 - 7.19 (m, 5H), 5.10 - 5.03 (m, 1H), 2.60 (dd, J = 10.2 Hz, 4.4 Hz, 1H), 1.88 - 1.66 (m, 4H), 1.65 (s, 3H), 1.40 (s, 3H), 1.37 (bs, 1H), 1.18 (s, 3H), 1.17 (s, 3H).

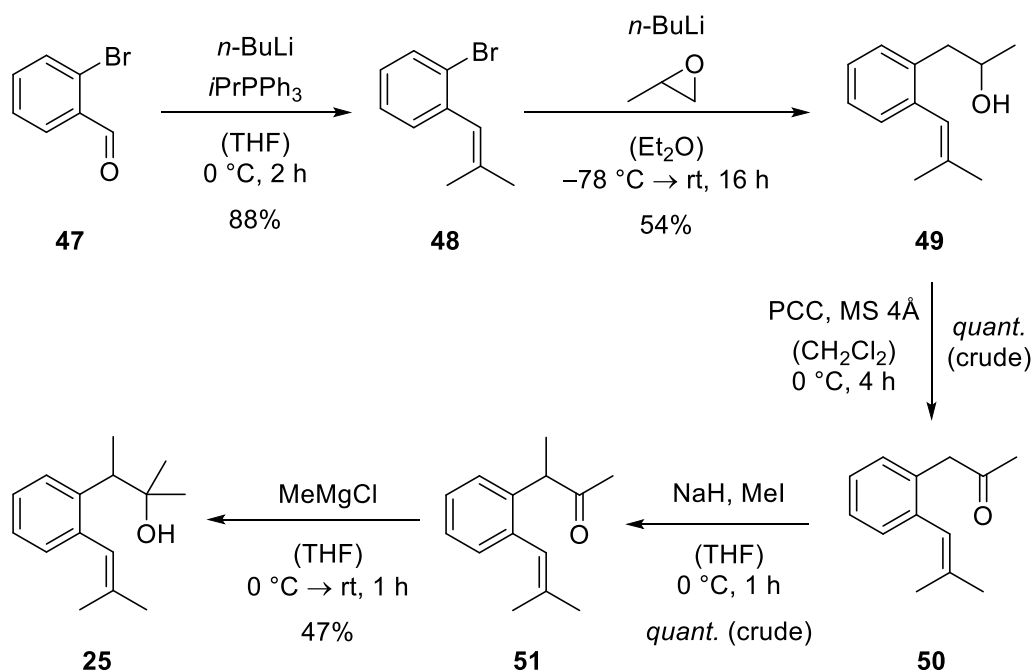
¹³C NMR (101 MHz, CDCl₃): δ [ppm] = 141.3, 131.9, 129.8 (2C), 128.2 (2C), 126.7, 124.4, 72.9, 56.8, 29.8, 28.2, 27.9, 26.7, 25.9, 17.8.

HRMS (EI): calcd for C₁₆H₂₂⁺ [(M-H₂O)⁺]: 214.1716, found: 214.1652.

IR (ATR): $\tilde{\nu}$ [cm⁻¹] = 3569, 3433, 3083, 3060, 3027, 2968, 2930, 2877, 1598, 1493, 1452, 1375, 1330, 1207, 1126, 1083, 947, 918, 896, 836, 752, 727, 701.

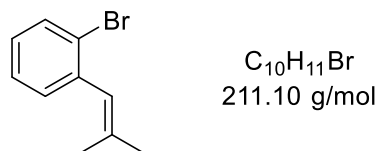
TLC: R_f = 0.62 (pentane/Et₂O = 2/1) [KMnO₄].

Synthesis of compound 25:



Scheme S6. Synthesis of substrate 25.

1-Bromo-2-(2-methylprop-1-en-1-yl)benzene (48)



Isopropyltriphenylphosphonium iodide (14.0 g, 32.4 mmol, 1.2 eq.) was suspended in anhydrous THF (65 mL) and cooled to 0 °C before slowly adding *n*-butyllithium (2.5 M in hexanes, 11.9 mL, 29.7 mmol, 1.1 eq.), resulting in a dark red suspension. After stirring for 30 min at 0 °C, aldehyde **47** (3.13 mL, 27.0 mmol, 1.0 eq.) was added dropwise. Following 2 h at 0 °C and another 1.5 h at rt, pentane (200 mL) was added, giving a white precipitate. The suspension was filtered through a plug of silica and washed with pentane. Concentration under vacuum yielded the crude product, which was purified by flash column chromatography (pentane) to afford compound **48** (4.99 g, 23.7 mmol, 88%) as a colorless liquid.

$^1\text{H NMR}$ (300 MHz, CDCl_3): δ [ppm] = 7.59 - 7.52 (m, 1H), 7.29 - 7.20 (m, 2H), 7.10 - 7.02 (m, 1H), 6.27 - 6.22 (m, 1H), 1.93 (d, J = 1.5 Hz, 3H), 1.75 (d, J = 1.4 Hz, 3H).

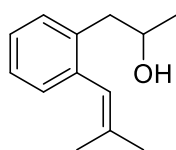
^{13}C NMR (75 MHz, CDCl_3): δ [ppm] = 138.8, 136.9, 132.6, 131.1, 127.8, 126.9, 124.9, 124.4, 26.3, 19.5.

HRMS (EI): calcd for $\text{C}_{10}\text{H}_{11}^+$ [(M-Br) $^+$]: 131.0855, found: 131.0855.

IR (ATR): $\tilde{\nu}$ [cm^{-1}] = 3062, 2972, 2931, 2909, 2854, 1656, 1588, 1560, 1466, 1428, 1376, 1181, 1116, 1060, 1041, 1022, 981, 943, 870, 827, 744, 717, 668, 626.

TLC: R_f = 0.88 (pentane) [KMnO_4].

1-(2-(2-Methylprop-1-en-1-yl)phenyl)propan-2-ol (**49**)



$\text{C}_{13}\text{H}_{18}\text{O}$
190.29 g/mol

To a solution of bromide **48** (5.00 g, 23.7 mmol, 1.0 eq.) in anhydrous Et_2O (120 mL), *n*-butyllithium (2.5 M in hexanes, 10.9 mL, 27.2 mmol, 1.2 eq.) was added dropwise at $-78\text{ }^\circ\text{C}$. The solution was subsequently stirred for 3 h at rt. After cooling again to $-78\text{ }^\circ\text{C}$, a solution of propylene oxide (3.31 mL, 47.4 mmol, 2.0 eq.) in Et_2O (3.4 mL) was added dropwise to the yellow solution, and the reaction mixture was allowed to warm to rt over 16 h. The reaction was then quenched with water. The aqueous phase was extracted with Et_2O ($3 \times 150\text{ mL}$), and the combined organic phases were washed with brine, dried over Na_2SO_4 , filtered and concentrated under vacuum. Purification by flash column chromatography (pentane/ Et_2O = 5/1 \rightarrow 2/1) yielded alcohol **49** (2.43 g, 12.8 mmol, 54%) as a colorless oil.

^1H NMR (300 MHz, CDCl_3): δ [ppm] = 7.24 - 7.11 (m, 4H), 6.32 - 6.28 (m, 1H), 4.03 - 3.91 (m, 1H), 2.82 - 2.65 (m, 2H), 1.91 (d, J = 1.5 Hz, 3H), 1.68 (d, J = 1.4 Hz, 3H), 1.21 (d, J = 6.1 Hz, 3H).

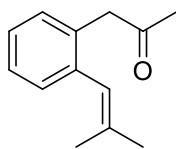
^{13}C NMR (75 MHz, CDCl_3): δ [ppm] = 138.4, 137.0, 136.0, 130.4, 130.2, 126.7, 126.3, 124.1, 68.4, 43.4, 26.2, 23.0, 19.4.

HRMS (EI): calcd for $\text{C}_{13}\text{H}_{18}\text{O}^+$ [(M) $^+$]: 190.1352, found: 190.1350.

IR (ATR): $\tilde{\nu}$ [cm^{-1}] = 3360, 3060, 3016, 2967, 2927, 2912, 2871, 2856, 1482, 1445, 1375, 1347, 1118, 1107, 1075, 1052, 1035, 935, 832, 746.

TLC: R_f = 0.92 (pentane/ Et_2O = 2/1) [KMnO_4].

1-(2-(2-Methylprop-1-en-1-yl)phenyl)propan-2-one (**50**)



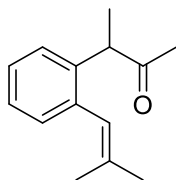
C₁₃H₁₆O
188.27 g/mol

Alcohol **49** (1.70 g, 8.93 mmol, 1.0 eq.) was dissolved in anhydrous DCM (80 mL) and cooled to 0 °C. To the solution were added successively 4Å molecular sieve (25 g) and pyridinium chlorochromate (3.85 g, 17.9 mmol, 2.0 eq.) and the mixture was subsequently stirred for 4 h at 0 °C. The suspension was then filtered through a plug of silica and washed with Et₂O. Concentration under vacuum yielded the crude product, which was used without further purification in the next step as shown in scheme S6.

¹H NMR (400 MHz, CDCl₃): δ [ppm] = 7.25 - 7.13 (m, 4H), 6.19 - 6.14 (m, 1H), 3.66 (s, 2H), 2.06 (s, 3H), 1.89 (d, *J* = 1.5 Hz, 3H), 1.65 (d, *J* = 1.3 Hz, 3H).

TLC: *R*_f = 0.61 (pentane/Et₂O = 5/1) [KMnO₄].

3-(2-(2-Methylprop-1-en-1-yl)phenyl)butan-2-one (**51**)



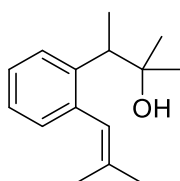
C₁₄H₁₈O
202.30 g/mol

To a suspension of NaH (60% suspension in paraffin oil, 66.9 mg, 2.79 mmol, 1.1 eq.) in THF (3.3 mL) was added a solution of crude ketone **50** (500 mg, 2.66 mmol, 1.0 eq.) in THF (2.2 mL) dropwise at 0 °C. The mixture was then allowed to warm to rt over a period of 30 min. After cooling to 0 °C, MeI (260 μL, 4.17 mmol, 1.6 eq.) was slowly added and stirring was continued for 1 h at 0 °C, followed by 1.5 h at rt. The reaction was subsequently quenched by the addition of saturated aqueous NH₄Cl, and this mixture was extracted with Et₂O (3 × 30 mL) and washed with brine. The combined organic phases were dried over Na₂SO₄, filtered and concentrated under vacuum. The crude product was used without further purification in the next step as shown in scheme S6.

¹H NMR (400 MHz, CDCl₃): δ [ppm] = 7.23 - 7.04 (m, 4H), 6.32 - 6.27 (m, 1H), 3.96 (q, *J* = 6.9 Hz, 1H), 1.95 (s, 3H), 1.93 (d, *J* = 1.5 Hz, 3H), 1.68 (d, *J* = 1.3 Hz, 3H), 1.31 (d, *J* = 6.9 Hz, 3H).

TLC: $R_f = 0.79$ (pentane/Et₂O = 5/1) [KMnO₄].

2-Methyl-3-(2-(2-methylprop-1-en-1-yl)phenyl)butan-2-ol (25)



C₁₅H₂₂O
218.34 g/mol

According to the general procedure for the addition of Grignard reagents, crude ketone **51** (450 mg, 2.22 mmol, 1.0 eq.) was added to methylmagnesium chloride (3.0 M in THF, 2.41 mL, 7.23 mmol, 3.3 eq.) and the mixture was stirred for 1 h at rt. After flash column chromatography (pentane/Et₂O = 10/1 → 5/1), alcohol **25** (227 mg, 1.04 mmol, 47%) was obtained as a colorless oil.

¹H NMR (400 MHz, CDCl₃): δ [ppm] = 7.38 - 7.33 (m, 1H), 7.24 - 7.13 (m, 2H), 7.11 - 7.06 (m, 1H), 6.37 - 6.33 (m, 1H), 3.14 (q, $J = 7.2$ Hz, 1H), 1.90 (d, $J = 1.4$ Hz, 3H), 1.63 (d, $J = 1.3$ Hz, 3H), 1.42 (bs, 1H), 1.29 (d, $J = 7.2$ Hz, 3H), 1.20 (s, 3H), 1.09 (s, 3H).

¹³C NMR (101 MHz, CDCl₃): δ [ppm] = 142.5, 138.8, 135.6, 130.4, 127.3, 126.6, 125.8, 125.2, 73.6, 44.4, 28.5, 27.6, 26.0, 19.3, 16.3.

HRMS (EI): calcd for C₁₅H₂₀⁺ [(M-H₂O)⁺]: 200.1560, found: 200.1564.

IR (ATR): $\tilde{\nu}$ [cm⁻¹] = 3566, 3446, 3094, 3061, 3022, 2970, 2930, 2911, 2876, 1654, 1483, 1444, 1372, 1300, 1206, 1180, 1164, 1137, 1100, 1068, 1041, 1001, 982, 943, 875, 858, 831, 768, 741, 717.

TLC: $R_f = 0.30$ (pentane/Et₂O = 5/1) [KMnO₄].

4. Determination of substrate densities

In order to allow for the direct addition of substrates to the catalyst solution, their densities were determined using a microbalance (Table S1). For this purpose, defined volumes (4.00 μL , 6.00 μL and 10.00 μL) of the corresponding substrate were weighed, by transferring them into tared GC vials using a Microman M1 pipette.

Table S1. Determination of densities.

Compound	m [mg] (4.00 μL)	d₁ [g/mL]	m [mg] (6.00 μL)	d₂ [g/mL]	m [mg] (10.00 μL)	d₃ [g/mL]	d(mean) [g/mL]
3	3.717	0.929	5.438	0.906	9.316	0.932	0.92
9	3.822	0.956	5.654	0.942	9.448	0.945	0.95
10	3.916	0.979	6.090	1.015	10.216	1.022	1.01
12	3.597	0.899	5.604	0.934	8.872	0.887	0.91
14	3.605	0.901	5.284	0.881	8.751	0.875	0.89
16	3.776	0.944	5.564	0.927	9.348	0.935	0.94
18	3.445	0.861	5.180	0.863	8.608	0.861	0.86
19	4.336	1.084	6.329	1.055	10.846	1.085	1.07
21	3.833	0.958	5.677	0.946	9.576	0.958	0.95
23	3.391	0.848	5.165	0.861	8.588	0.859	0.86
25	3.992	0.998	6.085	1.014	10.293	1.029	1.01
27	3.700	0.925	5.560	0.927	9.310	0.931	0.93
30	3.485	0.871	5.431	0.905	8.665	0.867	0.88

5. Cyclization-rearrangement: determination of yields

General procedure:

All substrates were tested in triplicate applying a *C*-undecylcalix[4]resorcinarene (**1**) stock solution in CDCl₃. The stock solution was prepared by homogenizing a mixture of *C*-undecylcalix[4]resorcinarene (**1**) and CDCl₃ (less than full capacity) in a 2 mL- or 5 mL- volumetric flask by gentle heating with a heat gun and agitation. The volumetric flask was then filled up to the calibration mark with CDCl₃ and again homogenized by agitation to give a clear orange solution. An aliquot of the stock solution containing 11.0 mg *C*-undecylcalix[4]resorcinarene (**1**) (9.95 μmol, 6.0 eq.) was then transferred to a GC vial. Next CDCl₃ was added to adjust an overall CDCl₃ volume of 0.50 mL. To this solution, *n*-decane (internal standard) (2.59 μL, 13.3 μmol, 8.0 eq.) and the substrate (16.6 μmol, 10.0 eq.) were added successively in one portion and the mixture was immediately sampled after 30 s of vigorous agitation. The small sample (approximately 10 μL) was diluted with *n*-hexane (0.1 mL) containing 0.08% (v/v) DMSO – the addition of *n*-hexane containing DMSO results in termination of the reaction in this sample and precipitation of the catalyst (protects the GC instrument) – centrifuged, decanted and subjected to GC analysis (initial sample). The GC vial was kept at 50 °C (±1 °C) using a thermostated heating block made from alumina. Based on preliminary studies regarding reaction time optimization, a second sample (final sample) was taken after a given time frame. All three reactions were performed in parallel together with a control reaction using TBAB (**2**) (see chapter 9.1) employing the same catalyst stock solution. In order to precisely calculate the conversion and yield, GC-response factors to *n*-decane as internal standard (IS) were determined for the investigated substrates and their corresponding products. For this purpose, the substance of interest was directly weighed into a GC vial using a microbalance. After diluting with 0.48 mL CDCl₃, 20 μL of a stock solution of *n*-decane in CDCl₃ (166 mmol/L) were added and the mixture was homogenized by agitation. A small sample (approximately 10 μL) of this mixture was then diluted with *n*-hexane (0.1 mL) and subjected to GC analysis. For each compound, this was performed in triplicate and the calculated mean value was used for the equations. The concentrations of analytes approximately matched the range observed in the reactions. The response factor determination for the reaction products containing inseparable, unknown side products required assessing their purity (w/w) by GC analysis. This procedure assumed that all side products and the desired product possess the same molecular weight. This assumption is valid, since only dehydration products are stable

under the reaction conditions (secondary and primary alcohols are unlikely to be formed due to the instability of the required secondary and primary cations). This assumption was furthermore verified for all products by GC/MS analysis. Additionally, the same response factor for the product and the side products had to be assumed. This assumption is acceptable, since the response factor mainly depends on the chemical formula, which is identical for all dehydration products.^[14] In the absence of heteroatoms, only slight variations are observed for compounds having the same chemical formula.^[15] Due to strong variations, the response factors of the aromatic substrates (**10**, **19**, **21** and **25**) and their corresponding products (**11**, **20**, **22** and **26**) could not be determined using the described method. In those cases, the identity of substrate and product response factor had to be assumed. The similarity between substrate and product response factor is confirmed by the aliphatic substrates and their corresponding products (see Table S2). Additionally, according to the ECN theory, the influence of a tertiary hydroxy group on the response factor corresponds to the influence of a quaternary carbon center, which is formed during the reaction.^[15] The error for this assumption is estimated to be around 5%. To further confirm the determined yields for the aromatic substrates, the purity of the crude product mixture obtained from large scale isolation was assessed under the above mentioned assumptions using GC to get a theoretical isolated yield (see chapter 7). This was not performed for the aliphatic products due significant losses during isolation caused by volatility.

The response factors were calculated according to equation 5.1 and are listed in Table S2.

$$RF = \frac{(A_X \cdot C_{IS})}{(A_{IS} \cdot C_X)} \quad (5.1)$$

RF = response factor; A_X = GC area of analyte; A_{IS} = GC area of internal standard; C_X = concentration of analyte; C_{IS} = concentration of internal standard.

Table S2. Response factors.

Compound	C_X/C_{IS}	A_X/A_{IS}	RF	Mean value
3	1.306	1.785	1.37	1.35
	2.389	3.219	1.35	
	5.464	7.309	1.34	
8	1.431	2.014	1.41	1.37
	1.459	1.953	1.34	
	2.674	3.636	1.36	

9	1.187	1.581	1.33	1.33
	1.717	2.285	1.33	
	6.161	8.270	1.34	
12	0.909	1.150	1.27	1.26
	2.527	3.169	1.25	
	5.757	7.245	1.26	
13	1.895	2.329	1.23	1.24
	3.187	3.982	1.25	
	5.587	6.908	1.24	
14	1.105	1.541	1.39	1.37
	2.401	3.229	1.34	
	5.003	6.854	1.37	
15	0.247	0.305	1.23	1.28
	1.198	1.557	1.30	
	1.294	1.689	1.31	
16	0.937	0.857	0.91	1.01
	2.601	2.474	0.95	
	3.278	3.875	1.18	
17	1.613	1.664	1.03	1.06
	3.984	4.285	1.08	
	4.786	5.176	1.08	
18	1.742	1.808	1.04	1.07
	2.327	2.565	1.10	
	4.005	4.345	1.08	
23	1.029	0.945	0.92	0.90
	2.579	2.307	0.89	
	6.125	5.382	0.88	
24	2.538	2.302	0.91	0.92
	3.460	3.252	0.94	
	4.225	3.863	0.91	
27	1.218	1.277	1.05	1.08
	3.954	4.297	1.09	
	6.934	7.597	1.10	
28	1.485	1.494	1.01	1.03
	1.896	1.928	1.02	
	2.272	2.393	1.05	

30	1.343	2.883	2.15	2.19
	2.138	4.660	2.18	
	4.327	9.646	2.23	
31	1.082	2.191	2.02	2.03
	1.504	3.066	2.04	
	2.495	5.102	2.04	

Conversions and yields were calculated by employing the following equations (5.2 – 5.6).

$$n(\text{sm})_0 = \frac{(A_{\text{sm}})_0}{\text{RF}_{\text{sm}} \cdot (A_{\text{IS}})_0} = x \quad (5.2)$$

$$n(\text{sm})_n = \frac{(A_{\text{sm}})_n}{\text{RF}_{\text{sm}} \cdot (A_{\text{IS}})_n} = y \quad (5.3)$$

$$n(\text{p})_n = \frac{(A_{\text{p}})_n}{\text{RF}_{\text{p}} \cdot (A_{\text{IS}})_n} = z \quad (5.4)$$

$$\text{conversion}(\text{sm}) = \left(\frac{x - y}{x} \right) \cdot 100\% \quad (5.5)$$

$$\text{yield}(\text{p}) = \left(\frac{z}{x} \right) \cdot 100\% \quad (5.6)$$

$n(\text{sm})_n$ = amount of starting material in the n-th measurement; $(A_{\text{sm}})_0$ = area of starting material in the initial measurement; $(A_{\text{IS}})_0$ = area of internal standard in the initial measurement; $(A_{\text{sm}})_n$ = area of starting material in the n-th measurement; $(A_{\text{IS}})_n$ = area of internal standard in the n-th measurement; $(A_{\text{p}})_n$ = area of product in the n-th measurement; RF_{sm} = response factor of starting material; RF_{p} = response factor of product.

The mean value was calculated by employing equation 5.7.

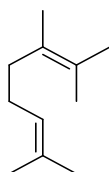
$$\text{mean value} = \bar{x} = \frac{1}{n} \sum_{i=1}^n x_i \quad (5.7)$$

The standard deviation was calculated according to equation 5.8.

$$\text{standard deviation} = \sqrt{\frac{1}{n-1} \sum_{i=1}^n (x_i - \bar{x})^2} \quad (5.8)$$

6. Synthesis of a GC reference compound

2,3,7-Trimethylocta-2,6-diene (52)



$C_{11}H_{20}$
152.28 g/mol

To a solution of potassium *tert*-butoxide (1.33 g, 11.9 mmol, 3.0 eq.) in anhydrous THF (15 mL) was added isopropyltriphenylphosphonium iodide (3.75 g, 12.3 mmol, 3.1 eq.) in portions. The dark red suspension was stirred for 30 min at rt before a solution of 6-methylhept-5-en-2-one (500 mg, 3.96 mmol, 1.0 eq.) in anhydrous THF (15 mL) was added dropwise. The reaction mixture was subsequently refluxed for 18 h. After cooling to rt, the suspension was filtered through a plug of silica and washed with Et₂O. Concentration under vacuum yielded the crude product, which was purified by flash column chromatography (pentane) to afford diene **52** (241 mg, 1.58 mmol, 40%) as a colorless liquid.

¹H NMR (400 MHz, CDCl₃): δ [ppm] = 5.16 - 5.09 (m, 1H), 2.05 - 1.99 (m, 4H), 1.68 (s, 3H), 1.66 - 1.63 (m, 9H), 1.61 (s, 3H).

¹³C NMR (101 MHz, CDCl₃): δ [ppm] = 131.5, 127.8, 124.8, 124.2, 34.9, 27.0, 25.9, 20.7, 20.3, 18.6, 17.7.

HRMS (EI): calcd for C₁₁H₂₀⁺ [(M)⁺]: 152.1560, found: 152.1486.

IR (ATR): $\tilde{\nu}$ [cm⁻¹] = 2967, 2915, 2859, 1447, 1375, 1178, 1151, 1117, 1097, 986, 829.

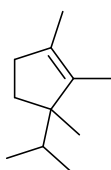
TLC: R_f = 0.77 (pentane) [KMnO₄].

7. Large scale isolation of rearranged cyclodehydration products

General procedure for large scale isolation:

In order to characterize the cyclodehydration products as well as side products and to obtain material for response factor determination large scale reactions (13-40 × GC scale) were performed. In a general large scale reaction, *C*-undecylcalix[4]resorcinarene (**1**) (330.0 mg, 298 μmol, 6.0 eq.) was weighed into a 40 mL pressure tube, CDCl₃ (15 mL) was added and the mixture was homogenized by gentle heating with a heat gun and agitation to give a clear orange solution. After allowing the solution to cool to rt, the substrate (497 μmol, 10.0 eq.) was added in one portion and the tube was sealed with an Ace-Thred PTFE bushing (caution: small overpressure). The pressure tube was then kept at 50 °C (±2 °C) using a thermostated silicone oil bath until GC indicated full conversion of the starting material and complete equilibration of the product mixture. The mixture was subsequently poured onto a packed silica column (SiO₂ = 100 mL) and the catalyst (as well as a large amount of CDCl₃) was separated from the highly apolar products by eluting with pentane (~200 mL). Subsequent solvent evaporation under vacuum, considering the product volatility, then gave the corresponding cyclopentene together with inseparable, dehydrated side products. To obtain product fractions of suitable purity for full characterization, a second chromatography step using AgNO₃-coated silica and pentane as the eluent was applied. In this process, using a large amount of AgNO₃-coated silica (30-80 mL) proved to be crucial for obtaining a high product purity. The purity of the fractions was analyzed by AgNO₃-coated TLC plates and GC. Isolation and purification of the cyclization product was performed for all substrates listed in Table 1 (see manuscript), except for substrate **9** and **18**, since they give the same product as substrate **3** and **16** respectively. Product formation in the case of **9** and **18** was confirmed via GC and ¹H NMR of the reaction mixture. In all cases, a GC purity of 85% or higher was achieved.

3-Isopropyl-1,2,3-trimethylcyclopent-1-ene (**17**)



C₁₁H₂₀
152.28 g/mol

¹H NMR (500 MHz, CDCl₃): δ [ppm] = 2.23 - 2.05 (m, 2H), 1.80 - 1.72 (m, 1H), 1.67 - 1.60 (m, 1H), 1.60 - 1.56 (m, 3H), 1.46 - 1.43 (m, 3H), 1.31 - 1.24 (m, 1H), 0.96 (s, 3H), 0.84 (d, J = 6.8 Hz, 3H), 0.67 (d, J = 6.8 Hz, 3H).

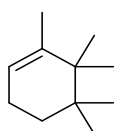
¹³C NMR (126 MHz, CDCl₃): δ [ppm] = 137.1, 129.9, 54.1, 36.1, 33.8, 29.6, 25.2, 18.4, 17.7, 14.2, 9.8.

HRMS (EI): calcd for C₁₁H₂₀⁺ [(M)⁺]: 152.1560, found: 152.1565.

IR (ATR): $\tilde{\nu}$ [cm⁻¹] = 2955, 2923, 2872, 2841, 2358, 2343, 1457, 1381, 1369, 1180, 1161, 1100, 1087, 1033, 827, 789.

TLC: R_f = 1.00 (pentane) [KMnO₄].

1,5,5,6,6-Pentamethylcyclohex-1-ene (**53**)



C₁₁H₂₀
152.28 g/mol

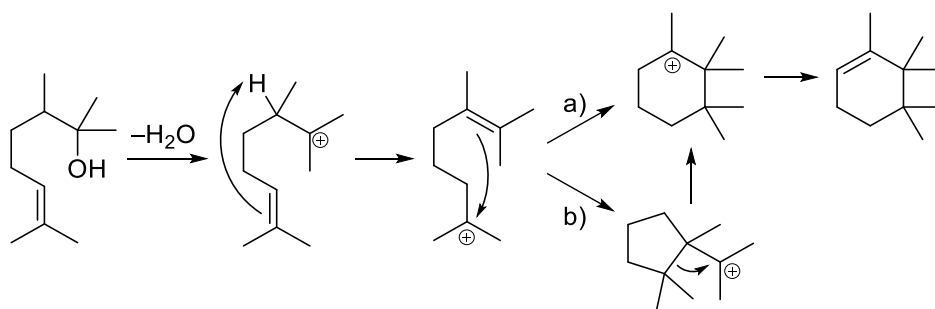
NMR data obtained from an enriched mixture of compound **53** and compound **17**.

¹H NMR (500 MHz, CDCl₃): δ [ppm] = 5.31 – 5.27 (m, 1H), 1.98 - 1.90 (m, 2H), 1.66 - 1.62 (m, 3H), 1.40 (t, J = 6.5 Hz, 2H), 0.93 (s, 6H), 0.87 (s, 6H).

¹³C NMR (126 MHz, CDCl₃): δ [ppm] = 140.4, 120.9, 39.8, 34.7, 33.3, 24.4 (2C), 23.0, 22.5 (2C), 20.0.

TLC: R_f = 1.00 (pentane) [KMnO₄].

The formation of cyclohexene **53** is likely to be caused by an intramolecular deprotonation via a 5-membered transition state (scheme S7).^[16] Starting from substrate **18**, the formation of cyclohexene **53** is favored by the additional possibility to deprotonate via a 6-membered transition state. According to GC, no significant amount of diene **52** is formed during the reaction. The ¹H NMR of a mixture of **17** and **53** is shown in Figure S1.



Scheme S7. Postulated mechanism for the formation of side product **53**.

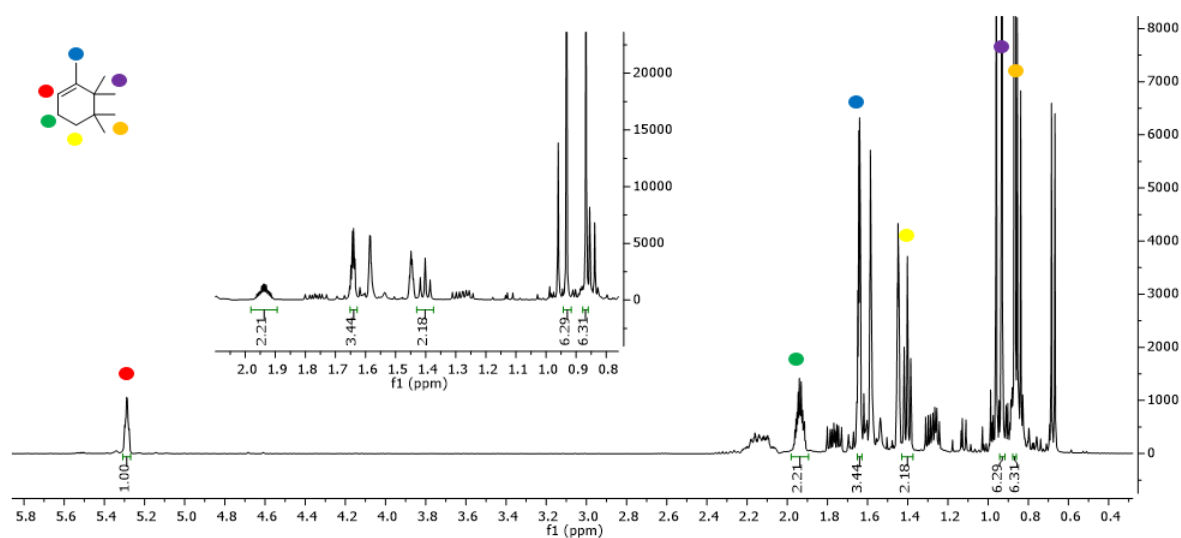
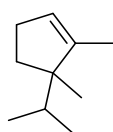


Figure S1. ^1H NMR spectrum of a mixture of compound **17** and compound **53**.

5-Isopropyl-1,5-dimethylcyclopent-1-ene (**24**)



$\text{C}_{10}\text{H}_{18}$
138.25 g/mol

^1H NMR (500 MHz, CDCl_3): δ [ppm] = 5.25 - 5.22 (m, 1H), 2.24 - 2.15 (m, 1H), 2.15 - 2.06 (m, 1H), 1.89 - 1.81 (m, 1H), 1.70 - 1.61 (m, 1H), 1.58 - 1.55 (m, 3H), 1.40 - 1.33 (m, 1H), 0.99 (s, 3H), 0.86 (d, $J = 6.8$ Hz, 3H), 0.73 (d, $J = 6.8$ Hz, 3H).

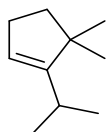
^{13}C NMR (126 MHz, CDCl_3): δ [ppm] = 146.6, 123.7, 52.8, 33.3, 31.0, 29.9, 25.2, 18.3, 17.8, 12.7.

HRMS (EI): calcd for $\text{C}_{10}\text{H}_{18}^+$ [(M) $^+$]: 138.1403, found: 138.1396.

IR (ATR): $\tilde{\nu}$ [cm^{-1}] = 3036, 2956, 2935, 2871, 2851, 1456, 1377, 1370, 1093, 1022, 822, 794.

TLC: $R_f = 1.00$ (pentane) [KMnO_4].

1-Isopropyl-5,5-dimethylcyclopent-1-ene (54)



$\text{C}_{10}\text{H}_{18}$
138.25 g/mol

^1H NMR (500 MHz, CDCl_3): δ [ppm] = 5.31 - 5.28 (m, 1H), 2.25 - 2.16 (m, 3H), 1.68 - 1.63 (m, 2H), 1.05 (d, $J = 6.8$ Hz, 6H), 1.02 (s, 6H).

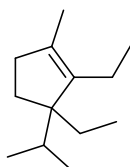
^{13}C NMR (126 MHz, CDCl_3): δ [ppm] = 159.0, 120.0, 46.6, 41.2, 29.0, 27.2 (2C), 26.2, 24.5 (2C).

HRMS (EI): calcd for $\text{C}_9\text{H}_{15}^+$ [(M- CH_3) $^+$]: 123.1168, found: 123.1166.

IR (ATR): $\tilde{\nu}$ [cm^{-1}] = 3043, 2955, 2934, 2868, 2849, 1465, 1379, 1362, 1311, 1111, 1093, 1045, 822, 794, 670.

TLC: $R_f = 1.00$ (pentane) [KMnO_4].

2,3-Diethyl-3-isopropyl-1-methylcyclopent-1-ene (15)



$\text{C}_{13}\text{H}_{24}$
180.34 g/mol

^1H NMR (500 MHz, CDCl_3): δ [ppm] = 2.16 - 2.03 (m, 2H), 1.92 - 1.82 (m, 2H), 1.67 - 1.60 (m, 2H), 1.64 (s, 3H), 1.55 - 1.46 (m, 1H), 1.37 - 1.30 (m, 1H), 1.27 - 1.17 (m, 1H), 0.97 (t, $J = 7.7$ Hz, 3H), 0.92 (d, $J = 6.7$ Hz, 3H), 0.69 (d, $J = 6.8$ Hz, 3H), 0.67 (t, $J = 7.4$ Hz, 3H).

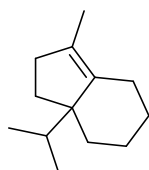
^{13}C NMR (126 MHz, CDCl_3): δ [ppm] = 139.2, 132.9, 59.5, 37.2, 34.4, 30.6, 26.1, 18.8, 18.4, 17.6, 14.2, 14.1, 9.3.

HRMS (EI): calcd for $\text{C}_{13}\text{H}_{24}^+$ [(M) $^+$]: 180.1873, found: 180.1874.

IR (ATR): $\tilde{\nu}$ [cm^{-1}] = 2960, 2933, 2874, 2858, 2841, 1465, 1384, 1376, 1367, 1187, 1088, 1056.

TLC: $R_f = 0.96$ (pentane) [KMnO_4].

7a-Isopropyl-3-methyl-2,4,5,6,7,7a-hexahydro-1H-indene (8)



C₁₃H₂₂
178.32 g/mol

¹H NMR (500 MHz, CDCl₃): δ [ppm] = 2.33 - 2.27 (m, 1H), 2.19 - 2.13 (m, 2H), 2.11 - 2.04 (m, 1H), 2.00 - 1.94 (m, 1H), 1.88 - 1.82 (m, 1H), 1.80 - 1.72 (m, 2H), 1.60 - 1.57 (m, 3H), 1.57 - 1.47 (m, 2H), 1.20 - 1.02 (m, 3H), 0.84 (d, J = 6.8 Hz, 3H), 0.67 (d, J = 6.9 Hz, 3H).

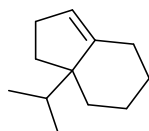
¹³C NMR (126 MHz, CDCl₃): δ [ppm] = 139.3, 127.0, 54.5, 38.8, 37.2, 30.3, 28.3, 27.8, 23.5, 22.1, 17.3, 17.2, 13.5.

HRMS (EI): calcd for C₁₃H₂₂⁺ [(M)⁺]: 178.1716, found: 178.1713.

IR (ATR): $\tilde{\nu}$ [cm⁻¹] = 2952, 2926, 2853, 2841, 1466, 1445, 1382, 1365, 1328, 1254, 1160, 1147, 1101.

TLC: R_f = 1.00 (pentane) [KMnO₄].

7a-Isopropyl-2,4,5,6,7,7a-hexahydro-1H-indene (13)



C₁₂H₂₀
164.29 g/mol

The position of the double bond was assigned based on 2D NMR spectra and literature data.^[1]

¹H NMR (500 MHz, CDCl₃): δ [ppm] = 5.22 - 5.18 (m, 1H), 2.29 - 2.23 (m, 1H), 2.22 - 2.12 (m, 2H), 2.10 - 2.04 (m, 1H), 2.03 - 1.98 (m, 1H), 1.98 - 1.90 (m, 2H), 1.81 - 1.74 (m, 1H), 1.56 - 1.43 (m, 2H), 1.29 - 1.16 (m, 2H), 1.15 - 1.07 (m, 1H), 0.86 (d, J = 6.8 Hz, 3H), 0.73 (d, J = 6.9 Hz, 3H).

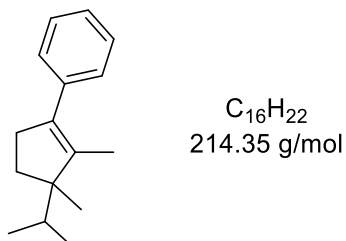
¹³C NMR (126 MHz, CDCl₃): δ [ppm] = 148.8, 119.9, 53.2, 39.0, 31.5, 31.0, 28.5, 27.9, 26.5, 22.2, 17.3, 17.2.

HRMS (EI): calcd for C₁₂H₂₀⁺ [(M)⁺]: 164.1560, found: 164.1553.

IR (ATR): $\tilde{\nu}$ [cm^{-1}] = 3039, 2953, 2928, 2852, 1465, 1446, 1383, 1366, 1161, 1088, 1024, 992, 919, 823, 799, 783.

TLC: R_f = 0.97 (pentane) [KMnO_4].

(3-Isopropyl-2,3-dimethylcyclopent-1-en-1-yl)benzene (20)



According to the general procedure, *C*-undecylcalix[4]resorcinarene (**1**) (330 mg, 298 μmol , 6.0 eq.) and substrate **19** (108 μL , 497 μmol , 10.0 eq.) were dissolved in CDCl_3 (15 mL) and kept at 50 $^\circ\text{C}$ for 2 d. Flash column chromatography (pentane) gave 83.0 mg crude product, which corresponds to 54.7 mg of compound **20** (51% theoretical isolated yield) according to GC analysis.

^1H NMR (500 MHz, CDCl_3): δ [ppm] = 7.35 - 7.31 (m, 2H), 7.30 - 7.26 (m, 2H), 7.22 - 7.18 (m, 1H), 2.74 - 2.65 (m, 1H), 2.58 - 2.49 (m, 1H), 1.95 - 1.88 (m, 1H), 1.81 - 1.74 (m, 1H), 1.71 - 1.67 (m, 3H), 1.48 - 1.41 (m, 1H), 1.08 (s, 3H), 0.91 (d, J = 6.8 Hz, 3H), 0.80 (d, J = 6.9 Hz, 3H).

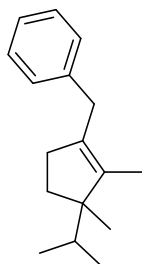
^{13}C NMR (126 MHz, CDCl_3): δ [ppm] = 141.5, 139.4, 134.2, 128.1 (2C), 128.0 (2C), 126.1, 55.2, 34.8, 33.9, 29.5, 24.8, 18.5, 17.7, 11.6.

HRMS (EI): calcd for $\text{C}_{13}\text{H}_{15}^+$ [(M-C₃H₇)⁺]: 171.1168, found: 171.1175.

IR (ATR): $\tilde{\nu}$ [cm^{-1}] = 3077, 3056, 3020, 2955, 2870, 2847, 1599, 1493, 1457, 1442, 1370, 1094, 1072, 968, 910, 761, 697.

TLC: R_f = 0.78 (pentane) [KMnO_4].

((3-Isopropyl-2,3-dimethylcyclopent-1-en-1-yl)methyl)benzene (22)



$C_{17}H_{24}$
228.38 g/mol

According to the general procedure, *C*-undecylcalix[4]resorcinarene (**1**) (330 mg, 298 μ mol, 6.0 eq.) and substrate **21** (129 μ L, 497 μ mol, 10.0 eq.) were dissolved in $CDCl_3$ (15 mL) and kept at 50 $^{\circ}C$ for 2 d. Flash column chromatography (pentane) gave 112 mg crude product, which corresponds to 65.0 mg of compound **22** (57% theoretical isolated yield) according to GC analysis.

1H NMR (500 MHz, $CDCl_3$): δ [ppm] = 7.28 - 7.23 (m, 2H), 7.19 - 7.11 (m, 3H), 3.39 (d, J = 14.8 Hz, 1H), 3.34 (d, J = 14.8 Hz, 1H), 2.15 - 2.07 (m, 1H), 2.06 - 1.99 (m, 1H), 1.78 - 1.67 (m, 2H), 1.62 - 1.58 (m, 3H), 1.30 - 1.24 (m, 1H), 1.01 (s, 3H), 0.86 (d, J = 6.8 Hz, 3H), 0.71 (d, J = 6.8 Hz, 3H).

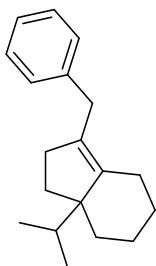
^{13}C NMR (126 MHz, $CDCl_3$): δ [ppm] = 141.0, 139.1, 133.0, 128.6 (2C), 128.3 (2C), 125.7, 54.2, 35.2, 33.7, 33.4, 29.4, 25.2, 18.4, 17.7, 10.2.

HRMS (EI): calcd for $C_{17}H_{24}^+$ [(M) $^+$]: 228.1873, found: 228.1875.

IR (ATR): $\tilde{\nu}$ [cm^{-1}] = 3084, 3062, 3026, 2954, 2870, 2844, 1602, 1494, 1453, 1379, 1370, 1320, 1181, 1160, 1091, 1077, 1030, 729, 697.

TLC: R_f = 0.76 (pentane) [$KMnO_4$].

3-Benzyl-7a-isopropyl-2,4,5,6,7,7a-hexahydro-1H-indene (11)



$C_{19}H_{26}$
254.42 g/mol

According to the general procedure, *C*-undecylcalix[4]resorcinarene (**1**) (330 mg, 298 μmol , 6.0 eq.) and substrate **10** (134 μL , 497 μmol , 10.0 eq.) were dissolved in CDCl_3 (15 mL) and kept at 50 $^\circ\text{C}$ for 2 d. Flash column chromatography (pentane) gave 116 mg crude product, which corresponds to 42.8 mg of compound **11** (34% theoretical isolated yield) according to GC analysis. In this case, the reaction was stopped before full equilibration was reached in order to isolate and characterize the main intermediate of the reaction. The main intermediate could be identified as the non-cyclized diene bearing an endocyclic double bond. The low affinity of this diene to the capsule interior explains the prolonged reaction time, required for full equilibration.

$^1\text{H NMR}$ (500 MHz, CDCl_3): δ [ppm] = 7.28 - 7.23 (m, 2H), 7.18 - 7.13 (m, 3H), 3.37 (s, 2H), 2.51 - 2.46 (m, 1H), 2.19 - 2.12 (m, 1H), 2.12 - 2.07 (m, 2H), 2.04 - 1.98 (m, 1H), 1.95 - 1.89 (m, 1H), 1.88 - 1.80 (m, 2H), 1.64 - 1.46 (m, 2H), 1.34 - 1.20 (m, 1H), 1.19 - 1.11 (m, 2H), 0.85 (d, $J = 6.8$ Hz, 3H), 0.69 (d, $J = 6.9$ Hz, 3H).

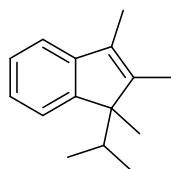
$^{13}\text{C NMR}$ (126 MHz, CDCl_3): δ [ppm] = 141.3, 141.1, 130.0, 128.7 (2C), 128.3 (2C), 125.7, 54.7, 39.0, 34.6, 34.4, 30.1, 28.4, 28.2, 23.8, 22.2, 17.4, 17.2.

HRMS (EI): calcd for $\text{C}_{19}\text{H}_{26}^+$ [(M) $^+$]: 254.2029, found: 254.2043.

IR (ATR): $\tilde{\nu}$ [cm^{-1}] = 3083, 3061, 3025, 2927, 2849, 1602, 1494, 1452, 1382, 1365, 1329, 1255, 1154, 1092, 1072, 1030, 987, 846, 732, 697.

TLC: $R_f = 0.68$ (pentane) [KMnO_4].

1-Isopropyl-1,2,3-trimethyl-1*H*-indene (**26**)



$\text{C}_{15}\text{H}_{20}$
200.33 g/mol

According to the general procedure, *C*-undecylcalix[4]resorcinarene (**1**) (385 mg, 348 μmol , 6.0 eq.) and substrate **25** (125 μL , 580 μmol , 10.0 eq.) were dissolved in CDCl_3 (17.5 mL) and kept at 50 $^\circ\text{C}$ for 6 d. Flash column chromatography (pentane) gave 108 mg crude product, which corresponds to 70.4 mg of compound **26** (61% theoretical isolated yield) according to GC analysis.

¹H NMR (500 MHz, CDCl₃): δ [ppm] = 7.32 - 7.29 (m, 1H), 7.25 - 7.22 (m, 1H), 7.19 - 7.16 (m, 1H), 7.12 - 7.08 (m, 1H), 2.01 - 1.93 (m, 4H), 1.83 - 1.80 (m, 3H), 1.21 (s, 3H), 1.07 (d, J = 6.9 Hz, 3H), 0.39 (d, J = 6.8 Hz, 3H).

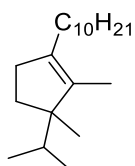
¹³C NMR (126 MHz, CDCl₃): δ [ppm] = 149.8, 146.5, 146.5, 130.5, 126.3, 123.5, 122.6, 117.9, 56.4, 33.8, 21.6, 18.3, 17.4, 10.5, 10.2.

HRMS (EI): calcd for C₁₅H₂₀⁺ [(M)⁺]: 200.1560, found: 200.1565.

IR (ATR): $\tilde{\nu}$ [cm⁻¹] = 3063, 3020, 2963, 2929, 2871, 1638, 1602, 1469, 1451, 1382, 1370, 1362, 1314, 1240, 1157, 1097, 1082, 1065, 1018, 930, 874, 842, 771, 751, 742, 676.

TLC: R_f = 0.57 (pentane) [KMnO₄].

1-Decyl-3-isopropyl-2,3-dimethylcyclopent-1-ene (31)



C₂₀H₃₈
278.52 g/mol

¹H NMR (500 MHz, CDCl₃): δ [ppm] = 2.21 - 2.08 (m, 2H), 2.06 - 1.92 (m, 2H), 1.78 - 1.70 (m, 1H), 1.68 - 1.60 (m, 1H), 1.46 - 1.42 (m, 3H), 1.36 - 1.20 (m, 17H), 0.96 (s, 3H), 0.88 (t, J = 6.9 Hz, 3H), 0.84 (d, J = 6.8 Hz, 3H), 0.68 (d, J = 6.8 Hz, 3H).

¹³C NMR (126 MHz, CDCl₃): δ [ppm] = 137.2, 134.5, 54.1, 33.7, 33.5, 32.1, 29.8, 29.8, 29.7, 29.6, 29.5, 29.5, 28.7, 28.1, 25.3, 22.9, 18.4, 17.7, 14.3, 9.9.

HRMS (EI): calcd for C₁₇H₃₁⁺ [(M-C₃H₇)⁺]: 235.2420, found: 235.2419.

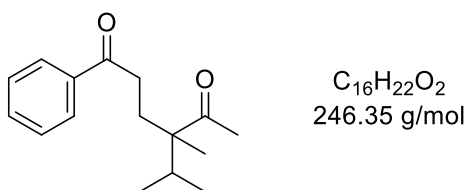
IR (ATR): $\tilde{\nu}$ [cm⁻¹] = 2955, 2923, 2871, 2853, 1457, 1378, 1370, 1090, 1032, 721.

TLC: R_f = 1.00 (pentane) [KMnO₄].

Substrate **30** is converted selectively to product **31** under the standard reaction conditions. Full conversion requires ~1.5 d.

8. Product derivatization

4-Isopropyl-4-methyl-1-phenylhexane-1,5-dione (**55**)



According to the general procedure for isolation, *C*-undecylcalix[4]resorcinarene (**1**) (440 mg, 398 μ mol, 6.0 eq.) and substrate **19** (144 μ L, 663 μ mol, 10.0 eq.) were dissolved in $CDCl_3$ (20 mL) and kept at 50 °C for 2 d. Flash column chromatography (pentane) gave the desired cyclopentene **20** together with inseparable, unknown dehydrated side products. The crude mixture was dissolved in MeCN (1.33 mL), water (1.99 mL) and CCl_4 (1.33 mL). $NaIO_4$ (582 mg, 2.72 mmol) and $RuCl_3 \cdot xH_2O$ (6.7 mg, 32.5 μ mol) were then added successively to the biphasic mixture at rt. After 15 h of vigorous stirring at rt, the mixture was diluted with DCM and the phases were separated. The aqueous phase was extracted with DCM (3×30 mL), and the combined organic phases were dried over Na_2SO_4 , filtered and concentrated under vacuum. The resulting residue was diluted with Et_2O , filtered through a pad of Celite and concentrated again under vacuum. Purification by flash column chromatography (pentane/ Et_2O = 10/1 \rightarrow 5/1) yielded the expected diketone **55** (92.0 mg, 373 μ mol, 56% over 2 steps) as a white solid.

1H NMR (400 MHz, $CDCl_3$): δ [ppm] = 7.97 - 7.91 (m, 2H), 7.58 - 7.52 (m, 1H), 7.48 - 7.42 (m, 2H), 2.88 - 2.68 (m, 2H), 2.13 (s, 3H), 2.11 - 1.99 (m, 2H), 1.94 - 1.84 (m, 1H), 1.84 (s, 3H), 0.91 (d, J = 6.9 Hz, 3H), 0.82 (d, J = 6.8 Hz, 3H).

^{13}C NMR (101 MHz, $CDCl_3$): δ [ppm] = 214.0, 200.0, 136.9, 133.2, 128.7 (2C), 128.7 (2C), 54.2, 34.0, 34.0, 30.2, 25.9, 18.2, 17.2, 15.3.

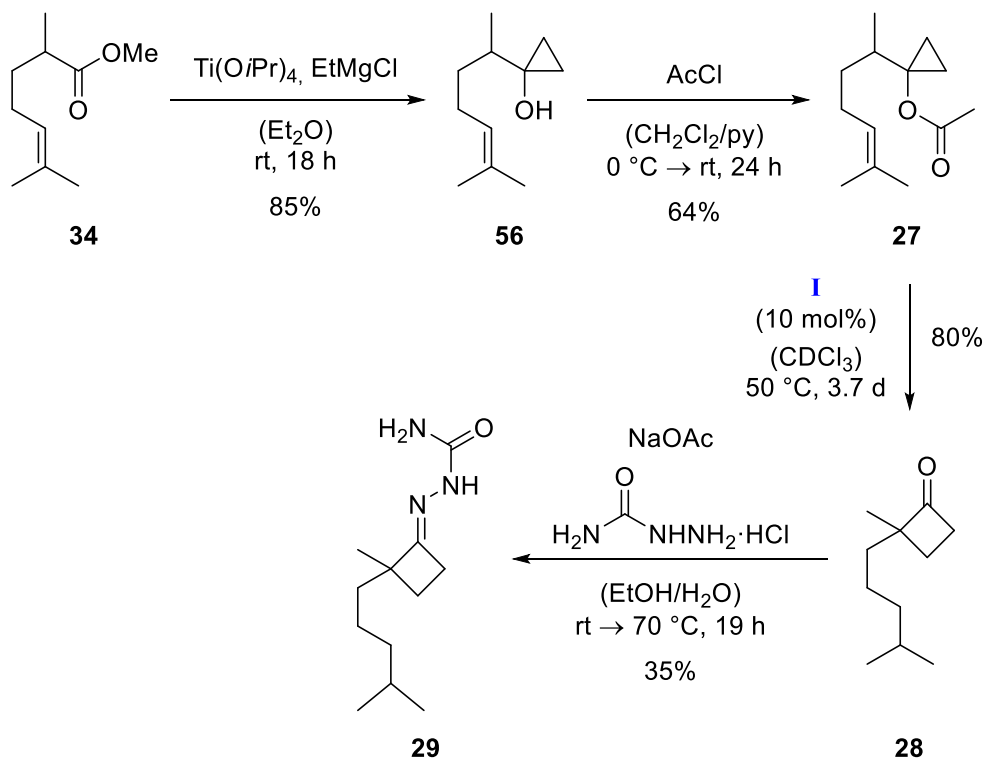
HRMS (ED): calcd for $C_{16}H_{22}O_2^+$ [(M) $^+$]: 246.1614, found: 246.1624.

IR (ATR): $\tilde{\nu}$ [cm^{-1}] = 3066, 2965, 2880, 1697, 1685, 1597, 1580, 1448, 1415, 1393, 1358, 1287, 1215, 1180, 1158, 1115, 1002, 981, 742, 690.

TLC: R_f = 0.30 (pentane/ Et_2O = 5/1) [$KMnO_4$].

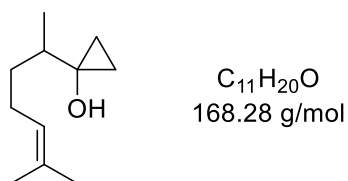
9. Intramolecular 1,5-hydride transfer

Synthesis of cyclobutanone **28** and its crystalline derivative **29**:



Scheme S8. Synthesis of cyclobutanone **28** and its crystalline derivative **29**.

1-(6-Methylhept-5-en-2-yl)cyclopropan-1-ol (**56**)



To a solution of ester **34** (6.00 g, 35.2 mmol, 1.0 eq.) in anhydrous Et₂O (300 mL) was added Ti(OiPr)₄ (10.4 mL, 35.2 mmol, 1.0 eq.). The mixture was subsequently stirred for 15 min at rt, before ethylmagnesium chloride (2.0 M in THF, 70.5 mL, 141 mmol, 4.0 eq.) was added dropwise. After stirring for 18 h at rt, the reaction was quenched by the addition of 10% aqueous H₂SO₄ (160 mL). The crude product was extracted with Et₂O (3 × 500 mL) and the combined organic phases were washed with brine (2 × 700 mL), dried over Na₂SO₄, filtered and concentrated under vacuum. Purification by flash column chromatography (pentane/Et₂O = 10/1 → 2/1) yielded alcohol **56** (5.02 g, 29.8 mmol, 85%) as a colorless oil.

¹H NMR (400 MHz, CDCl₃): δ [ppm] = 5.14 - 5.07 (m, 1H), 2.14 - 1.97 (m, 2H), 1.68 (s, 3H), 1.61 (s, 3H), 1.61 - 1.56 (m, 1H), 1.41 - 1.32 (m, 1H), 1.08 - 1.00 (m, 1H), 1.03 (s, 3H), 0.80 - 0.73 (m, 1H), 0.71 - 0.64 (m, 1H), 0.52 - 0.45 (m, 1H), 0.41 - 0.34 (m, 1H).

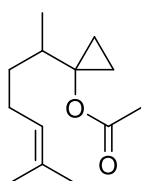
¹³C NMR (101 MHz, CDCl₃): δ [ppm] = 131.7, 124.9, 59.6, 40.0, 33.5, 26.0, 25.9, 17.9, 16.4, 14.5, 12.8.

HRMS (EI): calcd for C₁₁H₂₀O⁺ [(M)⁺]: 168.1509, found: 168.1485.

IR (ATR): $\tilde{\nu}$ [cm⁻¹] = 3350, 3084, 2964, 2925, 2876, 2857, 1709, 1453, 1376, 1270, 1118, 1008, 956, 931, 870, 827.

TLC: R_f = 0.31 (pentane/Et₂O = 10/1) [KMnO₄].

1-(6-Methylhept-5-en-2-yl)cyclopropyl acetate (**27**)



C₁₃H₂₂O₂
210.32 g/mol

To a solution of alcohol **56** (4.00 g, 23.8 mmol, 1.0 eq.) in pyridine (20 mL) and anhydrous DCM (100 mL) was added acetyl chloride (10.2 mL, 143 mmol, 6.0 eq.) dropwise at 0 °C. The yellow suspension was subsequently stirred for 24 h at rt. After addition of saturated aqueous NaHCO₃ (50 mL), the crude product was extracted with Et₂O (3 × 100 mL) and successively washed with saturated aqueous Cu₂SO₄ (3 × 100 mL) and brine (1 × 100 mL). The combined organic phases were dried over Na₂SO₄, filtered and concentrated under vacuum. The organic mixture was purified via flash column chromatography (pentane/Et₂O = 50/1 → 10/1) to give acetate **27** (3.18 g, 15.1 mmol, 64%) as a colorless oil.

¹H NMR (400 MHz, CDCl₃): δ [ppm] = 5.12 - 5.04 (m, 1H), 2.12 - 1.94 (m, 2H), 1.98 (s, 3H), 1.87 - 1.78 (m, 1H) 1.68 (s, 3H), 1.60 (s, 3H), 1.56 - 1.46 (m, 1H), 1.16 - 1.05 (m, 1H), 0.89 (d, J = 6.9 Hz, 3H), 0.82 - 0.66 (m, 4H).

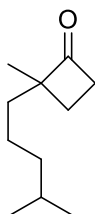
¹³C NMR (101 MHz, CDCl₃): δ [ppm] = 170.9, 131.6, 124.7, 63.8, 36.3, 33.6, 25.9, 25.9, 21.7, 17.8, 16.3, 10.7, 9.5.

HRMS (EI): calcd for C₁₂H₁₉O₂⁺ [(M-CH₃)⁺]: 195.1380, found: 195.1370.

IR (ATR): $\tilde{\nu}$ [cm^{-1}] = 2966, 2924, 2878, 2857, 1748, 1454, 1367, 1241, 1251, 1021, 989.

TLC: R_f = 0.61 (pentane/Et₂O = 10/1) [KMnO_4].

2-Methyl-2-(4-methylpentyl)cyclobutan-1-one (28)



$\text{C}_{11}\text{H}_{20}\text{O}$
168.28 g/mol

According to the general procedure, *C*-undecylcalix[4]resorcinarene (**1**) (165 mg, 149 μmol , 6.0 eq.) and substrate **27** (56.3 μL , 249 μmol , 10.0 eq.) were dissolved in CDCl_3 (7.5 mL) and kept at 50 °C for 4 d. Flash column chromatography (pentane/Et₂O = 1/0 \rightarrow 50/1 \rightarrow 20/1 \rightarrow 10/1) gave cyclobutanone **28** (27.0 mg, 160 μmol , 64%) as a colorless oil.

Due to the volatility of the product, the yield was additionally determined in triplicate *via* GC analysis, according to the standard procedure for the cyclization-rearrangement reaction. This gave a yield of $80 \pm 0\%$ after response factor correction.

¹H NMR (400 MHz, CDCl_3): δ [ppm] = 3.95 - 2.90 (m, 2H), 2.96 - 1.86 (m, 1H), 1.77 - 1.67 (m, 1H) 1.60 - 1.20 (m, 5H), 1.17 (s, 3H), 1.17 - 1.11 (m, 2H), 0.86 (d, J = 6.9 Hz, 3H), 0.86 (d, J = 6.9 Hz, 3H).

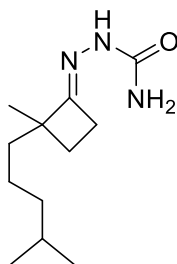
¹³C NMR (101 MHz, CDCl_3): δ [ppm] = 216.4, 64.5, 42.4, 39.5, 36.4, 28.0, 24.2, 22.8, 22.7, 22.4, 20.7.

HRMS (EI): calcd for $\text{C}_{11}\text{H}_{20}\text{O}^+$ [(M)⁺]: 168.1514, found: 168.1497.

IR (ATR): $\tilde{\nu}$ [cm^{-1}] = 2954, 2929, 2867, 1775, 1460, 1367, 1243, 1217, 1056.

TLC: R_f = 0.35 (pentane/Et₂O = 50/1) [KMnO_4].

(E)-2-(2-Methyl-2-(4-methylpentyl)cyclobutylidene)hydrazine-1-carboxamide (29)



C₁₂H₂₃N₃O
225.34 g/mol

To a solution of semicarbazide hydrochloride (133 mg, 1.19 mmol, 2.0 eq.) in water (1.0 mL) was added sodium acetate (97.5 mg, 1.19 mmol, 2.0 eq.) and the mixture was stirred until complete dissolution of the reagents. Subsequently a solution of cyclobutanone **28** (100 mg, 594 μ mol, 1.0 eq.) in EtOH (1.0 mL) was added dropwise to the mixture. The reaction was stirred for 16 h at rt, followed by 4 h at 70 °C. After cooling to 0 °C, the precipitate was filtered off and washed with cold water and pentane. After drying under high vacuum, product **29** (47.0 mg, 209 μ mol, 35%) was obtained as a colorless crystalline solid. Crystals suitable for X-ray analysis were grown by slow evaporation of a EtOH/water (2/1) solution.

¹H NMR (400 MHz, CDCl₃): δ [ppm] = 7.66 (s, 1H), 6.70 - 4.00 (m, 2H), 2.82 - 2.63 (m, 2H), 1.94 - 1.83 (m, 1H), 1.77 - 1.68 (m, 1H) 1.62 - 1.22 (m, 5H), 1.22 - 1.10 (m, 2H), 1.21 (s, 3H), 0.87 (d, J = 6.6 Hz, 6H).

¹³C NMR (101 MHz, CDCl₃): δ [ppm] = 157.5, 51.2, 39.5, 38.9, 28.0, 27.7, 26.8, 23.4, 22.8, 22.8, 22.4 (one carbon signal missing, probably due to slow relaxation).

HRMS (ESI): calcd for C₁₂H₂₃N₃NaO⁺ [(M+Na)⁺]: 248.1733, found: 248.1735.

IR (ATR): $\tilde{\nu}$ [cm⁻¹] = 3429, 3323, 3178, 3089, 2951, 2929, 2890, 2866, 2840, 1686, 1652, 1610, 1559, 1482, 1432, 1403, 1383, 1374, 1366, 1347, 1325, 1229, 1203, 1183, 1169, 1133, 1101, 1075, 982, 836, 794, 764, 749, 719, 676, 633, 606, 568, 493, 468, 425.

TLC: R_f = 0.29 (CH₂Cl₂/MeOH = 20/1) [CAM].

10. Control experiments

10.1 Blocked cavity

To verify that the reaction proceeds inside the cavity of the hexamer, the conversion and yield of all substrates were determined in the presence of a high affinity guest that would act as a competitive inhibitor by blocking the cavity. On the basis of previous reports^[17], tetrabutylammonium bromide (Bu₄NBr) (**2**) was chosen as suitable inhibitor. Additionally, it has been demonstrated that the acidity of the hexamer is increased upon encapsulation of Bu₄NBr (**2**).^[17] This enhances the quality of the control experiment, because the background reaction outside the cavity may even be favored when the inhibitor is encapsulated. For the control reactions a small excess (1.5 eq. relative to hexamer **I**) of guest **2** was utilized in order to ensure complete blocking of all cavities.

General procedure for the control reaction with inhibitor **2**:

An aliquot of a *C*-undecylcalix[4]resorcinarene (**1**) (11.0 mg, 9.95 μmol, 6.0 eq.) stock solution in CDCl₃ – prepared as described above – was added into a GC vial. Pure CDCl₃ was subsequently added until a total volume of 0.46 mL was obtained. Following this, 40 μL of Bu₄NBr (**2**) (2.49 μmol, 1.5 eq.) stock solution in CDCl₃ (62.3 mM) were added. Next, the sample was heated using a heat gun to ensure complete uptake of the inhibitor. After allowing the solution to cool to rt, *n*-decane (internal standard) (2.59 μL, 13.3 μmol, 8.0 eq.) and the substrate (16.6 μmol, 10.0 eq.) were added in one portion and the mixture was immediately sampled after 30 s of vigorous agitation. The small sample (approximately 10 μL) was diluted with *n*-hexane (0.1 mL) containing 0.08% (v/v) DMSO, centrifuged, decanted and subjected to GC analysis (initial sample). The GC vial was kept at 50 °C (±1 °C) using a thermostated heating block made from alumina. A second sample (final sample) was taken after the same time frame that is required for optimum yield in the absence of inhibitor. The conversion and yield were then determined by employing the equations above (5.2 – 5.6), utilizing the corresponding response factor. To ensure identical reaction conditions, the same stock solution of *C*-undecylcalix[4]resorcinarene (**1**) in CDCl₃ was used as for the yield determination in the absence of inhibitor.

All substrates showed a significantly reduced yield (≤ 13%) when exposed to the Bu₄NBr (**2**)-blocked cavity (Table S3). Only substrate **25** showed considerable product formation (55%) in the presence of inhibitor **2** due to its high preorganization-based reactivity. The high conversion

observed for most substrates is caused by dehydration of the substrate to the corresponding diene.

Table S3. Control reaction with blocked cavity.

Substrate	Background conversion [%]	Background yield [%]	Time [d]
3	98	7	4
9	99	12	3
10	100	12	7
12	100	3	2
14	64	13	2
16	42	10	3
18	65	3	3
19	12	1	2
21	29	6	2
23	6	0	1
25	100	55	5
27	6	0	3.7

10.2 Without catalyst

Control experiments in the absence of catalyst were performed to exclude a background reaction, catalyzed by trace amounts of HCl/DCl, potentially generated by photodegradation of CDCl₃. The substrate (16.6 μmol, 10.0 eq.) and *n*-decane (internal standard) (2.59 μL, 13.3 μmol, 8.0 eq.) were dissolved in CDCl₃ (0.50 mL), kept at 50 °C and analyzed by GC. This was performed with substrates **3**, **14** and **16**, representing the three different migrating groups. In all cases either no or negligible conversion was observed (Table S4).

Table S4. Control reaction without catalyst.

Substrate	Background conversion [%]	Background yield [%]	Time [d]
3	1	1	4
14	0	0	2
16	1	0	3

10.3 With catalytic amounts of TFA in solution

Substrate **3** (16.6 μmol , 1.0 eq.) and *n*-decane (internal standard) (2.59 μL , 13.3 μmol , 0.8 eq.) were dissolved in CDCl_3 (0.48 mL) and a small sample of this mixture (approximately 10 μL) was diluted with *n*-hexane (0.1 mL) and subjected to GC analysis (initial sample). Following this, 20 μL of TFA (0.12 μL , 1.66 μmol , 0.1 eq.) stock solution in CDCl_3 (83.0 mM) were added. The GC vial was subsequently kept at 50 °C (± 1 °C) using a thermostated heating block made from alumina. After 4 d, a second sample (approximately 10 μL) was diluted with Et_2O (0.1 mL), washed with saturated aqueous NaHCO_3 and subjected to GC analysis. Employing the equations above (5.2 – 5.6), a conversion of 24% and a yield of 5% of product **8** could be determined.

10.4 In the presence of methanol

Polar additives like methanol compete for the intermolecular hydrogen bonds of the assembly, and thus convert hexamer **I** into its monomeric subunits. DOSY-experiments by *Cohen et al.* have shown that at least 600 eq. of CD_3OD per hexamer are necessary to induce complete disassembly.^[18] This control experiment serves to exclude that formation of product **8** is enabled by simple hydrogen bonding from the phenolic OH-groups.

An aliquot of a *C*-undecylcalix[4]resorcinarene (**1**) (11.0 mg, 9.95 μmol , 6.0 eq.) stock solution in CDCl_3 – prepared as described above – was added into a GC vial. Pure CDCl_3 was subsequently added until a total volume of 0.42 mL was obtained. Following this, 80 μL of CD_3OD (1.99 mmol, 1200 eq.) were added. Next, *n*-decane (internal standard) (2.59 μL , 13.3 μmol , 8.0 eq.) and substrate **3** (16.6 μmol , 10.0 eq.) were added in one portion and the mixture was immediately sampled after 30 s of vigorous agitation. The small sample (approximately 10 μL) was diluted with *n*-hexane (0.1 mL) containing 0.08% (v/v) DMSO, centrifuged, decanted and subjected to GC analysis (initial sample). The GC vial was kept at 50 °C (± 1 °C) using a thermostated heating block made from alumina. A second sample (final sample) was taken after 4 d. Employing the equations above (5.2 – 5.6), a conversion of 29% to the two non-cyclized simple dehydration products **61** and **62** could be determined. However, formation of product **8** was completely suppressed. Performing the reaction with only 600 eq. of methanol gave a higher conversion of substrate **3** (76%), but also in this case no formation of product **8** could be detected.

11. Competition experiment

The control experiment with the blocked cavity provided strong evidence that the reaction proceeds inside the cavity. To provide further evidence, a competition experiment between substrate **16** and its long chain analogon, substrate **30**, was investigated.

Procedure for competition experiment in solution: Substrate **16** (1.50 μL , 8.29 μmol , 1.0 eq.), substrate **30** (2.79 μL , 8.29 μmol , 1.0 eq.) and *n*-decane (1.29 μL , 6.63 μmol , 0.8 eq.) as an internal standard were dissolved in anhydrous DCM (0.25 mL). At this point, a sample (approximately 10 μL) was diluted with *n*-hexane (0.1 mL) and subjected to GC analysis (initial sample). After cooling to $-5\text{ }^{\circ}\text{C}$, TFA (250 μL , 3.27 mmol, 394.5 eq.) was added in one portion and the mixture was immediately sampled (~ 10 s reaction time). The reaction in the sample was instantly quenched by diluting with Et_2O and washing with saturated aqueous NaHCO_3 . The organic phase was then subjected to GC analysis. After ~ 10 s, the ratio of conversion between substrate **16** and substrate **30** was determined to be 45:55, attributing a higher reactivity to the larger substrate in solution. In both cases, the main product was formed by cyclodehydration.

Procedure for competition experiment using catalyst I: *C*-Undecylcalix[4]resorcinarene (**1**) (11.0 mg, 9.95 μmol , 6.0 eq.) was weighed directly into a GC vial. After addition of CDCl_3 (0.50 mL), the mixture was homogenized by gentle heating with a heat gun and agitation. After allowing the solution to cool to rt, *n*-decane (internal standard) (1.29 μL , 6.63 μmol , 4.0 eq.), substrate **30** (2.79 μL , 8.29 μmol , 5.0 eq.) and substrate **16** (1.50 mL, 8.29 μmol , 5.0 eq.) were added successively and the mixture was immediately sampled. The small sample (approximately 10 μL) was diluted with *n*-hexane (0.1 mL) containing 0.08% (v/v) DMSO, centrifuged, decanted and subjected to GC analysis (initial sample). The GC vial was kept at $50\text{ }^{\circ}\text{C}$ ($\pm 1\text{ }^{\circ}\text{C}$) using a thermostated heating block made from alumina. The progress of the reaction was monitored via GC at specified intervals until nearly full conversion of substrate **16** was observed. After 3 h, the ratio of conversion between substrate **16** and substrate **30** was determined to be 96:4 (Figure S2).

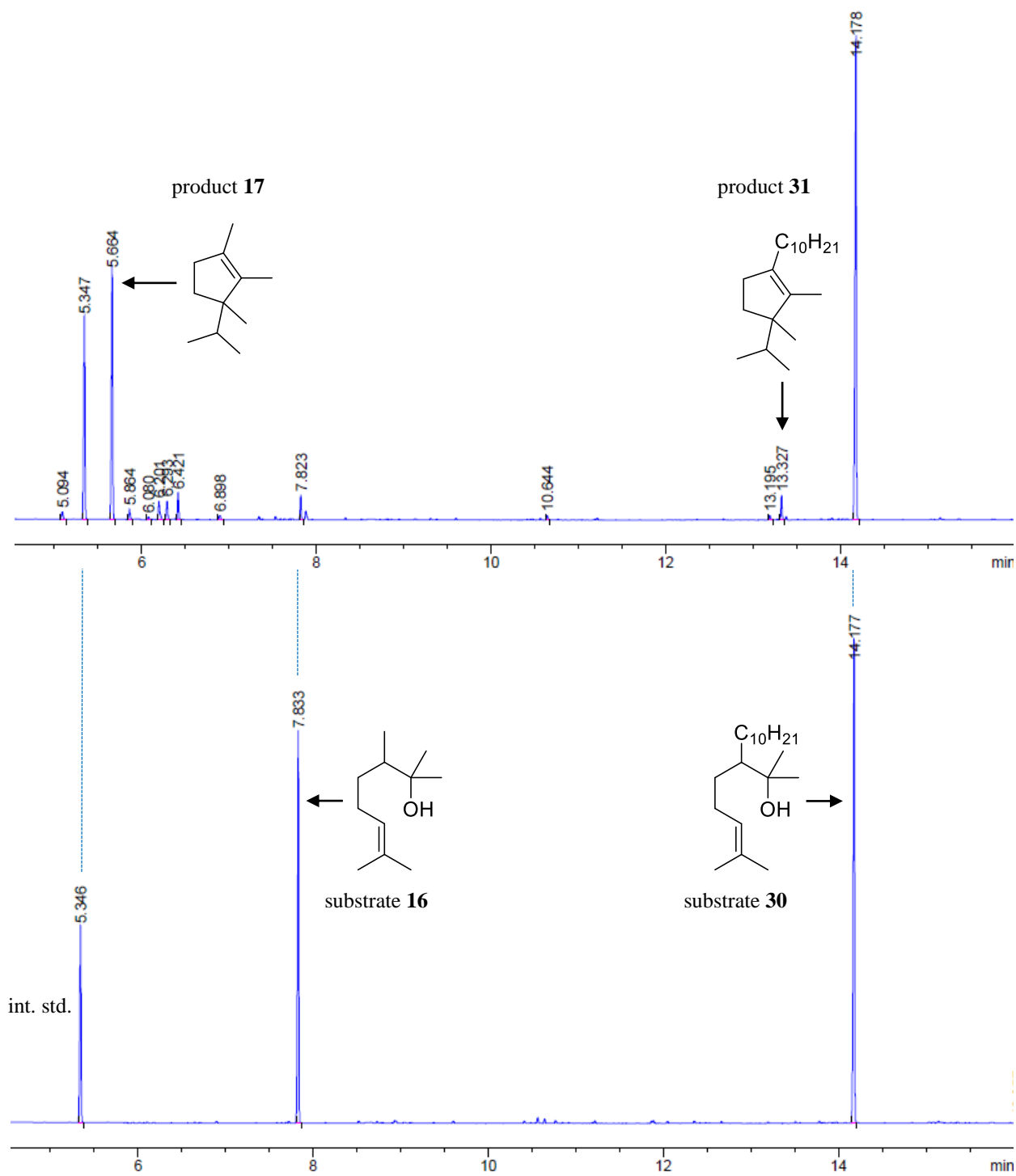
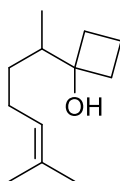


Figure S2. GC traces of the competition reaction with catalyst **I**. Bottom: Measured directly after addition of the substrates; Top: Measured after 3 h reaction time.

12. Substrates yielding no defined main product

1-(6-Methylhept-5-en-2-yl)cyclobutan-1-ol (**57**)



$C_{12}H_{22}O$
182.31 g/mol

Cyclobutanone (188 mg, 2.43 mmol, 1.0 eq.) was dissolved in anhydrous THF (2 mL) and added dropwise to (6-methylhept-5-en-2-yl)magnesium bromide (0.16 M in THF, 15.5 mL, 2.43 mmol, 1.0 eq.) – prepared according to a published procedure^[19] in one step from the corresponding bromide^[20] – at 0 °C. The solution was stirred for 1 h at this temperature. Stirring was continued for 16 h at rt before quenching with saturated aqueous NH_4Cl and dissolving the resultant white precipitate with water. The aqueous phase was subsequently extracted with Et_2O (3 × 50 mL). The combined organic phases were washed with brine, dried over Na_2SO_4 , filtered and concentrated under vacuum. Purification by column chromatography (pentane/ Et_2O = 10/1) yielded product **57** (103 mg, 566 μ mol, 23%) as a colorless liquid.

1H NMR (500 MHz, $CDCl_3$): δ [ppm] = 5.14 - 5.08 (m, 1H), 2.16 - 2.05 (m, 3H), 1.97 - 1.79 (m, 4 H), 1.69 (s, 3H), 1.62 (s, 3H), 1.59 - 1.44 (m, 4H), 1.16-1.07 (m, 1 H), 0.89 (d, J = 6.7 Hz, 3H).

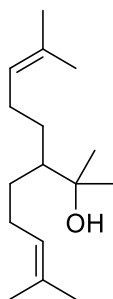
^{13}C NMR (75 MHz, $CDCl_3$): δ [ppm] = 131.5, 124.7, 79.0, 40.0, 34.5, 34.4, 30.0, 26.2, 25.7, 17.7, 12.3, 12.3.

HRMS (EI): calcd for $C_{12}H_{20}^+$ [(M- H_2O)⁺]: 164.1560, found: 164.1470.

IR (ATR): $\tilde{\nu}$ [cm^{-1}] = 3386, 2965, 2930, 2874, 1454, 1422, 1376, 1256, 1234, 1172, 1119, 1096, 1080, 1027, 954, 911, 822.

TLC: R_f = 0.56 (pentane/ Et_2O = 2/1) [$KMnO_4$].

2,7-Dimethyl-3-(4-methylpent-3-en-1-yl)oct-6-en-2-ol (58)



C₁₆H₃₀O
238.42 g/mol

NaH (60% suspension in paraffin oil, 125 mg, 5.23 mmol, 1.4 eq.) was suspended in anhydrous THF (36 mL) and cooled to 0 °C. The suspension was slowly treated with malonate **39** (800 mg, 3.73 mmol, 1.0 eq.) and the reaction mixture was stirred for 30 min at rt. Homoprenyl iodide (**37**) (1.18 g, 5.60 mmol, 1.5 eq.) was added dropwise and the mixture was stirred for 16 h at 55 °C. The reaction was subsequently quenched by the addition of saturated aqueous NH₄Cl, and this mixture was extracted with Et₂O (3 × 60 mL) and washed with brine. The combined organic phases were dried over Na₂SO₄, filtered and concentrated under vacuum. The crude alkylation product (*R_f* = 0.54 (pentane/Et₂O = 10/1) [KMnO₄]) was used without further purification in the next step. According to the general procedure for Krapcho decarboxylation, crude bishomoprenylated malonate was treated with LiCl and the reaction mixture was stirred for 1 h at 180 °C. Purification by flash column chromatography (pentane/Et₂O = 20/1) afforded the corresponding methyl ester (686 mg, 2.88 mmol, 77% over 2 steps) as a colorless oil. Following the general procedure for the addition of Grignard reagents, the ester (200 mg, 839 μmol, 1.0 eq.) was added to methylmagnesium chloride (3.0 M in THF, 909 μL, 2.73 mmol, 3.3 eq.) and the mixture was stirred over night at rt. After column chromatography (pentane/Et₂O = 10/1 → 5/1), alcohol **58** (158 mg, 662 μmol, 79%) was obtained as a colorless oil.

¹H NMR (400 MHz, CDCl₃): δ [ppm] = 5.16 - 5.09 (m, 2H), 2.16 - 1.92 (m, 4H), 1.69 (s, 6H), 1.62 (s, 6H), 1.58 - 1.48 (m, 2H), 1.26 - 1.10 (m, 3H), 1.17 (s, 6H).

¹³C NMR (101 MHz, CDCl₃): δ [ppm] = 131.6 (2C), 125.1 (2C), 74.1, 49.1, 31.6 (2C), 28.0 (2C), 27.4 (2C), 25.9 (2C), 17.9 (2C).

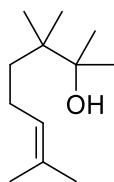
HRMS (EI): calcd for C₁₆H₂₈⁺ [(M-H₂O)⁺]: 220.2186, found: 220.2090.

IR (ATR): $\tilde{\nu}$ [cm⁻¹] = 3396, 2967, 2925, 2861, 1451, 1375, 1128, 984, 951, 895, 833.

TLC: *R_f* = 0.56 (pentane/Et₂O = 2/1) [KMnO₄].

13. Influence of a β -dimethyl group on product selectivity

2,3,3,7-Tetramethyloct-6-en-2-ol (**59**)



$C_{12}H_{24}O$
184.32 g/mol

Diisopropylamine (2.97 mL, 21.2 mmol, 18.0 eq.) was dissolved in anhydrous THF (50 mL) and cooled to $-78\text{ }^{\circ}\text{C}$. To the solution was added *n*-butyllithium (2.5 M in hexanes, 7.99 mL, 20.0 mmol, 17.0 eq.) dropwise and the reaction mixture was stirred for 30 min at $0\text{ }^{\circ}\text{C}$. After cooling to $-78\text{ }^{\circ}\text{C}$, a solution of ester **34** (200 mg, 1.17 mmol, 1.0 eq.) was slowly added and stirring was continued for 20 min at $-78\text{ }^{\circ}\text{C}$. MeI (1.76 mL, 28.2 mmol, 24.0 eq.) was subsequently added dropwise and the mixture was stirred for 2 h at $0\text{ }^{\circ}\text{C}$. The reaction was quenched by the addition of 1 M HCl, and this mixture was extracted with Et_2O ($3 \times 30\text{ mL}$) and washed with brine. The combined organic phases were dried over Na_2SO_4 , filtered and concentrated under vacuum. The crude product ($R_f = 0.75$ (pentane/ $\text{Et}_2\text{O} = 10/1$) [KMnO_4]) was purified via flash column chromatography (pentane/ $\text{Et}_2\text{O} = 50/1$). To a solution of the ester (102 mg, 554 μmol , 1.0 eq.) was added methyllithium (1.6 M in Et_2O , 865 μL , 1.38 mmol, 2.5 eq.) dropwise at $0\text{ }^{\circ}\text{C}$. The mixture was subsequently stirred for 2 h at $0\text{ }^{\circ}\text{C}$. The reaction was then quenched by the addition of water, and this mixture was extracted with Et_2O ($3 \times 30\text{ mL}$) and washed with brine. The combined organic phases were dried over Na_2SO_4 , filtered and concentrated under vacuum. Purification by flash column chromatography (pentane/ $\text{Et}_2\text{O} = 10/1$) yielded alcohol **59** (66.0 mg, 358 μmol , 65%) as a colorless oil.

$^1\text{H NMR}$ (400 MHz, CDCl_3): δ [ppm] = 5.15 - 5.09 (m, 1H), 2.00 - 1.91 (m, 2H), 1.68 (s, 3H), 1.61 (s, 3H), 1.38 - 1.30 (m, 3H), 1.18 (s, 6H), 0.91 (s, 6H).

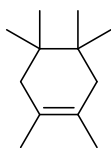
$^{13}\text{C NMR}$ (101 MHz, CDCl_3): δ [ppm] = 131.2, 125.5, 75.8, 40.0, 37.1, 25.8, 25.5 (2C), 23.5, 21.5 (2C), 17.7.

HRMS (EI): calcd for $\text{C}_{12}\text{H}_{22}^+$ [(M- H_2O) $^+$]: 166.1716, found: 166.1719.

IR (ATR): $\tilde{\nu}$ [cm^{-1}] = 3462, 2926, 2879, 2859, 1470, 1375, 1340, 1215, 1167, 1130, 1111, 941, 875, 840.

TLC: $R_f = 0.33$ (pentane/Et₂O = 5/1) [KMnO₄].

1,2,4,4,5,5-Hexamethylcyclohex-1-ene (60)



C₁₂H₂₂
166.31 g/mol

Isolation was performed according to the general procedure. The reaction displays a high selectivity.

¹H NMR (300 MHz, CDCl₃): δ [ppm] = 1.53 (s, 6H), 1.44 (s, 4H), 0.96 (s, 12H).

¹³C NMR (75 MHz, CDCl₃): δ [ppm] = 132.9 (2C), 35.9 (2C), 35.2 (2C), 28.2 (4C), 14.5 (2C).

HRMS (EI): calcd for C₁₂H₂₂⁺ [(M)⁺]: 166.1716, found: 166.1713.

IR (ATR): $\tilde{\nu}$ [cm⁻¹] = 2957, 2924, 2867, 1779, 1463, 1385, 1371, 1361, 1219, 1166, 1142, 1091, 1076, 1046, 868, 834, 778.

TLC: $R_f = 1.00$ (pentane) [iodine].

The rearrangement leading to structure **60** appears to require the generation of secondary cation intermediates. However, secondary cations are rarely found as intermediates.^[21] More often, a shift forming a secondary cation is combined with another shift in an asynchronous fashion (dyotropic rearrangement), leading to a tertiary cation.

14. Confirmation of substrate uptake by DOSY NMR

A DOSY-experiment was conducted to confirm that the new upfield-shifted resonances between 0.5 and -0.6 ppm correspond to encapsulated substrate **3**. Encapsulation results in formation of a diffusion unit and therefore the diffusion coefficient of the encapsulated species should be co-aligned with the diffusion coefficient of the host. To allow detection of encapsulated substrate **3** via DOSY NMR, the concentration of hexamer **I** (6.6 mM) and substrate **3** (66 mM) had to be doubled with respect to the standard reaction conditions, due to the low uptake. The spectrum shown in Figure S3, obtained 10 min after mixing of the two compounds, clearly indicates encapsulation of substrate **3**. The diffusion coefficient of the upfield-shifted resonances is drastically reduced compared to the not-encapsulated species and co-aligned with the diffusion coefficient of hexamer **I**.

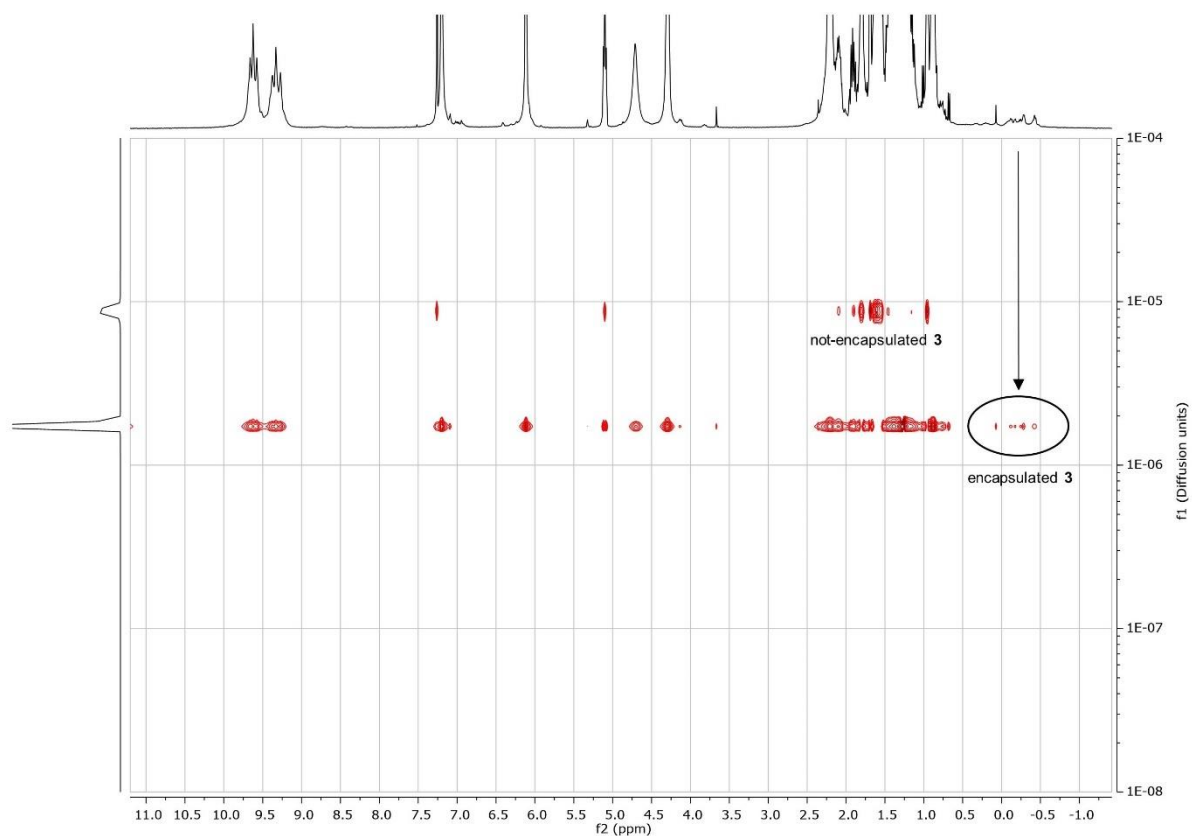


Figure S3. DOSY spectrum of a mixture of hexamer **I** (6.6 mM) and substrate **3** (66 mM) in CDCl₃, obtained 10 min after mixing. The deviation of the determined diffusion coefficient ($0.17 \times 10^{-5} \text{ cm}^2\text{s}^{-1}$) of hexamer **I** from the literature value ($0.24 \times 10^{-5} \text{ cm}^2\text{s}^{-1}$)^[22] results from the use of a pulse sequence that is not calibrated to the literature value. The same diffusion coefficient ($0.17 \times 10^{-5} \text{ cm}^2\text{s}^{-1}$) of hexamer **I** was also determined in the absence of substrate **3**. Nevertheless, the deviation from the literature value does not influence the validity of the experiment.

15. Elucidation of the initially formed side products in the cyclization of **3**

The cyclization of substrate **3** initially yields a mixture consisting of the desired product **8** and two side products, which slowly equilibrate to the desired product. According to GC analysis, these side products represent the main products in the control experiment with the Bu₄NBr (**2**)-blocked cavity (see chapter 10.1). In order to elucidate the structure of these intermediates, a large scale isolation in the presence of Bu₄NBr (**2**) was performed. Analog to the general procedure for isolation, *C*-undecylcalix[4]resorcinarene (**1**) (110 mg, 99.5 μmol, 6.0 eq.), Bu₄NBr (**2**) (8.03 mg, 24.9 μmol, 1.5 eq.) and substrate **3** (35.4 μL, 166 μmol, 10.0 eq.) were dissolved in CDCl₃ (5 mL) and kept at 50 °C for 4 d. Flash column chromatography (pentane) gave an inseparable mixture of the two side products in a ratio of ~2.2 to 1, according to GC analysis. The mixture furthermore contained traces of bicyclic product **8**. The ¹³C NMR spectrum of this mixture shows eight olefinic signals (excluding the signals corresponding to product **8**) (Figure S4). Eight olefinic signals can only be rationalized by assuming a mixture of the two non-cyclized dienes **61** and **62**, since cyclized products only have two olefinic carbons. The ¹H NMR spectrum further corroborates this and the integrals are in good agreement with the product ratio determined by GC analysis.

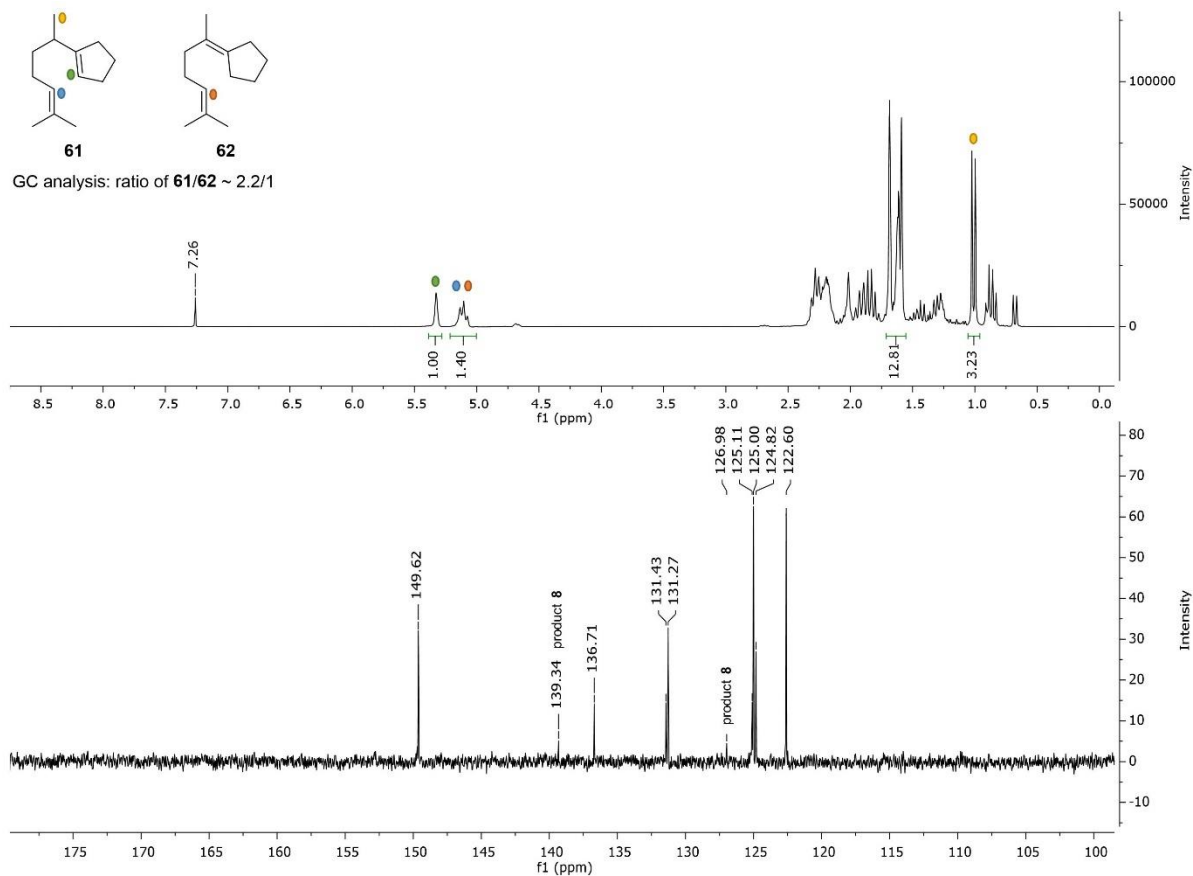


Figure S4. ¹H NMR (top) and ¹³C NMR (olefinic region) (bottom) of a mixture of **61** and **62** in CDCl₃, containing traces of bicyclic **8**.

16. SC-XRD determination of compound 29 (CCDC 1520534)

An extremely thin, clear colourless plate-like specimen of $C_{12}H_{23}N_3O$, approximate dimensions 0.010 mm x 0.142 mm x 0.162 mm, was used for the X-ray crystallographic analysis. The X-ray intensity data were measured on a Bruker D8 Venture TXS system equipped with a Helios optic monochromator and a Mo TXS rotating anode ($\lambda = 0.71073 \text{ \AA}$).

A total of 1544 frames were collected. The total exposure time was 23.23 hours. The frames were integrated with the Bruker SAINT software package using a narrow-frame algorithm. The integration of the data using a monoclinic unit cell yielded a total of 13705 reflections to a maximum θ angle of 21.02° (0.99 \AA resolution), of which 1467 were independent (average redundancy 9.342, completeness = 99.7%, $R_{int} = 6.79\%$, $R_{sig} = 3.40\%$) and 1235 (84.19%) were greater than $2\sigma(F_2)$. The final cell constants of $a = 17.0288(14) \text{ \AA}$, $b = 6.5418(5) \text{ \AA}$, $c = 13.0995(11) \text{ \AA}$, $\beta = 111.437(3)^\circ$, volume = $1358.32(19) \text{ \AA}^3$, are based upon the refinement of the XYZ-centroids of 67 reflections above $20 \sigma(I)$ with $6.642^\circ < 2\theta < 37.58^\circ$. Data were corrected for absorption effects using the Multi-Scan method (SADABS). The ratio of minimum to maximum apparent transmission was 0.809. The calculated minimum and maximum transmission coefficients (based on crystal size) are 0.9880 and 0.9990.

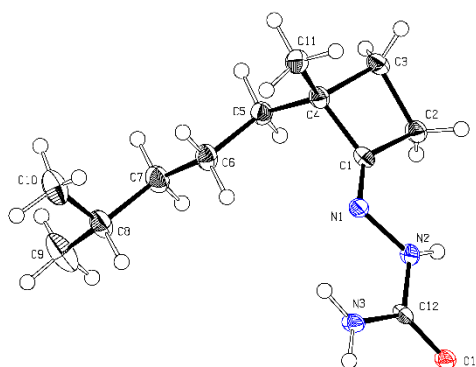


Table S5. Sample and crystal data for compound 29.

Identification code	CatLo1 AP9011-100
Chemical formula	$C_{12}H_{23}N_3O$
Formula weight	225.33
Temperature	100(2) K
Wavelength	0.71073 \AA
Crystal size	0.010 x 0.142 x 0.162 mm
Crystal habit	clear colourless plate
Crystal system	monoclinic
Space group	P 1 21/c 1
Unit cell dimensions	$a = 17.0288(14) \text{ \AA}$ $\alpha = 90^\circ$

	$b = 6.5418(5) \text{ \AA}$	$\beta = 111.437(3)^\circ$
	$c = 13.0995(11) \text{ \AA}$	$\gamma = 90^\circ$
Volume	1358.32(19) \AA^3	
Z	4	
Density (calculated)	1.102 g/cm ³	
Absorption coefficient	0.072 mm ⁻¹	
F(000)	496	

Table S6. Data collection and structure refinement for compound **29**.

Diffractometer	Bruker D8 Venture TXS	
Radiation source	TXS rotating anode, Mo	
Theta range for data collection	2.57 to 21.02°	
Index ranges	-17 ≤ h ≤ 17, -6 ≤ k ≤ 6, -13 ≤ l ≤ 13	
Reflections collected	13705	
Independent reflections	1467 [R(int) = 0.0679]	
Coverage of independent reflections	99.7%	
Absorption correction	Multi-Scan	
Max. and min. transmission	0.9990 and 0.9880	
Refinement method	Full-matrix least-squares on F ²	
Refinement program	SHELXL-2014/7 (Sheldrick, 2014)	
Function minimized	$\sum w(F_o^2 - F_c^2)^2$	
Data / restraints / parameters	1467 / 1 / 152	
Goodness-of-fit on F²	1.162	
Final R indices	1235 data; l > 2σ(l)	R1 = 0.0518, wR2 = 0.1185
	all data	R1 = 0.0642, wR2 = 0.1253
Weighting scheme	$w = 1/[\sigma^2(F_o^2) + (0.0286P)^2 + 2.3813P]$ where $P = (F_o^2 + 2F_c^2)/3$	
Extinction coefficient	0.0220(30)	
Largest diff. peak and hole	0.190 and -0.218 e \AA^{-3}	
R.M.S. deviation from mean	0.049 e \AA^{-3}	

17. References

- [1] K. Mandelt, L. Fitjer, *Synthesis* **1998**, 1998, 1523-1526.
- [2] A. Cert, W. Moreda, *J. Chromatogr. A* **1998**, 823, 291-297.
- [3] a) L. M. Tunstad, J. A. Tucker, E. Dalcanale, J. Weiser, J. A. Bryant, J. C. Sherman, R. C. Helgeson, C. B. Knobler, D. J. Cram, *J. Org. Chem.* **1989**, 54, 1305-1312; b) I. Elidrissi, S. Negin, P. V. Bhatt, T. Govender, H. G. Kruger, G. W. Gokel, G. E. M. Maguire, *Org. Biomol. Chem.* **2011**, 9, 4498-4506.
- [4] L. Avram, Y. Cohen, *Org. Lett.* **2008**, 10, 1505-1508.
- [5] L. Catti, K. Tiefenbacher, *Chem. Commun.* **2015**, 51, 892-894.
- [6] B. Flachsbarth, M. Fritzsche, P. J. Weldon, S. Schulz, *Chem. Biodivers.* **2009**, 6, 1-37.
- [7] L. Palais, A. Alexakis, *Chem. Eur. J.* **2009**, 15, 10473-10485.
- [8] B. D. Schwartz, D. P. Tilly, R. Heim, S. Wiedemann, C. M. Williams, P. V. Bernhardt, *Eur. J. Org. Chem.* **2006**, 2006, 3181-3192.
- [9] A. T. Placzek, R. A. Gibbs, *Org. Lett.* **2011**, 13, 3576-3579.
- [10] T. Heidt, A. Baro, A. Köhn, S. Laschat, *Chem. Eur. J.* **2015**, 21, 12396-12404.
- [11] D. Noutsias, G. Vassilikogiannakis, *Org. Lett.* **2012**, 14, 3565-3567.
- [12] E. Gorobets, V. Stepanenko, J. Wicha, *Eur. J. Org. Chem.* **2004**, 2004, 783-799.
- [13] G. Cahiez, O. Gager, J. Buendia, C. Patinote, *Chem. Eur. J.* **2012**, 18, 5860-5863.
- [14] J. T. Scanlon, D. E. Willis, *Journal of Chromatographic Science* **1985**, 23, 333-340.
- [15] C. L. Faiola, M. H. Erickson, V. L. Fricaud, B. T. Jobson, T. M. VanReken, *Atmos. Meas. Tech.* **2012**, 5, 1911-1923.
- [16] Y. J. Hong, D. J. Tantillo, *J. Am. Chem. Soc.* **2015**, 137, 4134-4140.
- [17] Q. Zhang, K. Tiefenbacher, *J. Am. Chem. Soc.* **2013**, 135, 16213-16219.
- [18] L. Avram, Y. Cohen, *J. Am. Chem. Soc.* **2004**, 126, 11556-11563.
- [19] G. Liu, G. Mei, R. Chen, H. Yuan, Z. Yang, C.-c. Li, *Org. Lett.* **2014**, 16, 4380-4383.
- [20] J. R. Vyvyan, C. Loitz, R. E. Looper, C. S. Mattingly, E. A. Peterson, S. T. Staben, *J. Org. Chem.* **2004**, 69, 2461-2468.
- [21] D. J. Tantillo, *Chem. Soc. Rev.* **2010**, 39, 2847-2854.
- [22] L. Avram, Y. Cohen, *Org. Lett.* **2002**, 4, 4365-4368.

18. NMR spectra

